NITROGEN IN HSLA AND DUAL PHASE STEELS

A Thesis

presented for the Degree of

Doctor of Philosophy

in

Mechanical Engineering

in the University of Canterbury

by

Ratnasabapathy Ratnaraj

University of Canterbury

Christchurch, New Zealand

December, 1989

ABSTRACT

Nitrogen is universally present in all steels, and although its solubility under normal steelmaking conditions is small it can exert large effects on steel properties. Some of these effects are detrimental, often being associated with various embrittlement phenomena. This has led to liquid steel refining processes designed, amongst other things, to decrease the nitrogen content. However nitrogen also has beneficial effects, and since it is abundant and cheap, different steels containing enhanced nitrogen have been developed.

Nitrogen levels obtained in the traditional steelmaking processes are well established. In the present investigation a detailed study of the origin and control of nitrogen in the New Zealand Steel iron and steelmaking process has been studied. The progress of 18 individual heats was followed by collecting samples at successive processing stages, and an attempt was made to correlate the observed nitrogen with recorded process variables.

It was found that hot metal from the melters had an average nitrogen content of 0.002% and a further increase in nitrogen content was observed at VRU. However, there was a drop in nitrogen content after oxygen blowing in the KOBM. It is suggested that nitrogen in solution in the liquid steel is absorbed into gas bubbles passing through the steel bath giving a flushing action, consequently carbon monoxide bubbles formed during oxygen lancing will effectively reduce the nitrogen content. There was a significant increase in nitrogen content between the KOBM samples and LTS samples, and a further increase in nitrogen content was observed in the CCM samples. These

increases at the LTS and CCM seem to result from the absorption of nitrogen during tapping, transferring the ladle to the LTS and teeming at the CCM where there is little protection of the molten stream from the atmosphere and consequential nitrogen absorption.

This investigation examines the effect of thermal treatments on the precipitation of vanadium nitride in high strength, low alloy steels. The thermal cycle of a hot rolling strip mill has been simulated in the laboratory and precipitation of vanadium nitride studied. The solubility of vanadium nitride in high strength, low alloy type steels was determined for temperatures from 900°C - 1250°C, and the ferrite grain size after the simulated thermal cycle determined. Change in yield strength, charpy transition temperature and strain age propensity as a result of vanadium nitride precipitation, have also been determined. The effect of a normalizing heat treatment subsequent to the simulated thermal cycle was also examined.

Analysed N_{insol} suggests that the precipitation of vanadium nitride is rapid in the high temperature ferrite phase range, and is diffusion controlled. Peak precipitation of vanadium nitride has been shown to occur at a simulated coiling temperature of 700°C for the high strength, low alloy steels examined. Minimum ferrite grain size for the simulated thermal cycle, and for samples subsequently normalized, suggest that vanadium nitride formed in the ferrite phase dominates the subsequent ferrite grain size. The mechanical properties of these high strength, low alloy steels have been shown to be dependent on both grain size and vanadium nitride precipitated during the simulated hot rolling thermal cycle.

Nitrogen also has an influence on the microstructure and properties of dual phase steels. Nitrogen increases the hardenability of the austenite phase formed at intercritical annealing temperature by partitioning. Manganese retards the partitioning of nitrogen by forming atom pairs within the iron lattice and providing low energy sites for nitrogen atoms. In this present investigation the partitioning of nitrogen has been investigated for a range of steels with manganese contents up to 1.5%. Significant partitioning of both nitrogen and manganese was shown to occur during the intercritical annealing heat treatment. Partitioning of nitrogen in low manganese steels was shown to be rapid, but with increased managanese content, partitioning of nitrogen retarded. This retardation was proportional to the manganese content. The effect of manganese partitioning on the formation of dual phase microstructure has also been examined.

ACKNOWLEDGEMENTS

I wish to express my gratitude to Professor L.A. Erasmus for his continual interest and supervision of this project. His encouragement, suggestions and time spent in discussion have been much appreciated.

I would also like to thank Dr J.S. Smaill and Dr J.M. Cowling for their invaluable advice and assistance, and Professor H. McCallion, Head of the Department of Mechanical Engineering, for the use of facilities for this project.

My sincere thanks also go to the technical staff of the Department of Mechanical Engineering, particularly Mr M.J. Flaws for his assistance with the image analysis and electron microscopy, the late Mr P.D. O'Hagan for his assistance with the mechanical testing, Mr O. Bolt for the preparation of test specimens, and Miss J. Shelton for her care in preparation of the diagrams and photographs.

My grateful thanks to Mrs J. Percival for her meticulous typing.

This project was assisted by the financial grants provided by the HERA and Todd Motors Research Scholarships. These are gratefully acknowledged. The financial support for this project by New Zealand Steel Limited is also gratefully acknowledged.

CONTENTS

CHAPTER PAGE

LIST OF FIGURES

LIST OF TABLES

SOME NOTATIONS OF FREQUENT OCCURRENCE

d	mean grain diameter
σ_{LY}	lower yield stress (LYS)
σ_o	friction stress in Hall-Petch equation
k_y	grain boundary strength coefficient in Hall-Petch equation
ΔY	increase in lower yield stress due to strain ageing
T	temperature
T_{27}	27 joule fracture transition temperature
K_s	solubility product
N_{sol}	'acid soluble' nitrogen
N_{insol}	'acid insoluble' nitrogen
N_{total}	total nitrogen
N_{VN}	nitrogen in the form of vanadium nitride
$N_{A\ell N}$	nitrogen in the form of aluminium nitride
N_{active}	'active' nitrogen

CHAPTER 1

INTRODUCTION

1.1 NITROGEN IN STEEL

Nitrogen is present in all commercial steels. Because the quantities of concern are generally small and its analysis is complex and expensive, its existence is generally ignored even in standard specifications. However, whether present as a residual element or added deliberately as an alloying element, the effects of nitrogen in steel are significant. Along with carbon it is responsible for the discontinuous yield point which characterises the stress-strain curve for low carbon steels. The dislocation pinning responsible for this yield point also contributes to the characteristic fatigue limit of these steels.

Nitrogen increases the strain hardening rate and can be used in a wide range of steels, including austenitic stainless steels, to produce solution hardening. Probably the hardest and best wearing steel surfaces are produced by the absorption of nitrogen into the surface of alloy steel components, generally with insignificant distortion and thus without any need for machining subsequent to nitriding.

When steels are microalloyed with titanium, vanadium or aluminium, the resultant nitrides play an important role in precipitation hardening, grain refinement and structure modification. This in turn affects steel behaviour and has led to simplified and cheaper heat

treatments, significantly enhanced strengths and improved deep drawability. Careful control of nitride precipitation is, however, important since excessive precipitation can lead to hot shortness, and to intergranular weakness in steel castings[1].

Nitrogen can also play a distinctively destructive role in the fracture toughness of structural steels[2]. Small changes in nitrogen content produce significant variations in the fracture mode transition temperature of these steels. These variations are complicated by consequential changes in precipitated nitrides[3], associated changes in grain size[4] and the interaction between nitrogen and manganese[5].

Nitrogen can also adversely affect the way in which steels behave after plastic deformation. This process is time dependent and is known as strain ageing. The embrittlement associated with strain ageing can be particularly troublesome in cold formed bends, bright drawn bars and cold formed hollow sections[6]. Conversely, there is presently great interest in using strain age hardening as a strengthening process in formed automobile panels or components where embrittlement is less likely because of the thin sections used[7]. Strain ageing can, however, be avoided by microalloying to form stable nitrides. These nitrides very often produce positive side effects leading to improved steel properties[8].

The effects of nitrogen in steel are then complex, interactive and, most cases, totally unexpected. Therefore, it is important to investigate the behaviour of nitrogen in steel, especially in widely used steels such as high strength, low alloy steels and dual-phase steels.

1.2 HIGH STRENGTH, LOW ALLOY STEELS

The American Iron and Steel Institute[9] states that high strength low alloy steels

> .....comprise a specific group of steels with chemical composition specially developed to impart higher mechanical properties values, and, in certain of these steels, materially greater resistance to atmospheric corrosion than is obtainable from conventional carbon steels. HSLA steel is generally produced with emphasis on mechanical properties requirements rather than to chemical composition limits. It is not considered to be alloy steel, even though the utilization of any intentionally added alloy content would technically qualify it as such.

High strength, low alloy (HSLA) steels are used for the construction of bridges, ships pressure vessels, tube and pipelines and vehicles[10]. Their continuing development has been stimulated by the demand for:

1. Higher yield strengths, for greater load bearing capacity by lighter sections.

2. A higher degree of weldability.

3. Higher resistance to brittle cleavage and low energy ductile fractures, as well as a low impact transition temperature.

4. Good cold formability, particularly in bending.

5. Increased ductility and fracture resistance in the through thickness direction.

6. Lower costs using hot-rolled rather than heat treated sections, plus higher ingot yields.

These stringent requirements have been met as knowledge has increased about the inter-relationships between microstructure and mechanical properties of HSLA steels.

The original HSLA steels, dating from the early 1900's, were mainly used for structural purposes[24] and were principally designed for tensile strength with little attention to toughness, formability and weldability in what were essentially riveted artefacts. The inexpensive alloying element carbon (about 0.3%) was used to achieve the tensile strength required[10]. Later, in 1934, attention was paid to yield strength of structural steels and it was improved by raising the manganese content to 1.5%[10]. The yield strength of this steel was 350 MPa in 3 cm thick plate and these steels were used successfully since neither cold forming nor welding was required[24,25].

During World War II, welding began to be much more widely used and major structural failures in the steels then available required an improvement in weldability and fracture resistance[11]. Better weldability and lower impact transition temperatures were obtained by lowering the carbon content of steel. At the same time, a high yield stress was found to be more important than a high tensile strength, although the full acceptance of this concept was slow in coming. A high manganese to carbon ratio[12], achieved by lower carbon contents, was advantageous since acicular transformation products could be by-passed in hot rolled or normalized sections.

By the early 1950's the beneficial effect of ferrite grain refinement on both yield strength and the ductile to brittle transition temperature had been demonstrated[13,14]. The significance

of manganese on grain refining through lowering the austenite transformation temperature, was not yet fully appreciated[4]. The newly developed methodology of structure-property relationships[15] hastened the introduction of normalized grain-refined steels. These steels had 75 to 125 MPa higher yield strengths together with sub-zero impact transition temperatures[15].

Initially grain refining was achieved by alloying with aluminium and nitrogen[16]. Later, other additives such as niobium, vanadium, or titanium were also found to contribute to grain refinement, precipitation hardening and higher yield strengths[17]. Niobium was the alloying addition which initially inspired the most interest[17,18]. It was believed that niobium carbide precipitation strengthening could only be achieved in the as-rolled condition, not after normalizing. The significance of niobium carbide solubility in austenite[4], and the effectiveness of vanadium in precipitation strengthening in normalized steels because of high vanadium carbide (V_4C_3) solubility in austenite[4] was established later.

Although the impact properties of these steels were not good because of their coarse as-rolled austenite grain size, which produced a coarse polygonal ferrite grain size or an acicular-ferrite transformation product, the high-ingot yields obtained with semi-killed niobium and vanadium steels provided an economic incentive [24,25]. The solution to this problem was the use of controlled rolling at a low finish-rolling temperature. This technique produced a fine grained austenite and consequently a fine ferrite grain size while preserving precipitation strengthening. As a result, yield strengths increased

to 450 - 525 MPa with impact transition temperatures as low as -80°C[19]. By accelerating the cooling of hot rolled strip products, maximum refinement of ferrite grain size was achieved by depressing the transformation temperature of the austenite[19,20]. At the same time, the use of exceptionally low carbon pearlite-free steels was considered[21]. The economic and production difficulties associated with these steels led to somewhat higher carbon contents of 0.03% to 0.08%. Together with about 1.5% manganese and appropriate grain refining additions, these steels produced yield strengths of 550 MPa and impact transition temperatures of -70°C[21,22].

The economic advantages of using accelerated cooling instead of expensive, scarce and strategically sensitive alloying elements are attractive. Accelerated cooling of heavy plates by air or water, and particularly of hot rolled strip by water cooling on the run-out table prior to coiling has led to the processing technology of controlled cooling, with or without controlled rolling.

More recently, attention has been focused on the ductility and charpy shelf-energy values of the microalloyed steels, particularly in the through thickness direction[23]. This resulted from lamellar tearing and from cracking which accompanied certain bending operations in hot rolled flat products[19]. Elongated stringers or ribbons of manganese sulphide, especially in more or less co-planer aggregates or discontinuous stringers of alumina, were found[19] to cause premature ductile fracture. This problem has been overcome in recent years by the extensive use of the technology of inclusion shape control, in which the plasticity of inclusions is decreased by additions of zirconium, cerium or calcium[24], so that elongated stringers of

inclusions are not produced. This provides increased ductility as well as improved charpy shelf-energy values in the through thickness direction, minimizing the anisotropy in these properties.

During the last ten years, there has been a revolution in high strength, low alloy steel technology in which combinations of the conventional microalloying elements are used, together with the new generation of such elements[24]. The understanding of the interactions of these multiple microalloying additions with nitrogen is far from complete, especially in terms of their dependence on processing variables. Most recently, there have been moves to design the composition of the HSLA steels so that they do not need to utilise the rather sophisticated controlled rolling technology in which the control of the low finishing rolling temperatures can be difficult[25]. Instead, the aim is to alloy so that the more conventional rolling processing can be used on mills not specifically designed for controlled rolling. Microalloying additions have also been applied to other types of steel, such as cold worked and annealed materials, quenched and tempered engineering steels and even the fully pearlitic steels[24].

1.3 DUAL-PHASE STEELS

The high strength, low alloy steels suffer from the disadvantage of showing lower formability compared with conventional low carbon steels, which can necessitate a redesign of components and forming equipment. To overcome this disadvantage, dual-phase steels were developed which combined the conflicting requirements of high strength and improved formability[26].

Dual-phase steels comprise microstructures in which islands of hard non-pearlitic phases occur in a fine grained ferrite matrix. The non-pearlite islands or second-phase particles, consist of martensite with some retained austenite and are referred to as the M-A constituent[27]. The usual range of volume fractions of M-A constituent is 0.10 - 0.30. Compared with conventional HSLA steels, dual-phase steels show lower yield strengths but higher work-hardening rates, tensile strengths and ductility values. The increased ductility is shown by both an increased uniform strain before plastic instability and increased strain at fracture. The high uniform strain before plastic instability results mainly from the high work-hardening rate, and confers improved resistance to necking during deformation. When tested in tension, the steels show continuous rather than discontinuous yielding and give typical 0.2% proof stress values of 350 - 400 MPa with tensile strengths of 550 - 800 MPa. At a typical tensile strength of 600 MPa, the total elongation would be 30% compared with 20% for a conventional HSLA steel[28].

There are two main methods of producing dual-phase structures. The first involves intercritical annealing, i.e. annealing at a temperature between the Ac_1 and Ac_3 temperatures to produce a microstructure of polygonal ferrite and austenite. The steel is then cooled at a rate sufficient to cause the austenite to transform and produce the required martensite content. Obviously, the required cooling rate depends on the alloy content in the steel. While it is possible to add sufficient alloying elements to ensure the formation of martensite, even during the batch annealing of large coils, the high alloy contents are expensive and may have severe disadvantages if the steels have to undergo subsequent welding operations. The main

method of intercritical annealing involves using a continuous annealling furnace[26], which may be equipped with accelerated cooling facilities to minimize the required alloy content.

The second method of producing the dual-phase structure is by direct hot rolling[29]. In this case, the alloy content and the finishing rolling, coiling temperatures on the hot mill are adjusted to enable sufficient polygonal ferrite to form, but to inhibit the formation of pearlite. The typical dual-phase structure of polygonal ferrite and M-A constituent is thus produced.

It has been shown[30] that the strength and work-hardening rate both increase with increasing volume fraction of M-A constituent, and this is increased by increasing the intercritical annealing temperature. On the other hand, it has also been shown[24] that the smaller the particle size of M-A constituent, the greater the strength parameters, particularly the flow stress and the work-hardening rate. A refinement of the particle size of M-A constituent, however, increases the work-hardening rate more than the flow stress[30], and therefore is likely to result in greater maximum uniform strain and hence better formability. The particle size of the M-A constituent tends to increase with increasing intercritical annealing temperature. Therefore, some compromise is required to achieve the required combination of a high volume fraction and a small particle size of the M-A constituent to give an optimum combination of strength and formability.

The required microstructural profile of a large volume fraction of very small particles of M-A constituent involves a high rate of

nucleation of the austenite during the intercritical annealing treatment, and a slow rate of growth of the austenite. It has been suggested[31] that fine microalloy carbide/nitride precipitates can pin the interface of the M-A constituent and hence inhibit its growth.

High nitrogen contents tend to produce finer particles of M-A constituent, and there seems to be a correlation between the microstructural effect and the resulting increased strength levels and work hardening rates obtained at higher nitrogen contents[30]. The reason for the finer M-A constituent particle size in the higher nitrogen steels are not clear, but could be due to:

(1) The increased pinning effect of nitride precipitates on the M-A constituent interface, thus inhibiting their growth.

(2) An increased nucleation rate for austenite. It has been suggested[31] that the increased nitrogen may increase the nucleation rate of austenite through a nucleating effect of increased numbers of nitride precipitates.

(3) The nitrogen increasing the hardenability of the austenite islands formed at the intercritical annealing temperature, possibly by a partitioning effect of any nitrogen in solution. Partitioning could cause a refinement of the acicular ferrite formed on cooling, which would break the austenite islands into smaller particles[30] which would then transform to the M-A constituent.

Therefore, the required microstructural profile of a large volume fraction of very fine particles of the M-A constituent can be achieved by:

(1) An initial highly refined microstructure;

(2) As high an intercritical annealing temperature as possible without producing too large particles of the M-A constituent;

(3) A rapid cooling rate from the intercritical annealing temperature;

(4) A high rate of nucleation and a low rate of growth of the austenite formed at the intercritical annealing temperature;

(5) Having a high nitrogen content in microalloyed steels.

1.4 SCOPE OF THESIS

As can be seen from the preceding discussion, nitrogen can have important effects on the structure and properties of steels. Its significance has been reinforced recently by the more stringent requirements for new types of products with low nitrogen specifications. Efficient control of these low nitrogen levels requires a comprehensive knowledge of the various sources of nitrogen. Many studies[2,8,38,42,93,95] have already been devoted to this question but recent modifications in liquid steel production and the introduction of new types of downstream processes lead to continuous reconsideration of this problem. This thesis describes research into

several aspects of the sources of nitrogen in steel and its influence on microsctructure of properties.

An investigation was made of the sources of nitrogen and variation of nitrogen level during iron and steel making at New Zealand Steel Limited. The factors influencing the nitrogen content of iron and steel at various stages of the iron and steel making processes were examined.

During thermomechanical processing of microalloyed steels, microalloying elements such as vanadium, titanium or aluminium combine with nitrogen to form stable nitride precipitates. These precipitates play a major role in controlling the mechanical properties of these microalloyed steels.

In order to study the nitride precipitation during a thermo-mechanical treatment and its effects on mechanical properties of microalloyed steels, the thermal cycle of a hot rolling strip mill was simulated in the laboratory. Precipitation of vanadium nitride and its effects on mechanical properties were examined.

Nitrogen also has an important influence on the microstructure and properties of dual-phase steels. Nitrogen increases the harden-ability of the austenite islands formed at intercritical annealing temperature by a partitioning effect of nitrogen in solution. Manganese retards the diffusion of nitrogen by forming atom pairs within the iron lattice and providing low energy sites for nitrogen atoms[32]. The partitioning of nitrogen and the effect of manganese on nitrogen partitioning were therefore also examined.

CHAPTER 2

NITROGEN ABSORPTION IN VARIOUS STEELMAKING PROCESSES AND ITS EFFECT ON STEEL PROPERTIES

2.1 INTRODUCTION

Nitrogen is universally present in steel. Because the quantities are small, generally less than 0.02%, and the analysis of nitrogen complex and expensive, its existence and effects are generally ignored. For instance, specifications rarely, if ever, acknowledge the existence of nitrogen in steel. However the effects of nitrogen in steel are significant.

In microalloyed steels (H.S.L.A. steels) some or all of this nitrogen may be combined as stable nitrides. Nitrogen not combined as stable nitrides has a major influence on steel properties. It produces enhanced strain hardening and improved creep and fatigue strengths, but raises the fracture mode transition temperature, gives strain age hardening and strain age embrittlement[8].

The nitrogen combined as stable nitrides also affect the properties of H.S.L.A. steels. These nitride precipitates may pin the grain boundaries or act as nuclei for new grains during phase transformation, thus refining ferrite grain size. Grain refinement substantially increases yield strength and also decreases the fracture mode transition temperature. The nitride precipitates also contribute to precipitation hardening and consequently increase yield strength[4].

Therefore, the nitrogen content of steels should be carefully controlled, to ensure desirable properties in a given alloy. To aid in control, the thermodynamics and kinetics of nitrogen behaviour in steel should be well understood. The subject of nitrogen in iron and steel has been studied extensively[8,42]. This chapter reports such a study.

2.2 BEHAVIOUR OF NITROGEN IN STEEL

2.2.1 Solubility of Nitrogen in Pure Iron

The solubility of Nitrogen at a partial pressure of one atmosphere in iron is known with reasonable accuracy and is shown in Figure 2.1[35]. It is to be noted that the solubility of nitrogen in iron is influenced by temperature, and it always undergoes an abrupt change at solidification and phase transformation temperatures.

At the temperatures of interest in steelmaking, gaseous nitrogen exists primarily as diatomic molecules which dissociate to dissolve in liquid iron:

$$N_{2(gas)} \rightleftharpoons 2N_{(dissolved)}$$

for which the equilibrium constant is:

$$K = \frac{[N]^2}{p_{N_2}}$$

whence $$[N] = (p_{N_2})^{\frac{1}{2}} \cdot K^{\frac{1}{2}}$$

As these essentially dilute solutions obey Henry's Law, this may be written as:

$$[\omega t\%\ N] = K_N \cdot (p_{N_2})^{\frac{1}{2}} \qquad \text{Eqn.2.1}$$

Equation 2.1 is closely obeyed for the solubility of nitrogen in liquid iron and it is an expression of the well known Sievert's Law,

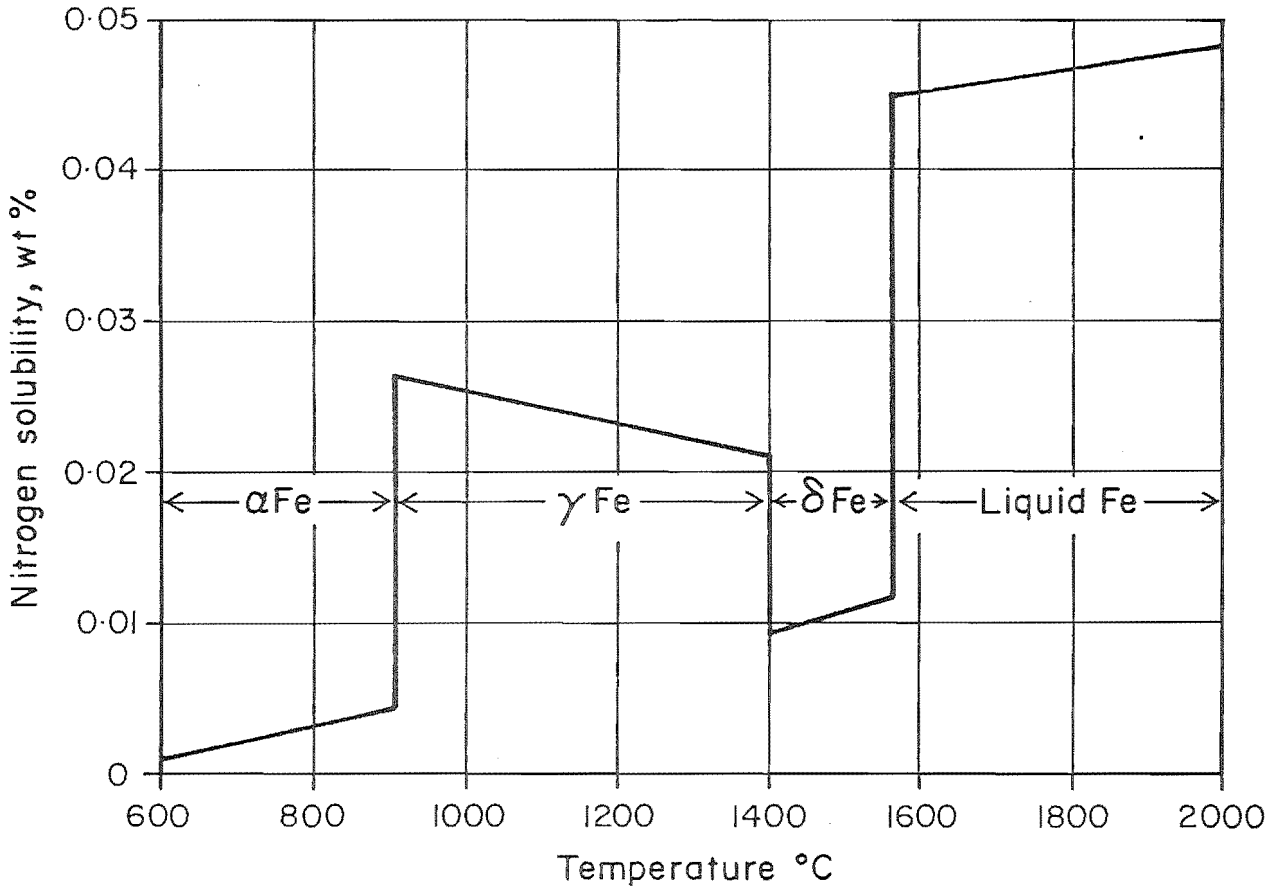

Figure 2.1: Solubility of nitrogen in pure iron under a nitrogen partial pressure of one atmosphere. (Ref. 35.)

which predicts a square root dependence of solubility in liquid metals on the partial pressure of diatomic gases. Sievert's Law is not applicable to the solution of nitrogen at the higher temperatures experienced under the electric arc, where considerable dissociation of normally diatomic molecules occurs(33).

The Sievert's constant K_N in equation 2.1, is equal to the solubility under one atmosphere of nitrogen and thus Figure 2.1 is also a plot of the variation of K_N with temperature. In liquid iron the dependence of K_N on the temperature is small and the plot in Fig.2.1 follows the following relationship(35):

$$\text{Log } K_N = -\frac{188.1}{T} - 1.246 \qquad \text{Eqn.2.2}$$

From equation 2.2 the solubility at 1600°C (T = 1873°K) under one atmosphere of nitrogen is 0.045 ωt%, and by application of equation 2.1 the solubility under air at a total pressure of one atmosphere for which p_{N_2} = 0.79 atmosphere is 0.040 ωt%.

2.2.2 Solubility of Nitrogen in Liquid Steel

Dissolved elements also influence the solubility of nitrogen in steel. The solubilities of nitrogen at one atmosphere pressure in binary iron alloys at 1600°C are shown in Figure 2.2, and these alloys all obey Sievert's Law(34).

If the simple and complex alloys are under the same partial pressure of nitrogen their nitrogen activities ([N]) will be the same, and as they obey Henry's Law they are given by:

$$[N] = [\omega t\%\ N]^{Fe} \text{ in pure iron}$$

$$[N] = [\omega t\%\ N]^{Fe.....i} \cdot f_N^{Fe.....i} \text{ in iron alloy}$$

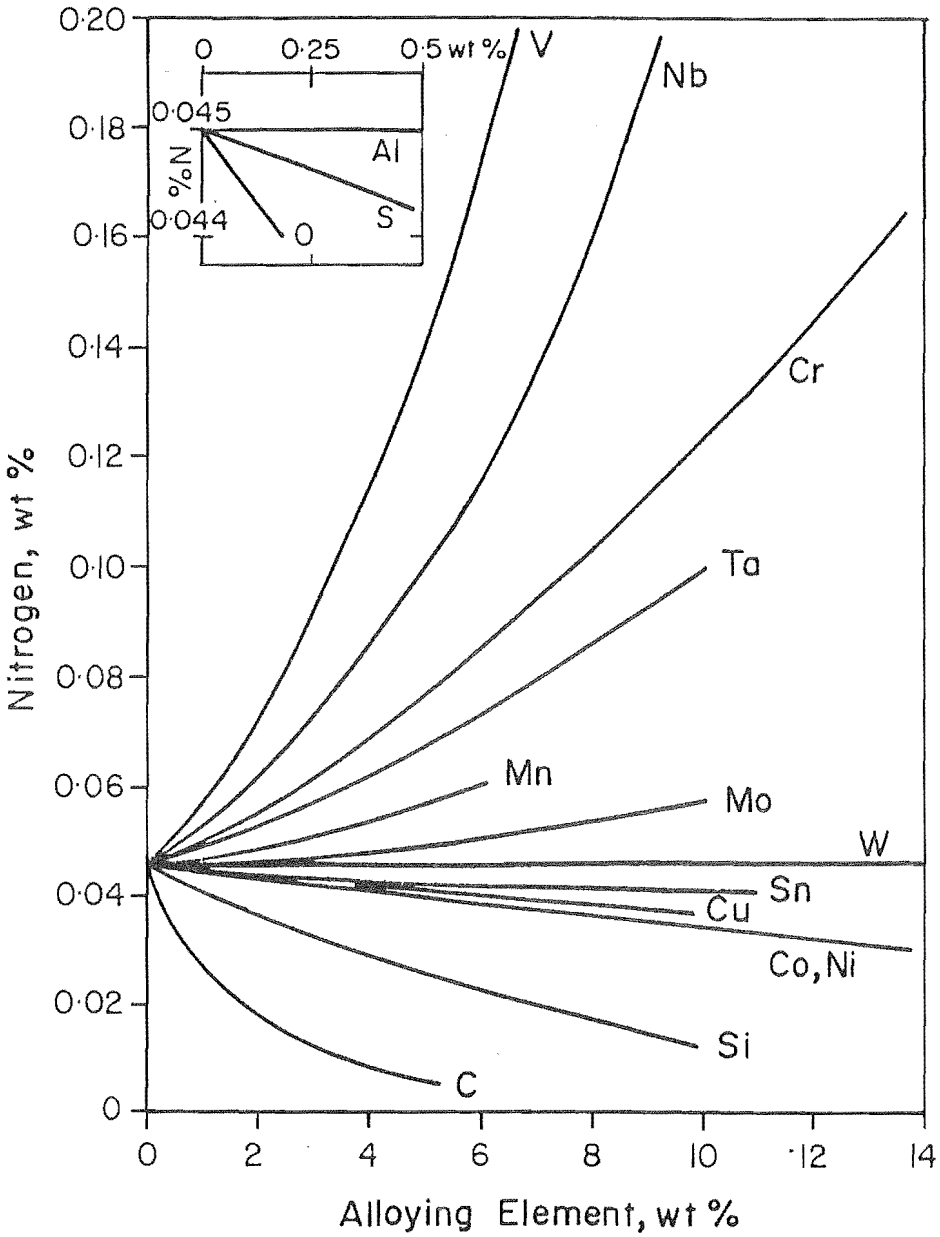

Figure 2.2: Effect of alloying elements on the solubility of nitrogen at one atmosphere pressure in liquid binary iron alloys at 1600°C. (Ref. 34.)

so that $[\omega t\%\ N]^{Fe.....i} = \dfrac{[\omega t\%\ N]^{Fe}}{f_N^{Fe....i}}$ Eqn.2.3

In this equation $[\omega t\%\ N]^{Fe}$ is known from equation 2.1, equal to $K_N(p_{N_2})^{\frac{1}{2}}$ and $f_N^{Fe.....i}$ can be found from the equation given below:

$$f_N^{Fe.....i} = f_N^N . f_N^C . f_N^{Si} . f_N^{Mn} ... f_N^i \qquad \text{Eqn.2.4}$$

where f_N^N is unity and $f_N^C, f_N^{Si}, f_N^{Mn}.....f_N^i$ are given for the Fe-N-i solutions by the application of equation 2.3 to simple ternary solution, that is:

$$f_N^{Fe-i} = f_N^i = \frac{[\omega t\%\ N]^{Fe}}{[\omega t\%\ N]^{Fe-i}} \qquad \text{Eqn.2.5}$$

The solubility of nitrogen in complex alloys is thus calculable if it is known in all possible binary alloys, (Fe-C), (Fe-Si), (Fe-Mn)..... (Fe-i), involved. Values of f_N^i are directly obtainable according to equation 2.5 from the measured solubility data given in Figure 2.2, and these values are shown plotted in Figure 2.3[34].

At low concentrations of the alloying elements the curves in Figure 2.3 are approximately linear and for Fe-N-X solutions may be expressed by equations of the form:

$$\text{Log } f_N^X = e_N^X . [\omega t\%\ X] \qquad \text{Eqn.2.6}$$

where e_N^X is the interaction coefficient. Values of the interaction coefficients for some elements in liquid Fe-N-X alloys at 1600°C are given in Table 2.1[33].

Therefore the solubility of nitrogen in complex alloys can be calculated from equation 2.3, i.e.:

TABLE 2.1: Values of the interaction coefficients, e_N^X, in liquid Fe-N-X alloys at 1600°C. (Ref. 33.)

Element, X	Interaction Coefficient, e_N^X
C	0.250
P	0.051
O	0.050
Si	0.047
As	0.018
S	0.013
Co	0.011
Ni	0.010
Cu	0.0092
Sb	0.0082
Sn	0.0071
Aℓ	0.0025
Se	0.000
W	-0.002
V	-0.100
Mo	-0.011
Mn	-0.020
Ta	-0.034
Cr	-0.045
Nb	-0.067
Ti	-0.640

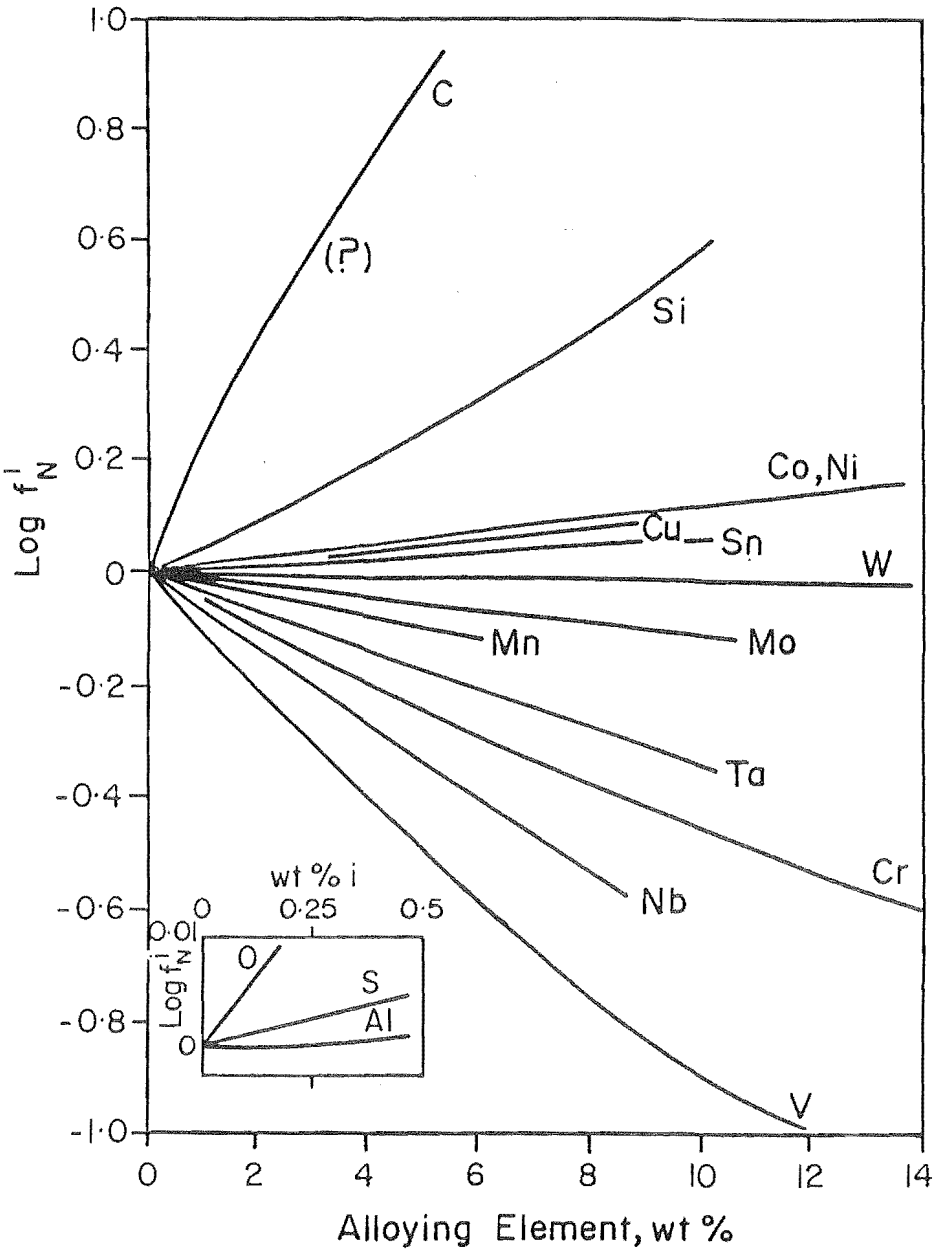

Figure 2.3: Activity coefficients of nitrogen in liquid binary iron alloys at 1600°C. (Ref. 34.)

$$[\omega t\%\ N]^{Fe,C,Si,Mn...i} = \frac{K_N.(p_{N_2})^{\frac{1}{2}}}{f_N^{Fe,C,Si,Mn....i}} \qquad \text{Eqn.2.7}$$

where

$$\text{Log } f_N^{Fe,C,Si,Mn...i} = e_N^C.[\omega t\%\ C] + e_N^{Si}.[\omega t\%\ Si] + e_N^{Mn}.[\omega t\%\ Mn]..... \ .....+ e_N^i.[\omega t\%\ i] \qquad \text{Eqn.2.8}$$

Equations 2.2, 2.7 and 2.8 have been used to predict the theoretical nitrogen solubility for the acid Bessemer[36] and BOF processes[37]. Both predictions indicate an increase in nitrogen solubility with blowing time, but show also that the normal nitrogen levels obtained with these processes are less than predicted.

Since the actual nitrogen content lags behind the increase in the equilibrium saturation value caused by the increasing temperature and the composition change, it becomes apparent that the time the steel is in contact with the nitrogen atmosphere is an important variable.

2.3 NITROGEN ABSORPTION IN STEELMAKING

The nitrogen content of steel can be derived from several sources: hot metal, scrap, ferroalloy additions, nitrogen additions and the atmosphere. The major source of nitrogen depends upon the steelmaking process[37]. The factors that affect the nitrogen content of steel are:

1. The composition of the melt.

2. The partial pressure of nitrogen in the gases in contact with the melt, or the nitrogen potential of the slag.

3. The duration of contact between the atmosphere and the liquid metal.

4. The temperature of the liquid metal.

5. Nitrogen additives.

Typical nitrogen content of commercial steels produced by different steelmaking practices are shown in Figure 2.4. Some steelmaking processes have been virtually superseded, e.g. the Bessemer, the Thomas air-pneumatic and the open-hearth processes. The decline in these steelmaking processes was linked with the problem of nitrogen strain-age effects and is one of the reasons for the frequent notes in steel specifications precluding the use of steel with these origins.

A brief description of the characteristics of the steelmaking processes is given below.

2.3.1 Air-Pneumatic Processes

(a) Bessemer Converter Process (Acid Bessemer Process)

In this process liquid iron was charged to a pear shaped vessel with a silicous (acid) lining, and the vessel turned upright. Air was blown through tuyeres in the vessel bottom and the carbon, silicon and manganese were oxidised by air bubbling through the iron. Sulphur and phosphorus were not removed, and the type of pig iron used was therefore very important.

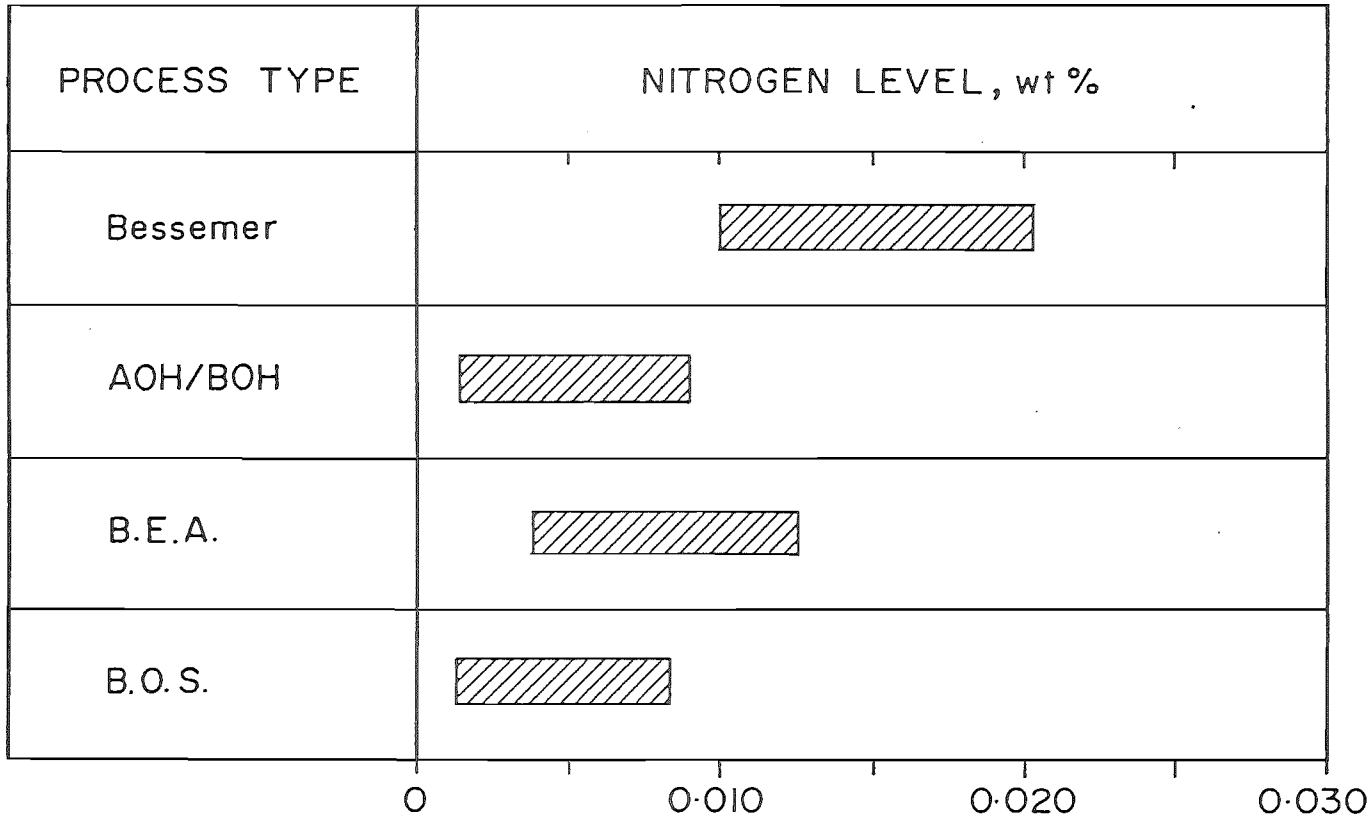

Figure 2.4: Typical nitrogen levels in finished products from different processes. (Ref. 38.)

(b) Thomas Process (Basic Bessemer Process)

The Thomas process was very similar to the acid Bessemer Process. In this process basic (dolomite) lining was used and it was therefore possible to remove phosphorus and sulphur in addition to carbon, silicon and manganese.

Since an air blast was used in both acid and basic Bessemer processes the resulting steel contained a fairly high level of nitrogen. Figures 2.5 and 2.6 show the change of steel composition with air blowing time in acid Bessemer converter and basic Bessemer converter processes[38].

2.3.2 Open Hearth Process

Open hearth furnaces were more versatile steelmaking units in that they would accept metal charges ranging from 100% liquid to 100% solid. Depending on availability and cost, a conventionally operated open-hearth furnace usually consumed between 30 and 70% of cold steel scrap. In this process heat is supplied by oil or gas flames over a wide, shallow "open-hearth".

The nitrogen content of open-hearth steels made from mixed scrap and hot metal charges generally varied little, except for a rise in nitrogen content during tapping when the stream was in contact with the atmosphere[39]. Whatever nitrogen elimination occurred during refining was accomplished by means of the carbon boil. The greater the amount of carbon eliminated after the bath was covered with slag, the larger the proportion of nitrogen removed. Brower et al[40] found that the nitrogen level of the open-hearth bath (samples taken from

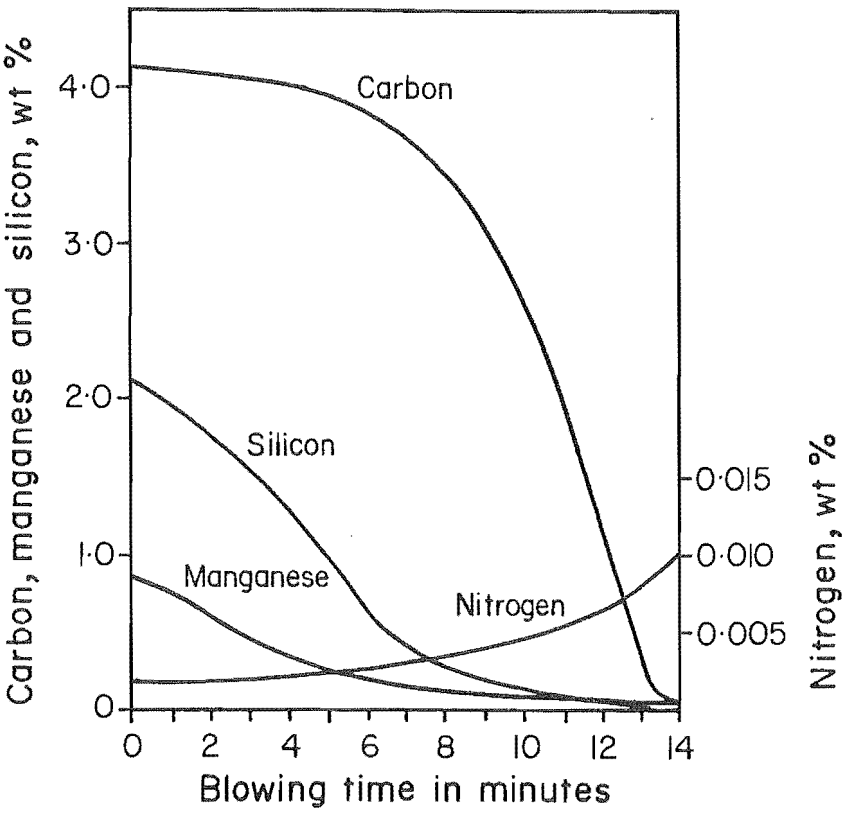

Figure 2.5: Change of steel composition with blowing time in the acid Bessemer converter process. (Ref. 38.)

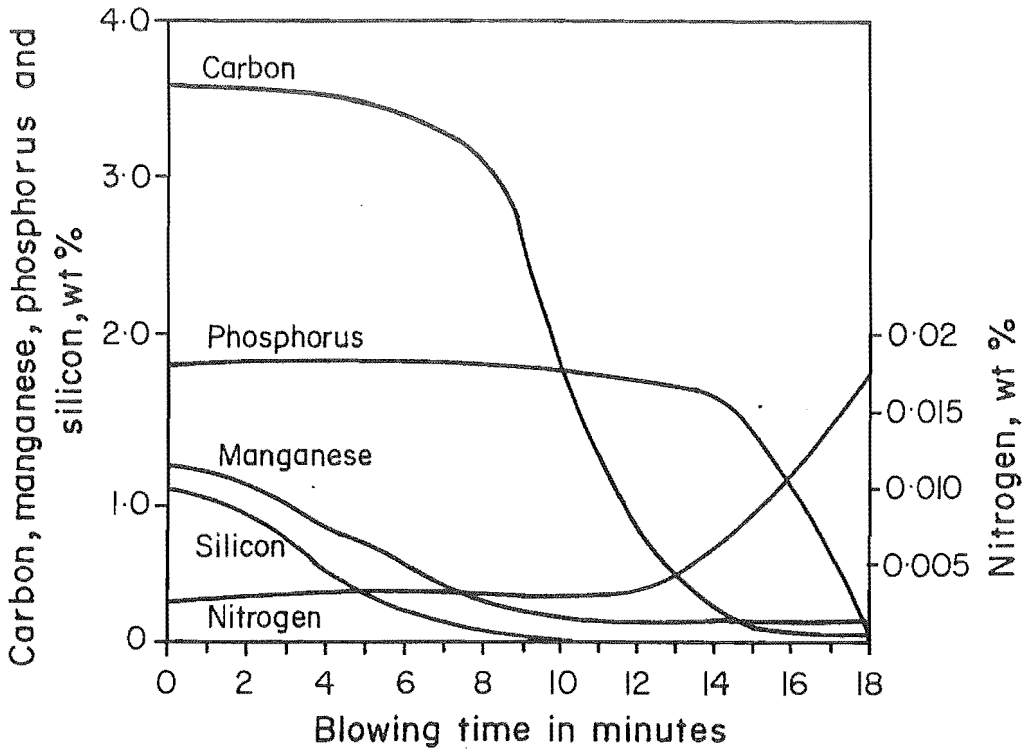

Figure 2.6: Change of steel composition with blowing time in the basic Bessemer converter process. (Ref. 38.)

the tapping stream) varied from 0.0010% to 0.0044%, with an average value of 0.0028%.

2.3.3 Basic Electric Arc Process

Precise temperature control and clear melting in a sulphur-free atmosphere made the electric arc furnace an alternative method for the melting of quality alloy steels. Arc furnaces are charged with clean scrap (steel, and pig iron), limestone and possibly anthracite or broken electrodes as a source of carbon, are melted as quickly as possible. Oxygen is blown into the melt during refining. Carbon is the main element removed by the oxygen blow but other elements in minor quantities are also removed. Carbon removal and carbon monoxide evolution produces the "carbon boil" which is an essential feature of all steelmaking processes. The carbon boil promotes stirring which results in good slag/metal mixing, elimination of temperature and concentration gradients, and the reduction of dissolved hydrogen and some nitrogen in the melt.

In an electric arc furnace, where nitrogen-bearing gases contact the metal surface at very high temperatures under the arc, nitrogen absorption by the bath is rapid. Hence the nitrogen content of the electric furnace steels is generally higher than the same steels made by the open-hearth process[39].

2.3.4 Basic Oxygen Pneumatic Steelmaking (BOS) Processes

The basic oxygen steelmaking processes were developed from the basic Bessemer process. In the oxygen steelmaking process oxygen is jetted on to the surface from a lance or blown through nozzles into the molten metal. Various oxygen steelmaking processes are in

practice, and depending on the converters and blowing pattern, they can be categorized into three groups:

1. Bottom blown Processes (Q-BOP,LWS): In these processes oxygen is injected through nozzles set in the converter bottom. Overheating of the nozzles is prevented by endothermic cracking of peripheral hydrocarbon surrounding ingoing oxygen.

2. Top blown Processes (LD,LD-AC): In these processes oxygen is admitted through a water cooled copper lance situated centrally in the vessel.

3. Combined, Top and Bottom, blown Process (KOBM): In this process oxygen is blown through nozzles in the converter bottom and a lance situated centrally in the vessel.

The factors that affect the nitrogen content of basic oxygen steel can be divided into two groups[40,41]:

1. The materials charged into the converter.
2. Blowing conditions.

1. Converter Inputs

The first parameter considered in the nitrogen content of the hot metal. It has been shown that an increase of 10 ppm in hot metal nitrogen leads to an increase of 1 ppm in the steel nitrogen level with all remaining conditions unchanged[43].

The use of regants based on carbonates and oxidising components such as $CaCO_3$, iron ores, etc. have been found to reduce the hot metal nitrogen content[42]. The nitrogen removed (30-60%) was accompanied

by a light decarburisation of the hot metal and the production of CO_2[44].

The second important parameter is the scrap input. It was observed that the greater the scrap input, the higher the steel nitrogen level at turndown[45]. This scrap effect can be controlled by increasing the hot metal input and using iron ore as a cooling agent.

The third input parameter is the oxygen purity, mainly its nitrogen content. An increase of 100 ppm of nitrogen content in the oxygen results in an increase of 1.5 ppm of the steel nitrogen level[42]. The purity of the blowing oxygen is therefore an important factor and must be controlled on a regular basis.

2. Blowing Conditions

Following the development of combined blowing processes, it has been possible to produce low carbon steels without increasing the nitrogen level at turndown. An important factor that should be considered in this field is the nature of the inert gas or the type of shielding medium used to protect the tuyeres when the oxygen is Bottom blown. It has been observed that in the case of the KOBM process the use of propane as a shielding gas rather than natural gas reduced the steel nitrogen level by more than 10 ppm[42].

Another factor exerting a major influence on the steel nitrogen level in the converter is the use of the reblow which always increases the nitrogen content of steel. After one reblow, the nitrogen pickup in low carbon steels can amount to 5-10 ppm and this value increases

up to 20 ppm after two reblows[42]. Therefore the avoidance of reblows is a pre-requisite to produce steels of low nitrogen content.

2.4 NITROGEN CONTROL IN LADLE

After the end of the oxygen blow in the converter, the most important aim during the various steps is to reduce, as effectively as possible, nitrogen pickup by the hot metal through avoidance of contact with air. The tapping of a rimming steel (aluminium-free tapping) represents an efficient action to restrict this nitrogen pickup. Investigations show that about 5-10 ppm less nitrogen can be achieved by decreasing the aluminium addition at tapping by 1-2 kg/tonne of steel[46]. An aluminium addition is performed at a later stage by high speed injection of aluminium wire. Argon with low nitrogen content must be used for bubbling with a moderate intensity. Under these conditions, the nitrogen pickup at the ladle station can be reduced to an average value of 2 ppm[42]. In the case of calcium injection for desulphurisation, inclusion shape control, etc., or when the stirring intensity is very important, a higher nitrogen pickup is observed[42].

2.5 NITROGEN CONTROL AT CONTINUOUS CASTER

The main reason for nitrogen pickup during continuous casting is insufficient protection of the stream between the ladle, the tundish and the mould. On a slab caster, the largest nitrogen pickup generally occurs between ladle and tundish. Casting tubes with nozzles submerged in the tundish are very often efficient in preventing nitrogen pickup[42].

On a billet caster with reduced mould size, stream protection from nitrogen pickup is more difficult. However, a significant reduction in nitrogen pickup has been achieved through the use of a cold tundish with complete stream protection[42]. Good surface insulation of the liquid steel in the cold tundish and the suppression of the mould aluminium wire injection lead to improved nitrogen control in a continuous caster.

2.6 EFFECTS OF NITROGEN IN STEEL

Nitrogen exists in steel in two forms:-

1. In the atomic form as interstitial nitrogen or as unstable and easily dissolved nitrides, e.g. Fe_4N, $Fe_{16}N_2$, is known as the active or free nitrogen in steel.

2. In the form of stable nitrides. In microalloyed steels (e.g. HSLA steels), some or all of the interstitial nitrogen combines with alloying elements (V, Ti or Al) and forms stable nitrides in the steel.

Both forms of nitrogen have a strong influence on the properties of steel.

2.6.1 Effects of Active Nitrogen

2.6.1.1 Solid Solution Strengthening.

Nitrogen increases the hardness and strength of steels in the hot rolled, annealed or cold rolled condition more than any other element[8]. It also increases the strain hardening rate in steels[8]. This strengthening results from the distortion of the iron lattice by interstitial nitrogen atoms and is caused by an increase in frictional

stress opposing the movement of dislocations. Figure 2.7 illustrates the change in yield stress due to solid solution strengthening caused by various interstitial and substitutional elements. Although theoretically both carbon and nitrogen can have a large effect through interstitial solid solution strengthening, their low solubilities in ferrite and high propensity to form carbides and nitrides means that in practice little advantage can be obtained from this effect.

A dependence of yield strength on grain size has long been established. In its basic form it is known as Hall-Petch equation[47]:

$$\sigma_{LY} = \sigma_o + k_y d^{-\frac{1}{2}} \qquad \text{Eqn.2.9}$$

An extension of this equation to:

$$\sigma_{LY} = \sigma_o + k'(\%\ \text{alloy}) + k_y d^{-\frac{1}{2}} \qquad \text{Eqn.2.10}$$

has been used to predict the effect of alloys on the yield strength[48]. Regression equations based on equation 2.10 give coefficients for active nitrogen ranging from 1540[49] to 5560[48] compared with coefficients of around 84 for silicon and 35 for manganese. Therefore the influence of nitrogen on the yield strength is large, and explains in part the reason for boosted nitrogen content in HSLA steels.

The grain boundary coefficient k_y is assumed constant in the above equations. However k_y has also been shown to be dependent on the active nitrogen content[50], see Figure 2.8. The grain boundary segregation of nitrogen and carbon at normal annealing or normalizing cooling rates means that these elements would exert a grain boundary

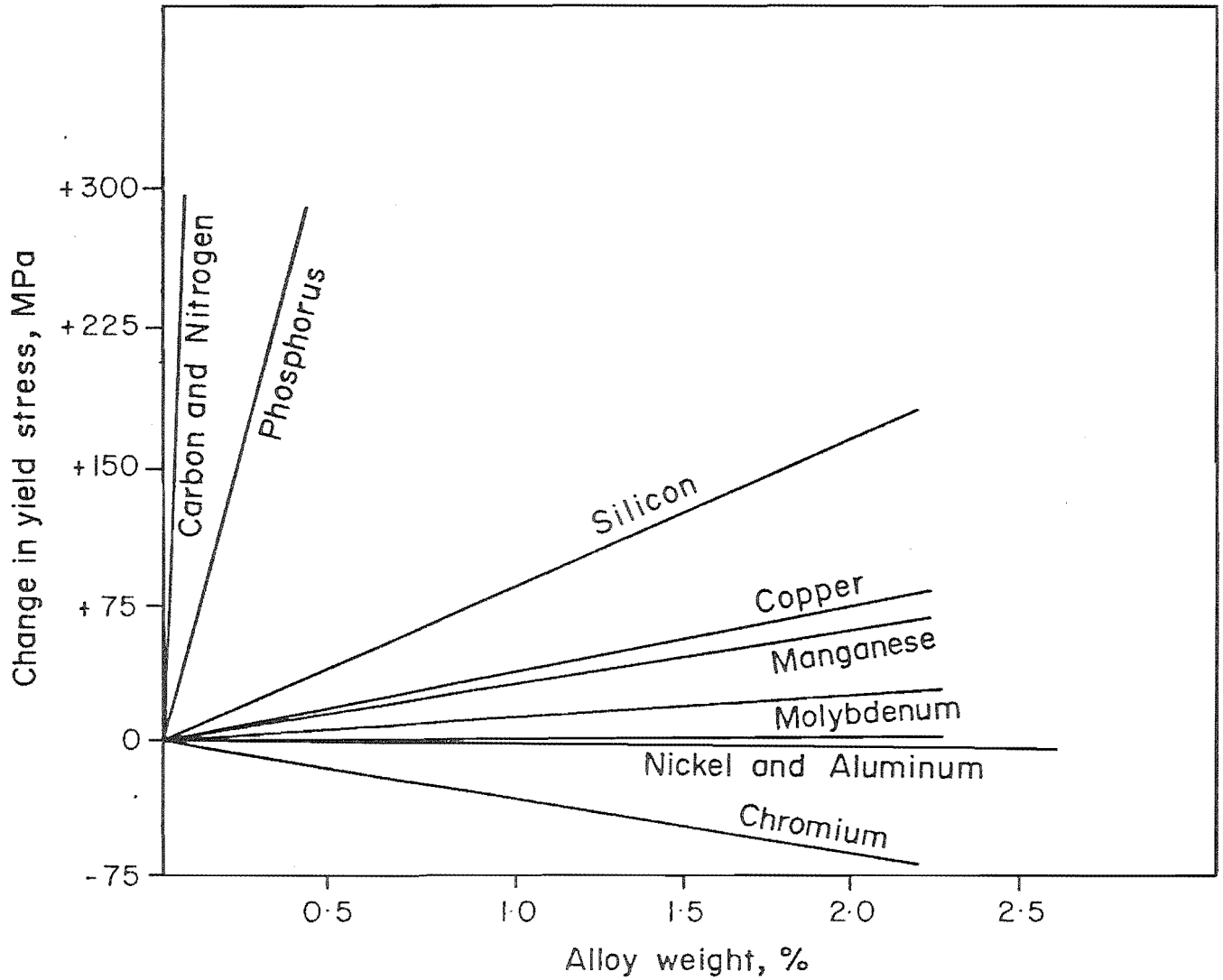

Figure 2.7: Solid solution strengthening effect in low carbon ferritic steels. (Ref. 25.)

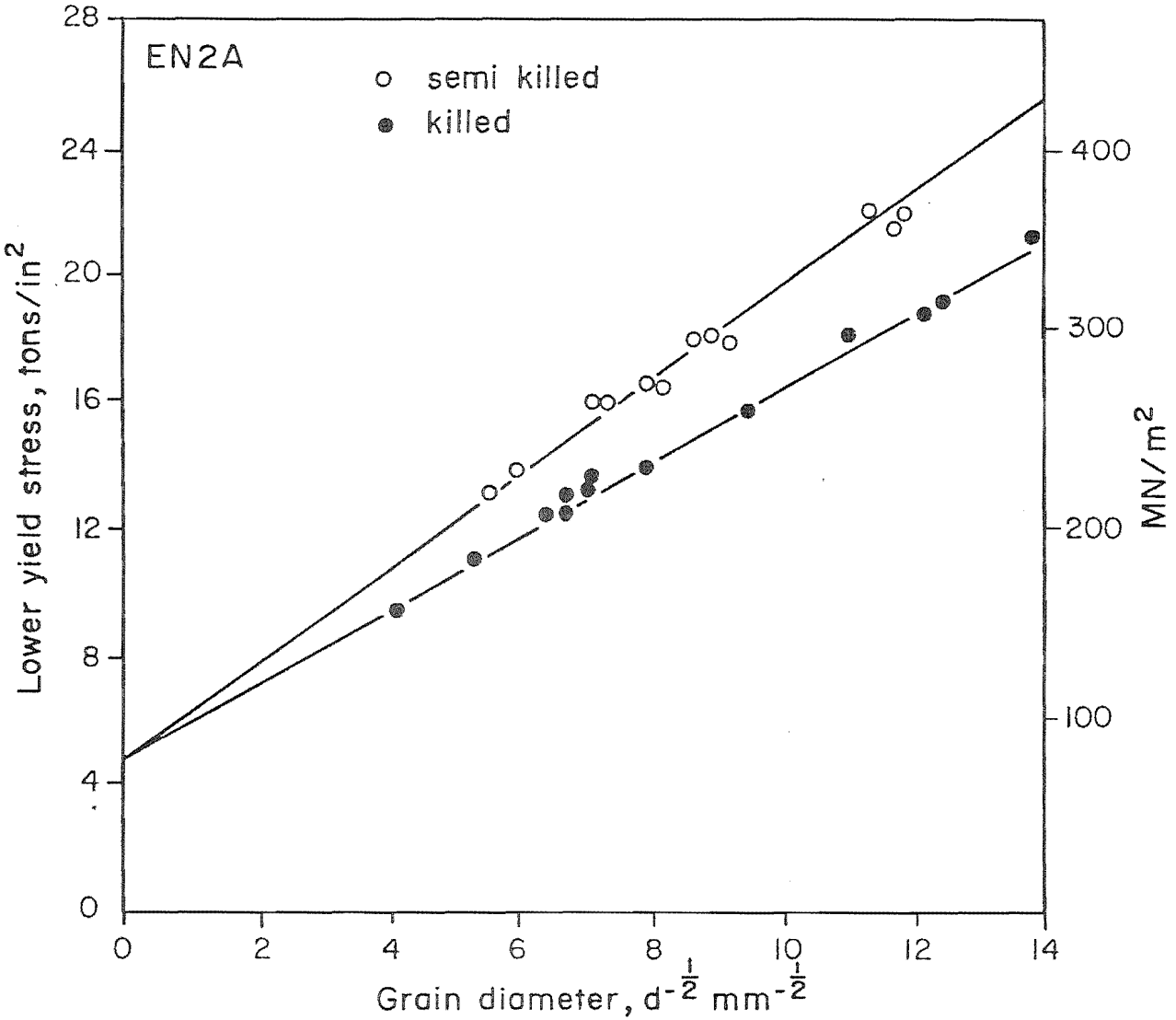

Figure 2.8: Grain size dependence of lower yield stress at 18°C for an aluminium killed and semi killed steels. (Ref.50.)

locking effect and have a strong influence on the grain boundary coefficient k_y. Petch[51] and Codd[52], established that nitrogen locking was stronger than carbon locking and that locking in an annealed semi-killed steel was predominantly due to nitrogen. The iron nitride precipitates Fe_4N and $Fe_{16}N_2$ have a higher solubility than iron carbide. Therefore, the re-solution of these iron nitrides, in the presence of dislocations, takes place more rapidly giving a ready supply of interstitial nitrogen for dislocation locking. Any mechanism where nitrogen is removed or prevented from segregating at grain boundaries would consequently weaken dislocation locking and lower the value of the grain boundary coefficient. Other published data has shown that the grain boundary coefficient k_y to be influenced by nitrogen, manganese and silicon contents[53,54,55], and interaction between these elements suggests that the solution may be more complex than suggested by equation 2.10.

2.6.1.2 The Yield Phenomenon.

Low carbon steels show a defined discontinuous yield point in contrast to many other non-ferrous metals. In these steels the yield phenomena can be characterised by an upper yield point (UYP), lower yield point (LYP) and Lüder's strain (or yield point elongation) whilst in most non-ferrous metals the yield point is generally taken as the stress required to produce 0.2% plastic strain (see Figure 2.9).

At the upper yield point plastic deformation is initiated as a discrete band of plastically deformed metal from some stress concentration and this yielding propagates along the specimen to give

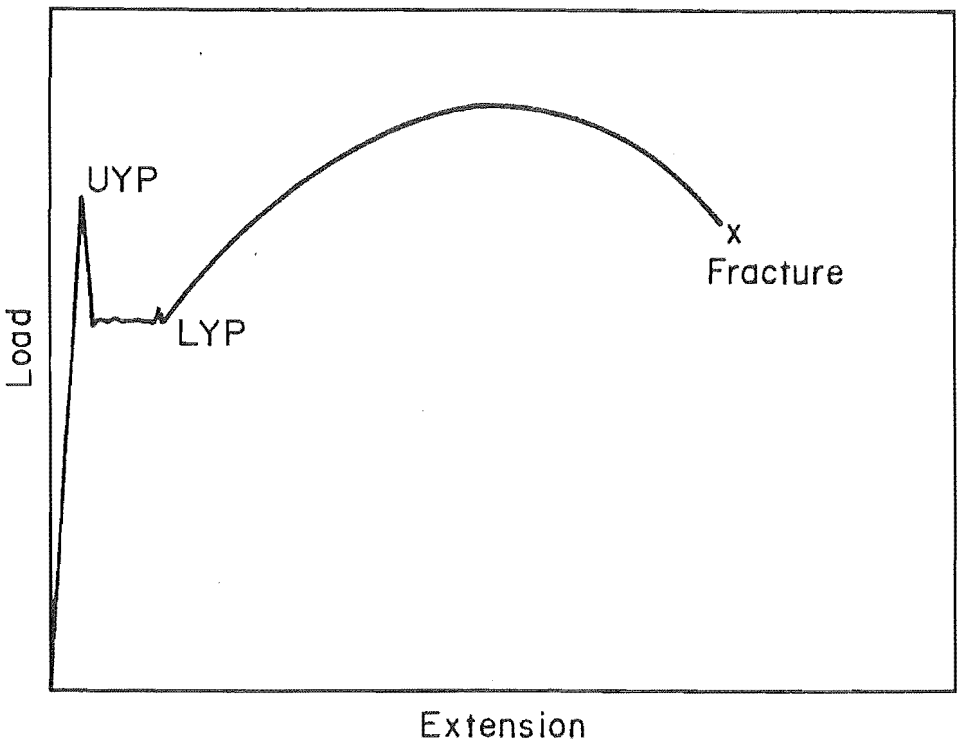

Figure 2.9(a): A typical load-extension curve for a low carbon steel tested in tension.

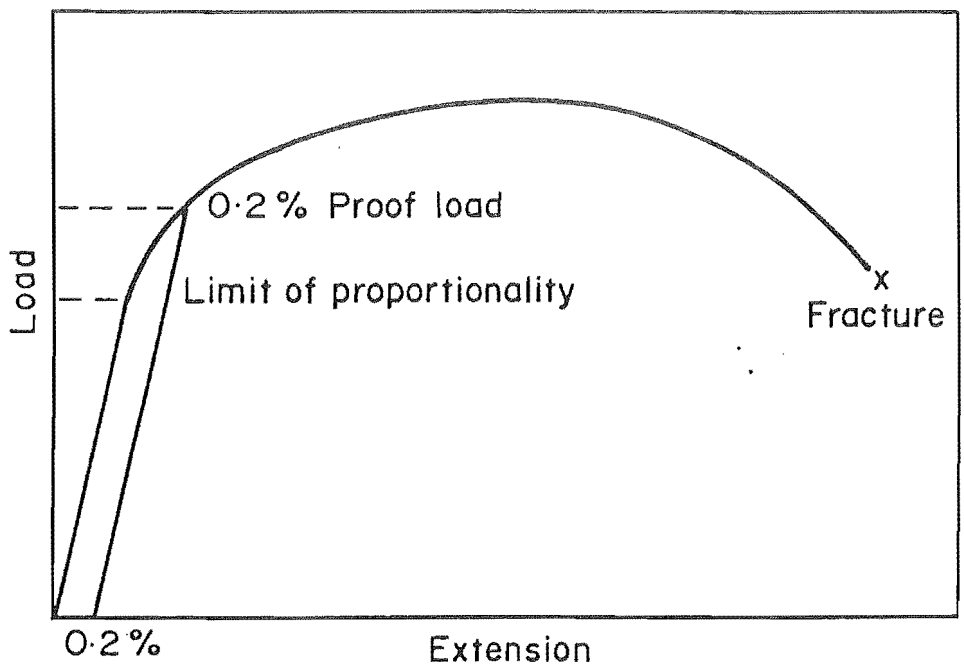

Figure 2.9(b): A typical load-extension for a non-ferrous metal tested in tension.

the full yield point elongation. These discrete bands which are usually at 45° to the loading axis, are known as Lüder bands. Further straining beyond this takes place with increased load due to strain hardening. The yield point is affected by strain rate, specimen surface finish and shape, axiality of loading and machine stiffness[56].

Reasons for the existence of yield point in low carbon steel has generated much debate. One of the early theories was proposed by Cottrell and Billby[57], who suggested that the interstitial atoms in solid solution in ferrite segregate to dislocations, locking them in position. The nitrogen atom is small, comparable in size to the carbon atom. Carbon and nitrogen atoms enter steel as interstitial solute in both the austenite and ferrite lattice. However solubility is limited in both lattice structures since the interstitial sites are appreciably smaller than these interstitial atoms, see Table 2.2. Dislocation sites, where the lattice is already dilated, are consequently attractive sites for interstitial clustering. Only very small quantities of either nitrogen or carbon are necessary to form interstitial atom atmospheres on dislocations.

It was estimated[57] that a concentration of approximately 10^{-6} ωt% nitrogen is sufficient to place one nitrogen atom on each dislocation per atom plane at normal dislocation density of $10^{8}cm^{-2}$ in an annealed ferrite. This would give a binding energy of approximately 0.5 eV per atom plane, which has to be overcome by the applied strain energy assisted by thermal activation for yielding to occur by the unlocking of the dislocation. It was later found[58] using internal friction measurements or electrical resistivity techniques,

TABLE 2.2(a): Longest sphere possible in interstices of FCC and BCC lattice of parent atom diameter = D. (Ref. 8.)

Structure	Largest Insterstitial Diameter	
	Ratio	In Fe(Å)
FCC tetrahedral	0.23D	0.28
octahedral	0.41D	0.51
BCC tetrahedral	0.290	0.36
octahedral	0.150	0.19

TABLE 2.2(b): Atomic size of elements. (Ref. 8.)

Element	Atom Diameter d(Å)	d/D_{Fe}
H	0.92	0.36
O	1.20	0.47
N	1.44	0.57
C	1.54	0.60
B	1.88	0.73
Fe_α	2.56	1.00

that the interstitial atoms per dislocation plane were usually in excess of 10. Therefore, it was suggested that the upper yield point corresponds to the stress which caused the dislocations to break from their "atmospheres" of interstitial atoms and multiply to form the first Luder band.

The above interstitial clusters are known as Cottrell atmospheres, and in most instances they act as a preliminary to the precipitation of carbides and nitrides on dislocations. Both the atmospheres and precipitates effectively pin dislocations, leading to the formation of the discontinuous yield point in annealed steels. With dilute atmospheres pinning may be weak enough to allow dislocations to escape from their atmospheres, but in annealed steels the dislocations are strongly pinned by precipitates of Fe_3C and Fe_4N. For yielding new mobile dislocations must be rapidly generated. The most likely sources of these new dislocations are grain boundaries[59]. However carbon and nitrogen should also rapidly segregate to the ferrite boundaries, and increase the difficulty of nucleating dislocations from the boundary regions.

Hence, it was postulated[59] that it was possible that new dislocations were nucleated from sources in grain boundaries. If yielding was dependent on the generation of new dislocations, which multiplied rapidly under the applied stress, it is possible to assume that the new dislocations can continue to move at a lower stress. This led to the theory by Hahn which analysed the yield point behaviour of iron and related b.c.c. metals[60]. Hahn assumed that most of the original dislocations remained locked by their precipitates, and that the dislocations responsible for slip were

heterogeneously nucleated and multiplied rapidly. The abrupt yield drop was then considered to be a consequence of rapid multiplication of dislocations and the stress dependence of dislocation velocity. The dislocation multiplication theory does not provide a satisfactory explanation for the effect of grain sizes. This is an important omission, because the yield strength of annealed low carbon steels is dominated by the grain size effect in tests at ambient temperature and at normal strain rates.

2.6.1.3 Strain Ageing.

Strain ageing is a yield related phenomenon and caused by nitrogen at temperatures below 150°C and by carbon above this temperature. When a low carbon steel specimen (in annealed, normalized or as-rolled condition) is strained to beyond the yield point elongation, it begins to strain harden and an increased load is required for continued deformation. If the test is arrested at A in Figure 2.10 and the load removed and then reloaded immediately, the specimen will behave elastically until the previously applied load (or flow stress) is reached at A in Figure 2.10. After this, plastic deformation and strain hardening will continue as if the test had not been interrupted at A, i.e. curve (a) in Figure 2.10. In other words, the steel behaves in the same way as any other metal where the dislocations are not pinned.

If a similar test is again interrupted at A in Figure 2.10, but on this occasion the steel is allowed to "age" for a period, the yield point is found to have returned on re-testing, i.e. the dislocations have again become pinned. This yield point returns at a higher stress, B in Figure 2.10, than the flow stress at A of the non-aged

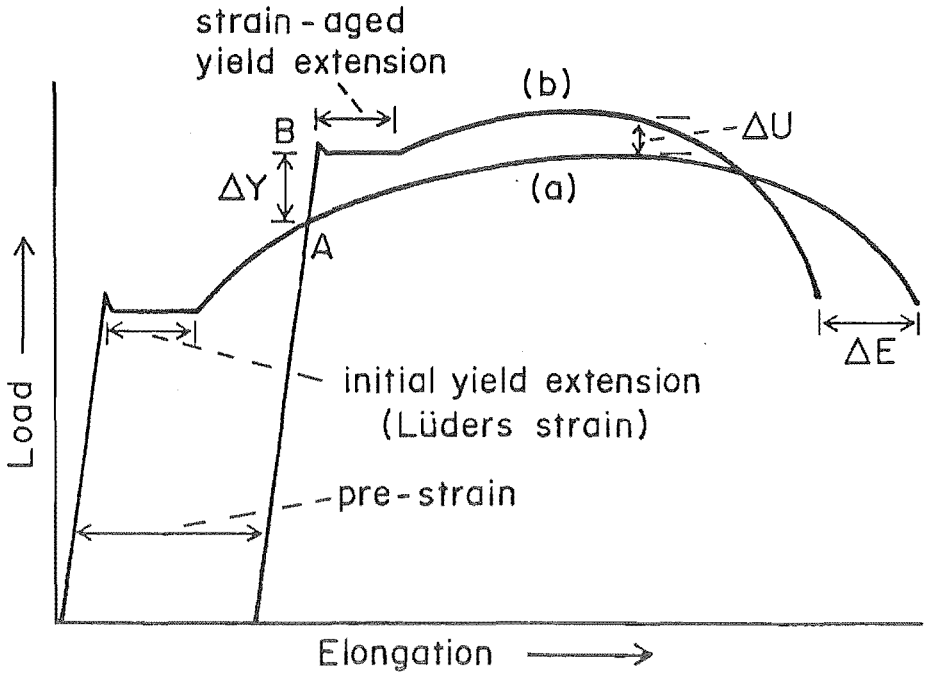

Figure 2.10: Load elongation curve for low carbon structural steel strained to point A, unloaded, and then re-strained immediately (curve a) and after ageing (curve b).

ΔY = change in yield stress due to strain ageing.
ΔU = Change in UTS due to strain ageing.
ΔE = Change in elongation due to strain ageing.
ΔY & ΔU - calculated on original area.

steel, and the steel is said to have strain aged. The return of the yield point after strain ageing is generally accompanied by an increase in tensile strength and a reduction in ductility, curve (b) in Figure 2.10, except where dislocation pinning is by dilute atmospheres and consequently weak. Strain ageing is generally measured by the values ΔY, ΔU and ΔE, as shown in Figure 2.10.

During ageing, the newly formed dislocations resulting from plastic straining or deformation, are locked in position by the segregation of interstitial atoms to these dislocation sites, and hence result in the re-emergence of the discontinuous yield point.

The kinetics of strain ageing have been explained by separating the ageing process into two main stages; mainly 'atmosphere formation' and 'precipitation on dislocations'[61]. During the first stage the interstitial solute atoms are assumed to migrate to the dislocation sites to form "Cottrell atmospheres" around the dislocations. On the earlier interpretation of yielding[57] this should affect only the locking portion of the curve (i.e. UYP, LYP and the Lüder strain) while the strain hardening portion remains unaltered, since on straining beyond the lower yield extension, the atmospheres are dispersed. Hence the tensile strength and elongation at fracture are not affected during this stage (i.e. stage 1 in Figure 2.11). With very low interstitial solute content, only ageing up to this stage takes place and is shown in Figure 2.12.

During the second stage of strain ageing, the interstitial solute atoms continue to segregate to the dislocations causing atmosphere formation to be exceeded so that precipitates form along the

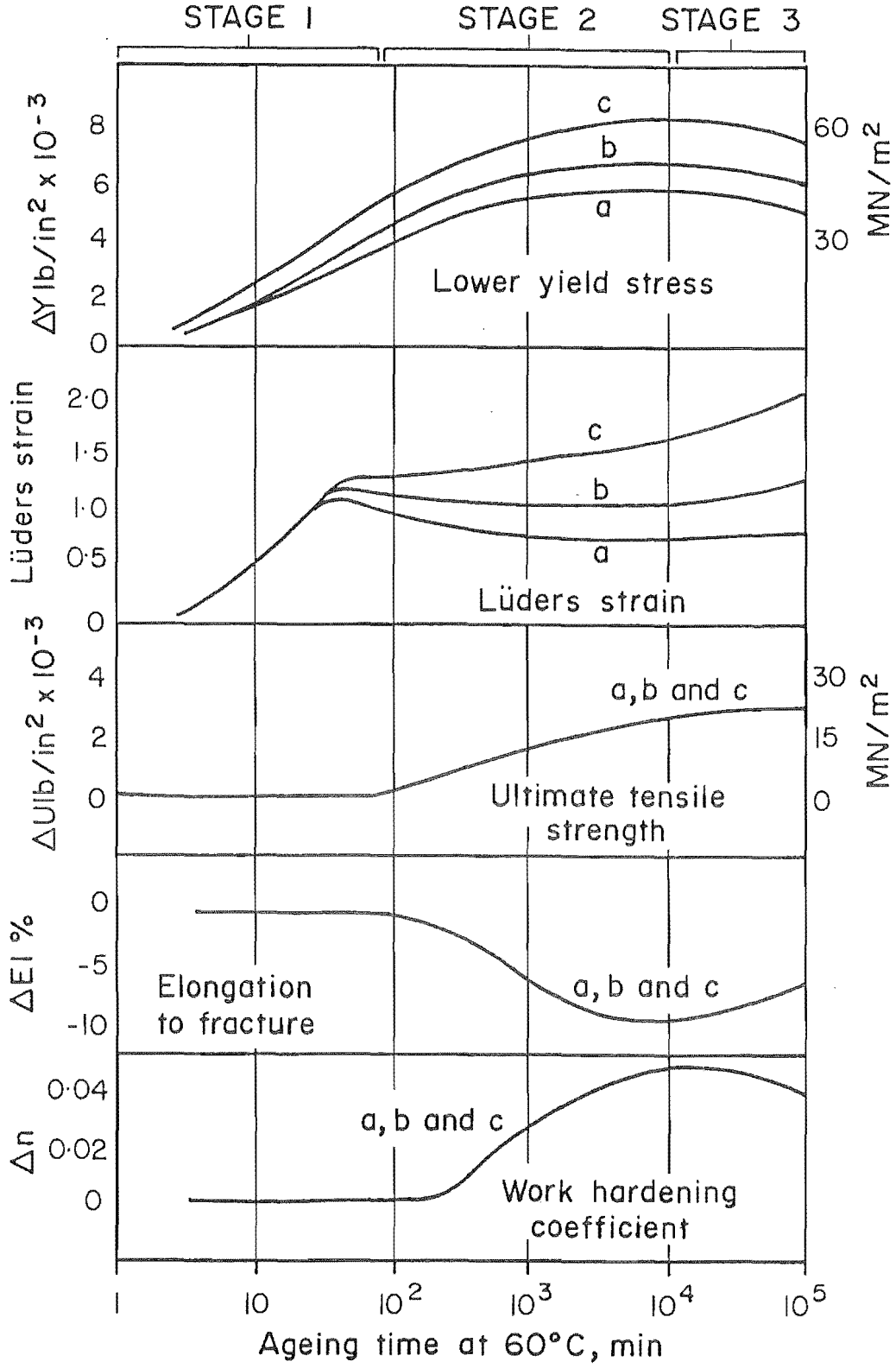

Figure 2.11: Effect of ageing time on changes in tensile properties due to strain ageing (pre-strain 4%) in low carbon rimmed steels having grain sizes (grains/mm²) (a) 50, (b) 195, (c) 1850. (Ref. 62.)

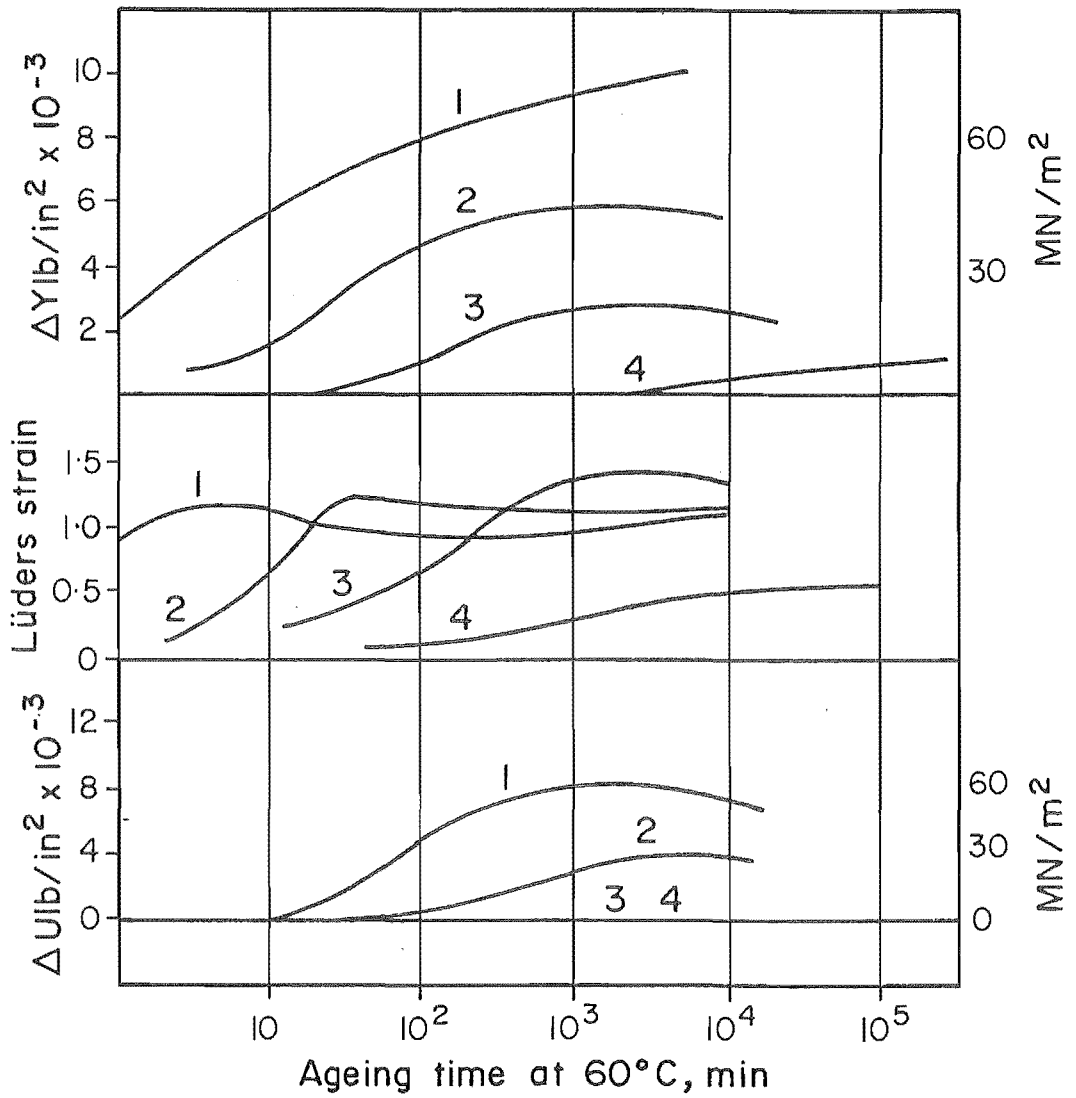

Figure 2.12: Effect of interstitial solute content on changes in tensile properties due to strain ageing (pre-strain 4%) in low carbon rimmed steels. Interstitial solute contents (1) 0.014%, (2) 0.0022%, (3) 0.0005%, (4) <0.0002%. (Ref. 62.)

dislocations. Since the dislocations are fully locked at the end of the first stage, the Lüder strain is little affected during the second stage. However, precipitates formation raises flow stress and the level of curve (b) (Figure 2.10), hence raising the tensile strength. The corresponding increase in the work hardening rate causes a reduction in the elongation at fracture. In most cases this stage of ageing takes place unless the interstitial content is extremely low (see Figure 2.12).

The effectiveness of carbon and nitrogen in producing strain ageing is a function of:

1. their solubilities in ferrite,
2. their diffusion coefficients, and
3. the severity with which each locks dislocations.

The main difference between carbon and nitrogen arises from their widely differing solubilities in ferrite. It is clear from Figure 2.13 that the solubility of nitrogen above 200°C (where rapid precipitation can take place), is higher than that of carbon, which is less than 10^{-4} ωt%. As a result, provided that well dispersed nuclei are present in which carbon atoms can precipitate, the quantity of carbon in interstitial solid solution will be very low below 200°C. However, as a result of its higher solubility, a reasonable proportion of nitrogen atoms may be held in super-saturated solid solution. In support of this, internal friction measurements show that in the absence of cold work precipitation from such super-saturations is very slow[63]. The solubility of nitrogen at room temperature extrapolates to 10^{-4} to 10^{-5} ωt% (Figure 2.13), but it is doubtful if this amount is ever approached, even on very slow cooling. It can be

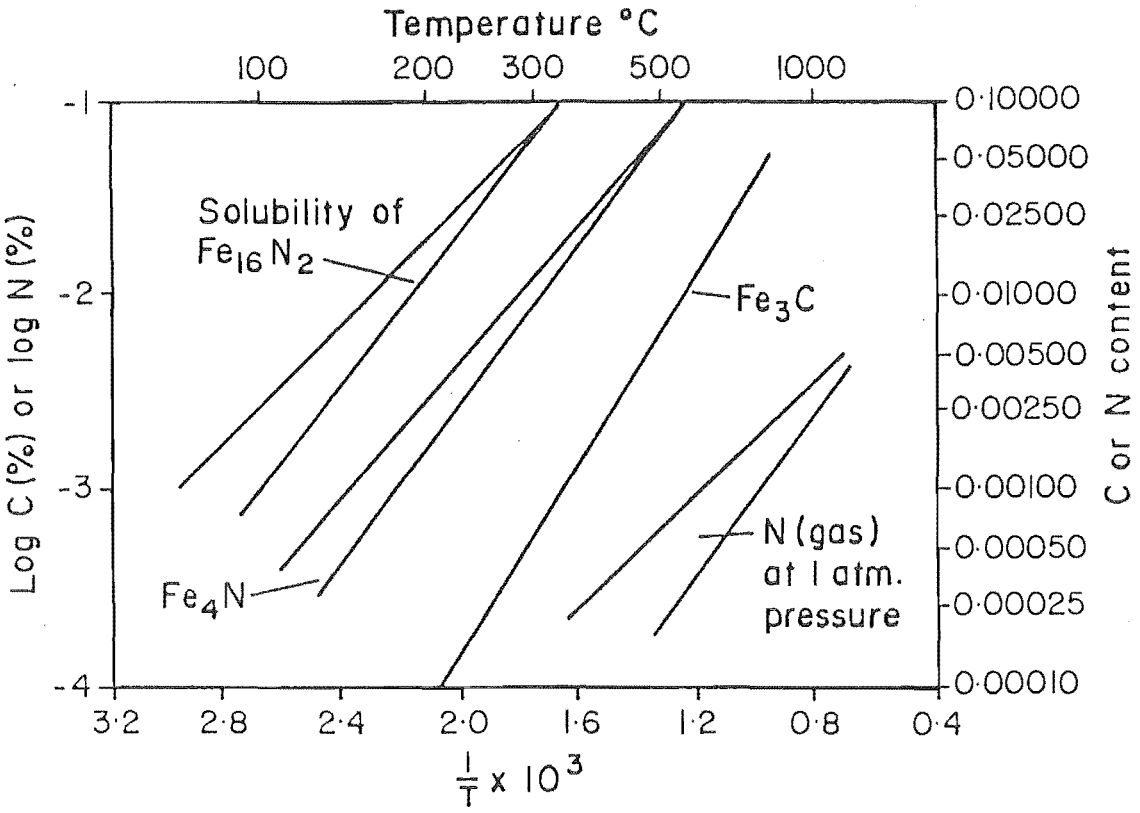

Figure 2.13: Solubilities of nitrogen and carbon in iron. (Ref.61.)

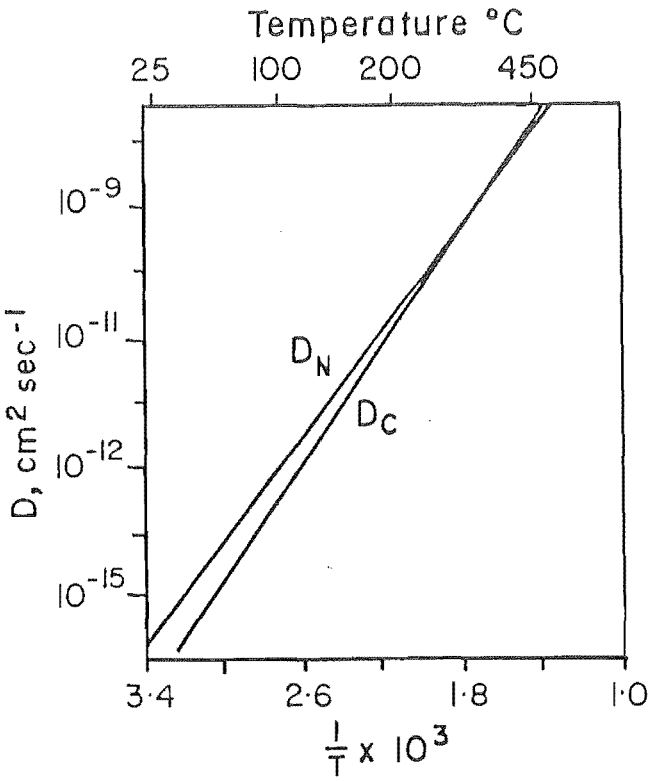

Figure 2.14: Diffusion coefficients of nitrogen (D_N) and carbon (D_C) in α-iron. (Ref. 61.)

deduced[64] that precipitates of Fe_4N and less stable $Fe_{16}N_2$ should dissolve in the presence of dislocations to provide nitrogen atoms for dislocation locking. These observations suggest the effect of nitrogen on strain ageing may not be greatly dependent on the prior heat treatment[65], and hence nitrogen can cause appreciable strain ageing at 100°C or less.

From the solubility data of carbon (Figure 2.13), it may be said that interstitial carbon in solid solution at room temperature in annealed or normalized low carbon steels is insufficient to cause strain ageing. Evidence from internal friction studies[66,67] suggests that re-solution of iron carbide (Fe_3C) precipitates is much less extensive than iron nitride (Fe_4N) precipitates, as may be expected in view of the much greater stability of Fe_3C compared to Fe_4N. Further evidence[68] shows that carbon strain ageing in slowly cooled steels is negligible below 100°C. However, Low and Gensamer[69] have shown that carbon produces strain ageing at 200°C. It has also been shown[70,71] that on strain ageing at temperatures above 100°C, there is evidence of fine iron carbide particles dissolving to produce extensive strain ageing. From these observations it appears that sufficient re-solution of Fe_3C can occur in normalized steels at temperatures of 150°C and above to give strain ageing due to carbon dislocation locking. Strain ageing may also be caused by interstitial carbon below this temperature due to it being held in super-saturated solid solution after rapid cooling from the austenite range[70].

Diffusion coefficients for nitrogen and carbon in ferrite is plotted against reciprocal of absolute temperature in Figure 2.14.

Comparison of the diffusion coefficients shows only negligible difference between the two interstitial elements. Considering the above aspects of carbon and nitrogen in causing strain ageing, it may be concluded that in low carbon steels, ageing below about 150°C almost entirely due to nitrogen, while above 150°C carbon appears to become increasingly effective.

In addition to the change in tensile behaviour shown in Figure 2.10, strain ageing also causes an increase in the fracture mode transition temperature, see Figure 2.15.

Cottrell and Petch[72] have both suggested fracturing laws to explain the transition temperature on a basis of dislocation pile-ups. This development requires that the Griffith equation to be written so that the energy of a dislocation pile-up can be equated to the surface energy of a crack. Using these models it can be shown that cleavage fracture will occur at the yield stress for some reference temperature when:

$$\sigma_y k_y d^{-\frac{1}{2}} \geq \beta G \gamma \qquad \text{Eqn.2.11}$$

Where σ_y is related to grain diameter d by equation 2.9, β is a constant representing the stress state, G is the shear modulus and γ is the energy required to produce a new surface. If in equation 2.11, the LHS is smaller than the RHS, ductile yielding results. If the LHS is greater than the RHS, cleavage fracture results.

Since strain age hardening results in an increase in σ_o (equation 2.9) and k_y attains its original value k_y^o in the fully aged

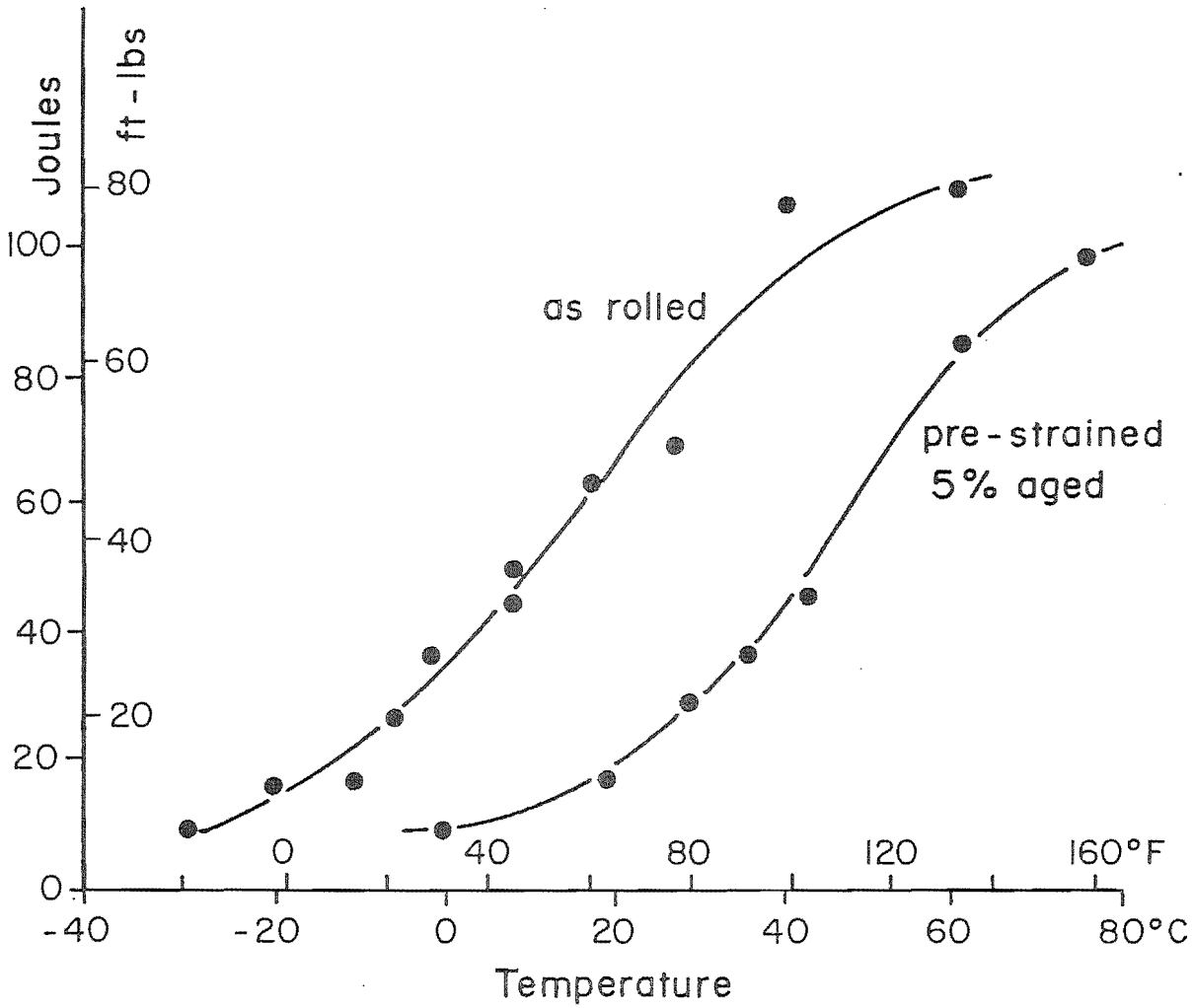

Figure 2.15: Charpy transition curve for low carbon steel in the as rolled and strain aged condition. (Ref.8.)

condition, the LHS of equation 2.11 increases in magnitude and cleavage fracture occurs, i.e. the transition temperature is increased. This is commonly known as "strain age embrittlement".

Ambient temperature strain age embrittlement only occurs when active nitrogen is present in the steel, and this in itself results in a higher transition temperature in the unstrained steel[73]. The increase in transition temperature resulting from prestrain in steels of different active nitrogen content is shown in Figure 2.16. The deleterious effect of nitrogen is then compounded by strain ageing.

2.6.1.4 The Fracture Transition Temperature.

Nitrogen increases the fracture mode transition temperature of steel. The detrimental effect of nitrogen on the fracture mode transition temperature has long been established on a qualitative basis[74]. A few attempts at quantitative analysis have been made, and the increases in transition temperature (°C) for 1% increase in nitrogen variously given as 2750[53] and 8700[4]. However, it has been shown that nitrogen interacts with manganese, and that this interaction has to be taken into consideration when attempting a quantitative analysis of the effect of nitrogen on the fracture mode transition temperature. The combined effect of manganese and nitrogen are given by the following emperical equation[73]:-

$$\Delta T_{27}(°C) = 28\ (\%\ Mn) - 140{,}000(F') + 3850\ (\%\ N) + Const. \qquad \text{Eqn.2.12}$$

where

$$F' = \frac{(\%\ Mn)(\%\ N)}{(\%\ Mn) + 1500(\%\ N)} \qquad \text{Eqn.2.13}$$

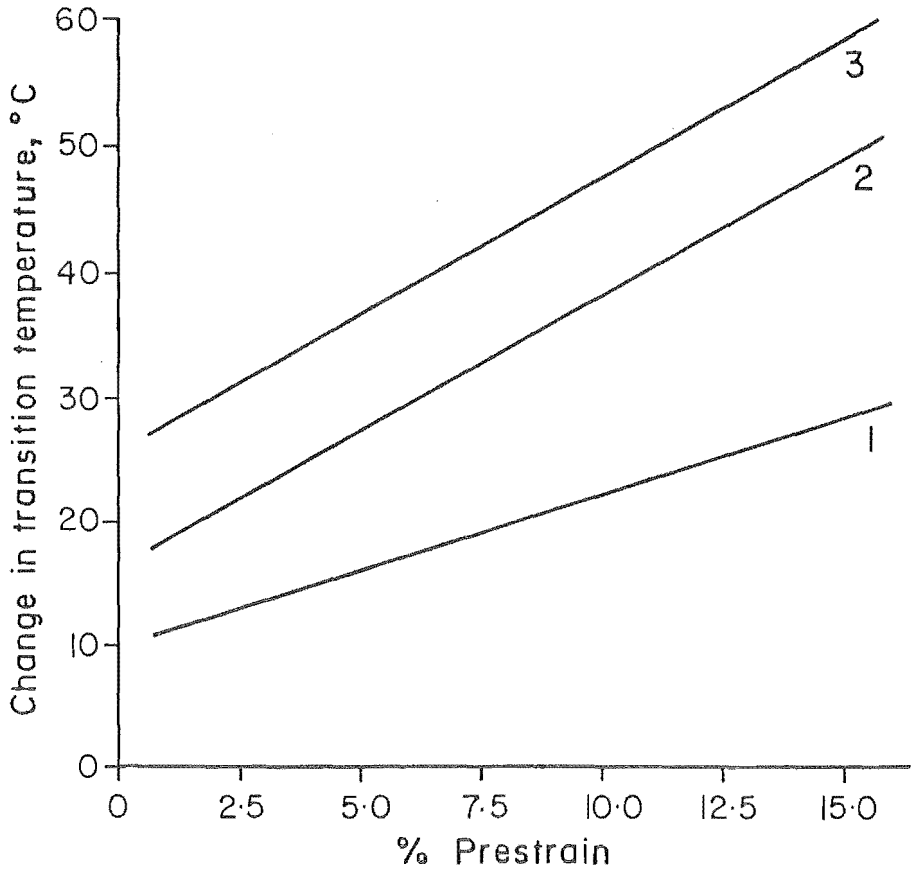

Figure 2.16: The effect of prestrain on the Charpy 27 joule transition temperature.
1. Unaged steel and steels containing greater than stoichiometric titanium
2. 0.0051% nitrogen steel aged at 100°C for 3 hours or 18°C for 1 year.
3. 0.012% nitrogen steel aged at 100°C for 3 hours or 18°C for 1 year.
(Ref. 8.)

ΔT_{27} is the change in Charpy 27 Joule energy transition temperature, and N is the "active" nitrogen content.

The change in transition temperature resulting from manganese for a range of nitrogen contents is shown in Figure 2.17, from where it can be seen that the transition temperature increases almost linearly with manganese content for steels of low nitrogen content (<0.0001%). However, for high nitrogen content steels (~0.01%) the transition temperature decreases almost linearly with manganese content. With zero manganese, nitrogen increases the transition temperature by 3850°C per one percent increase in nitrogen.

2.6.2 Effects of Nitrogen Combined as Nitrides

Ambient and low temperature (< 150°C) strain ageing can be eliminated, and the fracture mode transition temperature lowered, by reducing the active nitrogen content. The interstitial nitrogen (active nitrogen) content can be reduced or rendered inactive by the following methods:

1. By vacuum degassing of molten steel prior to casting to lower the nitrogen content. However this reduction is limited to about 20% for most tonnage commercial plant with maximum chamber vacuums of 0.5 torr[75].

2. By annealing the steel in dry hydrogen[76].

3. By retarding the rate of cooling from the austenite range. This may reduce the interstitial nitrogen content due to the possibility of attaining equilibrium solubility. A more effective method is by quench ageing in the region of

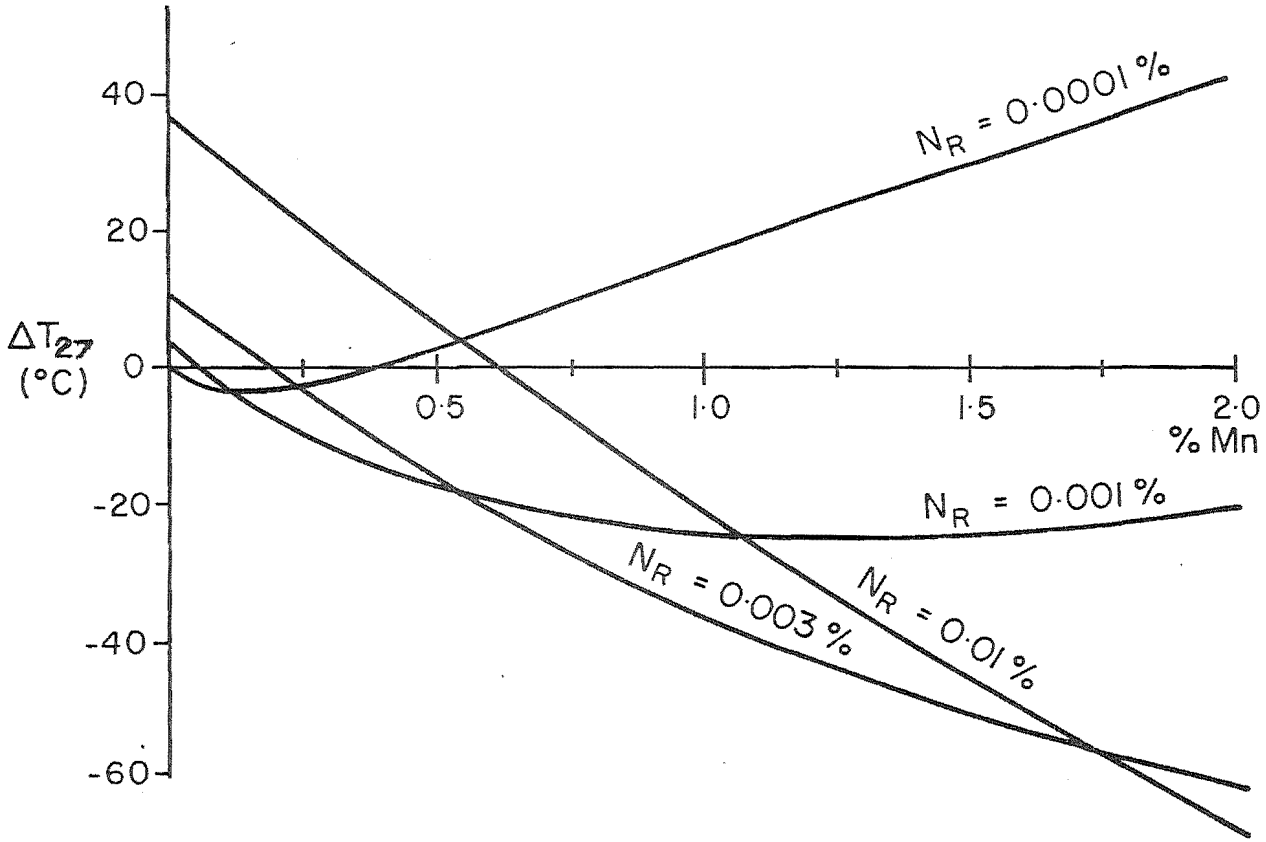

Figure 2.17: Changes in Charpy 27 joule transition temperature with manganese content as given by equation 2.12.

100-200°C[77], i.e. by rapid cooling from the austenite range to 100-200°C and holding at that temperature to attain equilibrium solubility. But the nitrogen precipitates Fe_4N and $Fe_{16}N_2$, formed by this treatment, could re-dissolve in the presence of dislocations to again become effective in locking them.

4. The precipitation of 'active' nitrogen in an inactive form by the addition of strong nitride forming elements in the steel.

5. By lowering the ageing temperature well below the ambient temperature, hence retarding the diffusion of interstitial nitrogen.

6. By the addition of alloying elements which interact with nitrogen atoms and hence restrict its mobility in the steel. These elements generally do not produce stable precipitates. Manganese and silicon belong to this category and are present in reasonable amounts in HSLA steels.

When comparing these methods, a more effective reduction in interstitial nitrogen content can be obtained by microalloying the steel with strong nitride forming elements such as titanium, aluminium or vanadium.

Titanium forms a very stable nitride which appears to be virtually insoluble in austenite at temperatures up to 1350°C[4]. The solubility curves for vanadium and aluminium in commercial grade low carbon steel are shown in Figure 2.18, from whence it can be seen that aluminium nitride is considerably more stable than vanadium nitride.

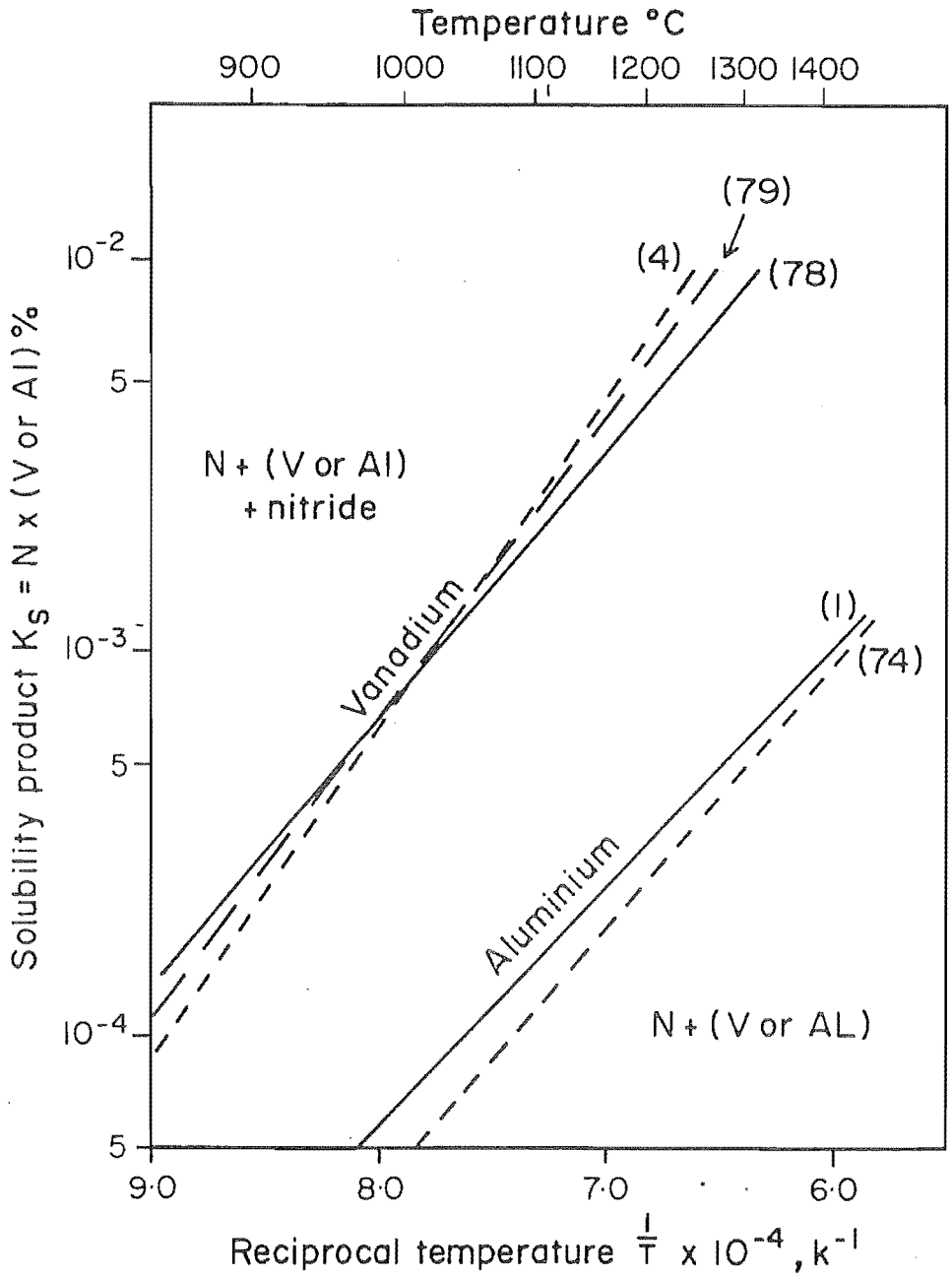

Figure 2.18: Solubility limits for vanadium and aluminium nitrides in commercial grade low carbon steel. (Ref. 1,4,74,78,79.)

However both nitrides will dissolve in austenite if the temperature is high enough relative to the solubility product.

The precipitation of aluminium nitride on cooling from above the solution temperature is sluggish and appreciable active nitrogen may exist in steels even where the aluminium content exceeds stoichiometric amount[80]. In steels containing both vanadium and aluminium, it is not unusual for only vanadium nitride to precipitate on cooling from high solution temperatures, but on reheating to lower temperatures an exchange of some nitrogen from vanadium nitride to aluminium nitride occurs[82].

The precipitation of stable nitrides reduces the active nitrogen content with a consequential lowering of fracture mode transition temperature and elimination of strain ageing. However, the reduction in grain size brought about by these precipitates has further very beneficial effects, viz. an increase in yield strength, and a further decrease in the fracture mode transition temperature. Also the nitride precipitate increases the yield strength and fracture mode transition temperature through precipitation strengthening.

2.6.2.1 Grain Refinement.

In high strength, low alloy steel grain refinement is accomplished by the addition of microalloying elements such as niobium, vanadium, titanium or aluminium. Nitrogen combines with these microalloying elements and forms stable nitrides in the steel. These nitride precipitates may pin the grain boundaries or act as nuclei for new grains during phase transformation, thus refines ferrite grain size. The effectiveness of nitride precipitates on grain refinement

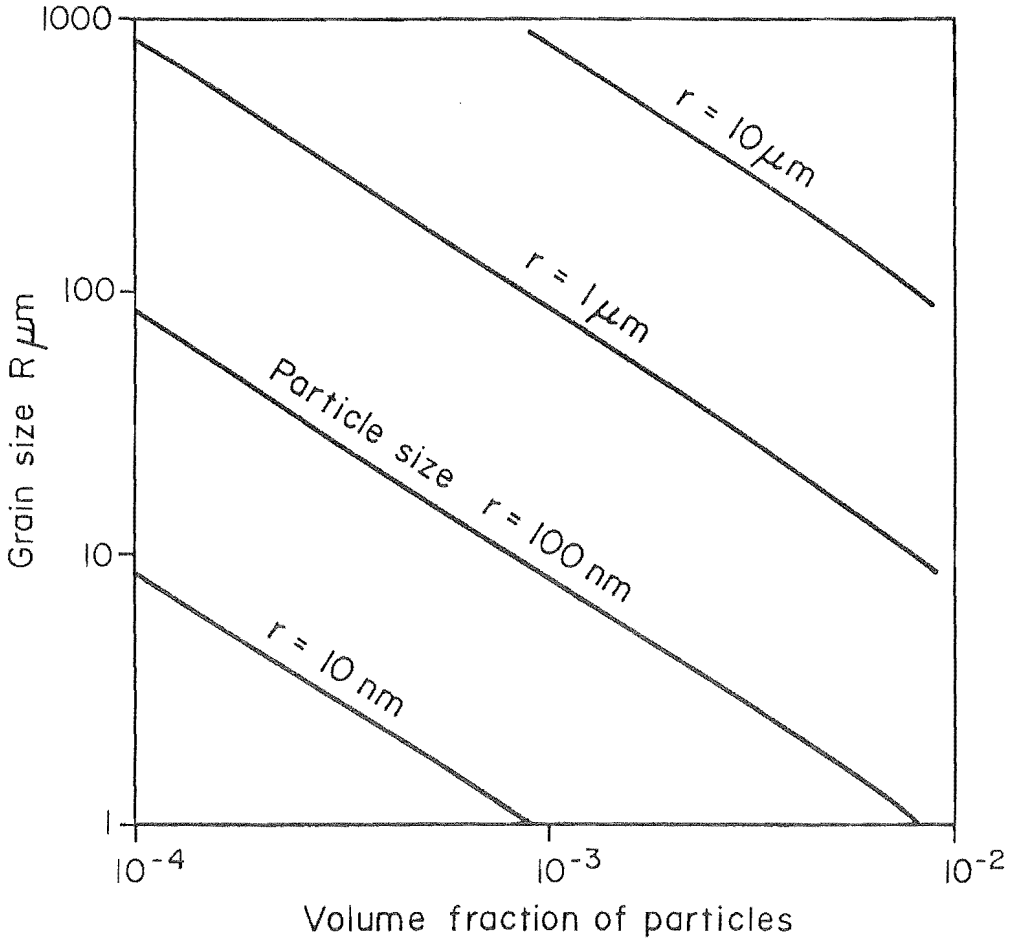

Figure 2.19: Relationship between refined grain size and volume fraction and particle size. (Ref.83.)

is dependent on the precipitate size and volume fraction of the precipitate. This is illustrated in Figure 2.19, where for a given volume fraction of fine precipitates the resultant grain size is finer than that for coarse precipitates. Although effective grain refinement could be achieved by the use of increased volume fractions of coarser precipitates, this practice is not generally carried out in high strength low alloy steels for economic considerations[84].

The grain refinement effect on the yield stress can be explained by assuming that a dislocation source operates within a crystal causing dislocations to move and eventually pile-up at the grain boundary. The pile-up causes a stress to be generated in the adjacent grain, which, when it reaches a critical value, operates a new source in that grain. In this way, the yielding process is propagated from grain to grain. The grain size determines the distance dislocations have to move from grain boundary pile-ups, and thus the number of dislocations involved. With coarse grain sizes, the pile-ups will contain larger numbers of dislocations which will in turn cause higher stress concentration in neighbouring grains. The shear stress τ_i at the head of a dislocation pile-up is equal to $n\tau$, where n is the number of dislocations involved, and τ is the shear stress on the slip plane. This means that the coarser the grain size, the easier it will be to propagate the yielding process. In practical terms, the finer the grain size, the higher the resulting yield stress and, as a result, in modern steel working much attention is paid to the final ferrite grain size.

The unique feature of grain refinement is that it is the only strengthening mechanism which also increases the toughness, i.e.

refining the grain size lowers the fracture mode transition temperature. Refining the ferrite grain size also increases the flow stress at any given strain during plastic deformation[85], and also the work-hardening rate in ferrite-pearlite steels[85]. In addition, the fracture stress is raised and the total strain at fracture is increased by refining the ferrite grain size[85].

2.6.2.2 Precipitation Strengthening.

Grain refinement is the preferred mode of strengthening in HSLA steels because it also improves toughness, but precipitation strengthening is the next most preferred mechanism. The Ashby-Orowan's precipitation strenghthening model predicts the following relationship[86]:

$$\sigma_D(\text{MPa}) = \frac{5.9\sqrt{f}}{\bar{x}} . \text{Ln} \left(\frac{\bar{x}}{2.5\text{x}10^{-4}}\right) \qquad \text{Eqn. 2.14}$$

where f = precipitate fraction, and is given by,

$$f = n_s . \frac{\pi \bar{x}^2}{4}$$

n_s = the number of precipitates per unit area of slip plane,

$\bar{x}$ = the mean planar-intercept diameter of a precipitate.

Figure 2.20 shows the dependence of precipitation strengthening on precipitate size and fraction according to the Ashby-Orowan model, compared with experimental observations for given microalloying additions. It is clear that the stress increment due to fine precipitates increases with the reduction in precipitate size and the increase in fine precipitate fraction.

This precipitate strengthening model predicts that to exploit the additional source of strength effectively, it is necessary to

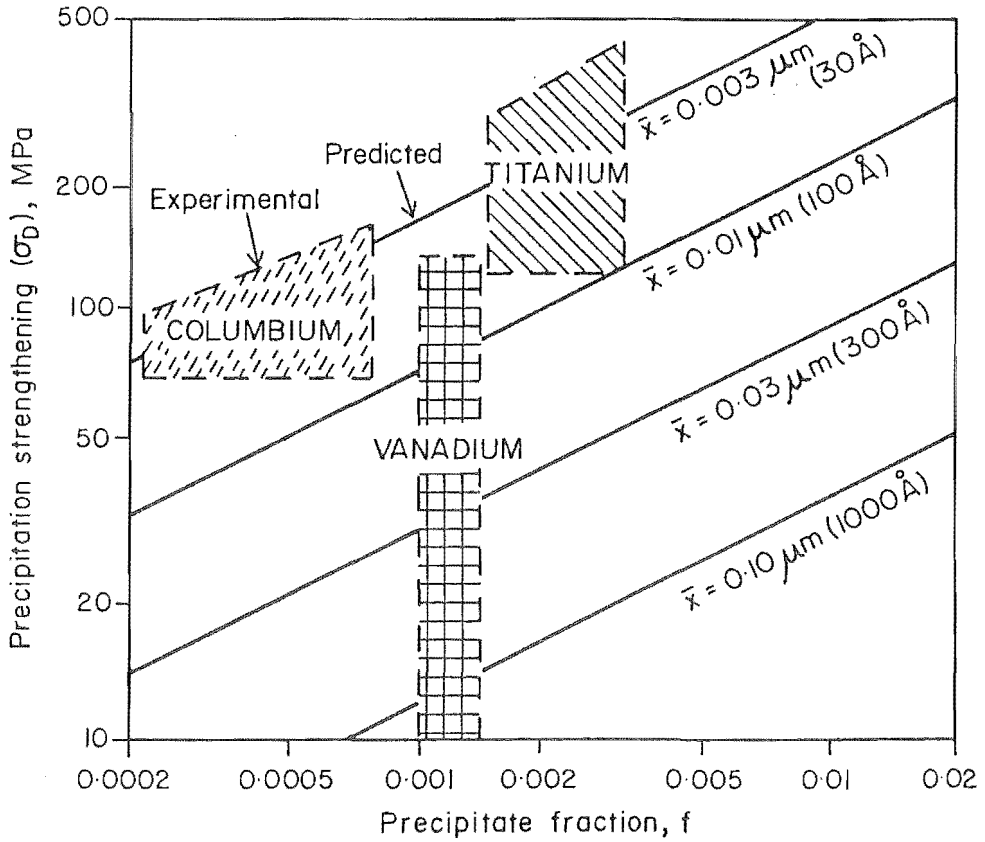

Figure 2.20: The dependence of precipitation strengthening on precipitate size ($\bar{x}$) and fraction according to the Ashby-Orowan model, compared with experimental observations for given microalloying additions. (Ref. 86.)

choose a microalloying addition and processing variables which produce a relatively large fraction of fine nitride or carbide precipitates.

Vanadium additions are widely used in HSLA steels to achieve both ferrite grain refinement and precipitation strengthening, but any precipitation in austenite before its transformation to ferrite will inevitably decrease the amount of subsequent precipitation in the ferrite, and thereby precipitation strengthening. It has been observed[87] (see Figure 2.21) that the addition of 0.011% nitrogen and 0.06% vanadium separately to a 0.10% carbon steel increases the yield strength of 9.6 mm thick carbon-manganese steel plate by 24 and 52 MPa respectively, but that when vanadium and nitrogen are both added to steel the increase in yield strength is greater than the sum of the increase produced by these elements individually[87]. This large increase in yield strength is due to the vanadium nitride precipitation which increases the yield strength through grain refinement and precipitation strengthening.

Nitrogen has many other effects in steel than discussed above. It increases the strain hardening rate in both ferritic and austenitic steels. Generally this is not of great significance except in the case of austenitic stainless steels, where boosted nitrogen contents have been used to increase the proof strength[88,89]. Nitrogen also increases creep strength, but only in the presence of manganese in steel. This improvement has been ascribed to a solid solution hardening mechanism resulting from small clusters of manganese and nitrogen atoms forming obstacles to dislocation movement[90,91]. However, the effect of nitrogen on strain hardening in austenitic steels and creep strength will not be discussed here, since they fall outside the scope

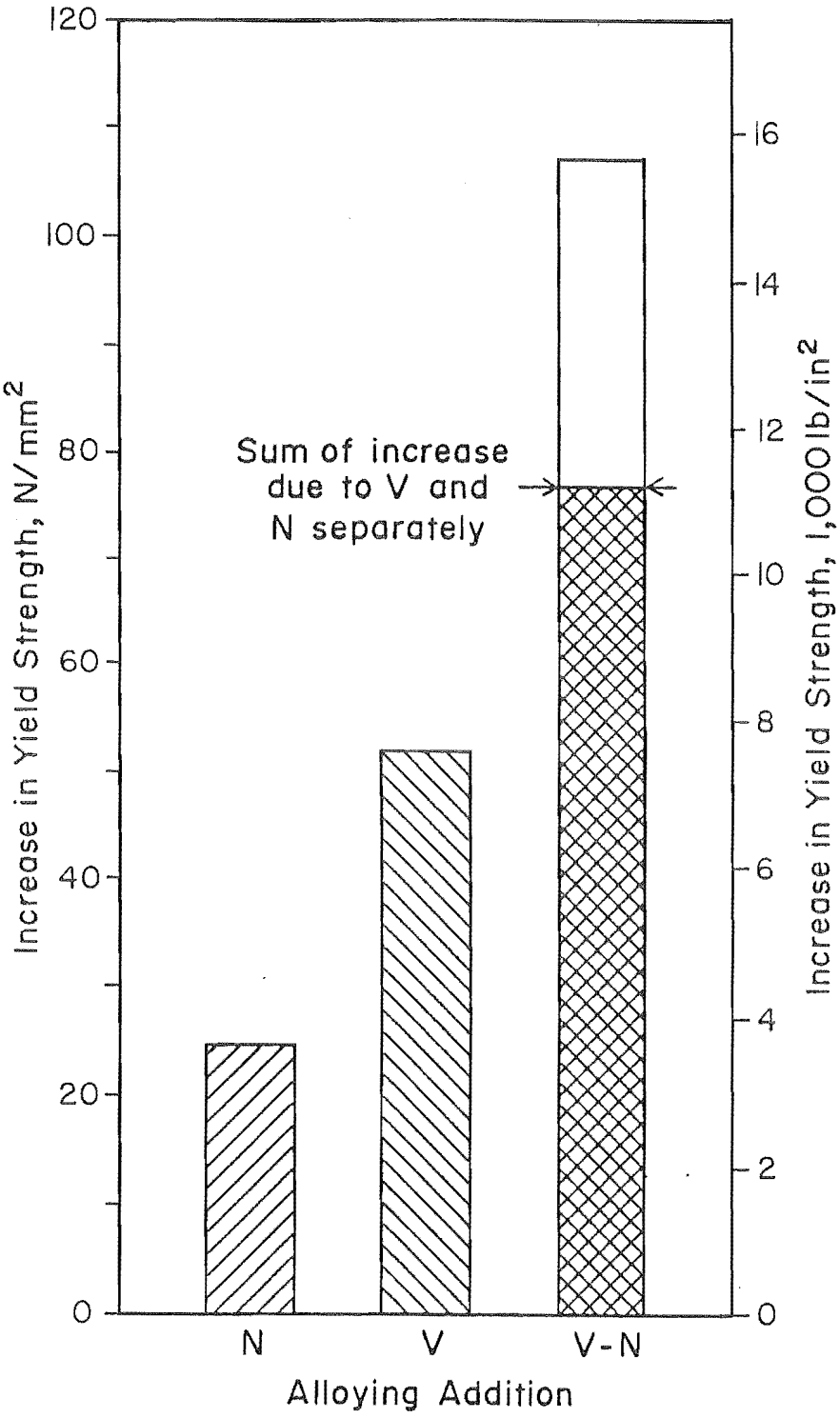

Figure 2.21: Increase in yield strength of as rolled 9.6 mm plates with vanadium and nitrogen addition to carbon-manganese steel. (Ref. 87.)

of HSLA steels. In conclusion, nitrogen can cause some problems in steel, but when combined with microalloying elements which form stable nitrides, a beneficial effect in the properties of steel can result.

CHAPTER 3

VARIATION OF NITROGEN LEVEL DURING STEELMAKING AT NEW ZEALAND STEEL LIMITED

3.1 INTRODUCTION

New Zealand Steel Limited is on the threshold of operating a fully integrated steel plant at Glenbrook, Auckland. The plant processes local raw materials of ironsand and coal into a range of steel products. The new oxygen steelmaking process currently in operation is similar to steelmaking operations at many of the world's most modern steel plants. Previously, the company produced steel by the basic electric arc steelmaking process. The new oxygen steelmaking process began in 1986 with the company's steelmaking expansions which increases the production capacity to 700,000 tonnes per year.

The following investigation was carried out to determine the variation of nitrogen level during the steelmaking process at New Zealand Steel Limited. Iron and steel samples were collected at various points of the steelmaking process for 18 heats. These iron and steel samples were analysed for nitrogen and regression equations were obtained by using the multiple linear regression technique. This chapter reports the results of such an investigation

3.2 STEEL PRODUCTION AT NEW ZEALAND STEEL LIMITED

3.2.1 Ironmaking

New Zealand Steel uses low grade raw materials (titanomagnetic iron sands) which require special ironmaking technology. The ironsand

deposits are mined and concentrated at the Waikato North Head mine site. The iron ore concentrated has an iron content of only 58%, contains a large quantity of gangue oxides (principally titanium dioxide) and has a small particle size of about 120 microns. The small particle size is exploited by using a slurry pipeline to transport the concentrated iron ore to the iron and steel making plants at Glenbrook.

New Zealand Steel currently uses coal from Huntly. These are sub-bituminous coals so they have high moisture contents of 20-25%, high volatile contents of over 40% (dry basis) but fortunately have low ash contents of 3-7%.

The ironsand concentrated and coal are blended in a ratio of about 1.8:1 and fed to vertical multihearth furnaces (MLF). In the multihearth furnace feed is moved across a succession of circular, bricked hearths, countercurrent to the hot waste gases which successively dry and heat the charge. As its temperature rises, the coal releases volatiles and these are burnt by air injected into the gas space above each hearth. This provides the multihearth's entire heat requirement and the product consists of dry concentrate and char at 600°C.

The pre-heated dry concentrate and char mixture is fed to rotary kilns where the reduction of iron ore takes place. The char in the feed provides carbon monoxide, which is both the reducing agent for iron and the energy source for the reduction reaction.

Energy source: $C + O_2 \rightarrow CO_2$

$2CO + O_2 \rightarrow CO_2$

Carbon monoxide production: $C + CO_2 \rightarrow 2CO$

Reduction reaction: $FeO + CO \rightarrow Fe + CO_2$

The kiln product is a mixture of reduced concentrate and char. The gangue oxides are intact because kiln temperatures (1100°C) are not high enough for their reduction. The products of the rotary kilns are continuously fed into two 6 in-line electrode melters each rated at 69 MVA with maximum current of about 90,000 amps. The melter feed enters at about 850°C and molten iron is produced at about 1470°C, with slag at about 1550°C. The heavier pig iron collects at the bottom of the furnace, and consists of iron reduced in the kiln, a small amount of iron which has been reduced during melting, small amounts of Si, Ti and V which are also reduced during melting and 3-4% of dissolved carbon[92]. Batches of pig iron are taken to the steel plant in charging ladles. Prior to steelmaking, the charging ladles are taken to the vanadium recovery unit (VRU). Vanadium is removed from the molten iron by controlled oxygen blowing in the charging ladle using a top lance. This re-oxidises the vanadium, as well as some of the Si, Ti and C and form a vanadium-rich slag on the surface of the metal. This slag is then mechanically skimmed and exported.

3.2.2 Steelmaking

The steelmaking facilities at New Zealand Steel Limited consists of an oxygen steelmaking furnace (KOBM). The KOBM is a combined top and bottom oxygen blown steelmaking vessel, shown in Figure 3.1.

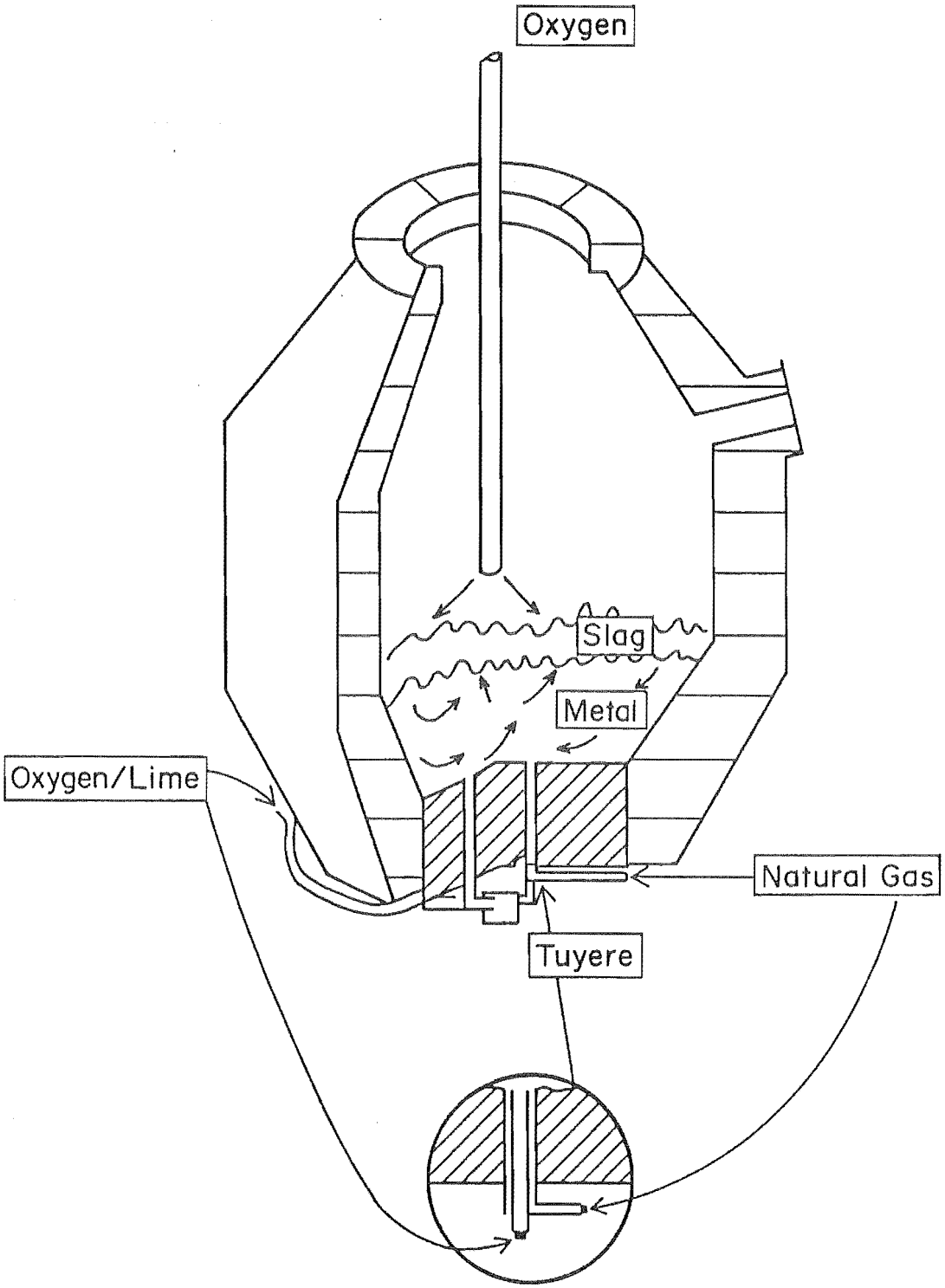

Figure 3.1: KOBM vessel

Oxygen and lime are injected through the centre pipe of each of the six concentric tuyers located at the bottom of the KOBM converter. Natural gas is feed through the outer annulus of the tuyers. This is to keep the tuyers cool as natural gas (mainly methane), cracks endothermally when it enters the molten metal.

The pig iron from the vanadium recovery unit or straight from the melters is charged into the vessel together with scrap (about 10% of the weight of the charged pig iron). Aluminium bars are added if required as a fuel. The whole steelmaking process is computer controlled, which calculates the amounts of fuel (aluminium) required, blow times, etc. based on the pig iron chemical composition, tonnage and the temperature before charging.

The charged hot metal is blown for about 18 minutes. Powdered lime is injected with the oxygen as a refining agent, mainly for desulphurisation and dephosphorisation. Nitrogen is blown through the tuyers when oxygen is not being blown to prevent the hot metal entering into the tuyers. This is done when charging the hot metal into the KOBM and tapping the steel. Before tapping, slag is removed from the KOBM vessel by tilting the vessel and pouring the slag into slag ladles. Once the liquid steel is ready for tapping the KOBM rotates to allow the steel to be poured into a casting ladle. Ladle additions such as ferromanganese, carbon, silicon and microalloy elements are fed into the ladle before the molten steel in the KOBM converter is tapped.

The ladle is then transferred to the ladle treatment station (LTS) where the liquid steel is purged with argon to improve the

homogenity of ladle temperature and composition. The liquid steel is purged with argon until it reaches the required composition and the required minimum temperature for casting. Rice Hull Ash (RHA) is dropped onto the surface of the molten steel for insulation. The ladle is then covered with a lid and transferred to the continuous casting machines (CCM) where the molten steel is teemed into a tundish and continuously cast into either billets or slabs.

3.3 SAMPLE COLLECTION

In order to prevent interruption to the normal production run in the iron and steel plant, samples taken for normal ironmaking and steelmaking processes control were used for nitrogen analysis. The New Zealand Steel process route and the locations where the samples were collected, are shown in Figure 3.2. Samples from each heat selected for examination were taken at the following stages of the iron and steelmaking processes[93]:

1. At melter.
2. At completion of VRU process.
3. At KOBM, just before slag-off.
4. At completion of LTS process.
5. At the CCM.

Altogether samples from 18 heats of steel were collected. Details of process variables such as blowing time, scrap additions, ladle additions, etc. were recorded as in the steel plant log sheet[93].

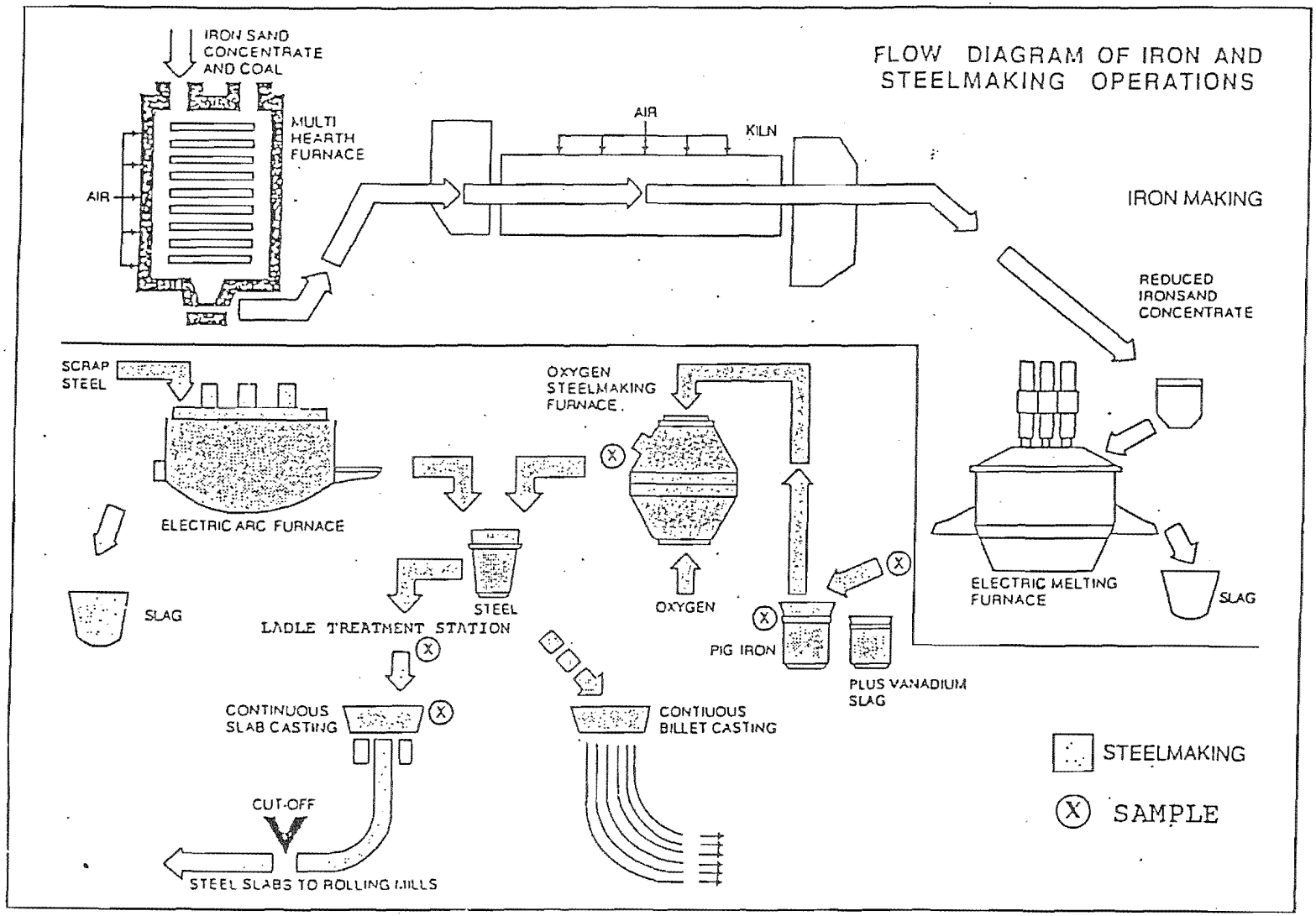

Figure 3.2: Process route and stations where sample collected.

3.4 CHEMICAL ANALYSIS

A detailed composition of each sample was obtained spectrographically from the ARL spectrometer at New Zealand Steel Limited. This data is summarized in Appendix B.

Nitrogen analysis was carried out on each sample from the 18 heats. A wet chemical method was used to determine the nitrogen content. This method[94] is detailed in Appendix A. The resultant nitrogen determination from the samples is given in Appendix B.

The total nitrogen was also determined using a LECO nitrogen analyser in the Technical Services Department of New Zealand Steel Limited. The total nitrogen content as determined by the two methods is compared in Figure 3.3.

3.5 DISCUSSION OF RESULTS

3.5.1 Variation of Nitrogen content during the steelmaking process at New Zealand Steel Limited.

The variation in nitrogen content, as determined by the wet analysis method, during the steelmaking process at New Zealand Steel Limited is shown in Figure 3.4. The variation of nitrogen content of the collected samples for each individual heat and major process additions between individual samples are given in Appendix B. The average nitrogen content at the melter was 0.0027%. This average nitrogen increases to 0.0033% at the VRU, before dropping to 0.0025% at the KOBM at turndown. This drop in nitrogen content may be due to the oxidation of carbon at KOBM. It has been suggested that nitrogen in solution in the liquid steel would be absorbed into gas

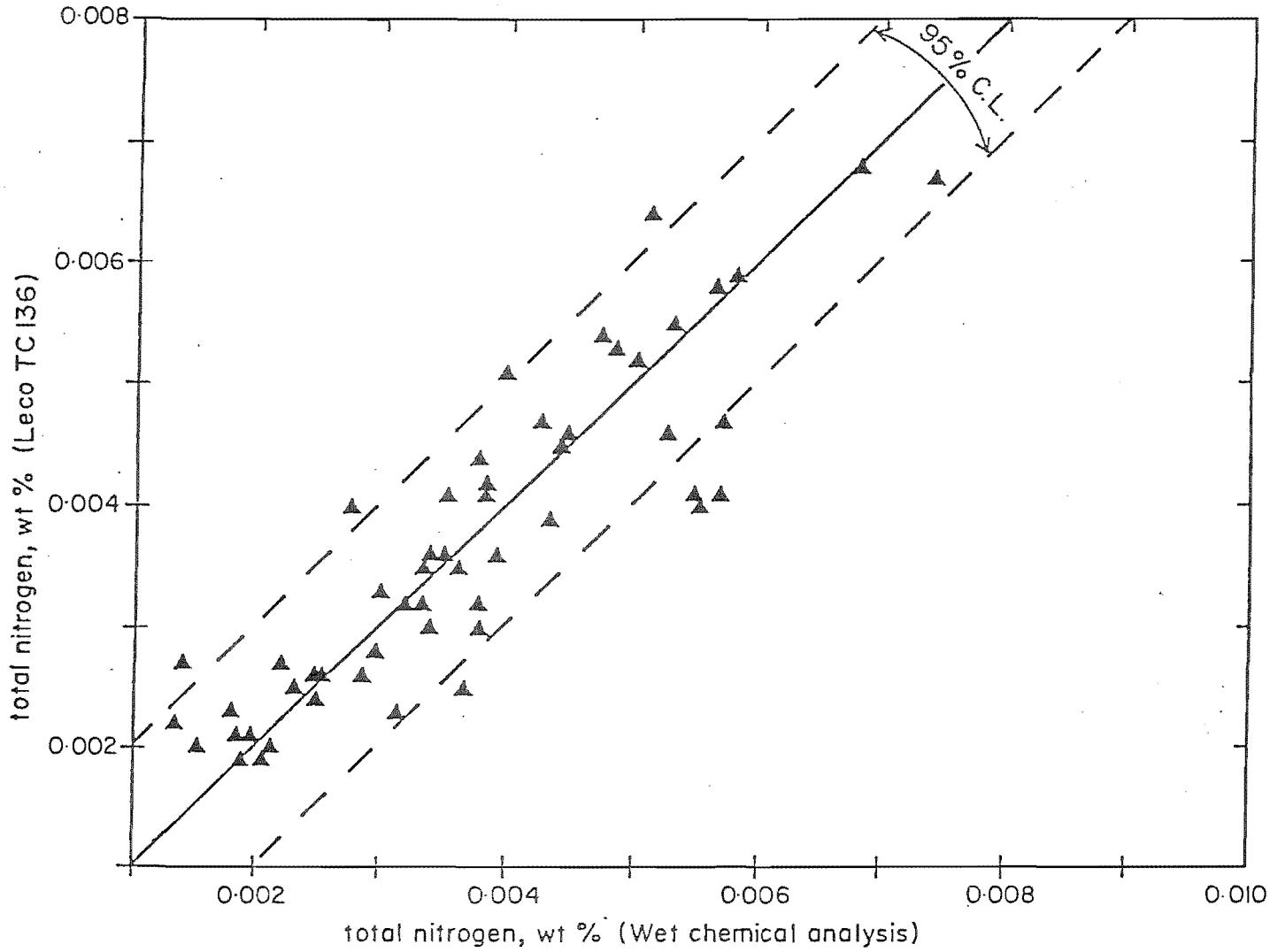

Figure 3.3: Comparison between the nitrogen content determined by LECO nitrogen analyser and wet chemical analysis.

Table 3.1: Summary of nitrogen data

Variable	Mean	St.Dev.	Max.	Min.	Sample Size
N(Melter)	0.0027	0.0006	0.0036	0.0016	18
N(VRU)	0.0033	0.0008	0.0043	0.0019	12
N(KOBM)	0.0026	0.0005	0.0040	0.0019	17
N(LTS)	0.0044	0.0007	0.0059	0.0035	17
N(CCM)	0.0055	0.0009	0.0068	0.0037	18

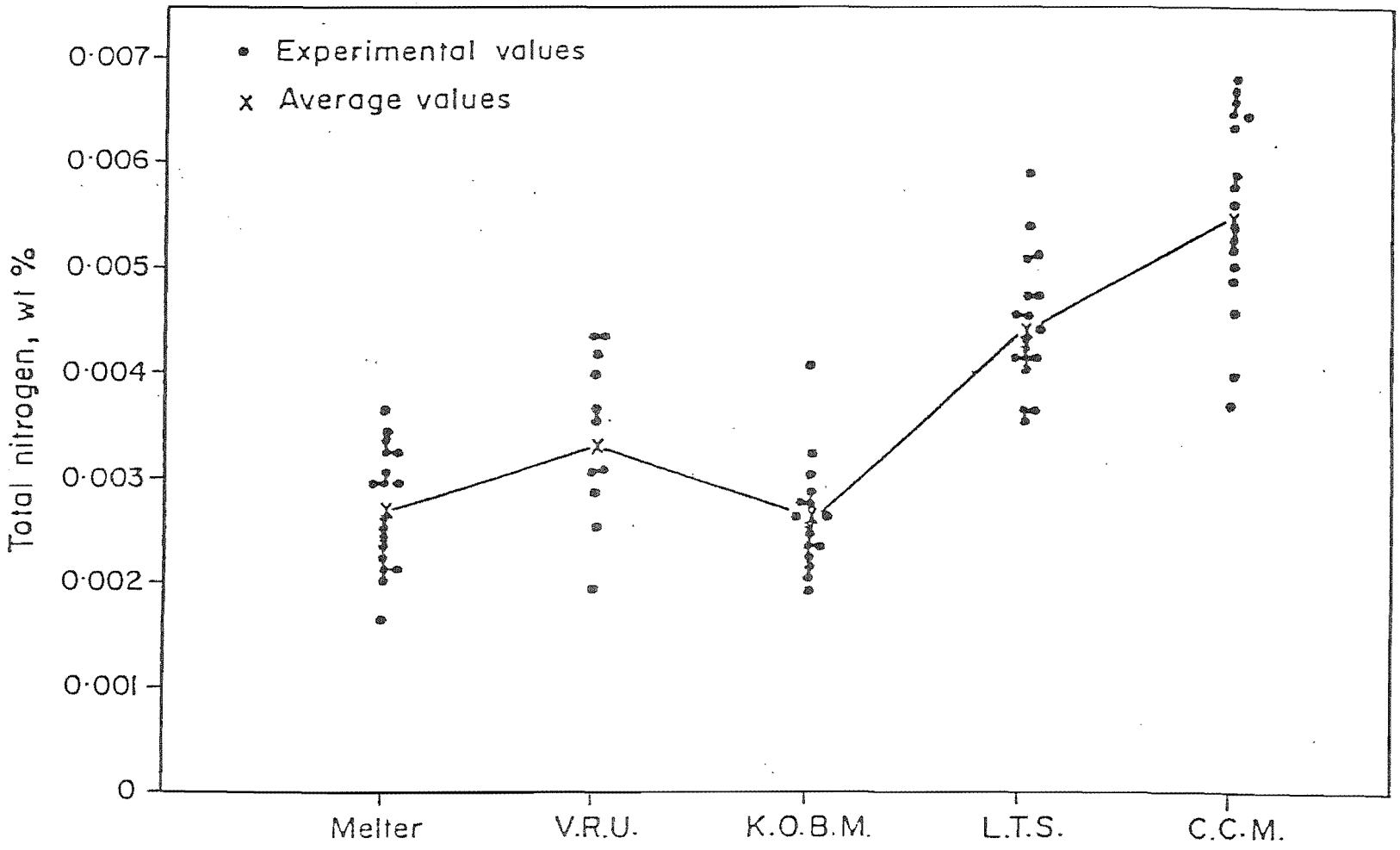

Figure 3.4: Variation in nitrogen content during steelmaking at New Zealand Steel Limited.

bubbles passing through the steel bath giving flushing action[95]. Consequently carbon monoxide bubbles formed during the "carbon boil" during oxygen lancing would effectively reduce the nitrogen content. It has also been suggested that the short residence time of the bubbles in the bath would inhibit equilibrium between the nitrogen in the bubbles and in the steel, and result in a consequential lag in nitrogen removal[96].

There is a significant increase in nitrogen content between the KOBM samples and LTS samples, and again a further increase in nitrogen content of the CCM samples is observed, see Figure 3.4.

These increases at the LTS and CCM probably result from the absorption of nitrogen when the molten stream is exposed to the atmosphere during tapping, transferring the ladle to LTS and teeming at CCM, where there is little protection against the absorption of nitrogen from the atmosphere.

3.5.2 Multiple Linear Regression

This form of analysis assumes that the regression can be referred to in terms of one dependent and several independent variables. The regression formulae are not restricted to variables having a dependent-independent relationship, but merely describe in mathematical terms the nature of the relationship between the variables. However, in evaluating the degree of the relationship, all the error or inaccuracy is assumed to be in the measurements of one of the variables and the other variables are assumed to be precisely known. That is, the imprecision is assumed to be associated with the

dependent variable and the independent variables are assumed to be the precise variables.

In general, a dependent variable Y may be expressed in terms of several independent variables, X_1, X_2, X_3.....as

$$Y = B_0 + B_1X_1 + B_2X_2 + B_3X_3 + \ldots\ldots\ldots \quad \text{Eqn.3.1}$$

where B_1, B_2, B_3.....are the respective regression coefficients.

A detailed description of the multiple linear regression techniques are given by Volk[97] and Williams[98]. All the multiple regression analysis reported here was carried out on an I.B.M. PC using a modified standard program (MLR).

A sample of the computer printout is shown in Table 3.2. From Table 3.2, the equation obtained is:

$$N_{\text{total}} \text{ (Melter)} = 0.0020 - 0.0002(\%C) - 0.0090(\%Si) + 0.0140(\%P) + 0.0066(\%Mn) \quad \text{Eqn.3.2}$$

The significance of the multiple linear regression may be tested by comparing the variance ratio (F value in Table 3.2) with tables of Fisher's F-values [99].

From Fisher's Tables (for 13 degrees of freedom and 4 independent variables)

$$5\% \ , \ F_{4,13} = 3.1791$$

$$2.5\% \ , \ F_{4,13} = 3.9959$$

$$1\% \ , \ F_{4,13} = 5.2053$$

In the example shown in Table 3.2 comparison of the variance ratio

Table 3.2: Computer printout, (Regression No.1, Nitrogen at Melter)

Multiple linear regression analysis of form:

$$Y = Bo + B_1X_1 + B_2X_2 + \ldots\ldots\ldots\ldots$$

Variable No.1 = % C
Variable No.2 = % Si
Variable No.3 = % P
Variable No.4 = % Mn
Variable No.5 = % N_t(Melter) (Dependent variable)

Variable (X)	Mean	Std. Dev.
1	3.0180	0.2200
2	0.2500	0.0750
3	0.0910	0.0121
4	0.3370	0.06100
Dependent (Y)		
5	0.0027	0.0006

Index	B	Std.Error	T-Ratio
0	1.9673E-3	1.5444E-3	1.2738
1	-1.7335E-4	4.6177E-4	-0.3754
2	-9.0419E-3	2.3031E-3	-3.9260
3	1.3967E-2	8.3904E-3	1.8646
4	6.5599E-3	2.8375E-3	2.3119

R^2 = 0.58592 R = 0.76545

Std.Error of Estimate = 4.08181E-4

D.F. = 13

F-value = 4.60

(F-value) with Fisher's F table values shows that the multiple regression is significant at the 2.5% probability level. That is we can say with 97.5% certainty, but not with 99% certainty, that there is a correlation. The right hand column of Table 3.2 (T-ratio) can also be used to determine the significance of any particular regression coefficient. In this example there are 18 sets of data and the computed T-values can be compared with t-test tables for the analysis of variance using (N-k-1) degrees of freedom. From such tables [99] for 13 degrees of freedom:

Significance	t-test value
0.1%	4.221
1%	3.012
2%	2.650
5%	2.160
10%	1.771
20%	1.350

Reference to Table 3.2 shows that carbon content has no significant effect on total nitrogen content at melter. The correlation of Mn with N_{total}(Melter) is significant at the 5% level and P has at the 10% significant level. Among all the independent variables Si has the best correlation with N_{total}(Melter) being significant at the 1% probability level. Carbon could therefore be removed from the multiple regression without much effect on the overall significance of the regression equation.

The multiple correlation coefficient, R and the variance ratio, F, are related by the following equation [97]

$$F = \frac{R^2(N-k-1)}{(1-R^2)k} \qquad \text{Eqn.3.3}$$

where N = number of data sets

K = number of independent variables

The confidence limits for the regression line may be determined about $\bar{Y}$ (mean) as ± t.s, where t is selected at the proper degrees of freedom and for the desired probability level, and s is the standard error of estimate.

In the example shown in Table 3.2, the 95% confidence limits for 13 degrees of freedom is found from the t-test tables

$$t_{0.05,13} = 2.160$$

From Table 3.2 $\bar{Y} = 0.0027$ and $s = 4.0818 \times 10^{-4}$

$\therefore$ 95% confidence limits $= 0.0027 \pm (2.160 \times 4.0818 \times 10^{-4})$

$= 0.0027 \pm 0.0009$

i.e. we can say with 95% confidence that all the value of $\bar{Y}$ will be within ± 0.0009 of the regression line.

One further factor needs brief mention here, that of the "fraction of variance". This usually means the fraction of variance accounted for the correlation and is equal to R^2. This fraction is also sometimes referred to as the "percentage of total variation in the dependent variable explained by the regression equation". From the Table 3.2, $R^2 = 0.586$ for this example regression equation, this means that 58.63% of the total deviation is explained by the regression line.

3.5.3 Nitrogen at Melter

The regression analysis of the 18 sets of data at melter yielded the following equation:-

$$N_{total}(\text{Melter}) = 0.0015 - 0.0089(\%Si) + 0.0139(\%P) + 0.0063(\%Mn) \qquad \text{Eqn.3.4}$$

The above multiple regression is significant at the 1% probability level but not at 0.5% probability level. That is, we can say with 99% certainty, but not with 99.5% certainty, that there is a correlation. The significance of each individual regression coefficient was determined by comparing the calculated t-values with t-test tables and the result is listed below.

Variable	Mean	Std. Deviation	Significant Level
Si	0.2501	7.471×10^{-2}	0.1%
P	0.0912	1.209×10^{-2}	10%
Mn	0.337	6.091×10^{-2}	5%
N_t(Melter)	0.0027	6.0×10^{-4}	1%

The nitrogen content at melter, calculated from equation 3.4 is plotted against the experimentally determined nitrogen in Figure 3.5. Also shown on this figure are lines representing the 95% confidence limits of ± 0.00085%.

As expected[33,34], equation 3.4 shows that increasing silicon content decreases the nitrogen content, while increasing manganese content increases nitrogen content. Phosporus is known[100] to reduce the nitrogen content in steel, but in equation 3.4 the effect is opposite. Since the phosphorus content of the iron is very low and the regression coefficient only significant at the 10% level the

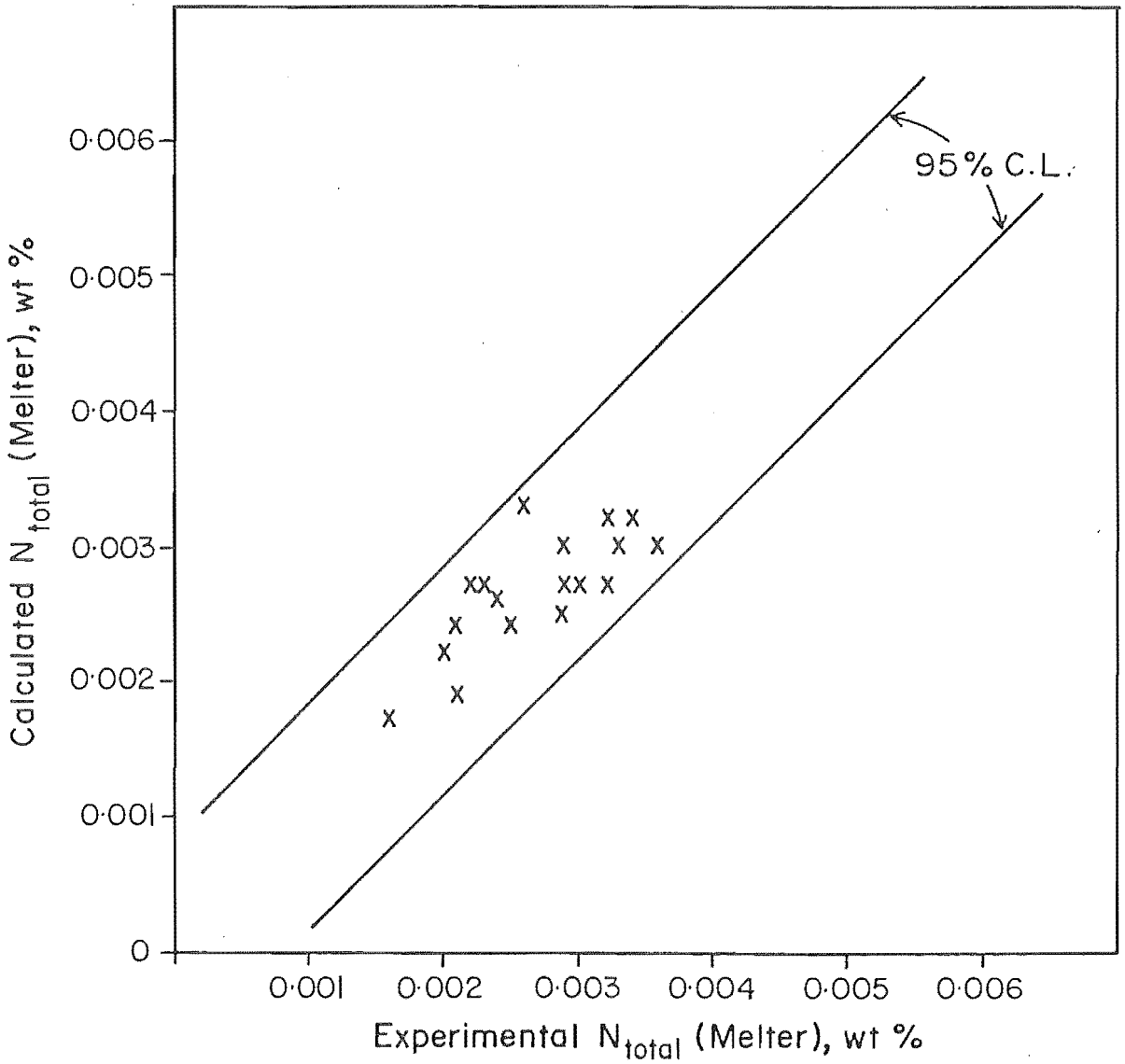

Figure 3.5: Calculated (using eqn.3.4) and observed nitrogen contents at melter

predicted increase in nitrogen content due to phosphorus can be ignored.

Only 76% of the total variation in nitrogen content is explained by equation 3.4 This is due to some unknown variables such as variations in nitrogen content of the feed to the melter, the amount of nitrogen absorbed due to high arc temperature etc. These variables have not been included in this regression analysis.

3.5.4 Nitrogen at VRU

The regression analysis of the data obtained at VRU resulted in the following equation:-

$$N_{total}(VRU) = 0.0005 + 0.9518(\%N_t(Melter)) - 0.0017(\%A\ell) - 0.0048(\%Mn) + 0.0259(\%P) - 0.0004(\%Si) \qquad \text{Eqn.3.5}$$

Equation 3.5 is significant at the 2.5% probability level, i.e. we can say with 97.5% certainty that there is a correlation. The significance of each individual regression coefficient was determined by comparing the calculated t-values with t-test tables and the result is listed below.

Variable	Mean	Standard Deviation	Significant Level
N_t(Melter)	0.0025	6.0126×10^{-4}	1%
Aℓ	5.9167×10^{-3}	3.2602×10^{-3}	5%
Si	0.2923	0.1529	5%
Mn	0.1766	5.8943×10^{-2}	5%
P	9.4666×10^{-2}	8.0149×10^{-3}	5%
N_t(VRU)	0.0033	7.8605×10^{-4}	2.5%

All regression coefficients except N_t(Melter) were significant at the 5% level and this latter variable at the 1% significant level. The correlation coefficient is such that 93% of the total variation in nitrogen content at VRU is explained by the equation 3.5; i.e. only 7% of the variation in nitrogen content at VRU has to be accounted for by unconsidered factors and experimental errors. The inclusion of other factors such as temperature, FeSi added decreased the percentage of the total variation in nitrogen content at VRU explained by equation 3.5 and since these individual variables were all of low significance they were dropped from the equation.

The nitrogen content at VRU, calculated from equation 3.5 is plotted against the experimentally determined nitrogen in Figure 3.6. Also shown on this figure are lines representing the 95% confidence limits of 0.0009%.

As expected[34], equation 3.5 shows that increasing silicon and aluminium contents decrease the nitrogen content. Manganese is known[4,34] to increase the nitrogen content in steel, while phosphorus is known[100] to reduce it, but in equation 3.5 the effect of these elements is opposite. A high correlation coefficient between nitrogen and the melter and nitrogen at VRU in equation 3.5 shows that N_t(Melter) has a major influence on the nitrogen content at VRU.

3.5.5. Nitrogen at KOBM

The regression analysis on KOBM data yielded the following equation:-

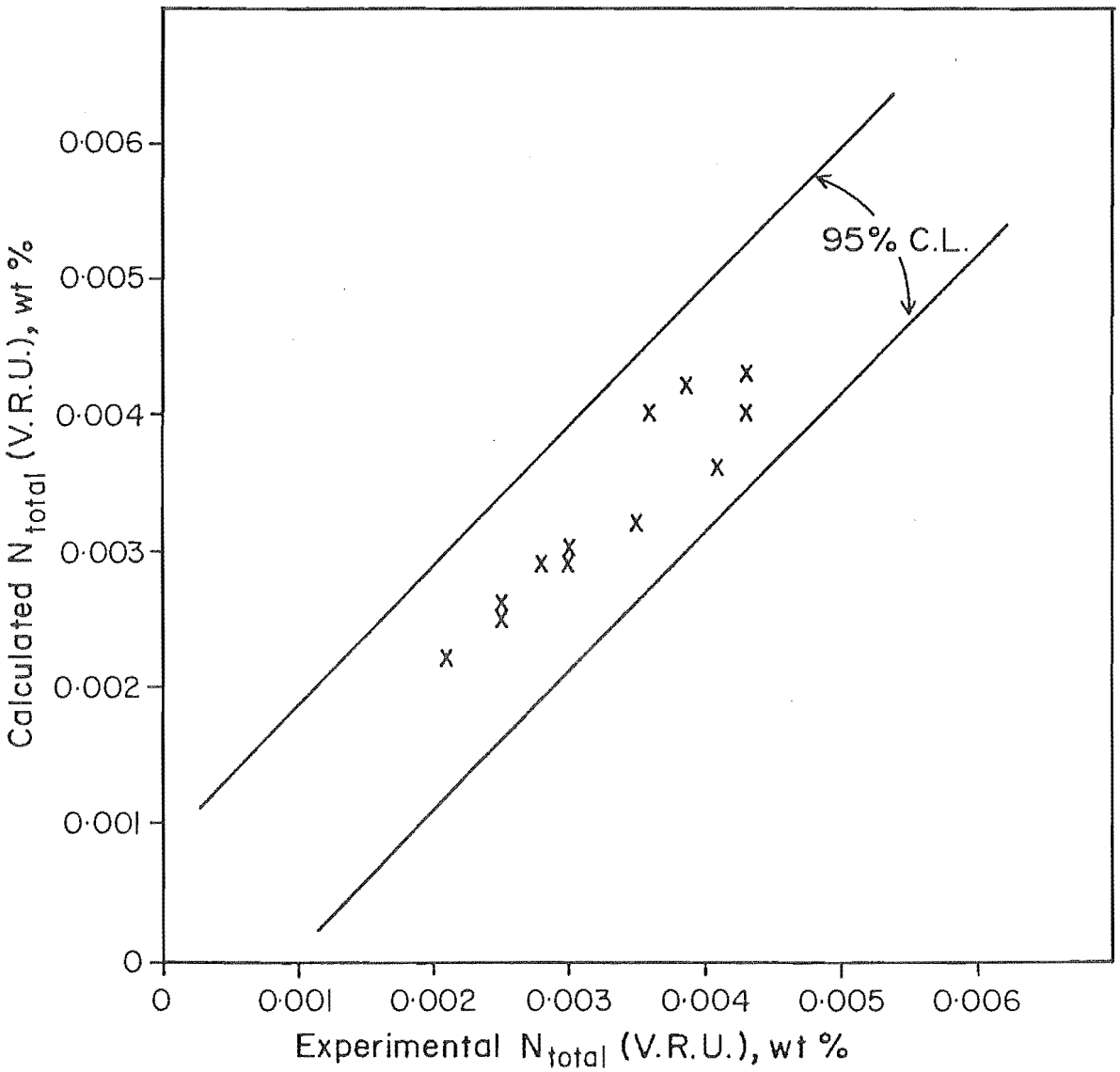

Figure 3.6: Calculated (using eqn.3.5) and observed nitrogen contents at VRU.

$$N_{total}(KOBM) = 0.00006 + 0.00004\ (\text{tonnes of scrap}) - 0.0685(\%C) + 1.1883(\%Ti) + 0.6956(\%Si) - 0.0102(\%Mn) - 0.2231(\%P) + 0.4364(\%V) - 0.00008(\text{kg of Al charged}) \quad \text{Eqn.3.6}$$

The equation 3.6 is significant at the 0.5% level, i.e. such a high degree of correlation will only occur by chance five times in a thousand. The significance of each individual regression coefficient was determined by comparing the calculated t-values with t-test tables and the result is listed below.

Variable	Mean	Standard Deviation	Significant Level
tonnes of scrap	2.646	2.998	10%
C	1.618×10^{-2}	1.0806×10^{-2}	0.5%
Ti	5.117×10^{-3}	4.8506×10^{-4}	1%
Si	4.7060×10^{-4}	1.375×10^{-3}	1%
Mn	0.104	6.89×10^{-2}	1%
P	9.824×10^{-3}	7.796×10^{-3}	0.5%
V	4.353×10^{-3}	3.277×10^{-3}	0.5%
kg of Al charged	18.38	2.335	2%
N_t(KOBM)	0.0026	4.9145×10^{-4}	0.5%

The correlation coefficient is such that 92% of the total variation in nitrogen content at KOBM is explained by the equation 3.6. The nitrogen content at KOBM, calculated from equation 3.6 is plotted against experimental values in Figure 3.7, for the 17 sets of data used in this regression analysis. Also shown on this figure are lines representing the 95% confidence limits of ± 0.00046%.

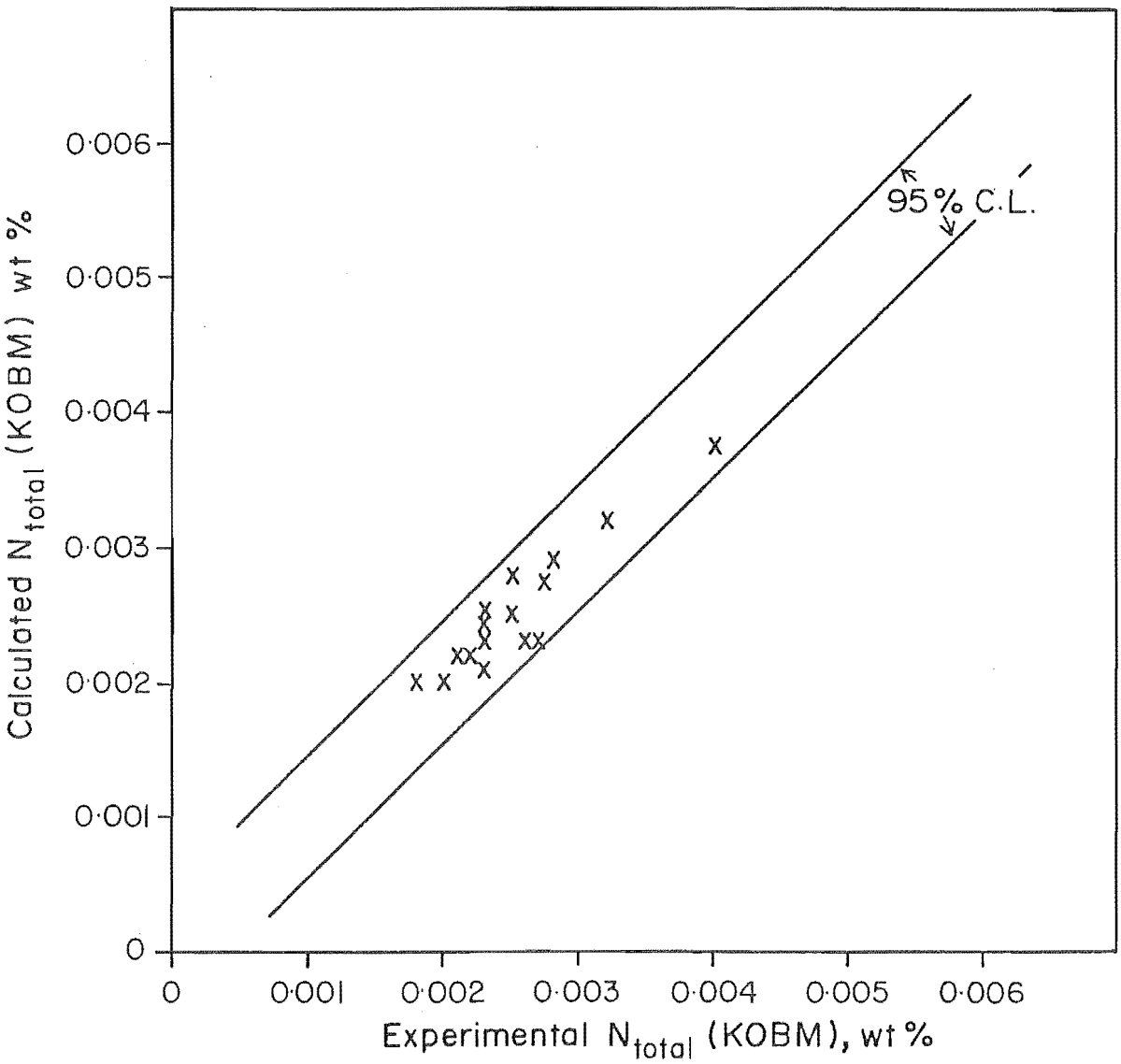

Figure 3.7: Calculated (using eqn.3.6) and observed nitrogen contents at KOBM.

The regression analysis shows that the scrap input increases the nitrogen content in steel. This may be due to the high nitrogen content of the recycled scrap. Figure 3.8 illustrates the influence of scrap additions on the nitrogen content of steel produced by the LD-HC process at COCKERILL-SAMBRE-Montignies[101]. In this case 2-6% of the total oxygen is blown through bottom tuyers, which is similar to the KOBM process at New Zealand Steel. The increase in nitrogen content due to scrap can be controlled by either using low nitrogen scrap or increasing the input hot metal to scrap ratio. The inclusion of other factors such as total carbon loss (ΔC) instead of carbon content, blowing time, lime addition etc. reduced the percentage of the total variation explained by equation 3.6 from 92% to 70% and since these individual factors were all of low significance they were dropped from the equation.

Equation 3.6 suggests that nitrogen content increases with decreasing carbon content. But according to the "carbon boil" theory decreasing carbon content should also decrease the nitrogen content. From the KOBM data (appendix B) it can be seen that average carbon content is decreased from 3% to 0.02% during the oxygen blow. During the first part of the oxygen blow a large proportion of carbon, say from 3% to 0.05%, is removed and nitrogen content consequently also decreases, as is explained by the carbon boil theory. Further carbon removal, say from 0.05 to 0.02%, requires a proportionally larger amount of oxygen to be blown. If the oxygen is contaminated with some nitrogen, then it is conceivable that the steel nitrogen content will again increase as the carbon is reduced from 0.05% to 0.02%, i.e. if it is assumed that 95% of the carbon data lies between

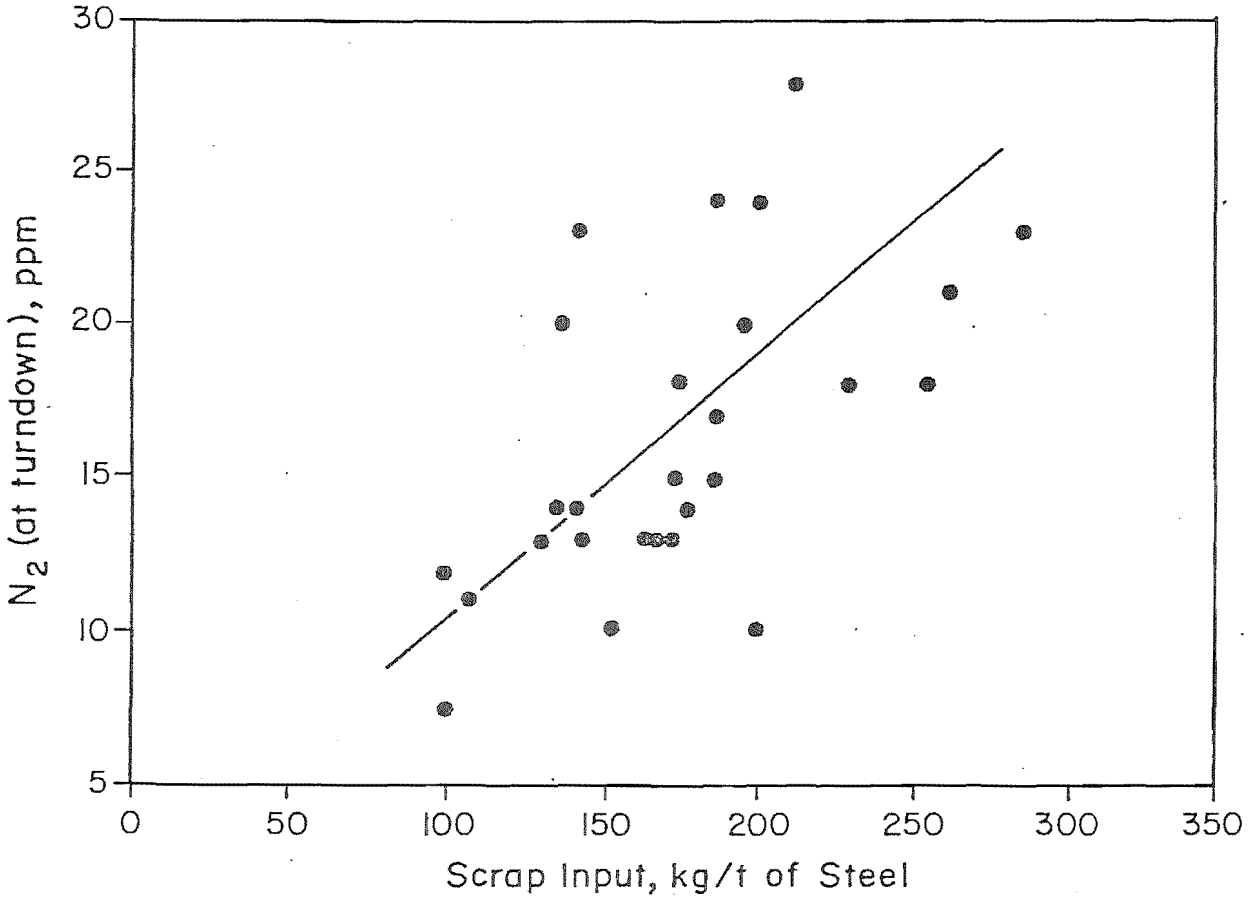

Figure 3.8: Relation between nitogen content at turndown and scrap input (Ref.101.)

the mean ± (1.96 standard deviation), then the examined variation in data lies between 0.038% and zero carbon. The regression coefficient in equation 3.6 shows that the nitrogen content will increase from zero to 0.0027% with the above decrease in carbon content.

Further regression analysis was carried out to study the relationship between ΔC (the total carbon loss between meltout and KOBM turndown) and oxygen lancing time (O_T). A significant correlation was found between the carbon loss (ΔC) and oxygen blown (minutes lancing).

$$\Delta C = 1.334 + 0.0598\ (O_T) \qquad \text{Eqn.3.7}$$

The equation is significant at the 1% level. Another important aspect observed in KOBM data (see Appendix B) is the reblow. It has been observed that reblowing increases the nitrogen content of steel. It has been found that after one reblow, the steel nitrogen pickup on low carbon steel can reach 5-10 ppm and this value increases up to 20 ppm after two reblow[102].

The oxygen purity also is an important factor in the control of nitrogen content of steel[41]. A reduction in nitrogen level at turndown can be obtained through the improvement of the oxygen quality. It has been observed that an increase of 100 ppm of the nitrogen content in the oxygen resulted in an increase of 1.5 ppm of the steel nitrogen level[42]. The purity of blowing oxygen is thus an important factor to control on a regular basis.

As expected [100,34], equation 3.6 shows that increasing titanium and vanadium content increases the nitrogen content, while

increasing phosphorus content reduces the nitrogen content. Silicon is known[34] to reduce the nitrogen content in steel, while manganese is known[34] to increase it, but in equation 3.6 the effect of these elements is opposite.

3.5.6 Nitrogen at LTS

The regression analysis on the data obtained at Ladle Treatment Station (LTS) resulted in the following equation

$$N_{total}(LTS) = 0.0068 + 0.00001(°C,\Delta T) + 0.0036(\%Mn) - 0.0478(\%A\ell) - 0.1985\ (\%V) \qquad \text{Eqn.3.8}$$

where; ΔT is the drop in temperature due to purging.

Equation 3.8 is significant at the 2.5% level, i.e. we can say with 97.5% certainty that there is a correlation. The significance of each individual regression coefficient was determined by comparing the calculated t-values with t-test tables and the result is listed below.

Variable	Mean	Standard Deviation	Significant Level
ΔT	56.35	16.53	10%
Mn	0.3826	0.2156	2%
Aℓ	5.52×10^{-2}	9.15×10^{-3}	2%
V	9.11×10^{-3}	4.15×10^{-3}	2%
N_t(LTS)	0.0044	6.55×10^{-4}	2.5%

All regression coefficients except ΔT were significant at the 2% level and this latter variable at the 10% significant level. The correlation coefficient is such that only 77% of the total variation in nitrogen content at LTS is explained by the equation. An attempt was made to improve this by including other factors such as lime addition, carbon addition, purging time etc. However, these new

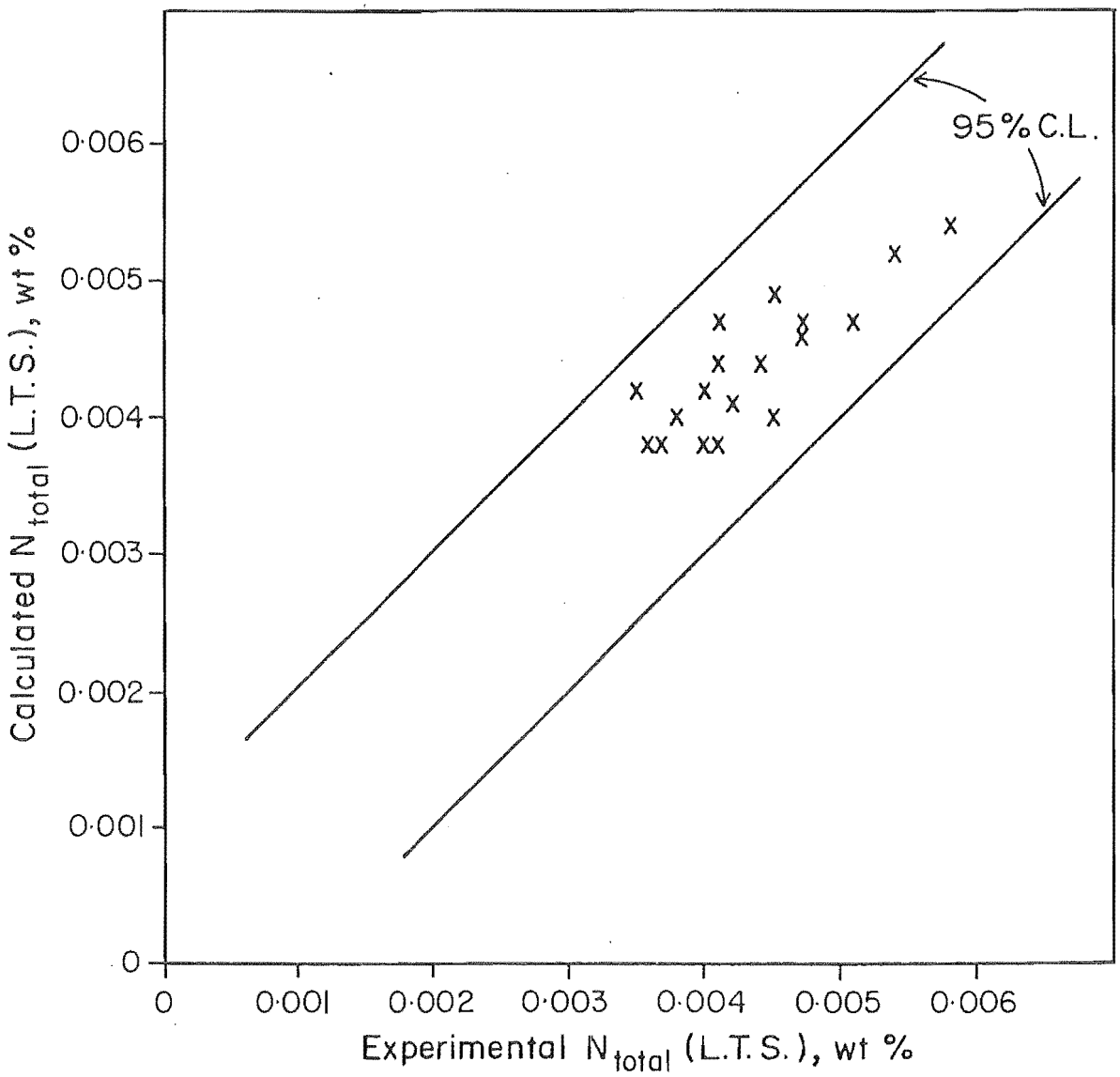

Figure 3.9: Calculated (using eqn.3.8) and observed nitrogen contents at LTS.

factors did not give any improvement in correlation coefficient. The nitrogen content calculated from equation 3.8 is plotted against the experimental values in Figure 3.9. Also shown on this figure are lines representing the 95% confidence limits of ± 0.0010%

As expected [34], equation 3.8 shows that increasing manganese content increases the nitrogen content, while increasing aluminium content decreases the nitrogen content in steel. Vanadium is known[34] to increase the nitrogen content in steel but in equation 3.8 the effect is opposite.

The most likely source of nitrogen at LTS would be atmosphere. During tapping and ladle transferring to the LTS, there is little protection of the molten surface from atmospheric nitrogen. The nitrogen content at LTS can be controlled by restricting liquid metal contact with air.

3.5.7 Nitrogen at CCM

Regression analysis of nitrogen content at the CCM was not attempted, since no further additions or other changes were made between the LTS and the CCM. However, there was an increase of 0.0011% nitrogen in the mean value between the LTS and CCM. Erasmus[95] investigated the nitrogen content at continuous casters and found that there was no correlation between the nitrogen at the continuous caster and the variables such as BOF tap nitrogen, fluorspar addition etc. However, he a observed significant increase in nitrogen content between the BOF treatment stage and the continuous casting stage. Similar increase in nitrogen content was observed in the present investigation, and is shown in Figure 3.10. The main reason for the nitrogen pick-up during continuous casting appears to

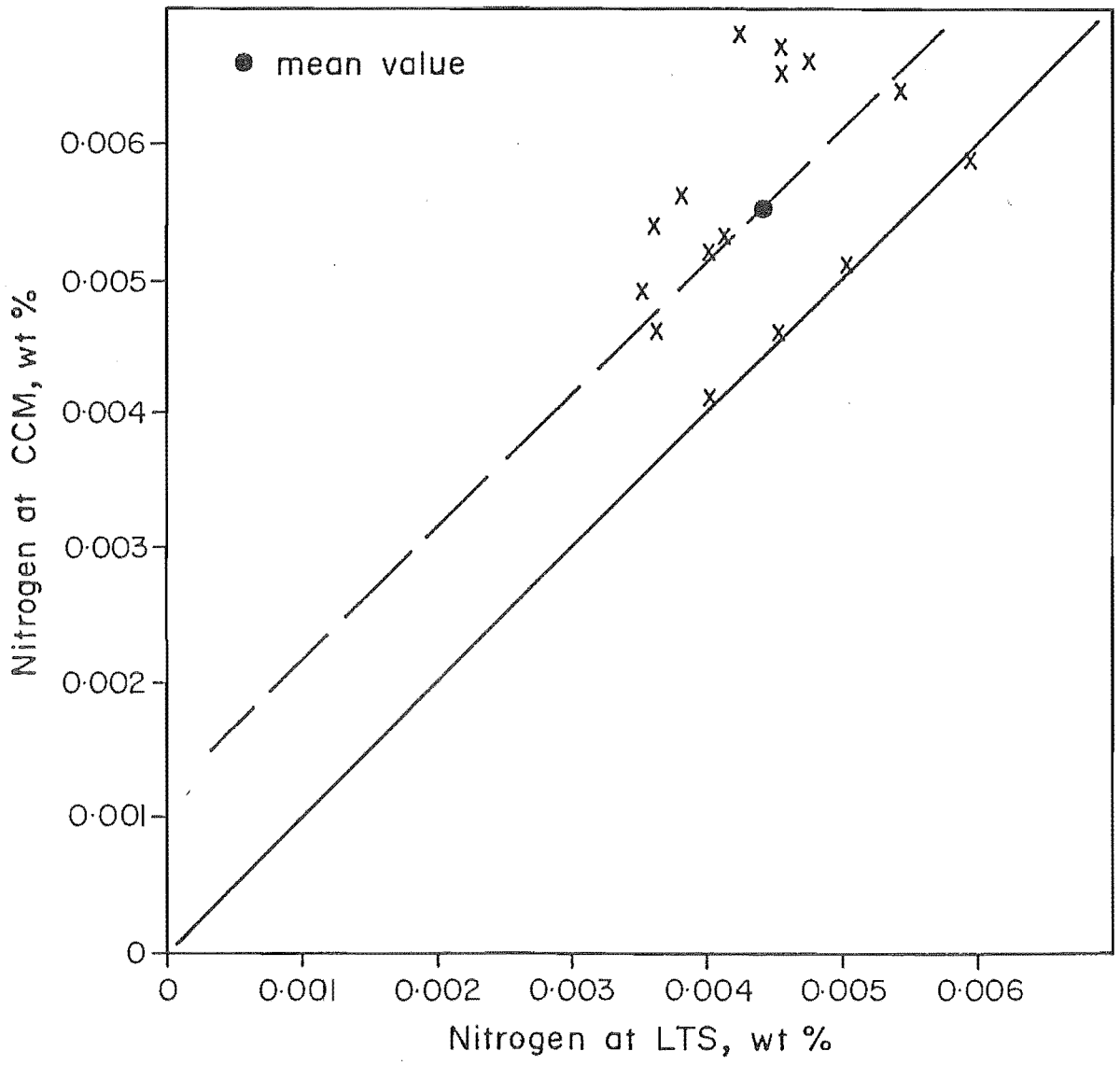

Figure 3.10: Comparison of nitrogen contents at CCM and LTS.

be insufficient protection of the liquid metal between the ladle and the tundish. Recent studies show that on a slab caster, the largest nitrogen pick-up generally occurs between ladle and tundish[42]. Casting tubes with nozzles submerged in the tundish may be used to prevent this nitrogen pick-up[42].

3.6 SUMMARY

A detailed investigation of the variations in nitrogen level during steel production between the melters and CCM at New Zealand Steel Limited has been carried out with samples taken at the Melters, VRU, KOBM, LTS and CCM. The multiple linear regression analysis has been used to establish a quantitative relationship between the nitrogen content and process variables.

It was found that hot metal from the melters had an average nitrogen content of 0.0027% and a further increase in nitrogen content was observed at VRU. However, there was a drop in nitrogen content observed at KOBM. An increase in nitrogen content was observed at LTS. Regression analysis on LTS data did not reveal a strong correlation between process variables. This increase in nitrogen content may be due to the nitrogen pick-up from the atmosphere. At the continuous caster, there was a further pick-up of nitrogen. Regression analysis of nitrogen content at the continuous caster was not analysed, since no further additions or other changes were made between the ladle treatment station and the continuous caster. Again, nitrogen pick-up from the atmosphere might be a major contributory factor to this increase in nitrogen level at the continuous caster.

CHAPTER 4

SOLUBILITY OF VANADIUM NITRIDE IN AUSTENITE

4.1 INTRODUCTION

During the thermomechanical processing of microalloyed steels, e.g. HSLA steels, microalloying elements such as vanadium, aluminium etc. combine with nitrogen to form stable nitride precipitates. These nitride precipitates play a major role in controlling the mechanical properties of microalloyed steels. The effect of these nitride precipitates on the mechanical properties depend on the precipitate size, distribution and the rate of precipitation at the processing temperature, which in turn depend on the solubility of the nitride precipitate at the processing temperature. Therefore, to provide a background to work on microalloyed steels, the present solubility studies have been made. In the present work the solubility product of vanadium nitride in austenite was determined as a function of temperature. This study was made on HSLA type steels containing 0.038% to 0.20% vanadium and 0.0065% to 0.0405% nitrogen over the temperature range of 900 to 1250°C. The nitrogen present as vanadium nitride was determined by chemical analysis[94]. This chapter reports results of such study.

4.2 EXPERIMENTAL STEELS

All the experimental steels were produced in a high frequency induction furnace. Four 72.5 kg of casts of steel were produced, each cast consisted of six ingots with varying amounts of nitrogen and vanadium, which were obtained by adding pre-determined amounts of

nitrovan and nitrided steel scrap. These molten steels were cast at a temperature of approximately 1600°C into 100 x 100 mm square ingots. These ingots were then forged down to 40 x 40 mm billets. Altogether 24 ingots were produced with vanadium varying from 0.02% to 0.22% and the nitrogen varying from 0.0050% to 0.0405%. Among these 24 steels only 15 steels were selected for the solubility product determination. These selected 15 steels were further forged down into 20 mm diameter bar.

4.3 HEAT TREATMENT

Specimens of 25 mm in length, cut from the forged 20 mm diameter bar, were used to determine the solubility of vanadium nitride in austenite. These samples were held at a series of temperatures between 900°C and 1250°C for four hours in an argon atmosphere before quenching into water. In order to minimize the temperature fluctuation a small tube furnace was used for this heat treatment. The temperature of the hot zone was monitered by an external 13% Pt-Rh/Pt thermocouple and controlled to within ± 5°C.

4.4 CHEMICAL ANALYSIS

4.4.1 Composition of Steels

A detailed composition of the experimental steels was obtained spectrographically from the spectrometer at Pacific Steel Limited, Auckland. The chemical composition of the steels obtained by this analysis is given in Table 4.1.

4.4.2 Determination of Nitrogen in the Steels

The amount of nitrogen combined as vanadium nitride in the heat

Table 4.1: Chemical composition of experimental steels

CAST	C	Mn	Si	S	P	Ni	Cr	Mo	Cu	Sn	V	Al	N
A5	0.09	1.38	0.15	0.012	0.012	0.03	0.02	-	0.01	-	0.072	-	0.0067
B2	0.11	1.35	0.31	0.016	0.014	0.03	0.01	-	0.01	-	0.038	-	0.0224
B3	0.09	1.30	0.30	0.012	0.011	0.03	0.01	-	0.01	-	0.054	-	0.0229
B4	0.10	1.29	0.30	0.012	0.011	0.03	0.01	0.004	0.01	0.004	0.070	0.001	0.0233
B5	0.12	1.33	0.30	0.015	0.013	0.03	0.01	0.002	0.01	0.001	0.085	-	0.0225
C2	0.11	1.28	0.20	0.011	0.011	0.03	-	-	0.01	-	0.044	-	0.0270
C3	0.12	1.29	0.20	0.014	0.012	0.03	-	-	0.01	-	0.061	0.004	0.0292
C4	0.12	1.27	0.19	0.014	0.012	0.03	-	0.001	0.01	-	0.078	-	0.0320
C5	0.11	1.25	0.18	0.013	0.011	0.03	-	-	0.01	-	0.088	-	0.0318
D1	0.14	1.57	0.19	0.012	0.020	0.04	0.05	0.005	0.01	0.002	0.07	0.007	0.0370
D2	0.14	1.35	0.18	0.011	0.019	0.04	0.05	0.004	0.01	0.001	0.10	0.007	0.0370
D3	0.14	1.34	0.18	0.011	0.019	0.04	0.05	0.005	0.01	0.002	0.12	0.006	0.0395
D4	0.15	1.33	0.17	0.011	0.019	0.04	0.05	0.004	0.01	0.001	0.15	0.005	0.0393
D5	0.15	1.27	0.15	0.011	0.019	0.04	0.05	0.004	0.01	0.001	0.17	0.005	0.0405
D6	0.16	1.24	0.13	0.012	0.020	0.04	0.05	0.003	0.01	-	0.20	0.005	0.0379

treated samples was determined by the chemical analysis method for nitrogen[94]. A weighed amount of drillings from each sample was dissolved in dilute (20%) sulphuric acid by heating in a steam bath. When the dilute sulphuric acid attack on the drillings was completed the nitrogen content of the steel was accurately separated by centrifuging into 'acid soluble' nitrogen (N_{sol} - represents the nitrogen in solution, as iron nitrides and aluminium nitride) and 'acid insoluble' nitrogen (N_{insol} - represents the nitrogen combined as stable nitrides, in this case vanadium nitride). The clear solution contains all the 'acid soluble' nitrogen as an ammonium salt solution. The insoluble residue was then decomposed by fuming with concentrated sulphuric acid at its boiling point. This solution was then diluted and contains all the 'acid insoluble' nitrogen as an ammonium salt solution. The nitrogen in these two solutions was absorbed as ammonia into boric acid solution by steam distillation with sodium hydroxide solution.

The total nitrogen content of the steel is given by:

$$N_{total} = N_{sol} + N_{insol}$$

The resultant nitrogen determination of the heat treated samples is given in Appendix C.

Figure 4.1 summarises the method used for nitrogen determination. The details of this chemical analysis method[94] are given in Appendix A.

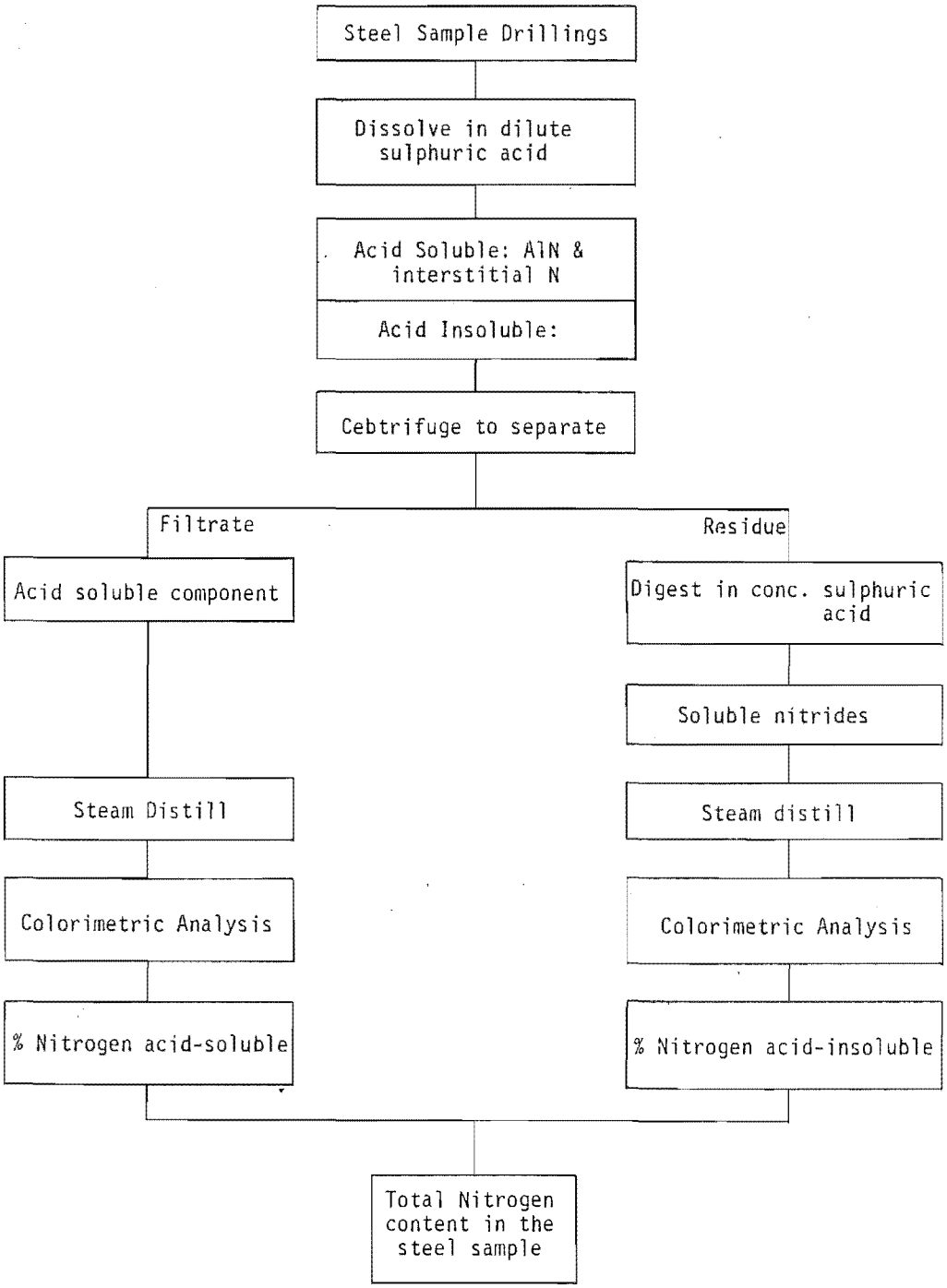

Figure 4.1: Format for nitrogen analysis of steel

4.5 DETERMINATION OF THE SOLUBILITY PRODUCT OF VANADIUM NITRIDE

The vanadium nitride precipitation process involves the combination of nitrogen in the steel with vanadium. This V + N → VN reaction is reversible. Reversible reactions such as this can be described by the Law of Mass Action, which states that the velocity of a reaction at a given temperature is proportional to the product of the active masses of the reacting substances[104].

Consider the reaction:

$$V + N \rightleftarrows VN \qquad \text{Eqn.4.1}$$

The forward rate of this reaction is given by

$$v_1 = k_1 [V][N] \qquad \text{Eqn.4.2}$$

Similarly the rate of reverse reaction is

$$v_2 = k_2 [VN] \qquad \text{Eqn.4.3}$$

where v_1 = rate of forward reaction

v_2 = rate of reverse reaction

[V], [N] and [VN] = active masses of V, N and VN respectively

Since equilibrium is a dynamic one in which the rate of the forward reaction is equal to the rate of the reverse reaction. At equilibrium

$$v_1 = v_2$$

$$\therefore \quad k_1 [V] [N] = k_2 [VN]$$

or

$$\frac{k_2}{k_1} = \frac{[V][N]}{[VN]} = K_c \qquad \text{Eqn.4.4}$$

Where Kc is the concentration equilibrium constant and is temperature dependent.

Now since the concentration term for the compound VN is constant at a constant temperature, equation 4.4 can be rewritten

$$[V][N] = Ks \qquad \text{Eqn.4.5}$$

where Ks is a new constant, called the solubility product and is numerically equal to Kc[VN].

Now the Arrhenuis equation, which can be deduced from the Van t Hoff isochore equation and the Law of Mass Action, gives the effect of temperature on the rate of reaction(104).

$$v = \theta e^{-\frac{Q}{RT}} \qquad \text{Eqn.4.6}$$

or

$$\text{Ln } v = -\frac{Q}{RT} + \text{Ln } \theta \qquad \text{Eqn.4.7}$$

or

$$\text{Log } v = \text{Log } \theta - \frac{Q}{2.303RT} \qquad \text{Eqn.4.8}$$

where v = specific reaction rate

θ = integration constant

Q = activation energy

R = gas constant

T = absolute temperature

By combining equations 4.2 and 4.5, it can be established that

$$v \propto Ks$$

Therefore by substitution in equation 4.8, a graph of Log Ks versus the reciprocal of absolute temperature should give a straight line.

A similar relationship was first proved by Darken[105] for for aluminium nitride dissolving in austenite to form a solid solution of aluminium and nitrogen. The solubility product was taken as the product of the weight percentages of aluminium and nitrogen in solution in austenite in equilibrium with aluminium nitride, these being considered equivalent to the activities.

Similarly, in the case of vanadium nitride the activities of vanadium and nitrogen can be taken as the weight percentage of vanadium and nitrogen in solution in austenite in equilibrium with vanadium nitride.

$$\text{i.e.} \quad K_s = [\text{wt\% } N_{sol}][\text{wt\% } V_{sol}] \qquad \text{Eqn.4.9}$$

Therefore the solubility product of vanadium nitride is the product of the weight percentages of nitrogen and vanadium in solution in austenite in equilibrium with vanadium nitride, and can be expressed as follows:

$$K_s = [N_{total} - N_{insol}][V - \frac{51}{14} N_{insol}] \qquad \text{Eqn.4.10}$$

where N_{total} = wt%, total nitrogen in steel

N_{insol} = wt%, 'acid insoluble' nitrogen (nitrogen combined as vanadium nitride)

V = wt%, vanadium content in steel

$\frac{51}{14} N_{insol}$ = wt%, vanadium combined as vanadium nitride

K_s = Solubility product of vanadium nitride at that temperature

The values for N_{total} and N_{insol} can be determined by the chemical analysis method for nitrogen and the solubility product of vanadium nitride can be calculated by using equation 4.10.

4.6 DISCUSSION OF RESULTS

4.6.1 Solubility Product of Vanadium Nitride in Austenite

The solubility product of vanadium nitride in austenite was first determined by Fountain and Chipman[106] in 1958. They proposed two solubility equations, Log K_A and Log K_B, depending on the size of precipitated vanadium nitride: K_A for the metastable smaller nitride precipitates ($\simeq$0.04 μm) and K_B for the stable larger nitride precipitates ($\simeq$0.6 μm). Both Log K_A and $_B$ included the activity coefficient of nitrogen, and the activity coefficient of vanadium was assumed to be approximately equal to one. These were expressed as functions of temperature by the following relations:

For metastable smaller nitride precipitates ($\simeq$0.04μm)

$$\text{Log } K_A = \text{Log(wt\% N)(wt\% V)}.f_N = -\frac{6430}{T} + 2.0 \qquad \text{Eqn.4.11}$$

For stable larger nitride precipitates ($\simeq$0.6μm)

$$\text{Log } K_B = \text{Log(wt\% N)(wt\% V)}.f_N = -\frac{7070}{T} + 2.27 \qquad \text{Eq.4.12}$$

where K_A, K_B = solubility product of vanadium nitride

f_N = activity coefficient of nitrogen

T = absolute temperature

In 1960 Frahberg and Graf[107] determined the solubility of vanadium nitride in high purity austenite and ferrite. The solubility relationship in austenite was:

$$\text{Log } K_s = - \frac{7070}{T} + 2.27 \qquad \text{Eqn.4.13}$$

Later in 1964 Erasmus[108] investigated the solubility of vanadium nitride in austenite for 0.2% carbon steels and proposed the following equation,

$$\text{Log } K_s = - \frac{6900}{T} + 2.35 \qquad \text{Eq.4.14}$$

In 1966 Narita and Koyama[109] measured the reaction of nitrogen and vanadium in γFe-V alloys equilibrated with 1 atm N_2-3% H_2 gas. They reported that the reaction was $V + N \rightleftarrows VN$ and the solubility product of vanadium nitride was expressed as:

$$\text{Log } K_s = \text{Log (wt\% N).(wt\% V)}$$
$$= - \frac{8700}{T} + 3.63 \qquad \text{Eqn.4.15}$$

In 1967 Irvine at al[4] determined the solubility relationship of vanadium nitride and vanadium carbide for commercial carbon-manganese steels. The relationship for vanadium nitride was:

$$\text{Log[V][N]} = - \frac{8330}{T} + 3.46 \qquad \text{Eqn.4.16}$$

Irvine extended his studies of the solubility of vanadium nitride to higher manganese steels and found that the solubility was increased significantly as the manganese content increased.

For higher manganese steels:

$$\text{Log}[V][N] = -\frac{8330}{T} + 3.40 + 0.12(\%\ Mn) \qquad \text{Eqn.4.17}$$

The addition of 1% Mn would thus increase the solubility product at a given temperature by about 30%. It was suggested[4] that this increased solubility of vanadium nitride is a result of the activity coefficient of nitrogen in austenite being lowered by manganese.

Later, in 1987, Harue Wada[110] studied the equilibrium nitrogen solubility and nitride formation in austenitic Fe-V alloys and proposed the following equation:

$$\text{Log } K_s = \frac{(-6777 \pm 372)}{T} + (2.07 \pm 0.3) \qquad \text{Eqn.4.18}$$

To provide a background to work on high strength low alloy steels microalloyed with vanadium the solubility of vanadium nitride has now been determined by the chemical analysis method, previously described. The 'acid insoluble' component of nitrogen was taken as the nitrogen precipitated as vanadium nitride. Silicon is unlikely to affect the formation of vanadium nitride and Konig et al[111] suggested that the formation of Si_3N_4 is unlikely to occur in steels containing strong nitride formers such as vanadium or aluminium. However, there is still a possibility of obtaining Si_3N_4 in steels containing vanadium if the silicon content is high (0.6%). Since all the experimental steels have silicon content less than 0.31%, the possibility of the formation of Si_3N_4 is small. Therefore the 'acid insoluble' component of the nitrogen would be the amount of nitrogen combined as vanadium nitride.

The solubility product of vanadium nitride was then calculated by substituting the values for N_{total} and N_{insol}, determined by the chemical analysis, in equation 4.10. Altogether 191 results from the chemical analysis were used in the solubility product determination. In order to find a relationship between the solubility product and temperature, the logarithms of solubility product values were plotted against the reciprocal of the absolute temperature. A best fit line was found by a linear regression analysis. Table 4.2 shows the computer printout of the linear regression analysis. The linear regression analysis gives the following solubility product relationship:

$$\text{Log } K_s = - \frac{7754}{T} + 3.02 \qquad \text{Eqn.4.19}$$

Equation 4.19 is significant at 1.0% probability level, i.e. we can say with 99% certainty that there is a correlation. The solubility relationship is shown graphically in Figure 4.2 with the individual experimental results. Also shown on this figure are lines representing the 95% confidence limits.

Figure 4.3 shows the present results compared with those reported previously in the literature. Although the numerical parameters given in Table 4.3 differ from those results reported in the literature, the actual solubilities at a given temperature in the austenite temperature range are very similar. The present results are in good agreement with all the results, previously reported, at low austenite temperatures. At higher austenite temperatures the present results show better agreement with the results reported by Irvine et al[4], Erasmus[108] and Nartia et al[109] than with the results

Table 4.2: Computer printout (solubility product of vanadium nitride as a function of temperature).

Multiple linear regression analysis of the form

$$Y = Bo + B_1X_1 + B_2X_2 + ...$$

Variable No.1 = $(_1/T) \times 1000$
Variable No.2 = log Ks

Regression number 2
2 is the dependent variable

Index	Means	Standard Deviations
1	0.7580161	4.766561E-02
2	- 2.858471	0.375535

Correlation coefficients

0.9999993	- 0.9841594
-0.9841595	0.9999924

Index	B	Std. Error	T-Value
0	3.018907	7.718063E-02	39.11483
1	- 7.753632	0.1016196	- 76.30057

R - Squard = 0.9685565 R = 0.9841527

Std. error of estimate = 6.676696E-02

D.F = 189

F value = 5821.786

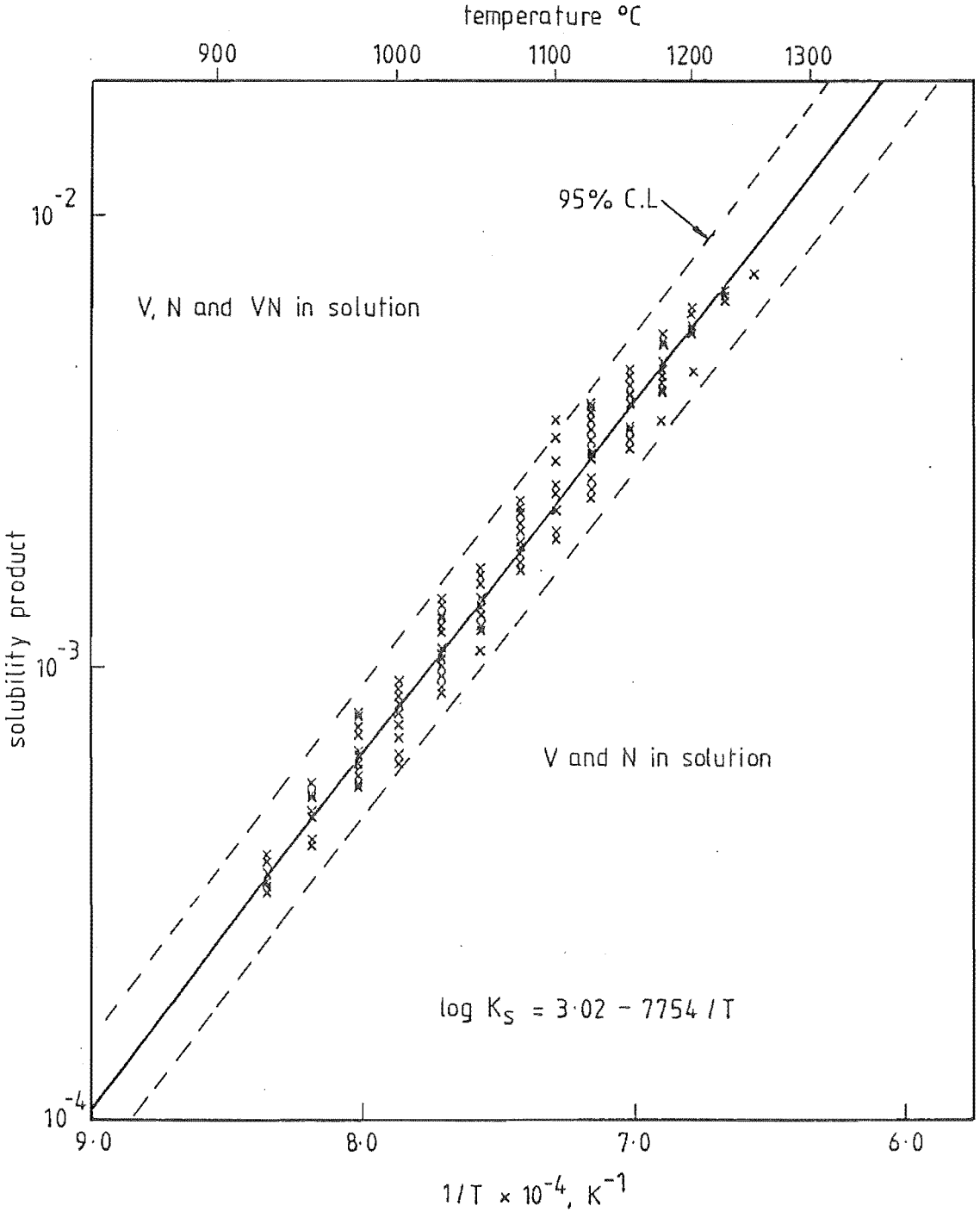

Figure 4.2: Solubility product of vanadium nitride in austenite as a function of temperature

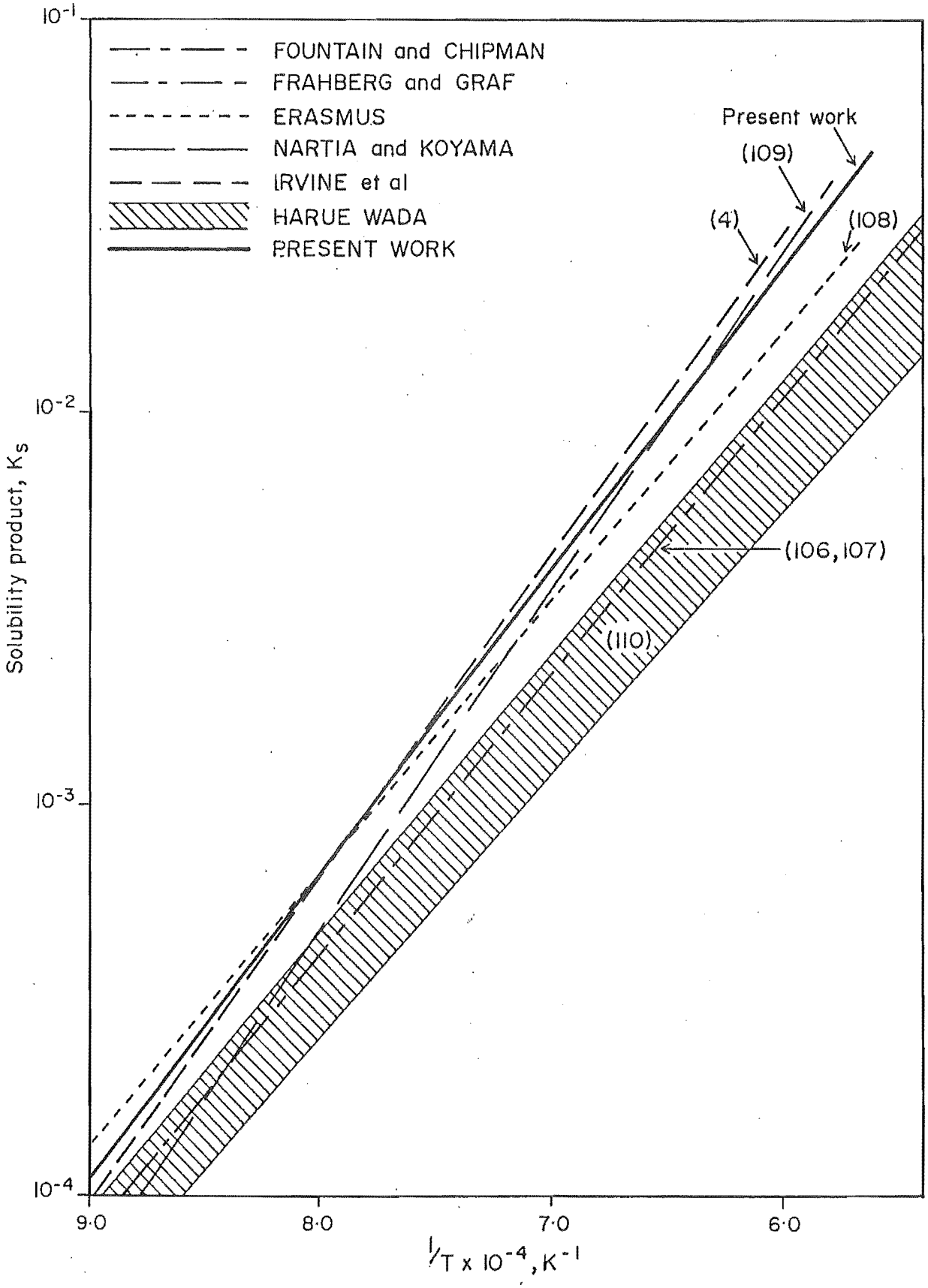

Figure 4.3: Solubility product of vanadium nitride in austenite (Ref. 4,106,107,108,109,110).

Table 4.3: Solubility product of vanadium nitride in austenite as a function of temperature.

$$\log K_S = A - \frac{B}{T}$$

Author	Year	A	B	Ref.
Fountain and Chipman	1958	* 2.0 2.27	* 6430 7070	106
Frahberg and Graf	1960	2.27	7070	107
Erasmus	1964	2.35	6900	108
Nartia and Koyama	1966	3.63	8700	109
Irvine et al	1967	3.46	8330	4
Harue Wada	1987	2.07 ± 0.3	6777 ± 372	110
Ratnaraj	1988	3.02	7754	Present study

* These values applicable only for smaller metastable precipitates (≈ 0.04 μm).

reported by Fountain and Chipmen[106], Frahberg and Graf[107] and Harue Wada[110]. Irvine et al[4] and Erasmus[108] used a chemical analysis method which is similar to the method used in the present investigation. This may be the reason for the better agreement of these results. Although Nartia and Koyama[109] used a different technique to determine the solubility of vanadium nitride, the relationship between solubility product and temperature proposed by them also agrees with the present results, within the experimental accuracy. However, the present relationship shows the effect of temperature on the solubility product of vanadium nitride in austenite for HSLA steels.

4.6.2 Solution temperature of Vanadium Nitride in HSLA steels

Figures 4.4 - 4.11 show the effect of temperature on the equilibrium solubility of vanadium nitride in all fifteen experimental HSLA steels. In these figures the weight percentage nitrogen combined as vanadium nitride, determined by the chemical analysis, is plotted against the temperature. Also shown are the calculated equilibrium curves, determined from all the experimental results by plotting Log K_S against the reciprocal of absolute temperature in Figure 4.2.

It is clear from figures 4.4 - 4.11 that the equilibrium solubility of vanadium nitride increases with increasing temperature. The solution temperature of vanadium nitride in all 15 experimental steels was obtained from the calculated equilibrium curves is given in Table 4.4. The results show that the solution temperature of vanadium nitride is dependent on the vanadium and nitrogen contents of the steel. The effect of solution temperature on the precipitation of vanadium nitride during a simulated hot rolling thermal cycle was

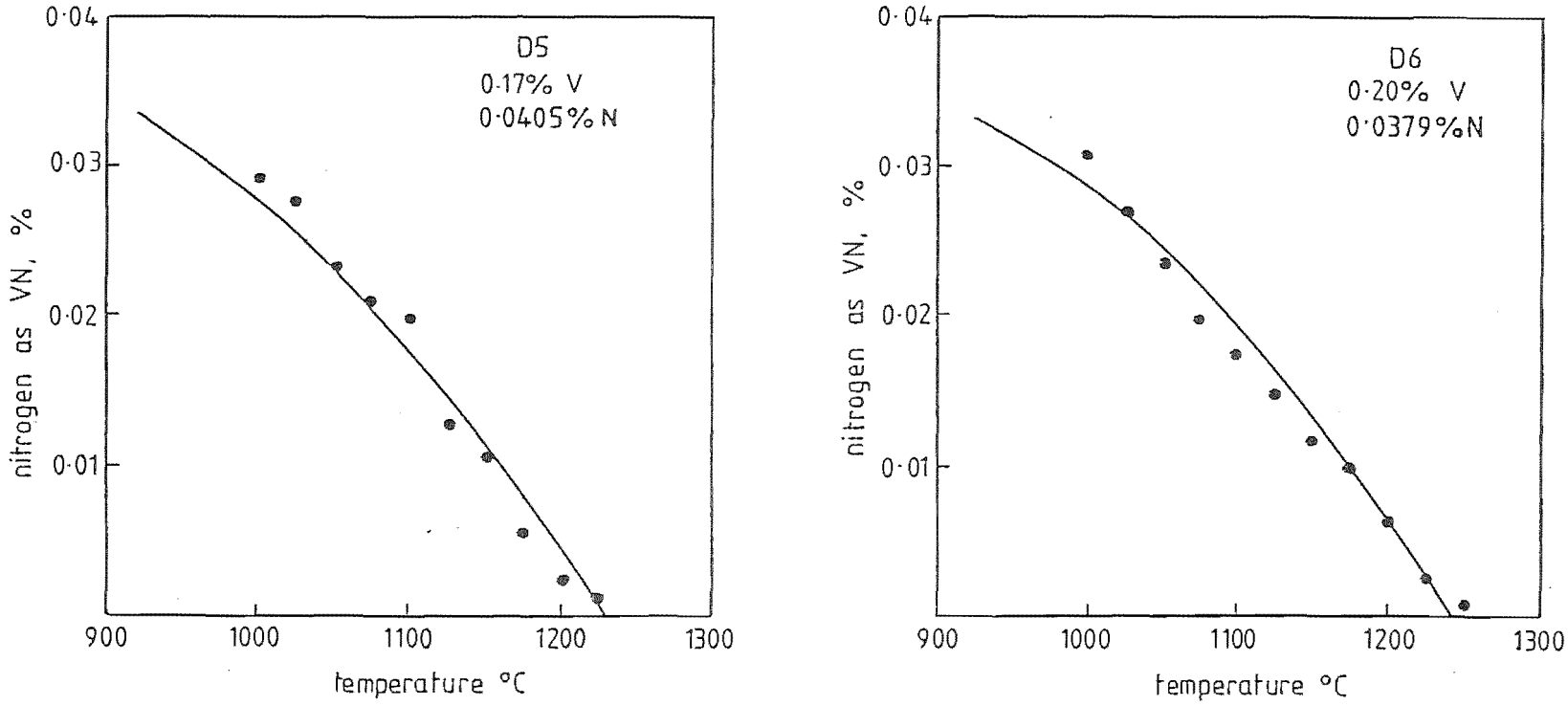

Figure 4.4: Solution of vanadium nitride in steels D5 and D6

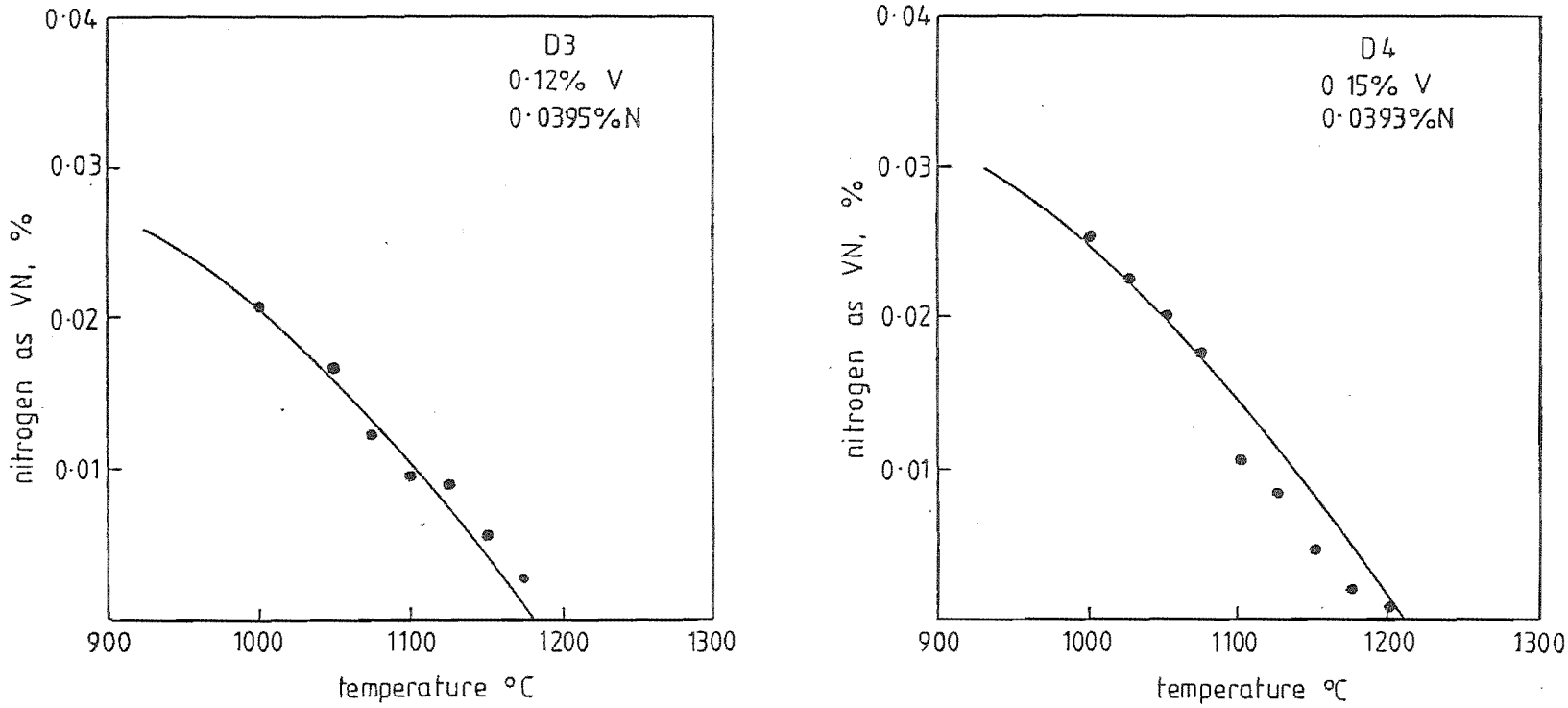

Figure 4.5: Solution of vanadium nitride in steels D3 and D4

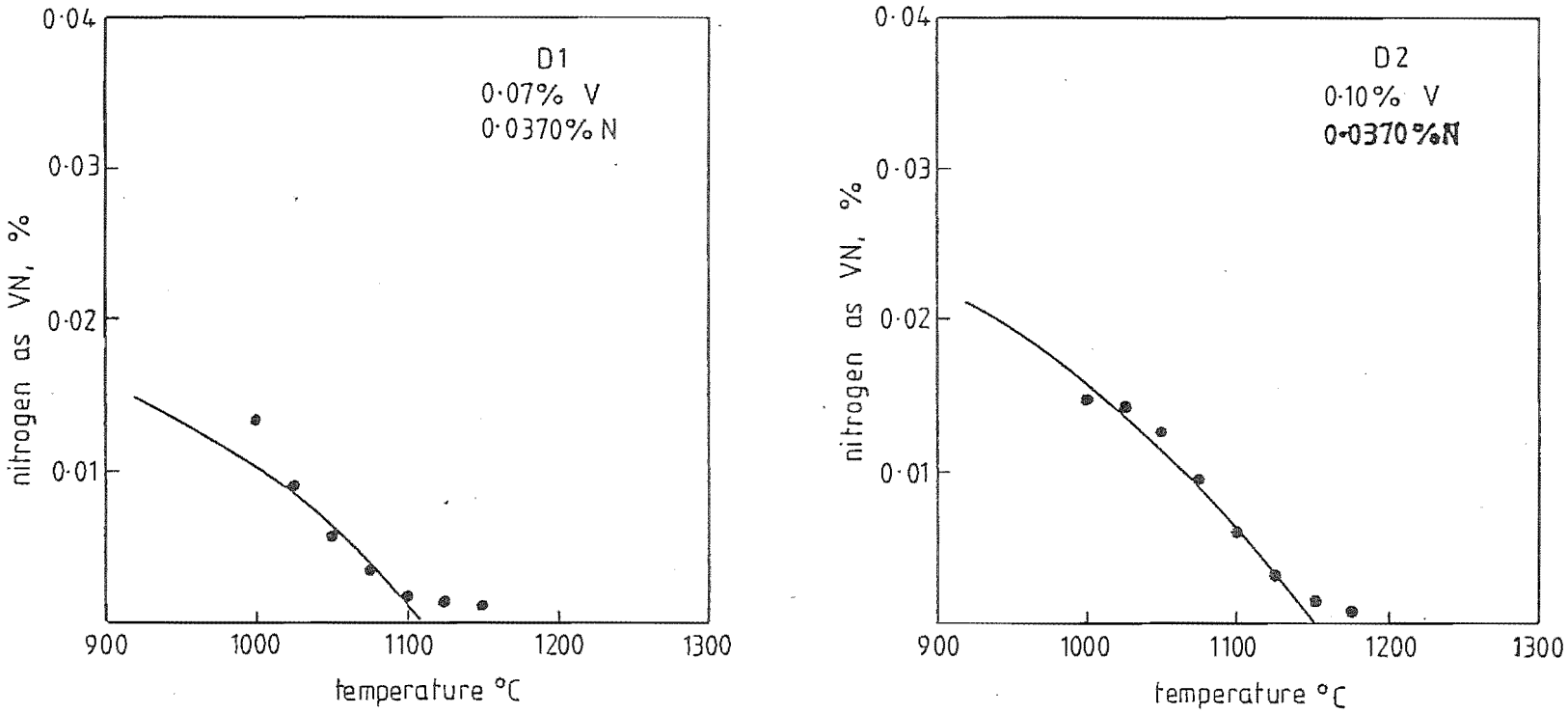

Figure 4.6: Solution of vanadium nitride in steels D1 and D2

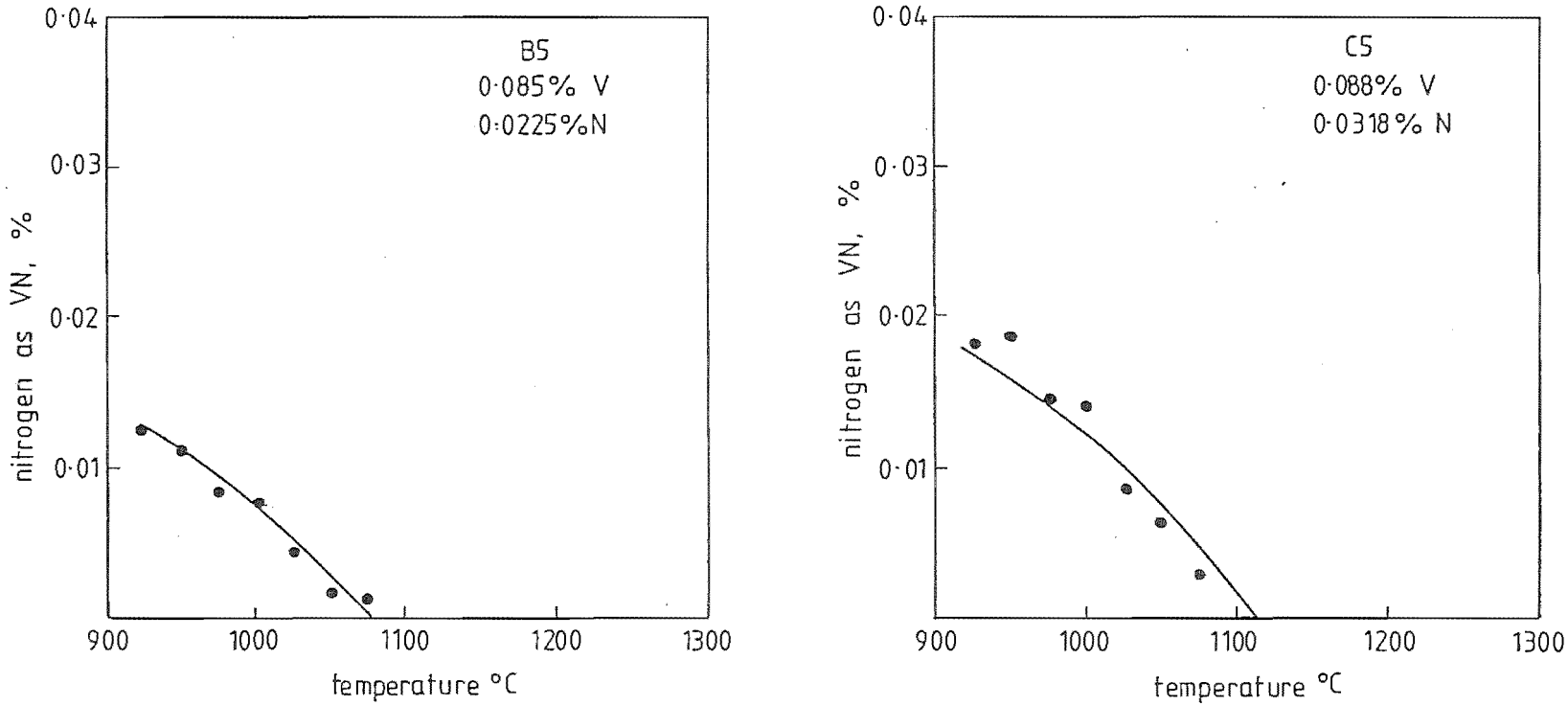

Figure 4.7: Solution of vanadium nitride in steels B5 and C5

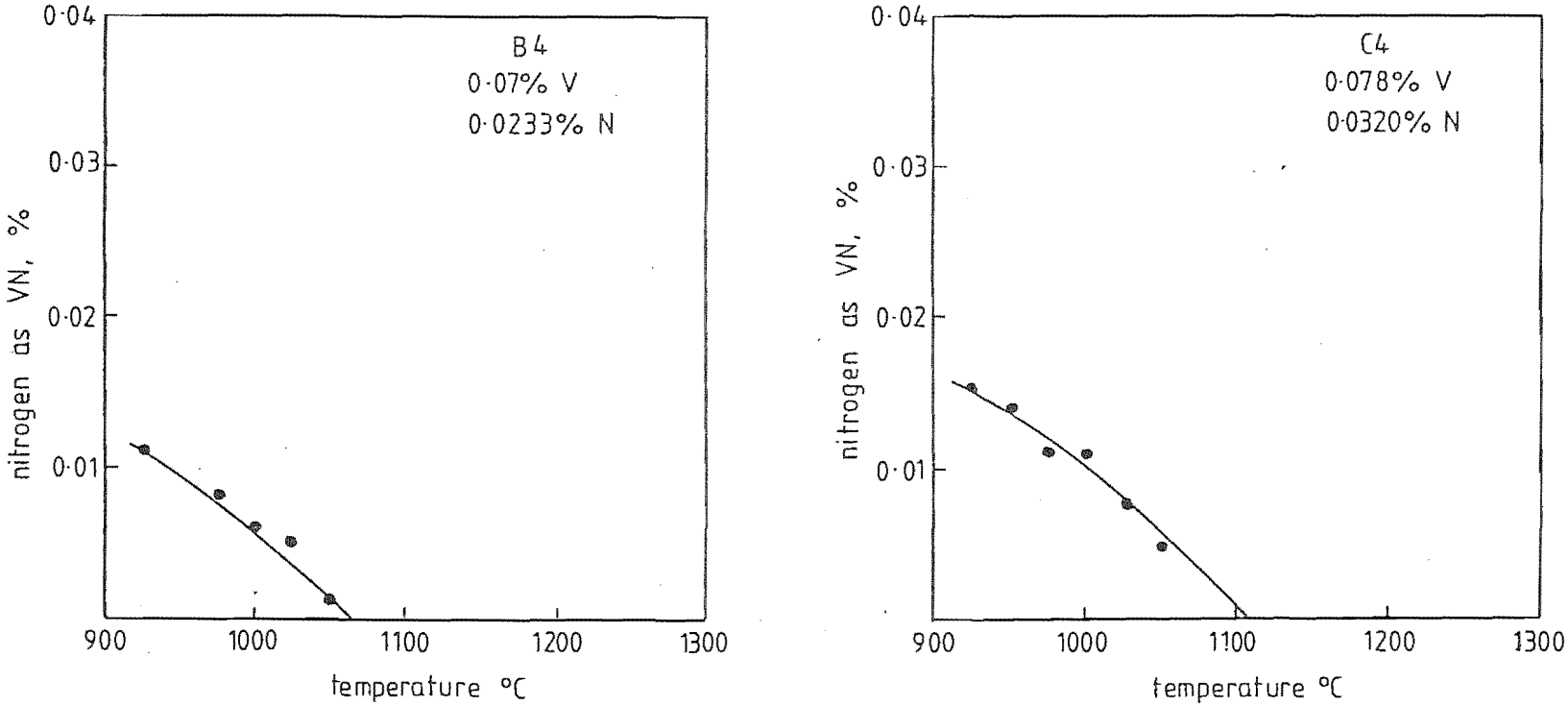

Figure 4.8: Solution of vanadium nitride in steels B4 and C4

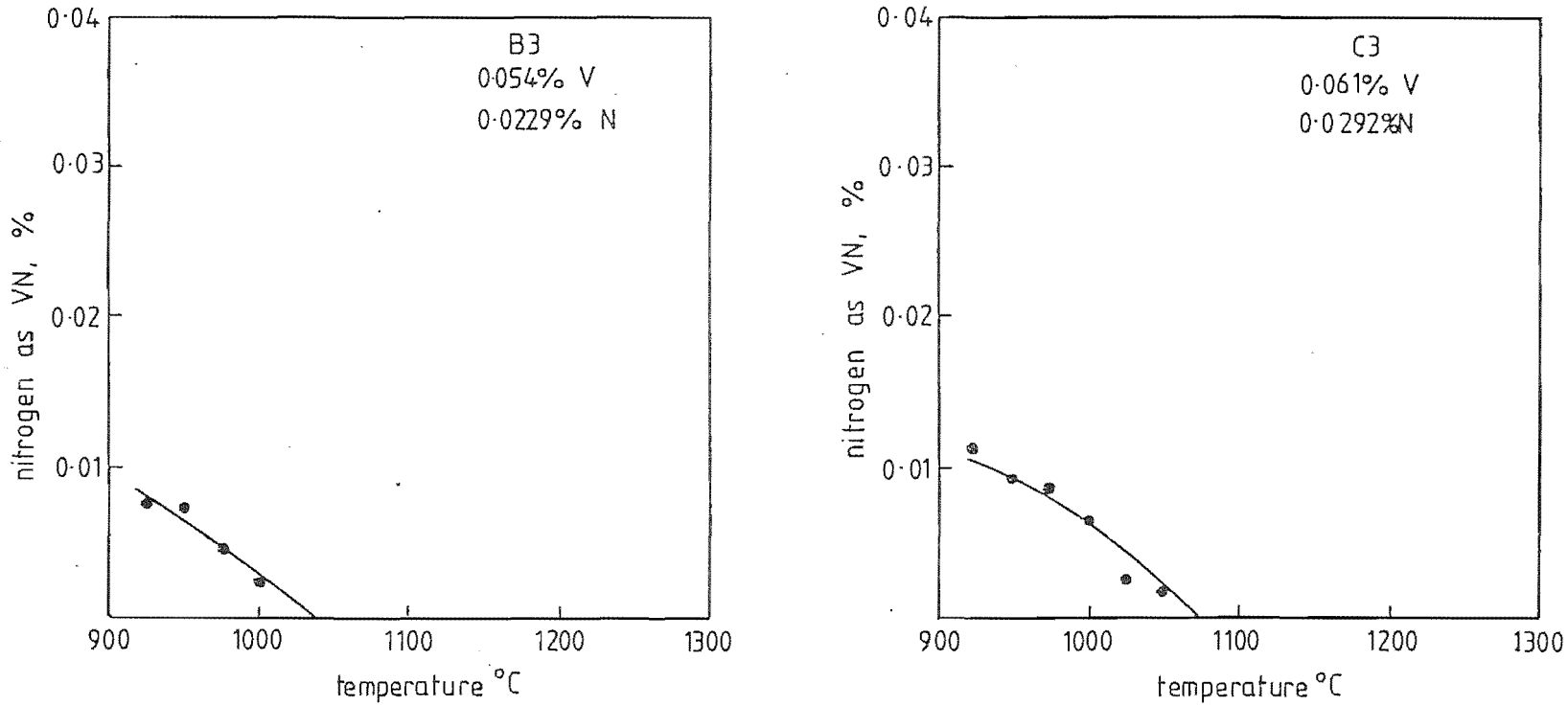

Figure 4.9: Solution of vanadium nitride in steels B3 and C3

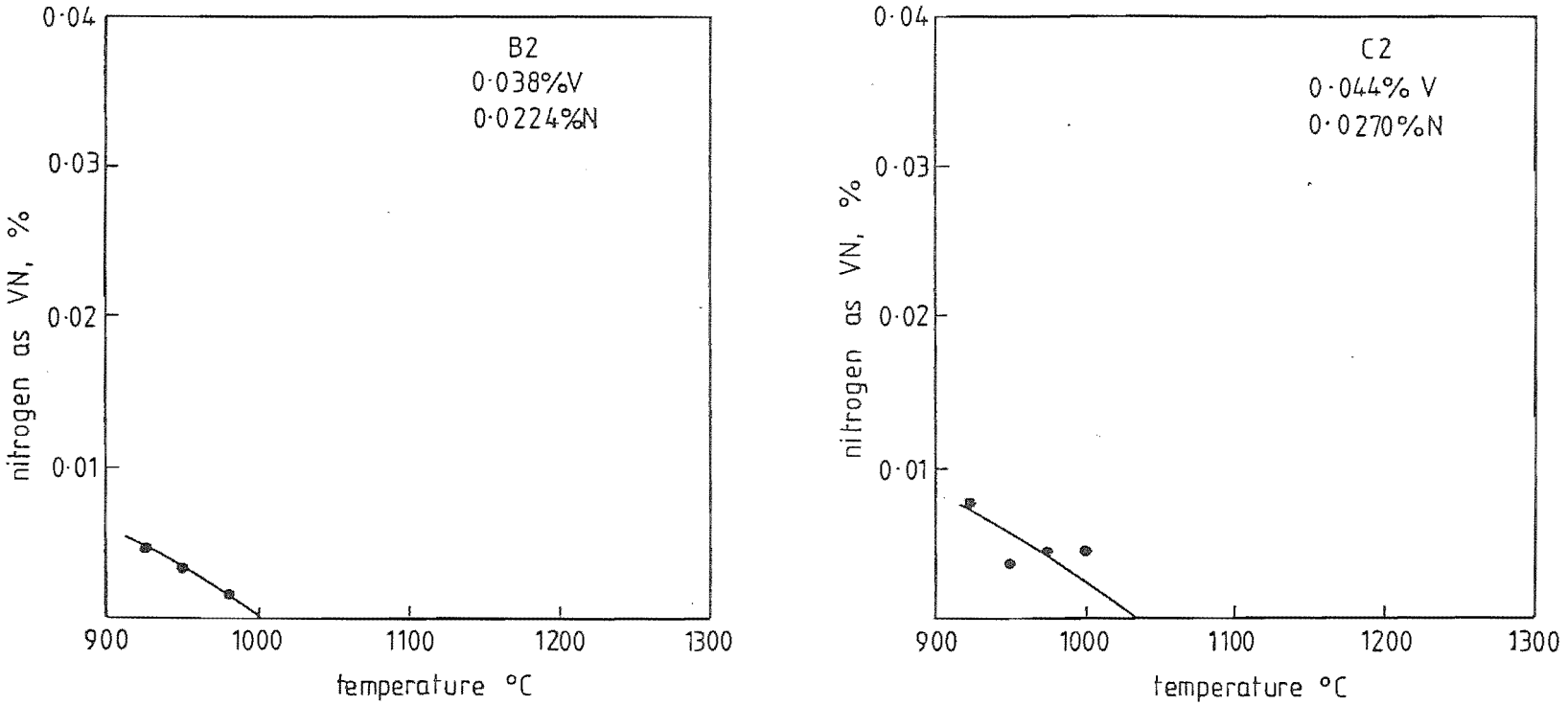

Figure 4.10: Solution of vanadium nitride in steels B2 and C2

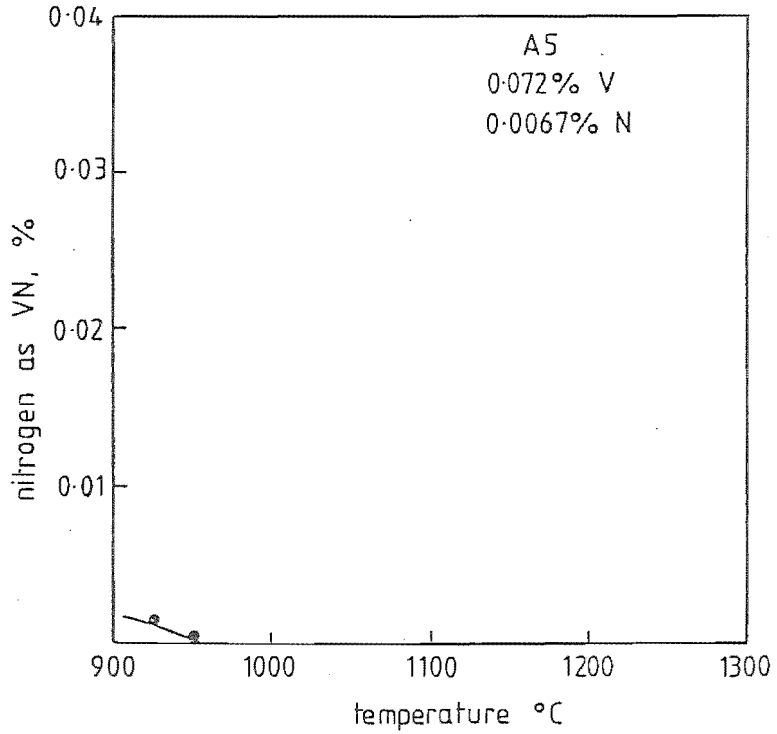

Figure 4.11: Solution of vanadium nitride in steel A5

Table 4.4: Solution temperature of vanadium nitride in experimental HSLA steels.

STEEL	V (wt %)	N (wt %)	SOLUTION TEMPERATURE (°C)
A5	0.072	0.0067	950
B2	0.038	0.0224	1000
C2	0.044	0.0270	1040
B3	0.054	0.0229	1040
C3	0.061	0.0292	1075
B4	0.070	0.0233	1075
C4	0.078	0.0320	1110
B5	0.085	0.0225	1075
C5	0.088	0.0318	1115
D1	0.070	0.0370	1110
D2	0.100	0.0370	1150
D3	0.120	0.0395	1175
D4	0.150	0.0393	1210
D5	0.170	0.0405	1235
D6	0.200	0.0379	1250

investigated. The results will be discussed in the next chapter.

4.7 SUMMARY

The solubility of vanadium nitride in HSLA steel was determined in the temperature range from 900°C to 1250°C. Since there was no other strong nitride formers present in the experimental steels, the 'acid insoluble' component of nitrogen was taken as the nitrogen combined as vanadium nitride. The solution temperature of vanadium nitride in each experimental steel was determined from the equilibrium solubility curves. The solubility product of vanadium nitride in austenite was determined as a function of temperature, and the result obtained was:

$$\text{Log } K_S = - \frac{7754}{T} + 3.02$$

where K_S = solubility produce of vanadium nitride, and

T = absolute temperature.

CHAPTER 5

PRECIPITATION OF VANADIUM NITRIDE DURING A SIMULATED HOT ROLLING THERMAL CYCLE

5.1 INTRODUCTION

The addition of strong nitride forming elements such as vanadium, aluminium and titanium to increase the strength of steel has been widely used in the metallurgical design of HSLA steels[112] These microalloying elements combine with nitrogen to form nitride precipitates during thermomechanical processing. These precipitates may pin grain boundaries or act as nuclei for new grains during phase transformation, thus refining the ferrite grain size. Grain refinement substantially increases the yield strength and also decreases the fracture mode transition temperature. The nitride precipitates also contribute to precipitation hardening and consequently further increase the yield strength.

Among all the microalloying elements vanadium shows the following advantages:

(1) It can be added to semikilled or rimmed steel, because of its lower affinity for oxygen than the other microalloying elements such as titanium.

(2) Vanadium nitride has medium solubility in austenite, therefore the rate of precipitation and thus mechanical properties can be controlled during thermomechanical processing.

During thermomechanical processing, vanadium combined with nitrogen forms vanadium nitride precipitates. The rate of precipitation of vanadium nitride depends on the thermomechanical processing parameters such as reheating temperature, finishing rolling temperature, cooling rate coiling temperature, etc. In the work reported here, an attempt has been made to simulate the thermal cycle of a typical commercial hot rolling mill. This chapter reports the results of such a study.

5.2 SIMULATION OF HOT ROLLING THERMAL CYCLE

With slight modification to the isothermal "down quenching" technique (i.e. quenching to some intermediate temperature from a higher temperature and holding at this temperature to allow isothermal precipitation) it is possible to simulate the thermal cycle conditions of slabs or billets passing through various stages of the rolling process.

Figure 5.1 shows the various stages of a hot rolling process. In the hot rolling mill slabs or billets are soaked at temperature in the reheating furnace for four hours. During rolling there will be a gradual decrease in temperature but the major temperature drop occurs on completion of rolling, when the strips or rods are cooled rapidly by artificial means (e.g. water spray) before coiling. The temperature of the strip or rod is then stabilised by coiling and the complete coil then continuous cooled at a much reduced rate in air.

Figure 5.2 illustrates schematically the simulated heat treatment of the thermal cycle of a hot rolling mill. In this

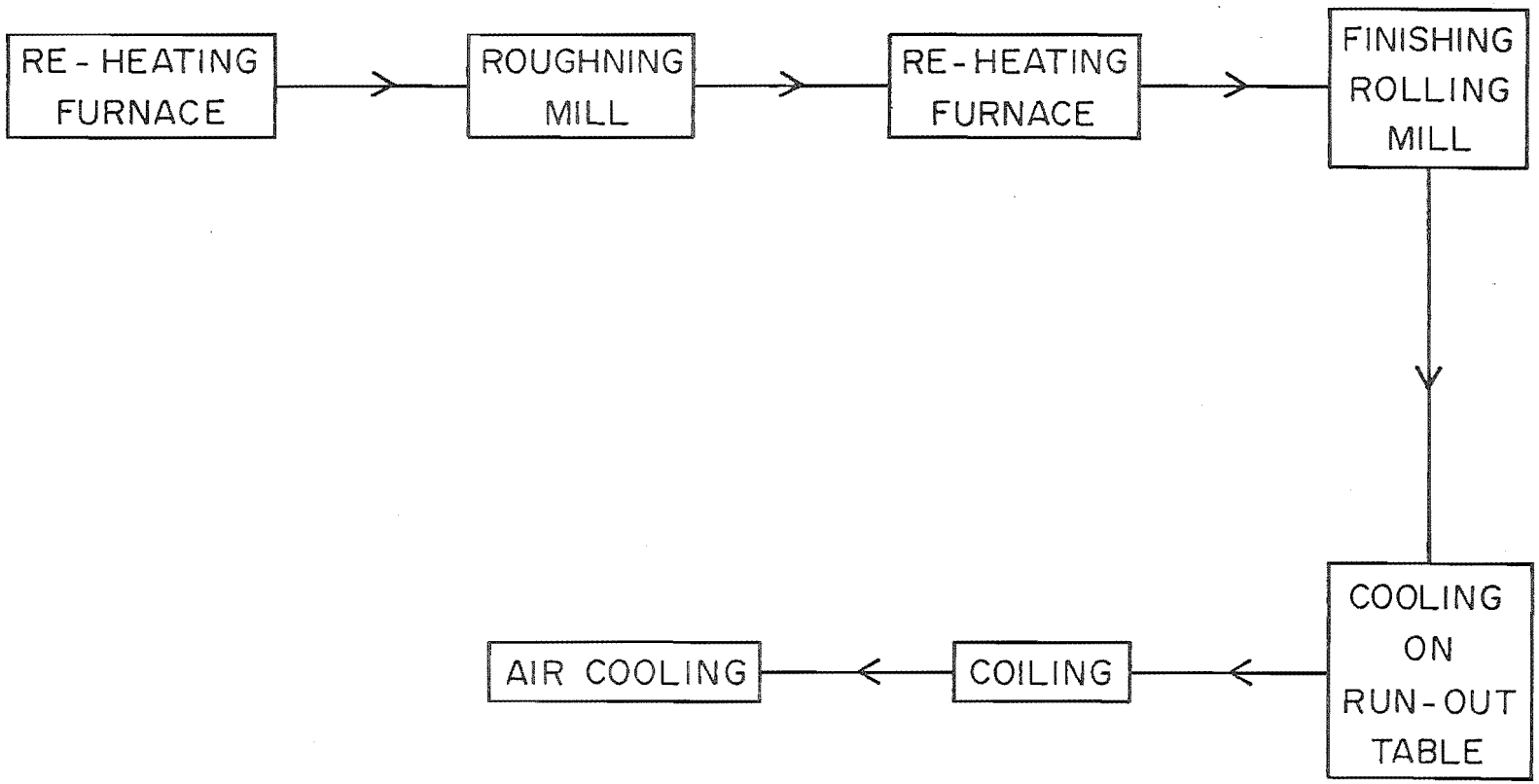

Figure 5.1: Schematic diagram of hot rolling mill

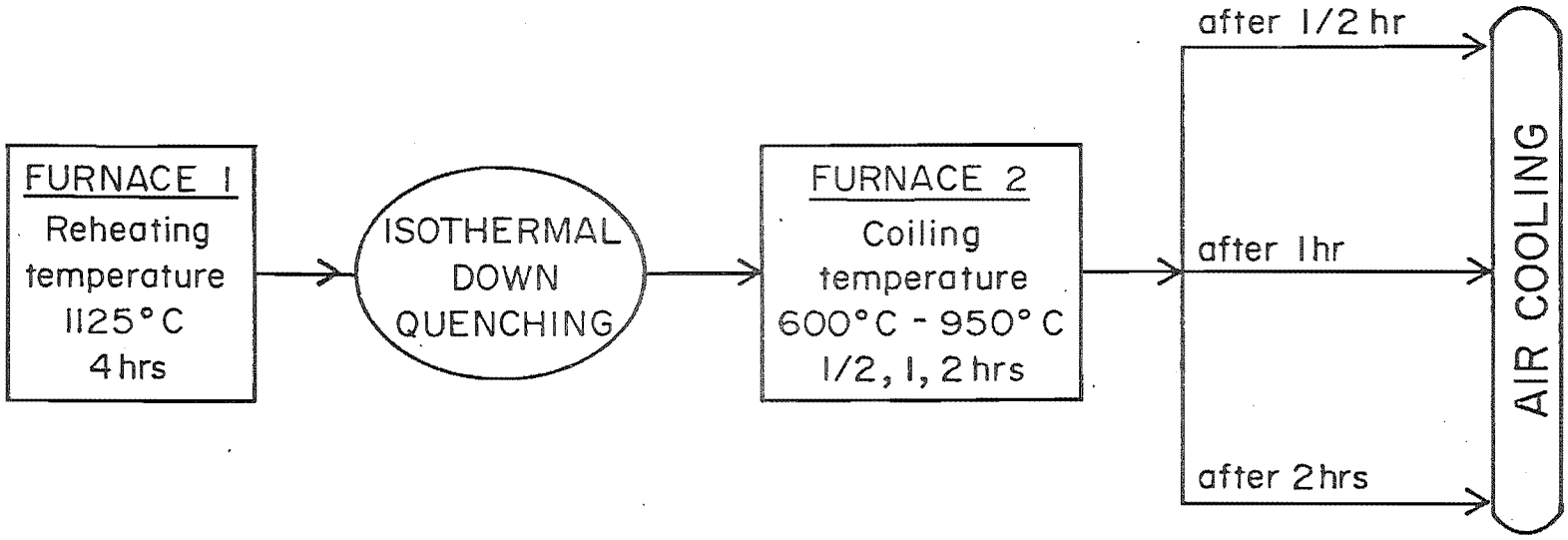

Figure 5.2: Simulated heat treatment

simulated heat treatment samples were soaked in a furnace which was at the reheating furnace temperature for four hours. After four hours the samples were transferred immediately into another furnace where the temperature was equal to the coiling temperature and varied between 600°C and 950°C. To simulate different coil sizes and thus varied cooling rates after coiling, the samples were kept for different periods of time in the second furnace, the temperature of which is called the simulated coiling temperature hereafter. The details of this simulated heat treatment are given in the following experimental procedure section.

5.3 EXPERIMENTAL STEELS

The steels used in this experiment were selected from the fifteen casts used in the previous solubility product determination work. To study the effect of initial undissolved vanadium nitride precipitates on the rate of precipitation of vanadium nitride during the simulated rolling treatment, two steels cast D2 and cast B5 were selected. Figure 5.3 shows the effect of temperature on the equilibrium solubility of vanadium nitride in these two selected steels. The solution temperatures of vanadium nitride in these two steels were determined from the equilibrium solubility curves. The solution temperatures of vanadium nitride for casts D2 and B5 were 1150°C and 1075°C respectively. Since the solution temperature of vanadium nitride for cast D2 is higher than the soaking temperature (1125°C), there would be some undissolved vanadium nitride precipitates even after reheating at 1125°C for four hours. However, in cast B5 all the vanadium nitride precipitate would dissolve after soaking at 1125°C for four hours, (i.e. all the nitrogen and vanadium would be in solution at 1125°C).

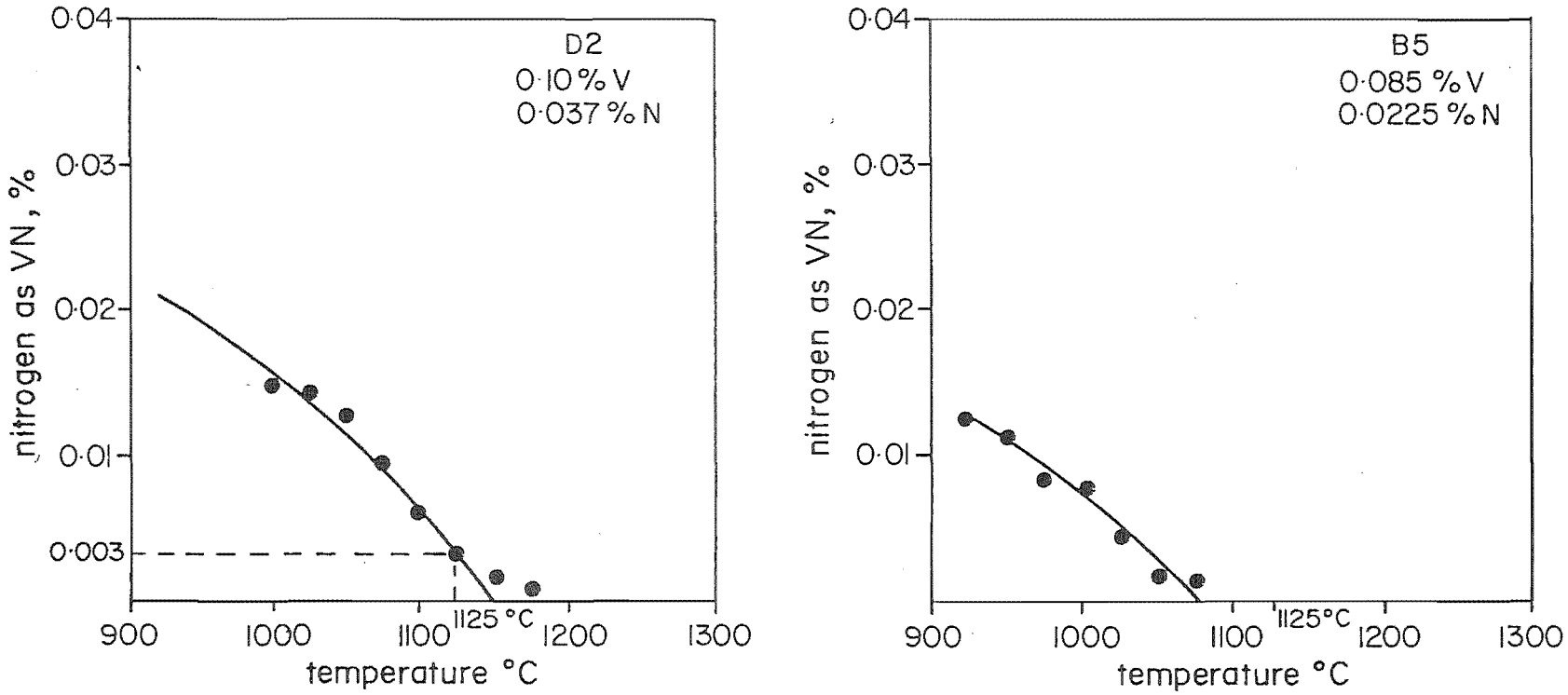

Figure 5.3: Effect of temperature on equilibrium solubility of VN in steels D2 and B5

Figure 5.4 shows this clearly. It can also be seen from Figure 5.4 that steel B5 has a vanadium content slightly in excess of stoichiometric for vanadium nitride, and in steel D2 the vanadium content is less than stoichiometric (0.0095% excess nitrogen). The chemical composition of these two steels is given in Table 5.1.

Table 5.1: Chemical composition of steels D2 and B5.

Cast	C	Mn	Si	S	P	Aℓ	V	N
D2	0.14	1.35	0.18	0.011	0.019	0.007	0.10	0.0370
B5	0.12	1.33	0.30	0.015	0.013	-	0.085	0.0225

5.4 EXPERIMENTAL PROCEDURE

5.4.1 Heat Treatment

Specimens 25 mm long, cut from forged 20 mm diameter bar were used in this heat treatment. These samples were soaked at 1125°C in an argon atmosphere for four hours, after which each sample was transferred immediately to a second furnace set at the coiling temperature. Samples were held at different coiling temperatures between 600°C and 950°C for 30 minutes, 1 and 2 hours to provide some assessment of precipitation and grain size changes which may occur after coiling, and then air cooled to ambient temperature.

Samples, as heat treated above, were analysed for vanadium nitride and then prepared for ferrite grain size measurements. The average ferrite grain size was measured from the optical micrographs by the linear intercept method. The samples were then normalized at

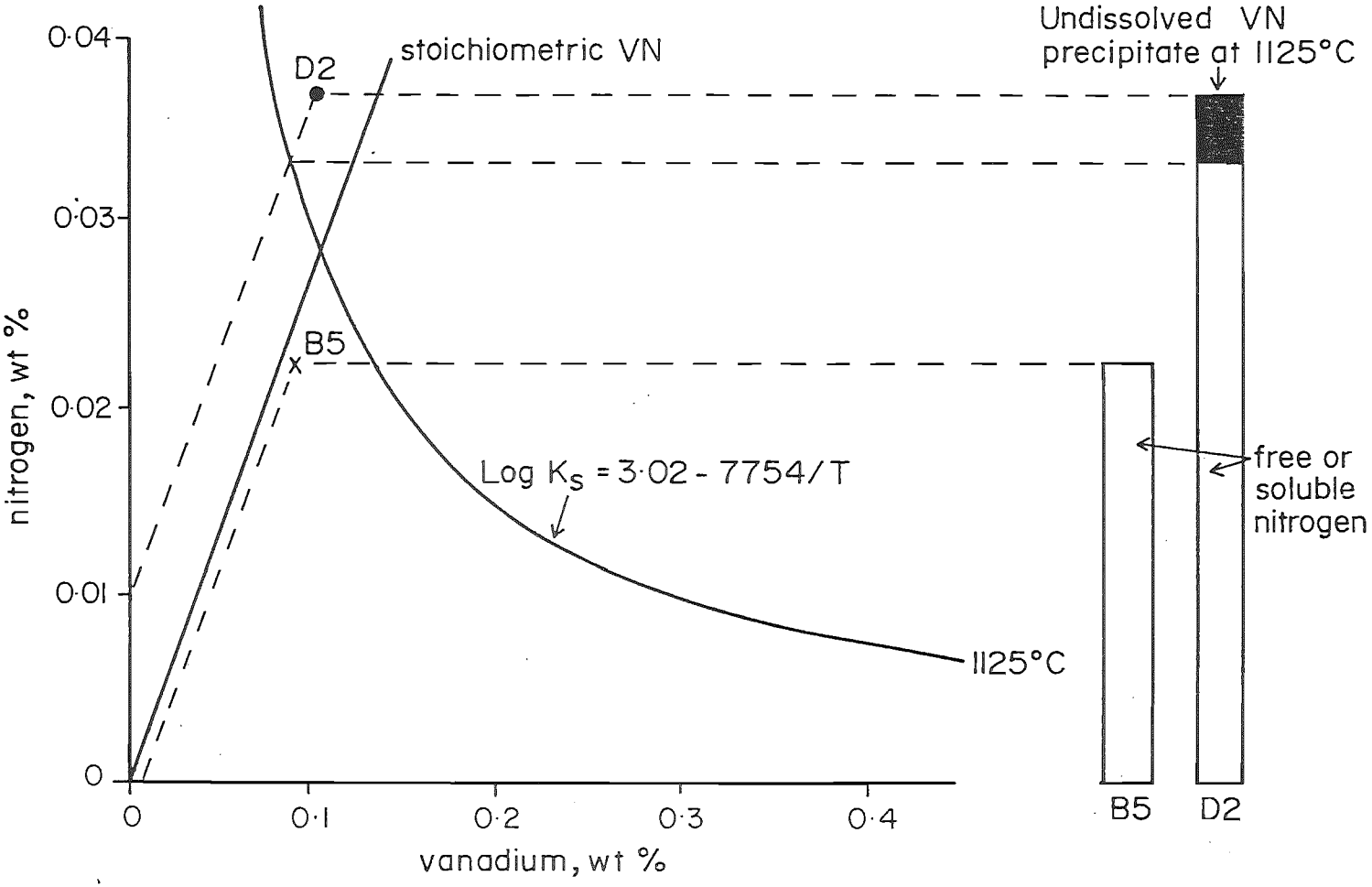

Figure 5.4: The relationship between solubility and precipitation of VN

900°C for 1 hour and the vanadium nitride content and average ferrite grain size again measured.

5.4.2 Chemical Analysis

The standard chemical method[94] was used to determine the nitrogen combined as vanadium nitride during the simulated heat treatment. In this analysis technique the sample is divided into two fractions after dissolution in dilute (20%) sulphuric acid. Nitrogen in each fraction is converted into ammonia and extracted from the solution by steam distillation. The nitrogen content is determined photometrically using Nessler's regent. The part of nitrogen determined on the sample which was insoluble in dilute sulphuric acid (N_{insol}) was assumed to be vanadium nitride. This has been proved by Konig et al [111].

The resultant nitrogen determination of the simulated heat treated sample is given in Table 5.2. The details of the method used for the nitrogen determination is given in Appendix A.

5.4.3 Grain Size Measurements

The 'effective ferrite grain size' was estimated in accordance with the ASTM standards (Designation E112-87). The linear intercept method was used for the determination, considering the steels to be of two phases (i.e. ferrite and pearlite). This method essentially consists of the following procedure:

(a) Drawing a set of parallel straight lines on a photomicrograph of known magnification.

(b) Determining the total length of these lines which fall in the ferrite area.

Table 5.2: Nitrogen analysis results for the simulated heat treated steels D2 and B5

SIMULATED COILING TEMP. °C	NITROGEN %	D2			B5		
		1/2 hr	1 hr	2 hr	1/2 hr	1 hr	2 hr
600	SOL 1	0.0298	0.0278	0.0278	0.0174	0.0164	0.0157
	INSOL 1	0.0072	0.0087	0.0099	0.0046	0.0051	0.0066
	TOTAL:	0.0370	0.0365	0.0377	0.0220	0.0215	0.0223
	SOL 2	0.0304	0.0293	0.0278	0.0176	0.0181	0.0163
	INSOL 2	0.0068	0.0082	0.0102	0.0049	0.0049	0.0064
	TOTAL:	0.0372	0.0375	0.0380	0.0225	0.0230	0.0227
650	SOL 1	0.0272	0.0263	0.0229	0.0150	0.0148	0.0132
	INSOL 1	0.0098	0.0112	0.0133	0.0082	0.0087	0.0095
	TOTAL:	0.0370	0.0375	0.0362	0.0232	0.0235	0.0227
	SOL 2	0.0265	0.0277	0.0250	0.0138	0.0133	0.0133
	INSOL 2	0.0095	0.0100	0.0125	0.0082	0.0086	0.0097
	TOTAL:	0.0360	0.0377	0.0375	0.0220	0.0219	0.0230
700	SOL 1	0.0263	0.0244	0.0221	0.0126	0.0114	0.0103
	INSOL 1	0.0117	0.0135	0.0149	0.0100	0.0106	0.0122
	TOTAL:	0.0380	0.0379	0.0370	0.0226	0.0220	0.0225
	SOL 2	0.0260	0.0240	0.0224	0.0132	0.0117	0.0099
	INSOL 2	0.0115	0.0137	0.0149	0.0099	0.0108	0.0120
	TOTAL:	0.0375	0.0377	0.0373	0.0231	0.0225	0.0219
750	SOL 1	0.0327	0.0307	0.0298	0.0161	0.0174	0.0155
	INSOL 1	0.0052	0.0058	0.0082	0.0066	0.0046	0.0062
	TOTAL:	0.0379	0.0365	0.0380	0.0227	0.0220	0.0217
	SOL 2	0.0324	0.0315	0.0296	0.0168	0.0180	0.0157
	INSOL 2	0.0047	0.0057	0.0080	0.0062	0.0050	0.0064
	TOTAL:	0.0371	0.0372	0.0376	0.0230	0.0230	0.0221
800	SOL 1	0.0351	0.0345	0.0344	0.0215	0.0204	0.0206
	INSOL 1	0.0020	0.0021	0.0028	0.0016	0.0020	0.0023
	TOTAL:	0.0371	0.0366	0.0372	0.0231	0.0224	0.0229
	SOL 2	0.0360	0.0342	0.0355	0.0211	0.0208	0.0215
	INSOL 2	0.0020	0.0023	0.0026	0.0018	0.0019	0.0022
	TOTAL:	0.0380	0.0365	0.0381	0.0229	0.0227	0.0237

Cont'd...

Table 5.2: (Continued)

SIMULATED COILING TEMP. °C	NITROGEN %	D2			B5		
		1/2 hr	1 hr	2 hr	1/2 hr	1 hr	2 hr
850	SOL 1	0.0350	0.0337	0.0337	0.0197	0.0204	0.0210
	INSOL 1	0.0031	0.0029	0.0032	0.0021	0.0026	0.0025
	TOTAL:	0.0381	0.0366	0.0389	0.0218	0.0230	0.0235
	SOL 2	0.0342	0.0348	0.0345	0.0200	0.0203	0.0204
	INSOL 2	0.0029	0.0028	0.0033	0.0020	0.0024	0.0025
	TOTAL:	0.0371	0.0376	0.0378	0.0220	0.0227	0.0229
900	SOL 1	0.0347	0.0340	0.0327	0.0204	0.0189	0.0202
	INSOL 1	0.0035	0.0035	0.0045	0.0024	0.0028	0.0027
	TOTAL:	0.0382	0.0375	0.0372	0.0228	0.0217	0.0229
	SOL 2	0.0336	0.0349	0.0330	0.0212	0.0187	0.0201
	INSOL 2	0.0034	0.0037	0.0047	0.0026	0.0029	0.0030
	TOTAL:	0.0370	0.0386	0.0377	0.0238	0.0216	0.0231
950	SOL 1	0.0347	0.0325	0.0315	0.0195	0.0189	0.0193
	INSOL 1	0.0035	0.0036	0.0055	0.0030	0.0030	0.0034
	TOTAL:	0.0382	0.0361	0.0370	0.0225	0.0219	0.0227
	SOL 2	0.0335	0.0328	0.0325	0.0202	0.0192	0.0194
	INSOL 2	0.0036	0.0038	0.0056	0.0029	0.0031	0.0035
	TOTAL:	0.0371	0.0366	0.0381	0.0231	0.0223	0.0229

Table 5.3(a): Ferrite grain size (after simulated hot rolling thermal cycle treatment).

Simulated Coiling Temperature, °C	Ferrite Grain Size, μm					
	Cast D2			Cast B5		
	1/2 hr	1 hr	2 hrs	1/2 hr	1 hr	2 hrs
600	18.1	20.0	22.1	22.2	23.4	24.3
650	19.2	21.4	24.3	21.5	25.2	27.7
700	19.5	24.3	26.4	23.3	24.8	32.8
750	21.7	24.5	30.7	25.8	29.3	36.8
800	23.8	28.6	32.7	26.4	32.2	37.2
850	25.2	30.0	33.6	28.5	34.2	39.8
900	25.7	30.8	35.3	29.2	33.8	39.8
950	26.5	31.8	36.8	28.4	34.9	41.8

Table 5.3(b): Ferrite grain size (normalized after the simulated hot rolling thermal cycle treatment.

Simulated Coiling Temperature, °C	Ferrite Grain Size, μm					
	Cast D2			Cast B5		
	1/2 hr	1 hr	2 hrs	1/2 hr	1 hr	2 hrs
600	6.5	5.9	5.2	7.3	7.1	6.3
650	6.2	5.2	4.6	6.6	6.8	5.7
700	5.9	4.8	4.1	6.4	6.0	5.2
750	7.6	6.1	6.2	7.9	6.3	6.5
800	8.3	6.4	6.7	8.9	7.3	7.2
850	8.0	5.9	5.8	8.7	7.2	6.7
900	7.9	5.8	5.5	8.4	6.7	6.3
950	7.8	5.6	5.4	8.2	6.4	6.0

(c) Determining the number of intercepts made in the ferrite area by these lines.

(d) From (b) and (c), and the magnification the mean intercept length is calculated and the 'effective ferrite grain diameter' is determined from this length.

Ferrite grain size estimations were made in the steels D2 and B5 for simulated heat treated and normalized conditions. Results are given in Table 5.3.

5.5 DISCUSSION OF RESULTS

5.5.1 Vanadium Nitride Precipitation

Figure 5.5 shows the variation in nitrogen precipitated as vanadium nitride with simulated coiling temperature (the second furnace temperature) in steels D2 and B5. It can be seen from this figure that the simulated coiling temperature and the holding time at this temperature have a strong effect on the precipitation of vanadium nitride. However, the effect of undissolved precipitates at the re-heating furnace temperature 1125°C (the first furnace temperature) on the precipitation of vanadium nitride is insignificant. In all three different holding time cases (30 minutes, 1 hour, and 2 hours) the vanadium nitride precipitation shows the same trend in the two steels D2 and B5 for the full simulated coiling temperature range.

It can be seen from Figure 5.5 that vanadium nitride precipitation peaks at a simulated coiling temperature of about 700°C and decreases sharply above and below this temperature. The vanadium nitride precipitation is a minimum at a simulated coiling temperature

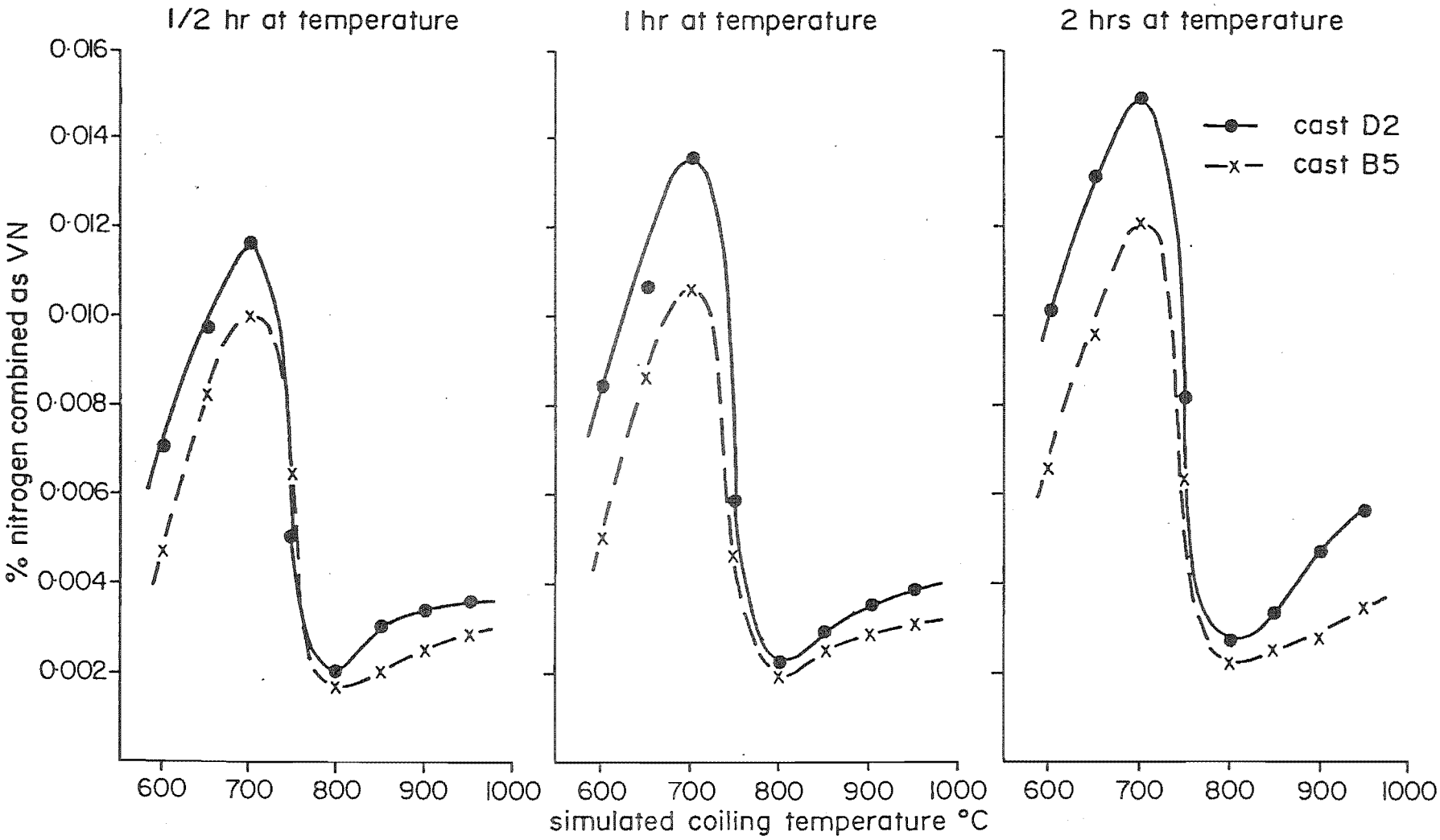

Figure 5.5: Precipitation of VN in steels D2 and B5

of 800°C, and although the precipitated vanadium nitride again increases at simulated coiling temperatures of above 800°C it does not, even at 950°C, match the amount precipitated at 700°C after holding at coiling temperature for 2 hours. The vanadium nitride precipitation peaks at 700°C coincides with the minimum temperature at which austenite exists in the structure (i.e. Ac_1 temperature for 1.3% Mn steels).

There are two possible explanations which can be given for the vanadium nitride precipitation peak at 700°C.

(1) As is shown in Figure 5.6, the solubility drop of vanadium nitride associated with the austenite/ferrite phase transformation [121]. The solubility product for vanadium nitride is given by:

In α - iron [107]:

$$\text{Log } K_S = 2.45 - 7830/_T \qquad \text{Eqn.5.1}$$

In γ - iron (present work):

$$\text{Log } K_S = 3.02 - 7754/_T \qquad \text{Eqn.5.2}$$

(2) The difference in diffusion coefficient of nitrogen in austenite and ferrite. The diffusion coefficient of nitrogen in α and γ iron is given by[120]:

In α - iron:

$$D_N^{\alpha} = 0.0066 \exp \left[- \frac{18600}{RT} \right] \text{ cm}^2/\text{s} \qquad \text{Eqn.5.3}$$

In γ - iron:

$$D_N^{\gamma} = 0.019 \exp \left[- \frac{28300}{RT} \right] \text{ cm}^2/\text{s} \qquad \text{Eqn.5.4}$$

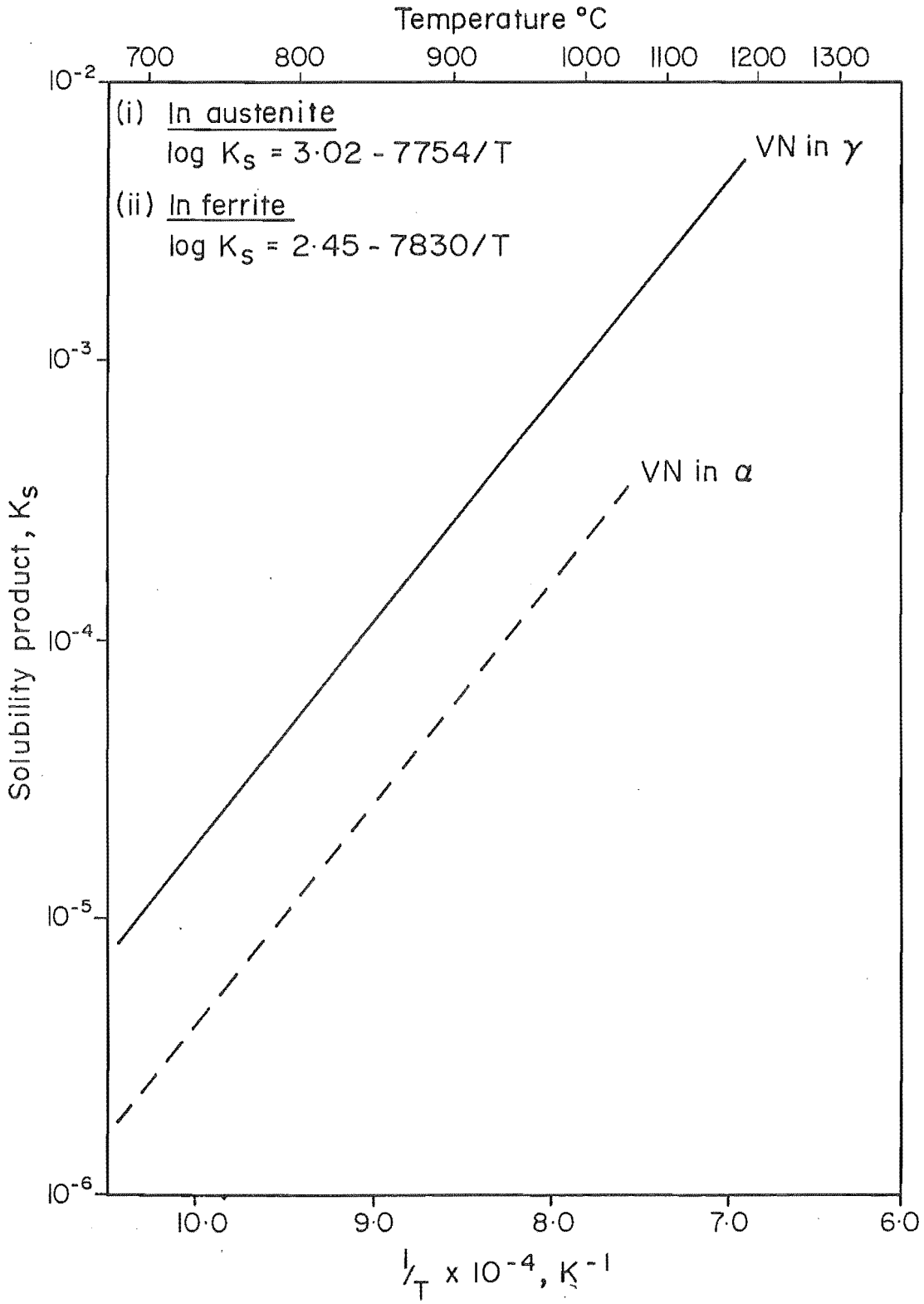

Figure 5.6: Solubility product for vanadium nitride in α and γ iron

The vanadium nitride precipitation peak occurring at 700°C appears to be controlled by diffusion in ferrite rather than by the decreased solubility of vanadium nitride in ferrite. It can be shown from equations 5.3 and 5.4 that the diffusion coefficient for nitrogen in ferrite at 700°C is about 53 times that for nitrogen in austenite at the same temperature [120]. The total weight of vanadium nitride detected as insoluble nitrogen will be the sum of precipitated vanadium nitride in both the ferrite and austenite phases. If appreciably more precipitate forms in ferrite relative to austenite, the nitrogen combined as vanadium nitride will largely depend on the volume fraction of ferrite phase. This will approach maximum at about 700°C for 1.3% Mn steels, giving a corresponding maximum in vanadium nitride precipitation, despite the higher diffusion rate of nitrogen in the ferrite formed at higher temperatures.

At simulated coiling temperatures below 700°C, there would not be any significant change in the volume fraction of ferrite phase. Since the weight percentage of nitrogen combined as vanadium nitride decreases rapidly at simulated coiling temperatures below 700°C, precipitation of vanadium nitride must again be controlled by diffusion as opposed to vanadium nitride solubility. If the vanadium nitride precipitation is controlled by solubility of vanadium nitride, the amount of nitrogen combined as vanadium nitride (vanadium nitride precipitated) should increase with decreasing temperature. Diffusion control in the ferrite temperature range is also confirmed by increased vanadium nitride precipitated with 'coil' temperature holding time.

The amount of nitrogen precipitated as vanadium nitride decreases sharply at simulated coiling temperatures above 700°C and reaches a minimum at 800°C. Although the rate of precipitation increases again with higher simulated coiling temperatures, precipitation of vanadium nitride throughout the austenite range is slow. Even at 900°C the amount of vanadium nitride precipitated is less than 20% of the amount predicted from the equilibrium solubility curve in Figure 5.3. These results indicate that the precipitation of vanadium nitride in the austenite temperature range is also controlled by diffusion and not by the decreased solubility of vanadium nitride, since the diffusion rate decreases with decreasing temperature. On the other hand, if the solubility of vanadium nitride was the controlling factor, the decreasing solubility with decreasing temperature should cause increased vanadium nitride precipitation, as the temperature decreased, which is not the case.

Konig et al [111] studied precipitation of aluminium and vanadium nitrides in microalloyed structural steels. In this investigation samples were solution treated at 1350°C for 2 hours and were then transferred immediately to a furnace maintained at the required precipitation temperature, so that the precipitation took place at approximately constant temperature. The samples were then quenched into water after holding for 1 hour, 3 hours and 6 hours at the precipitation temperature. The amount of nitrogen combined as vanadium nitride and aluminium nitride was determined by chemical analysis and the results are shown in Figure 5.7.

The results obtained in the present work are in good agreement with the results obtained by Konig et al[111]. In both cases peak

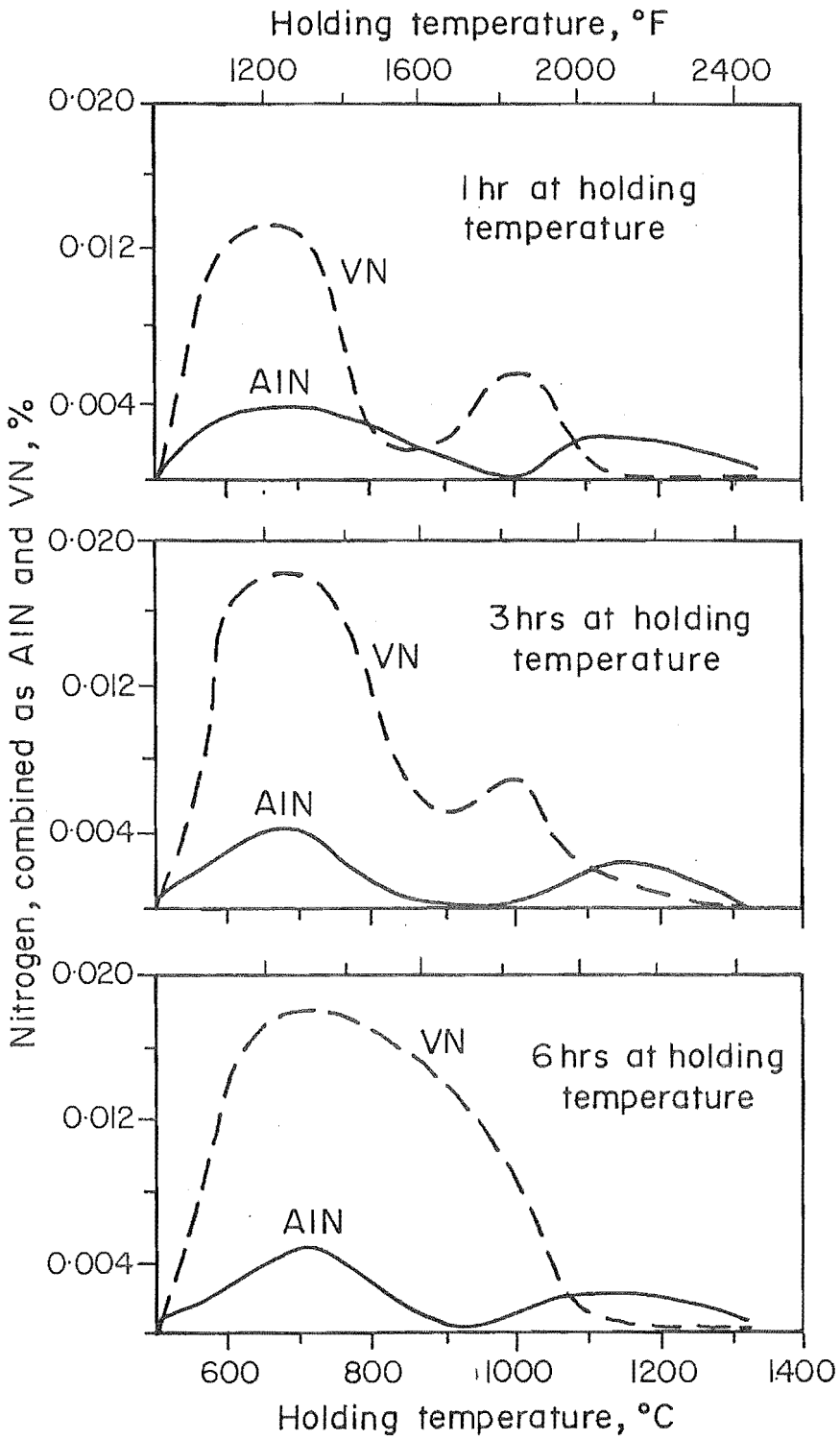

Figure 5.7: Precipitation of vanadium and aluminium nitrides in 0.2%C, 1.5%Mn, 0.14%V, 0.01%Aℓ, 0.0240%N steel. (Konig et al, Ref 111.)

vanadium nitride precipitation occurred at a holding temperature of 700°C and the vanadium nitride precipitation drops above and below this temperature with minimum precipitation at 800°C. Konig et al[111] carried out their work for a wide range of holding temperatures, up to 1350°C and found that there was a second peak of vanadium nitride precipitation occurring at a holding temperature of 1000°C for holding times of 1 hour and 3 hours. This second peak precipitation disappeared when the holding time was extended to 6 hours at temperature.

With shorter holding times (1 hour and 3 hours) a second peak of vanadium nitride precipitation occurred at 1000°C in the austenite region. However, this peak disappeared when sufficient time was available to approach equilibrium vanadium nitride precipitation. This suggests that the precipitation of vanadium nitride in austenite is controlled by nitrogen diffusion at lower temperatures and shorter holding times, but at higher temperatures and longer holding times the solubility of vanadium nitride becomes more significant.

It also appears from Figure 5.5 that undissolved precipitate at the reheating furnace temperature (1125°C) has no effect on the precipitation of vanadium nitride at the simulated coiling temperatures.

Erasmus[122] studied precipitation of aluminium nitride in a 0.53% carbon steel and suggested that the undissolved initial precipitates act as centres for subsequent precipitation at lower temperatures. It can be seen from Figure 5.5 that the difference between the amount of nitrogen precipitated as vanadium nitride in steels D2 and B5 is equal to or less than the initial 0.0030% nitrogen

as vanadium nitride for the full range of coiling temperatures studied.

5.5.2 Ferrite Grain Size

The ferrite grain size of microalloyed steels is controlled by the prior austenite grain size and by any ferrite grain growth which occurs after transformation. Austenite grains recrystallise during rolling and their size (and hence the resulting ferrite grain size) will be determined by the amount of deformation given to the steel, the temperature at which deformation occurs and the time allowed for recrystallisation[124].

In the case of thin plates and strips which are rolled on continuous or semi-continuous multi-stand mills, the time between successive deformation can be shorter than the time required for austenite grain to recrystallise. The final austenitic and hence ferritic, grain sizes will then be determined by the finishing rolling temperature at the last stand of the mill, the rate of cooling down to the transformation temperature on the runout table and the coiling temperature.

5.5.2.1 Ferrite Grain Size, After Simulated Hot Rolling Thermal Cycle Treatment.

Figure 5.8 shows the ferrite grain size of samples subjected to the simulated thermal cycle. In both steels D2 and B5, the ferrite grain size increases with the simulated coiling temperature. The ferrite grain size is significantly coarser than that normally expected in High Strength Low Alloy steels microalloyed with vanadium and nitrogen. This is due to the fact that there was no mechanical deformation subsequent to reheating at 1125°C for 4 hours and

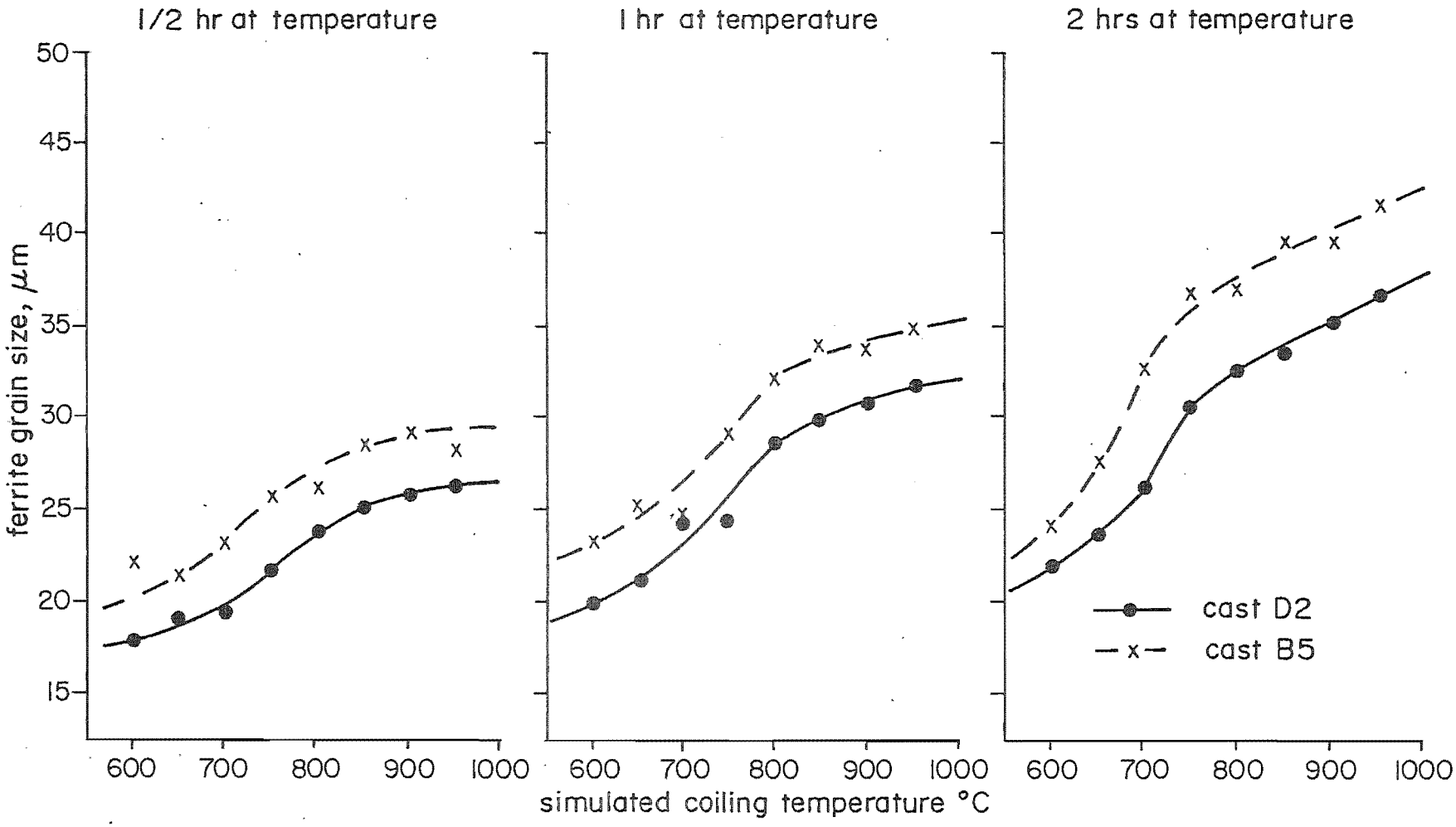

Figure 5.8: The variation of ferrite grain size with simulated coiling temperature

therefore initial austenite grain size would be coarse for all simulated coiling temperatures.

It is possible that the grain refinement induced by vanadium is due to retardation of austenite recrystallisation. This is because there are more high energy sites for the nucleation of ferrite grains in elongated unrecrystallised austenite grains. Cordea[123] suggested that the two principal causes of this retardation were:

(1) Vanadium in solid solution slowing down the migration rate of grain boundaries.

(2) Precipitation of vanadium nitride on sub-grain boundaries retarding sub-grain growth.

It is likely that the second mode will be favoured only at high mechanical deformation leading to strain-induced precipitation.

It was also identified that most of the vanadium nitride precipitation had taken place in ferrite, after the transformation, not in the austenite phase. The vanadium nitride precipitate formed in ferrite does not produce grain refinement, but the precipitates formed in the austenite inhibit grain growth by grain boundary pinning. The difference in grain size between steels D2 and B5 is consistent with impeded austenite grain coarsening from the 0.0030% of nitrogen precipitated as vanadium nitride in steel D2 at the reheat furnace temperature. This undissolved precipitate may exert a more important effect on grain size when combined with hot working.

It is seen from Figure 5.8, that there is some coarsening of grain size with increased holding time for all simulated coiling temperatures. This indicates continued grain coarsening with holding time in both ferrite and austenite despite the corresponding increase in vanadium nitride precipitation, see Figure 5.10. There is, however, a significant decrease in grain size at coiling temperatures below 750°C. Since cooling through the austenite-ferrite transformation range would be more rapid in those samples held at 'coiling' temperatures in the austenite temperature range, this reduction in ferrite grain size must be precipitate related and dependent on the vanadium nitride precipitate formed in the ferrite phase.

5.5.2.2 Ferrite Grain Size Of Steels D2 And B5, Normalized After The Simulated Hot Rolling Thermal Cycle Treatment.

Figure 5.9 shows the ferrite grain size of samples normalized at 900°C after the simulated thermal cycle. It is seen from this figure that the ferrite grain size is considerably reduced after normalizing and now lies within the range normally expected for High Strength Low Alloy Steels. When the samples were normalized at 900°C after the simulated thermal cycle, there would be a large volume fraction of undissolved precipitate in austenite at 900°C. This undissolved precipitate would refine the austenite grains by grain boundary pinning. The ferrite grain size of normalized steels is largely a function of the austenite grain size prior to transformation, as this determines the number of high energy sites available for nucleating ferrite. Hence the resultant ferrite grain size will be fine.

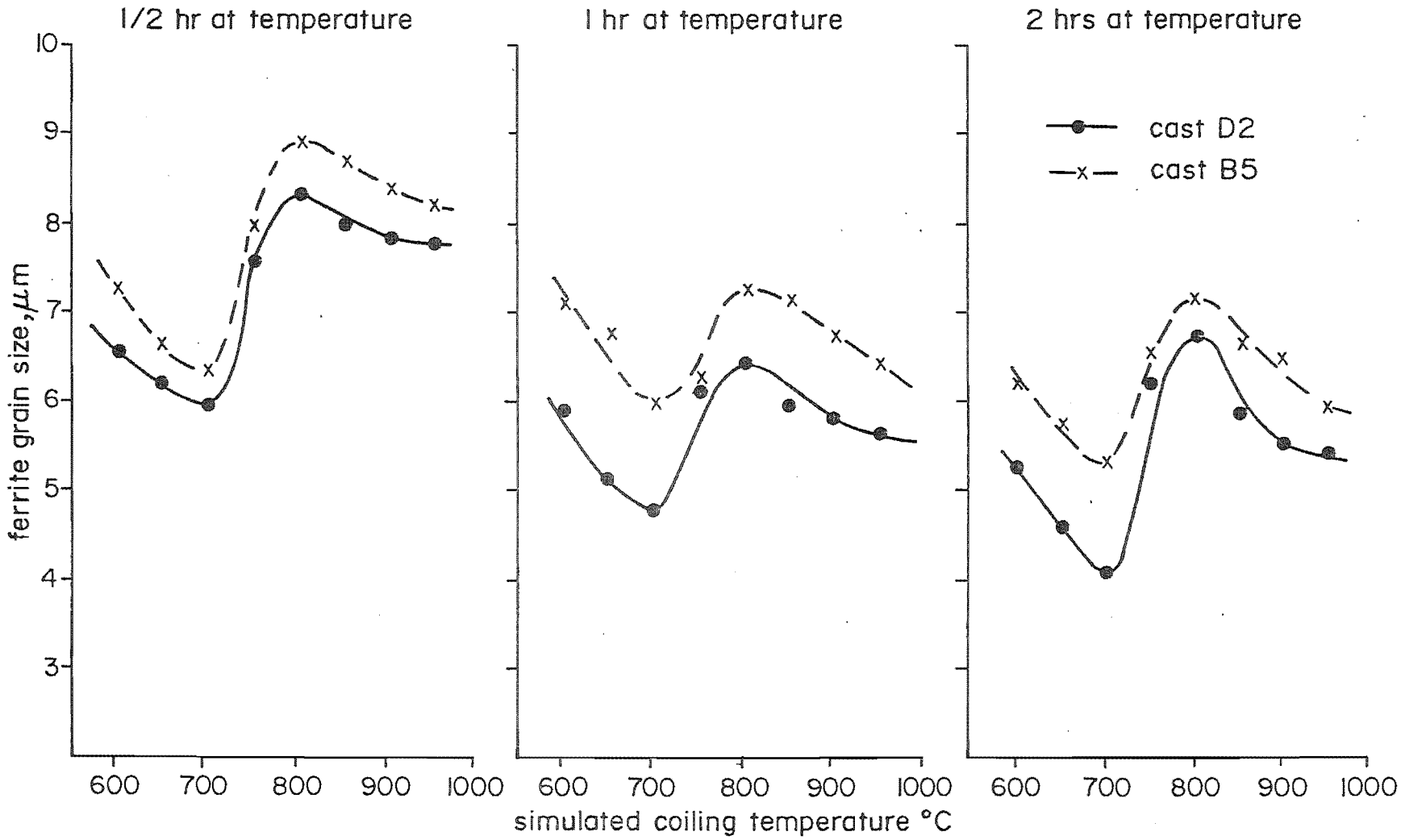

Figure 5.9: The effect of simulated coiling temperature on the normalised ferrite grain size

As can be seen from Figure 5.10, the vanadium nitride precipitated during the simulated thermal cycle has a strong effect on ferrite grain size after normalizing. There is a consistent sharp increase in grain size for a simulated coiling temperature of 750°C. The minimum grain size corresponds to the peak in precipitated vanadium nitride formed in the ferrite phase during the simulated hot rolling thermal cycle at 700°C. Analysis for nitrogen precipitated as vanadium nitride on the normalized samples gave an almost constant value, which is greater than that predicted by the equilibrium solubility of vanadium nitride for all simulated coiling temperatures (e.g. 0.0155% in steel B5, equilibrium prediction from Figure 4.2 gives 0.0145%). This shows that the precipitation of vanadium nitride is rapid on reheating to normalizing temperature. Although the volume fraction of precipitated vanadium nitride remains constant in normalized samples for all simulated coiling temperatures, the volume fraction of vanadium nitride precipitated in ferrite at the simulated coiling temperature continues to influence the grain size after normalizing. This is indicated by the relationship between the ferrite grain size after normalizing and the prior simulated coiling temperatures. The variation of ferrite grain size of the normalized samples is almost a mirror image of the variation in precipitated vanadium nitride during the simulated rolling thermal cycle. Steel D2 has more nitrogen precipitated as vanadium nitride than steel B5 and this is also reflected in the normalized ferrite grain size.

5.6 SUMMARY

The thermal cycle of a hot rolling strip mill has been simulated in the laboratory in order to study the precipitation of

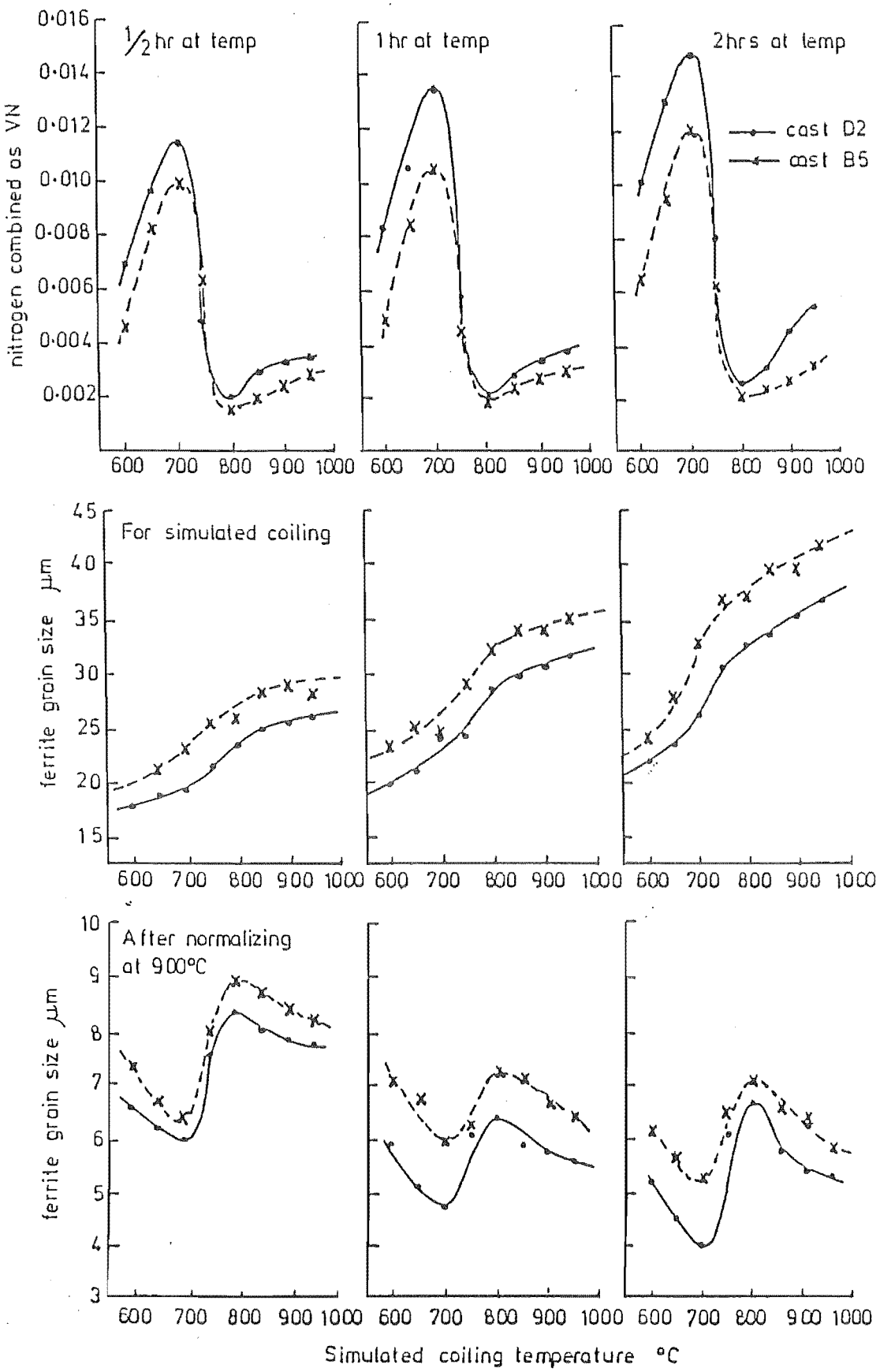

Figure 5.10: Changes in precipitated vanadium nitride; ferrite grain size and ferrite grain size after normalizing for steels D2 and B5

vanadium nitride during hot rolling in HSLA steels microalloyed with vanadium and its effect on the ferrite grain size. The analysis of nitrogen precipitated as vanadium nitride suggests that the precipitation of vanadium nitride is more rapid in the ferrite phase, and is diffusion controlled. Peak precipitation consequently occurs at a simulated coiling temperature of 700°C in the steels D2 and B5 examined. If any interphase vanadium nitride precipitate was formed during the simulated rolling thermal cycle, its volume fraction was too small to be detected by the chemical analysis. Minimum ferrite grain size for the simulated rolling thermal cycle, and for samples subsequently normalized, suggest that vanadium nitride formed in the ferrite phase dominates grain size effects.

CHAPTER 6

EFFECT OF VANADIUM NITRIDE PRECIPITATION ON MECHANICAL PROPERTIES OF HSLA STEELS

6.1 INTRODUCTION

The mechanical properties of as rolled steels are controlled by the grain size, solid solution hardening, and the precipitation of stable nitrides and carbides. Figure 6.1 shows the structural and compositional factors affecting yield strength and impact transition temperature[24]. In microalloyed steels, microalloy additions such as vanadium, aluminium or titanium combined with nitrogen to form stable nitride precipitates during thermomechanical processing. These nitride precipitates may pin grain boundaries or act as nuclei for new grains during phase transformation, thus refining ferrite grain size. This grain refinement substantially increases the yield strength, and also decreases the impact transition temperature. The nitride precipitates also contribute to precipitation hardening and consequently further increase the yield strength. Although the precipitation hardening increases the yield strength, it has an adverse effect on transition temperature. This is clearly illustrated by the vector diagram in Figure 6.1[24].

To avoid the economic disadvantages of aluminium killed steels, grain refinement can be obtained in semi-killed steels with vanadium or niobium additions[25]. Vanadium additions can produce both grain refinement and precipitation strengthening for steels in either the as

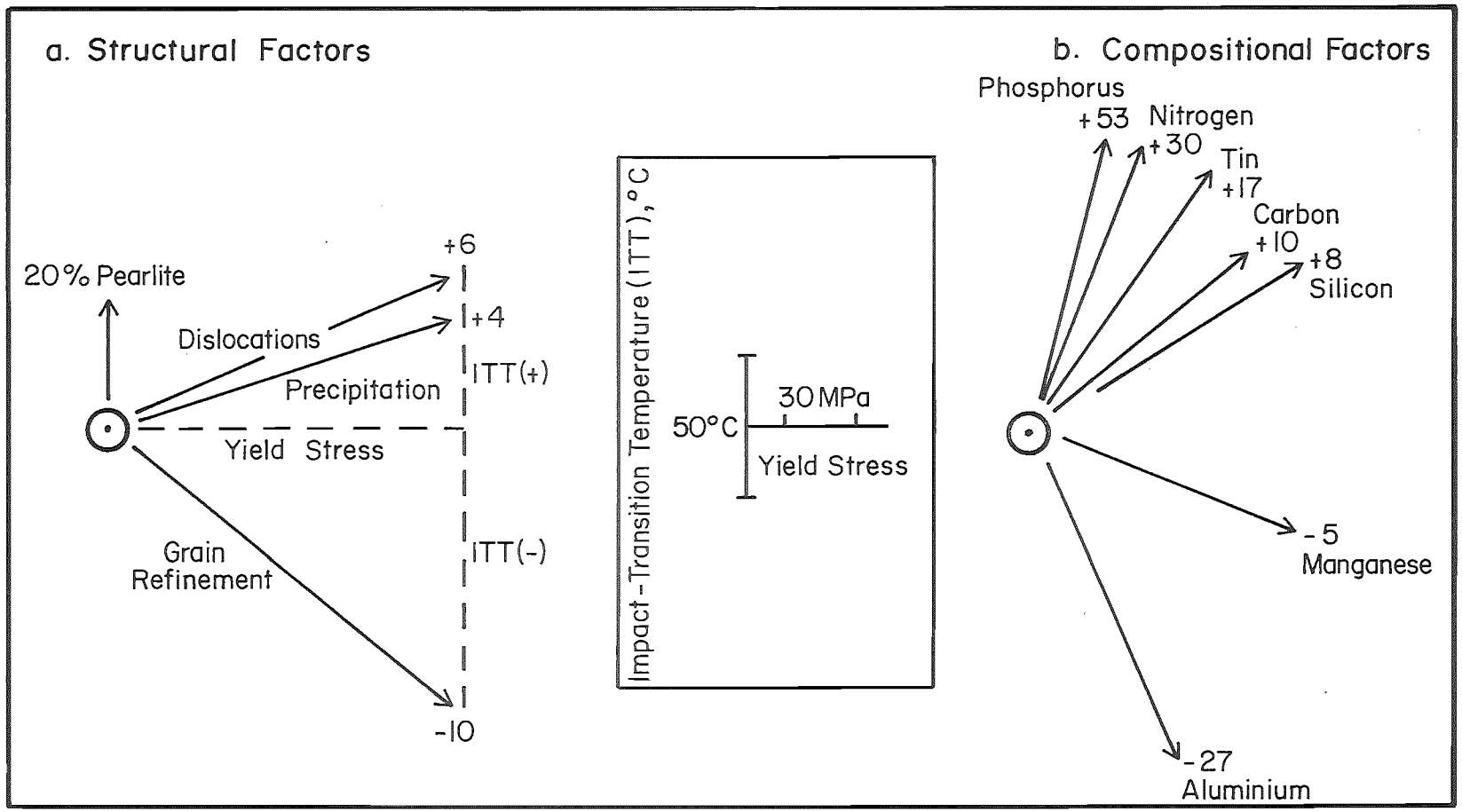

Figure 6.1: Factors affecting yield strength and impact-transition temperature. Ratios indicate the change in transition temperature per 15 MPa increase in yield strength. (Ref.24.)

rolled or normalized conditions[25]. Nitrogen addition to the vanadium microalloyed steels increases the strength still further.

In the present investigation hot rolling temperature profiles were simulated in the laboratory. The effect of vanadium nitride precipitation, occurring during the simulated hot rolling thermal cycle, on the mechanical properties was investigated. The results are discussed in this chapter.

6.2 EXPERIMENTAL STEEL

Steel B5, (0.12% C, 1.33% Mn, 0.30% Si, 0.085% V and 0.0225% N) was chosen to investigate the effect of the simulated thermal cycle vanadium nitride precipitation on the mechanical properties of the steel. The kinetics of vanadium nitride precipitation during the simulated thermal cycle have already been discussed in Chapter 5.

6.3 EXPERIMENTAL PROCEDURE

6.3.1 Simulated Heat Treatment

As described in Chapter 5, the simulation used for the hot rolling thermal cycle comprised the solution treatment of samples in an argon atmosphere at 1125°C for four hours, after which each sample was transferred to a second furnace set at the coiling temperature. Samples were held at different coiling temperature between 600°C and 950°C for two hours, and then air cooled to ambient temperature.

6.3.2 Tensile Testing

Tensile testing was performed on specimens with a diameter of 5 mm and a minimum gauge length of 35 mm, machined from heat treated

20 mm diameter bar. The dimensions of the specimen were based on the dimension of specimen No. 14A in the handbook of Hounsfield Tensometer tensile specimens[125]. However, some modifications to the gauge length and specimen heads were made in order to accommodate the Instron 25 mm gauge length extensometer and the specimen grips on the Instron testing machine. The detailed specimen dimensions are shown in Figure 6.2.

Tensile testing was carried out on a 250 kN Instron universal testing machine using the following specified conditions at ambient temperature:

Cross-head speed	=	0.2 mm/min, giving an approximate strain rate of 1×10^{-4}/sec.
Maximum load range	=	20 kN.
Extensometer sensitivity	=	5 , i.e.: 1% strain on 25 mm gauge length gives 26.25 mm on the load-extension graph.

The 25 mm gauge length Instron strain gauge extensometer was fixed to the gauge length to provide a load-extension curve and the curve was plotted directly on the machine chart recorder.

Tensile tests were carried out on two sets of specimens. One set was in the "simulated hot rolling thermal cycle" heat treatment condition and the second set was normalized from 900°C after the simulated heat treatment. In order to investigate the effect of nitrogen precipitated as vanadium nitride during the simulated heat treatment on strain ageing, both sets of tensile specimens were

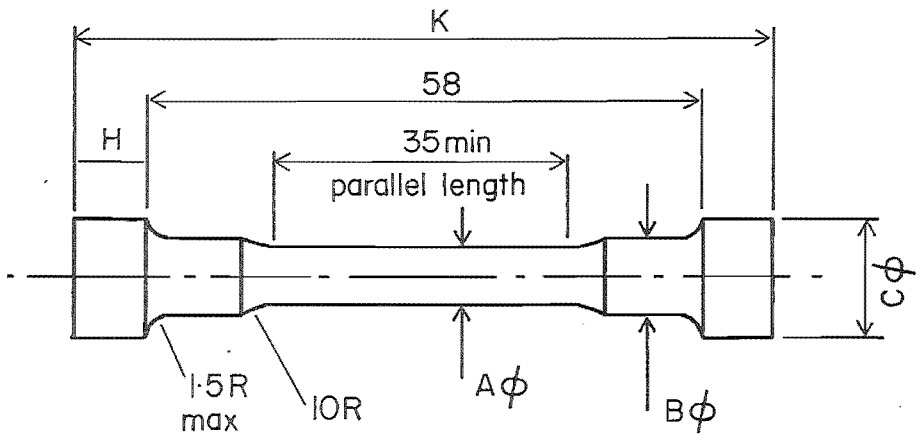

Machining sequence of gauge length

(1) Finish turn to A + 0·2mm dia.
(2) Grind to A + 0·025mm dia.
(3) Finish grind to A in two 0·0125mm cuts

Diameters (mm)			Lengths (mm)	
A	B	C	H	K
5·06 / 5·04	7·15 / 6·80	11·3 / 10·1	8	74

(all dimensions in mm)

Figure 6.2: Details of the tensile specimen.

prestrained to 3%, unloaded and subsequently aged at 100°C for three hours (equal to 293 days at 15°C) before finally testing to fracture. The resultant variation in tensile properties (i.e. lower yield strength and strain ageing parameter, ΔY) were determined from the recorded load-extension curves and are given in Table 6.1(a) and (b).

6.3.3 Charpy V-notch Impact Testing

Subsidiary, 7.5 mm x 10 mm charpy V-notch specimens were machined from two sets of heat treated bar. One set of samples were in the simulated hot rolled condition and the second set of samples were normalized subsequent to the hot rolling simulation.

Impact testing was performed on an Avery impact testing machine with a striking energy of 300 joules and a striker velocity of 5 m/s. For sub-ambient temperature tests the specimens were cooled by immersion in a petroleum ether and dry ice mixture, whilst hot oil was used as the heating medium in elevated temperature tests. A minimum soaking time of 15 minutes at the desired temperature was allowed to ensure temperature homogeneity. The resultant charpy impact transition curves are given in Appendix D. The 27 joules fracture transition temperatures (T_{27}) were obtained from the charpy impact transition curves and are given in Table 6.2

6.4 DISCUSSION OF RESULTS

6.4.1 Effect of simulated coiling temperature on lower yield stress

The variation in lower yield stress with simulated coiling temperature is shown in Figure 6.3. The lower yield stress decreases with increasing coiling temperature in the simulated hot rolled

Table 6.1(a): Variation in tensile properties (simulated hot rolled condition).

Simulated Coiling Temp.°C	Nitrogen, ωt%			Average Ferrite Grain Size μm	$d^{-\frac{1}{2}}$ $mm^{-\frac{1}{2}}$	σ_{LY} MN/m^2	ΔY MN/m^2
	Soluble	Insoluble	Total				
600	0.0158	0.0065	0.0223	24.3	6.42	487	38
650	0.0131	0.0096	0.0227	27.7	6.01	460	34
700	0.0101	0.0121	0.0222	32.8	5.52	403	24
750	0.0157	0.0063	0.0220	36.8	5.21	373	64
800	0.0210	0.0022	0.0232	37.2	5.18	* 343	98
850	0.0206	0.0024	0.0230	39.8	5.01	363	86
900	0.0201	0.0028	0.0229	39.8	5.01	352	82
950	0.0193	0.0034	0.0227	41.8	4.89	332	65

* 0.2% Proof stress

Table 6.1(b): Variation in tensile properties (normalized at 900°C, after the simulated heat treatment).

Simulated Coiling Temp.°C	Nitrogen, ωt%			Average Ferrite Grain Size μm	$d^{-\frac{1}{2}}$ $mm^{-\frac{1}{2}}$	σ_{LY} $MN/m^{\frac{1}{2}}$	ΔY MN/m^2
	Soluble	Insoluble	Total				
600	0.0068	0.0158	0.0226	6.33	12.6	386	78
650	0.0067	0.0157	0.0224	5.66	13.3	389	65
700	0.0069	0.0158	0.0227	5.21	13.9	400	60
750	0.0067	0.0158	0.0225	6.48	12.4	390	75
800	0.0066	0.0157	0.0223	7.22	11.8	378	85
850	0.0068	0.0158	0.0226	6.72	12.2	386	80
900	0.0070	0.0157	0.0227	6.33	12.6	390	75
950	0.0070	0.0158	0.0228	5.97	12.9	398	73

Table 6.2: Charpy Impact test results.

(a) Simulated heat treated condition.

Simulated Coiling Temp. °C	Grain Size μm	$d^{-\frac{1}{2}}$ $mm^{-\frac{1}{2}}$	T_{27} °C
600	24.3	6.42	48
700	32.8	5.52	55
800	37.2	5.18	72
900	39.8	5 01	77

(b) After normalizing at 900°C.

Simulated Coiling Temp. °C	Grain Size μm	$d^{-\frac{1}{2}}$ $mm^{-\frac{1}{2}}$	T_{27} °C
600	6.33	12.6	-43
700	5.21	13.9	-59
800	7.22	11.8	-32
900	6.33	12.6	-38

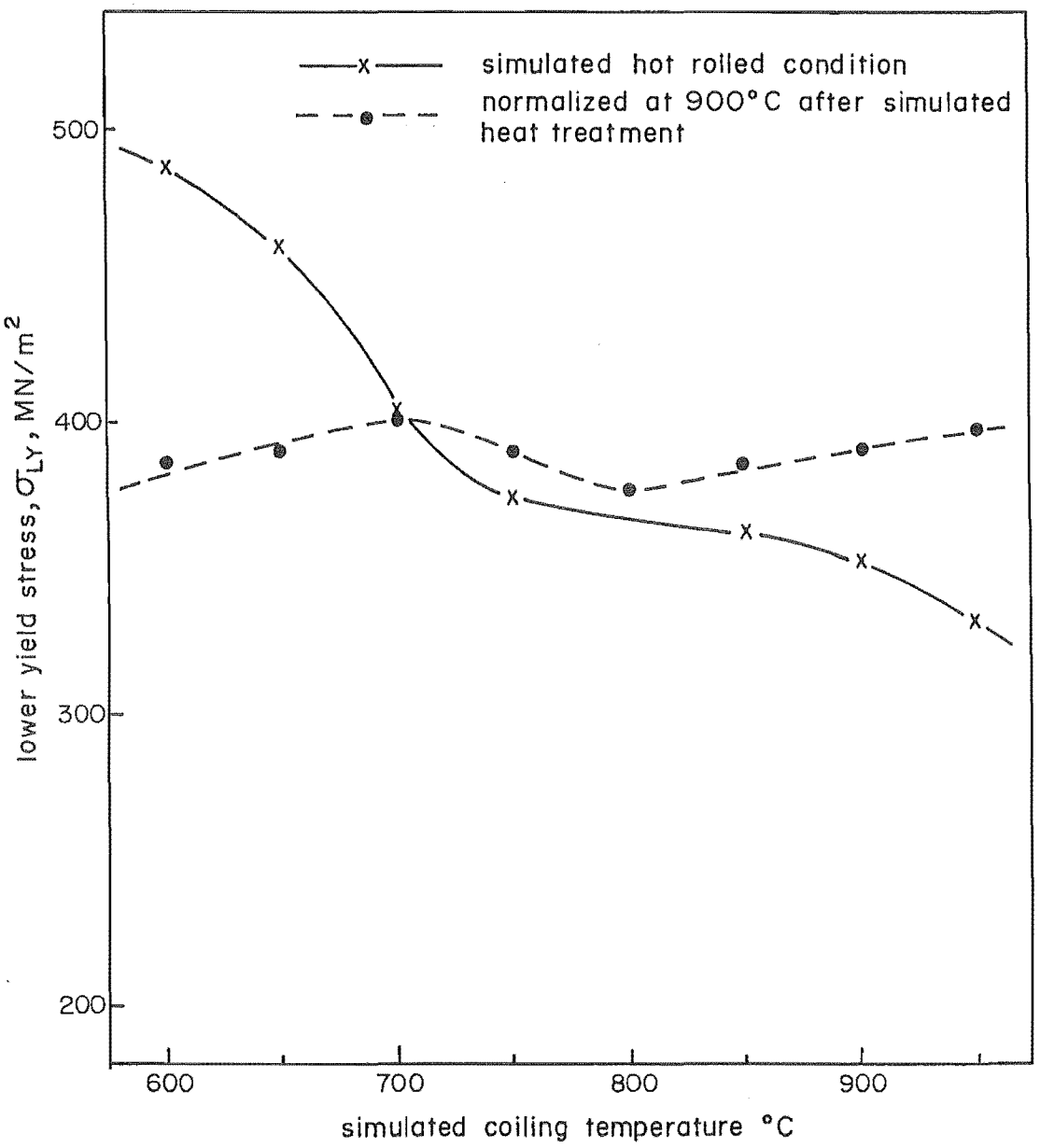

Figure 6.3: Variation in lower yield stress with simulated coiling temperature.

samples, while it remains relatively constant for all simulated coiling temperatures in the normalized samples.

Considering first the simulated hot rolled samples, although the ferrite grain size is significantly coarser than that normally expected in HSLA steels (see Figure 6.4), the yield stress falls within the normally expected range for these steels. It appears then that the yield strength is in this instance mainly dependent on the volume fraction, size and distribution of the vanadium nitride precipitates.

In order to investigate the size and distribution of vanadium nitride precipitates in these simulated hot rolled samples, carbon extraction replicas were prepared and analysed using the TEM. Figures 6.5(a)-(d) shows the precipitates observed in the sample with a simulated coiling temperature of 700°C. Some of these precipitates appear to be rod-like and of 10 nm in diameter, interdispersed with smaller cubic particles of approximately 5 nm in size (see Figures 6.5(a)-(d)). However, at a simulated coiling temperature of 800°C the precipitates appeared to be cubic only and of 10 nm in size, (see Figure 6.6(a)-(d)). It seems then that the vanadium nitride precipitate size increases with increasing simulated coiling temperature. Woodhead et al [130] observed similar changes in vanadium nitride precipitate size in a vanadium-bearing low carbon steel.

As the Ashby-Orowan[86] precipitation strengthening model illustrates in Figure 6.7, a large volume fraction of fine precipitates has a greater precipitation strengthening effect than a smaller volume fraction of coarse precipitates. The relatively large volume fractions of fine vanadium nitride precipitate (for example 0.072% of

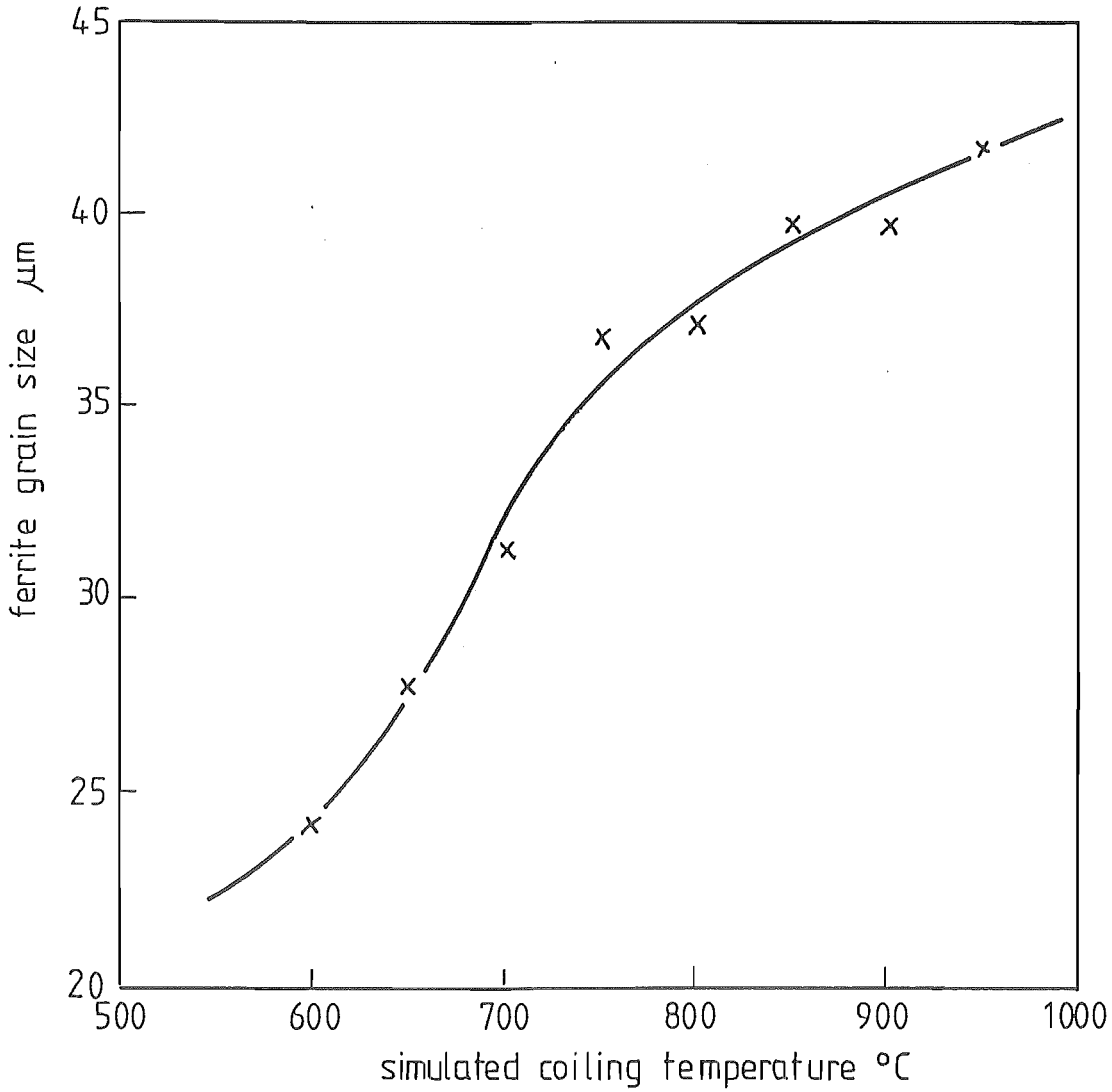

Figure 6.4: Changes in ferrite grain size with simulated coiling temperature (simulated hot rolled condition).

(a)

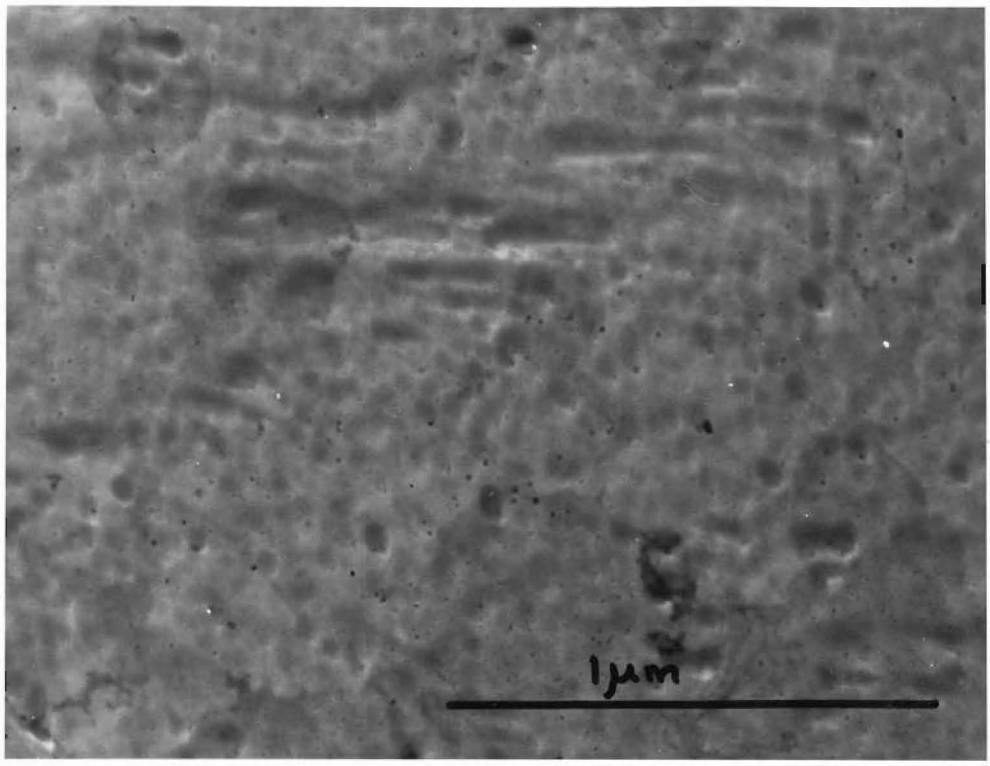

X 65,000

(b)

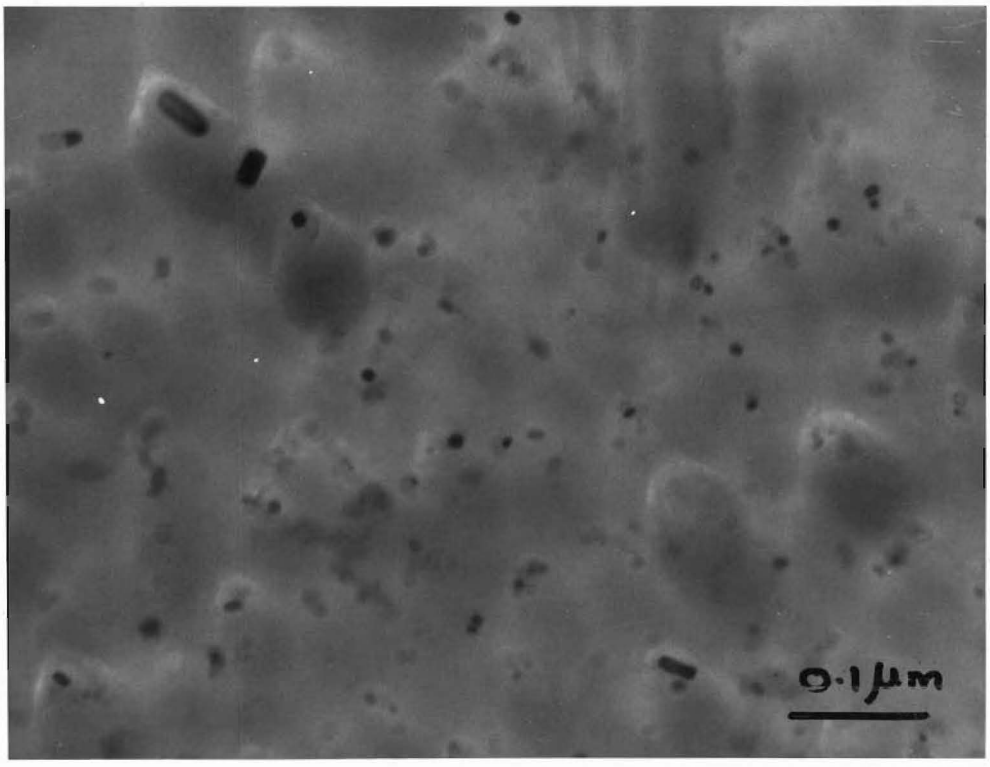

X 180,000

Figures 6.5(a)-(b): Vanadium nitride precipitate morphology in steel B5 at a simulated coiling temperature of 700°C (carbon extraction replica).

(c)

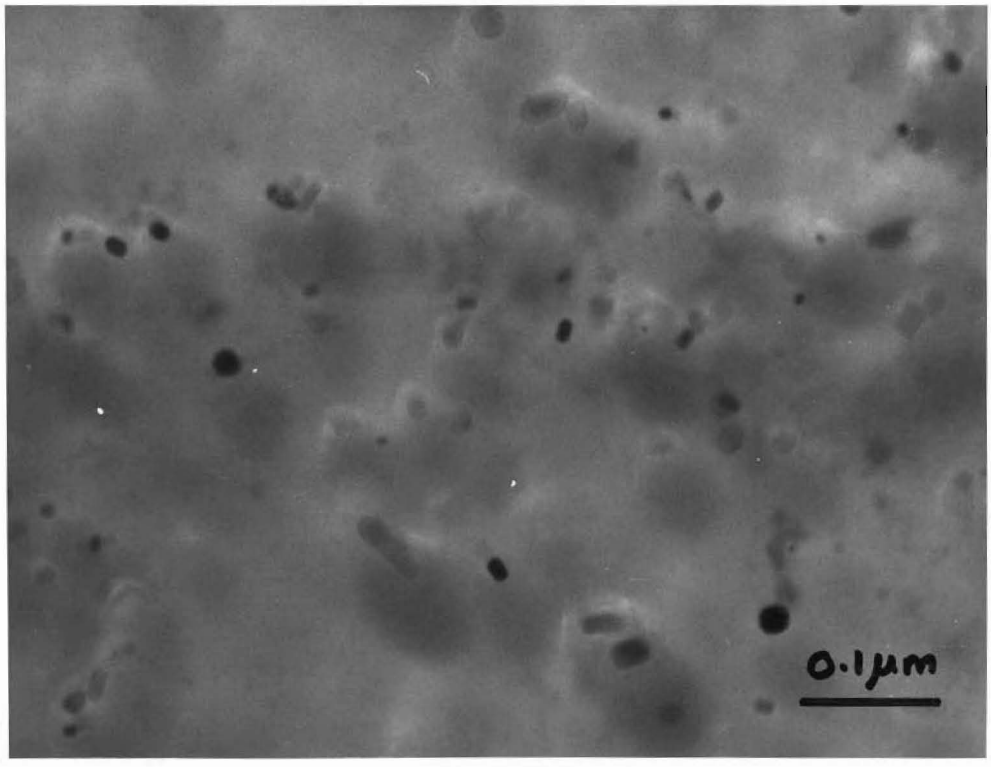

X 180,000

(d)

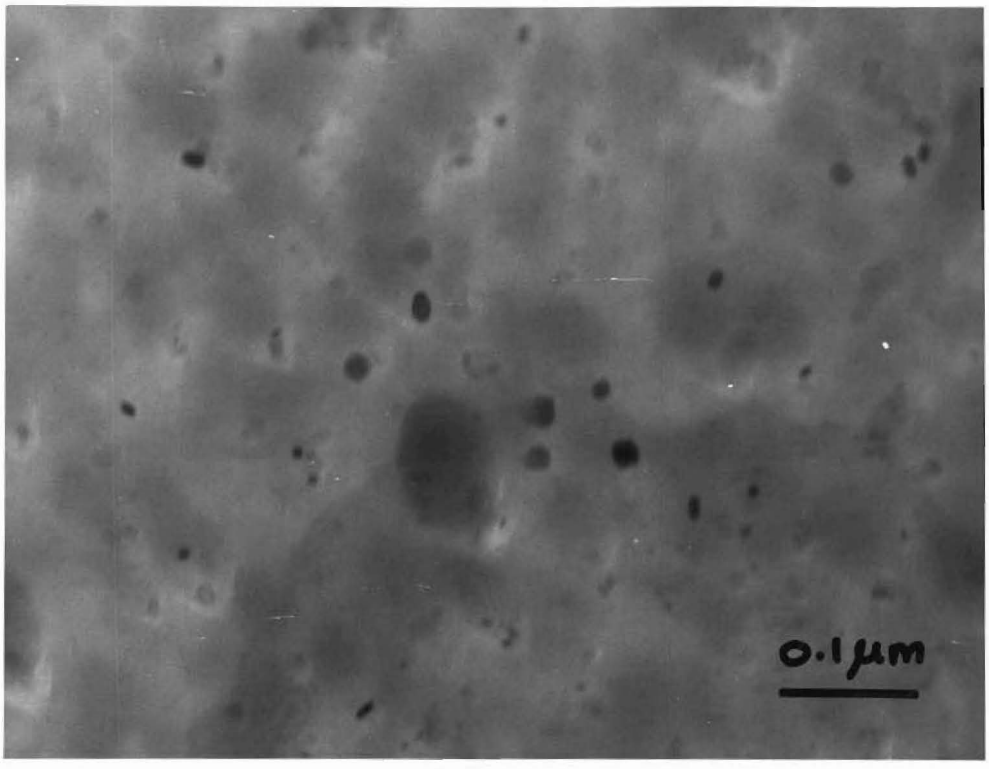

X 180,000

Figures 6.5(c)-(d): Vanadium nitride precipitate morphology in steel B5 at a simulated coiling temperature of 700°C (carbon extraction replica).

(a)

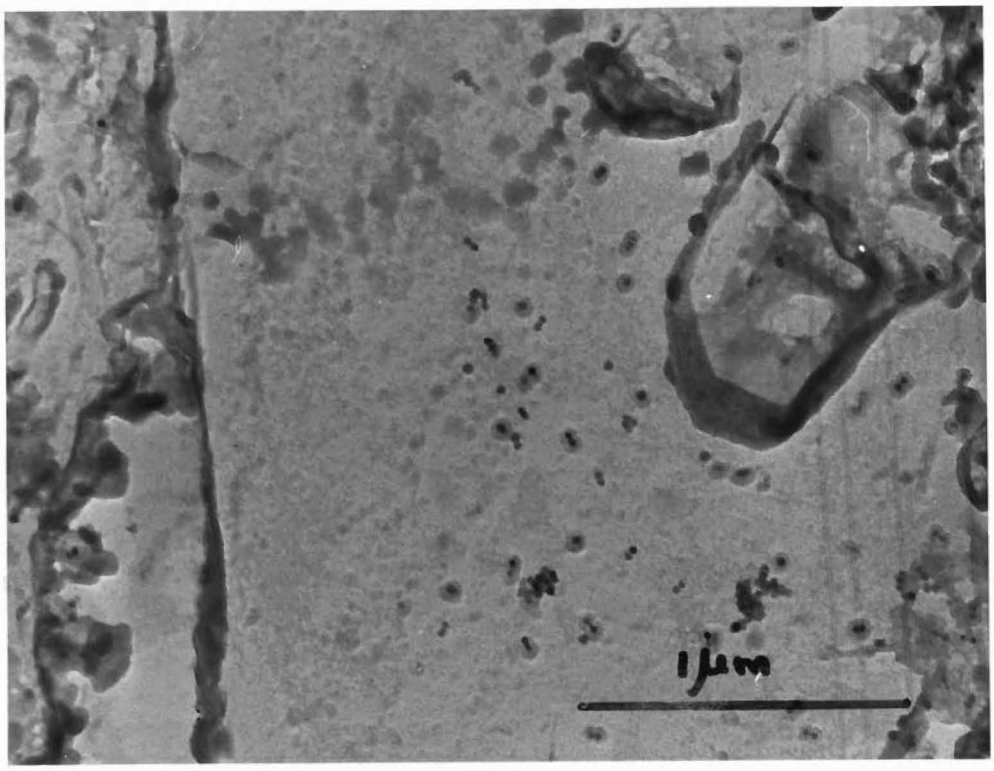

X 44,000

(b)

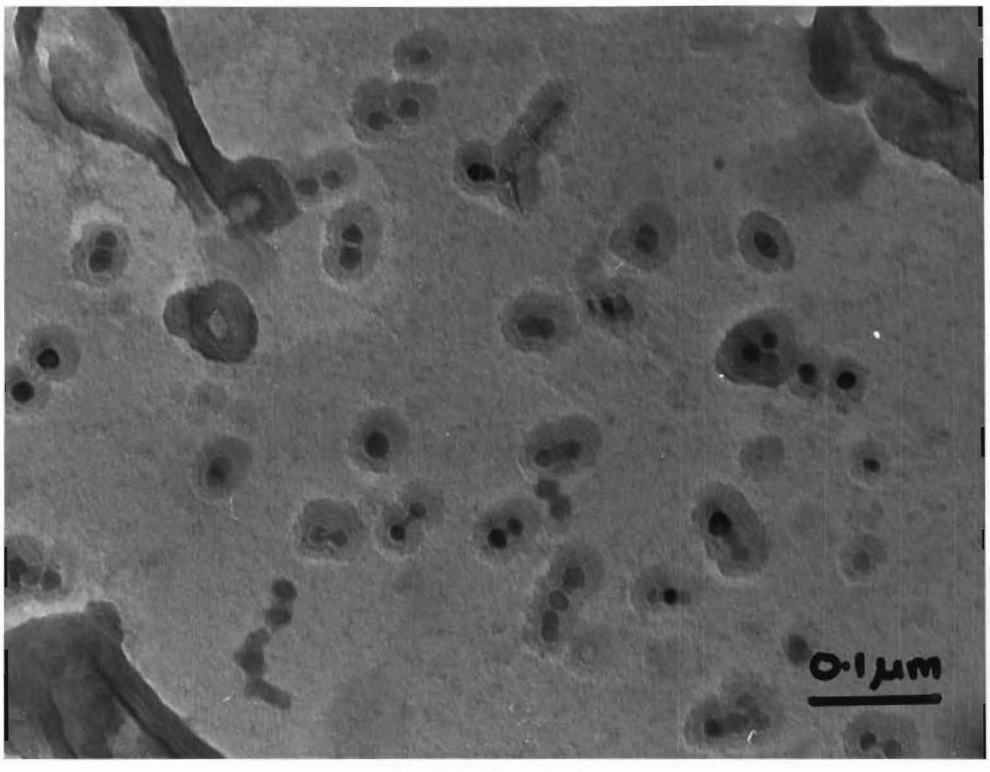

X 180,000

Figure 6.6(a)-(b): Vanadium nitride precipitate morphology in steel B5, at a simulated coiling temperature of 800°C (carbon extraction replica).

(c)

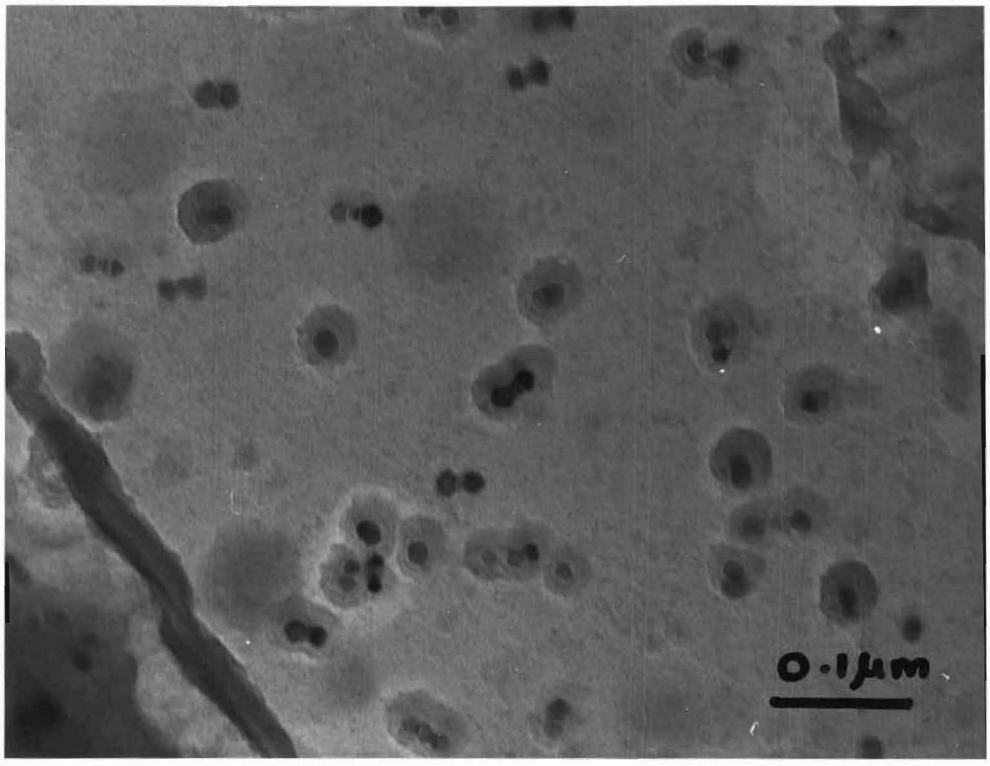

X 180,000

(d)

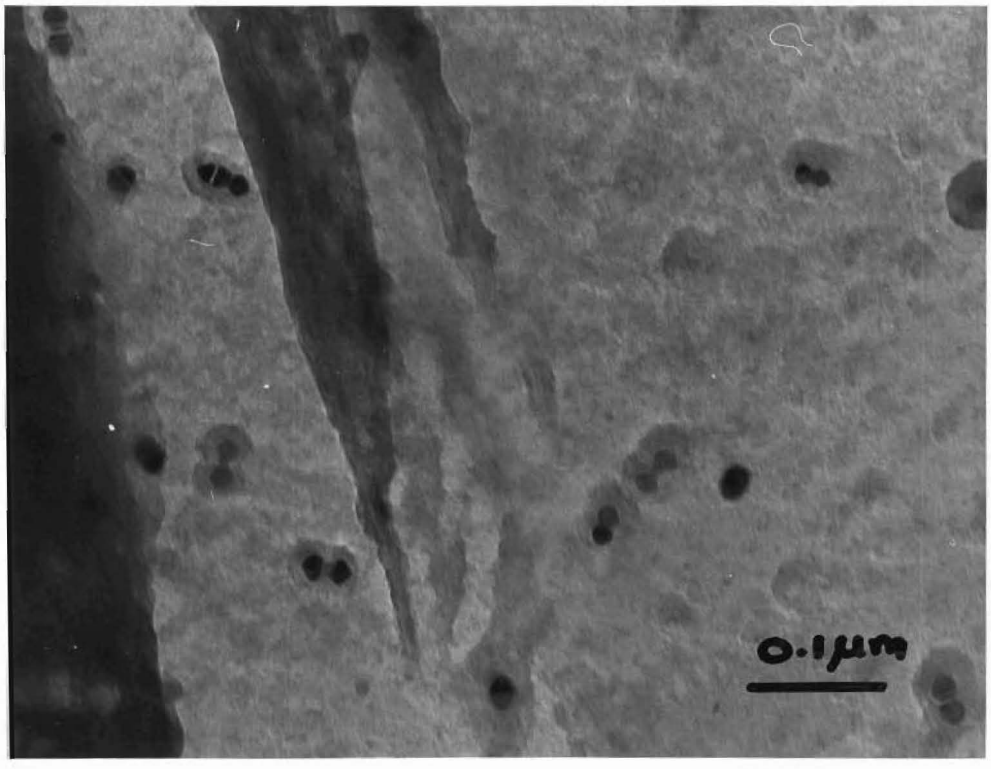

X 180,000

Figure 6.6(c)-(d): Vanadium nitride precipitate morphology in steel B5, at a simulated coiling temperature of 800°C (carbon extraction replica).

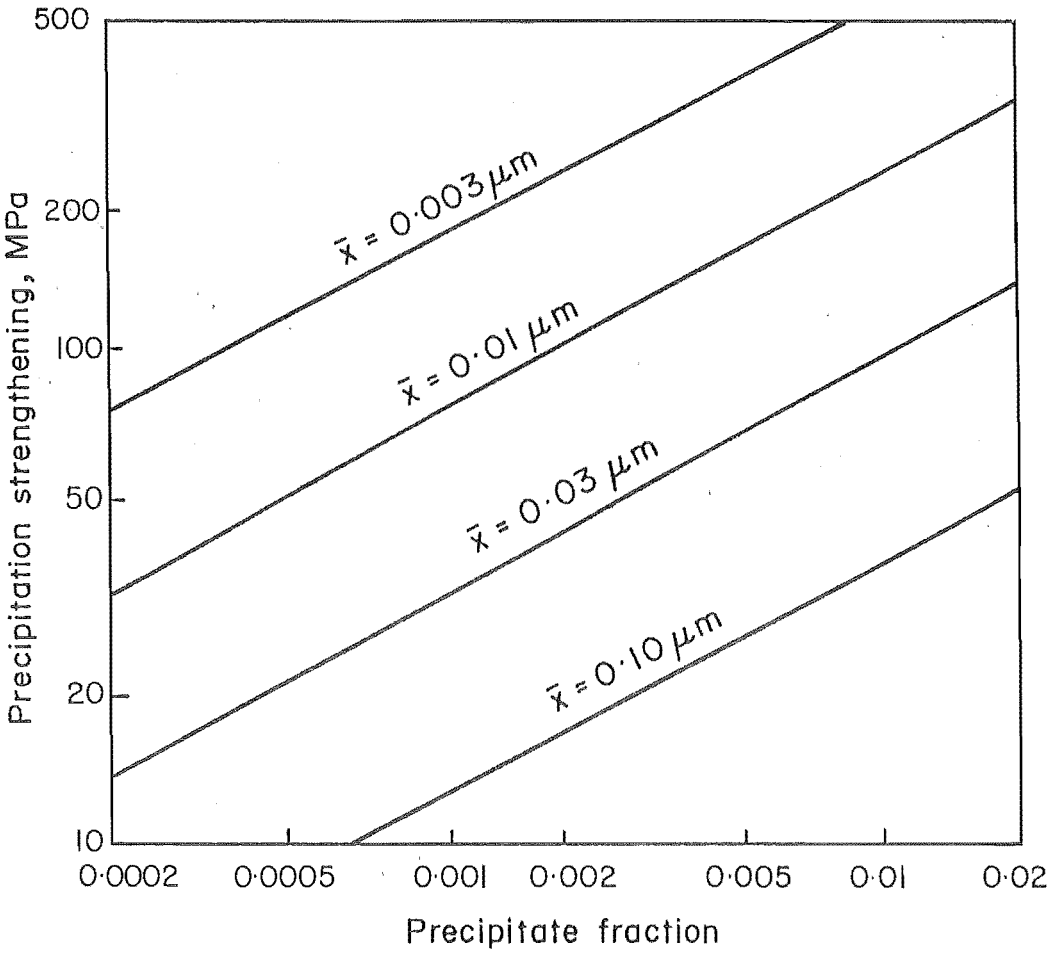

Figure 6.7: The dependence of precipitation strengthening on precipitate size ($\bar{x}$) and volume fraction according to the Ashby-Orowan model (Ref.86).

5 nm cubic precipitates at 700°C, see Figure 6.9) formed at simulated coiling temperatures of 600°C and 700°C has consequently contributed to this high yield strength. The precipitation strengthening model predicts that 0.072% (see Appendix G) of 5 nm cubic precipitates formed at 700°C would increase the yield strength by 70 MPa, (see Figure 6.7). There is also some variation in yield strength resulting from grain size effects, however this is considered to be of second order magnitude after precipitation strengthening.

In HSLA steels 20 - 40% of the yield strength is normally contributed by grain size[25]. As discussed in Chapter 2, the dependence of yield strength on grain size is given by the Hall-Petch equation [47]:

$$\sigma_{LY} = \sigma_o + k_y d^{-\frac{1}{2}} \qquad \text{Eqn.2.9}$$

where σ_{LY} is the lower yield stress, σ_o and k_y are constants and d is the average grain diameter. It has been shown [55] that σ_o may be considered to comprise two components, one which is temperature dependent representing the Peierlo-Nabarro force [127] and the other which is temperature independent representing the stress required to move free dislocations against the resistance of microstructural irregularities provided by dissolved solutes, fine precipitates, dislocations and other sub-structures [86,127]. Hence σ_o, besides being temperature dependent, also varies with the concentration of solute atoms and the degree of precipitation that has taken place.

The Hall-Petch relationship between grain size and yield strength is very relevant to microalloyed steels. Figure 6.8 shows

the variation in lower yield stress with $d^{-\frac{1}{2}}$ for steels in the simulated hot rolled condition and subsequent normalized condition. The graph of lower yield stress against $d^{-\frac{1}{2}}$ gives a slope (k_y) of 98 $Nmm^{-3/2}$ for simulated hot rolled samples and 12.5 $Nmm^{-3/2}$ for normalized samples. The normally expected values of k_y lie between 15.4 - 21.6 $Nmm^{-3/2}$(49).

The amount of vanadium nitride precipitated in the normalized samples is constant, (see Figure 6.9) so that the σ_o term would be constant for all normalized samples and the slope gives the sole effect of grain size on yield strength. Parallel lines having this slope were therefore drawn through the data points for the simulated hot rolled samples, shown in Figure 6.8, and the friction stress (σ_o) was found from the intercepts of these parallel lines with Figure Y axis. These calculated friction stress values are plotted as a function of nitrogen precipitated as vanadium nitride in Figure 6.10. As was discussed earlier, the resistance provided by the vanadium nitride precipitate to free dislocation motion should increase friction stress with volume fraction of vanadium nitride precipitate (assuming constant precipitate size). This is generally confirmed by Figure 6.10.

Considering the normalized samples, although there is some change in ferrite grain size (see Figure 6.11) the lower yield stress remains approximately constant for the range of simulated coiling temperatures examined (see Figure 6.4). The analysis of vanadium nitride in the normalized samples gave a constant value of 0.0158% N for all simulated coiling temperatures (see Figure 6.9). The volume

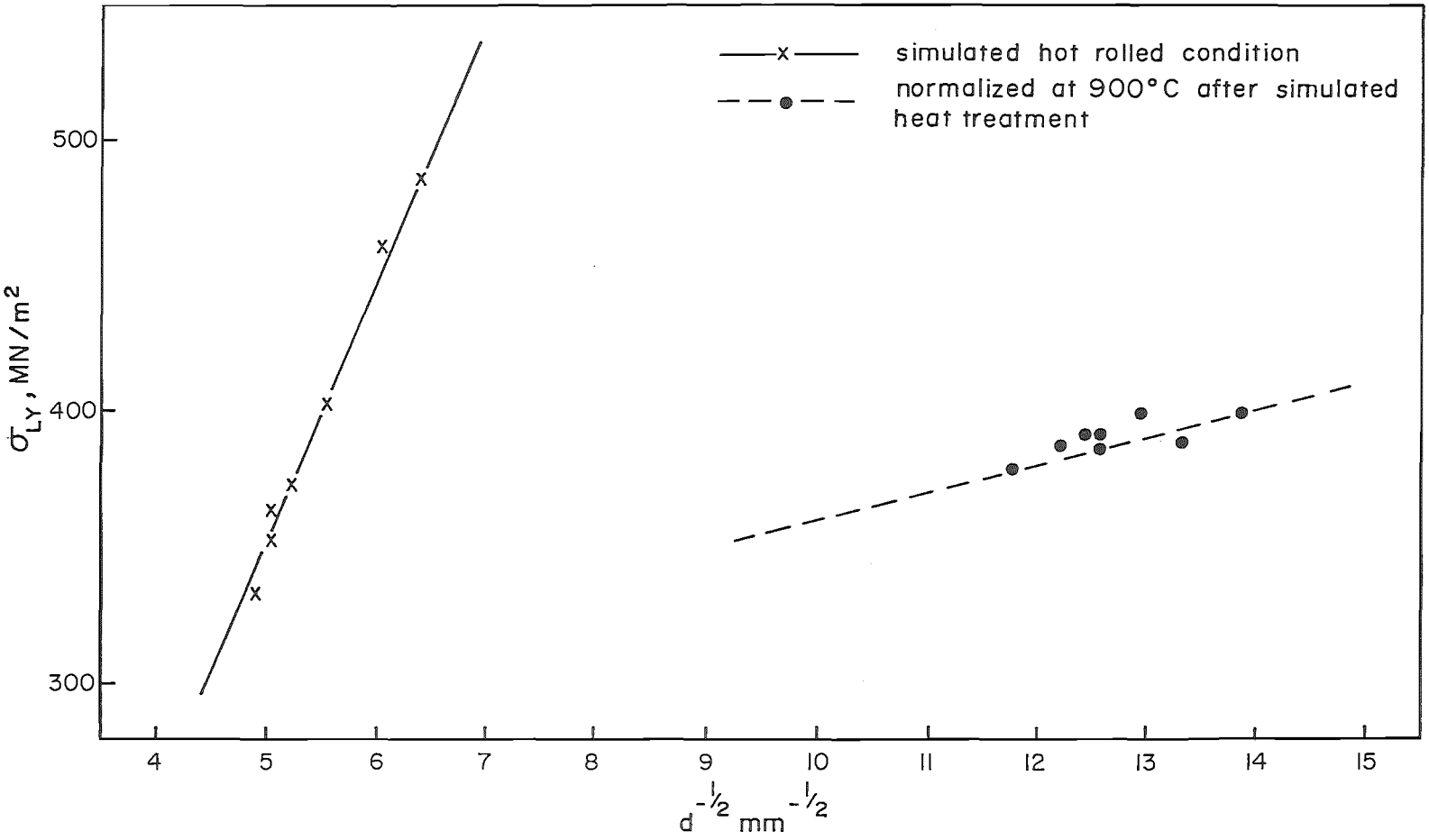

Figure 6.8: Variation in lower yield stress with $d^{-\frac{1}{2}}$.

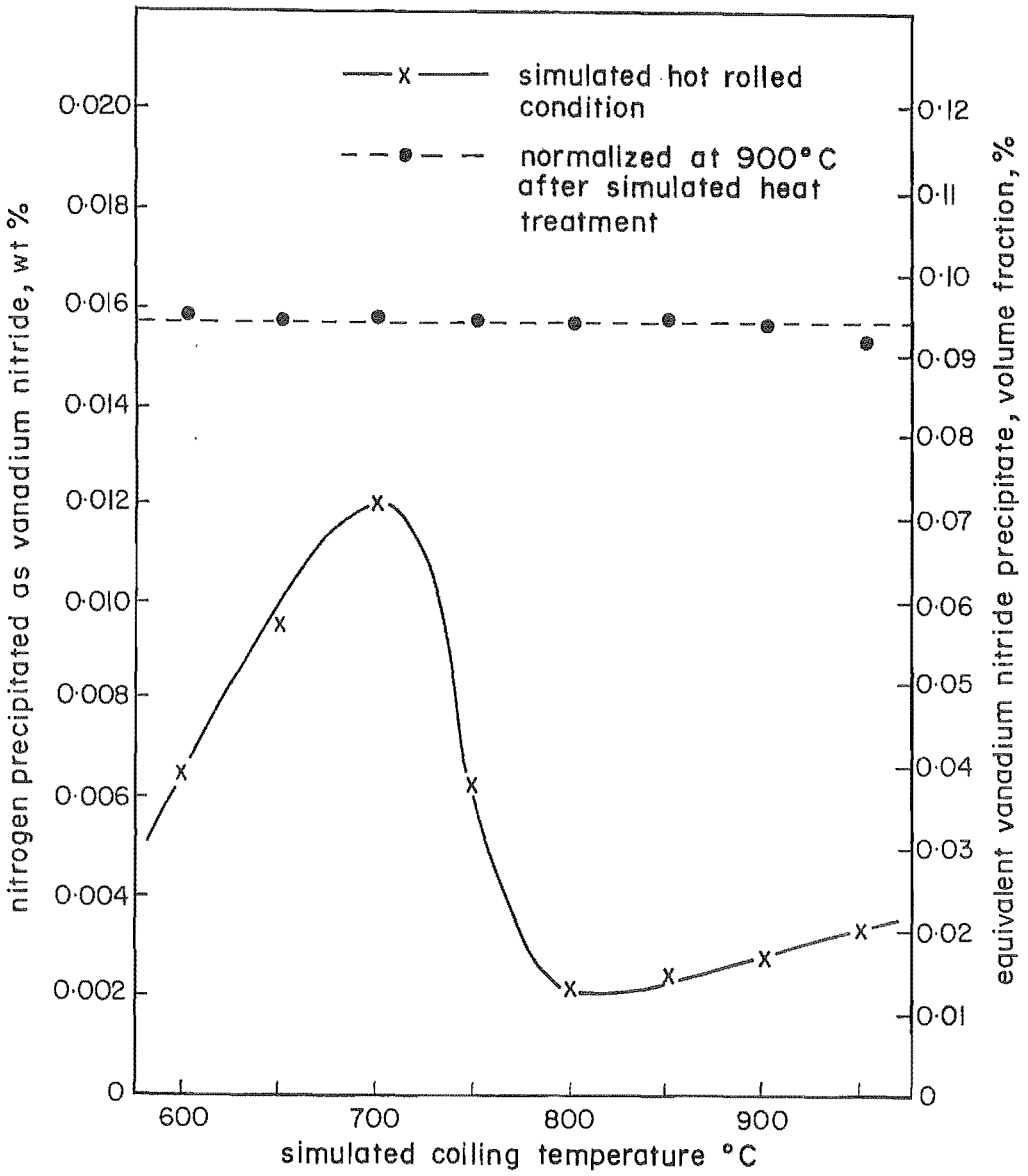

Figure 6.9: Variation in nitrogen precipitated as vanadium nitride with simulated coiling temperature.

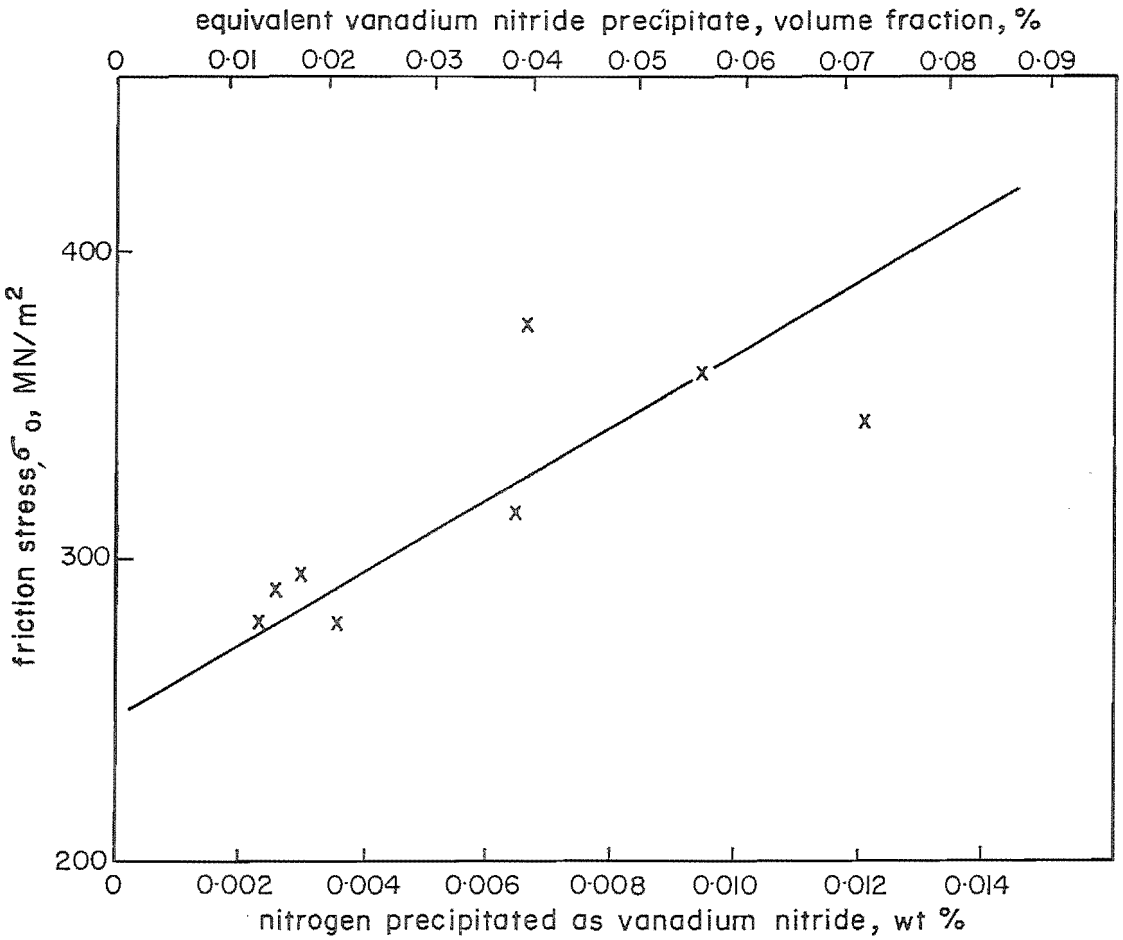

Figure 6.10: Effect of vanadium nitride precipitation on friction stress.

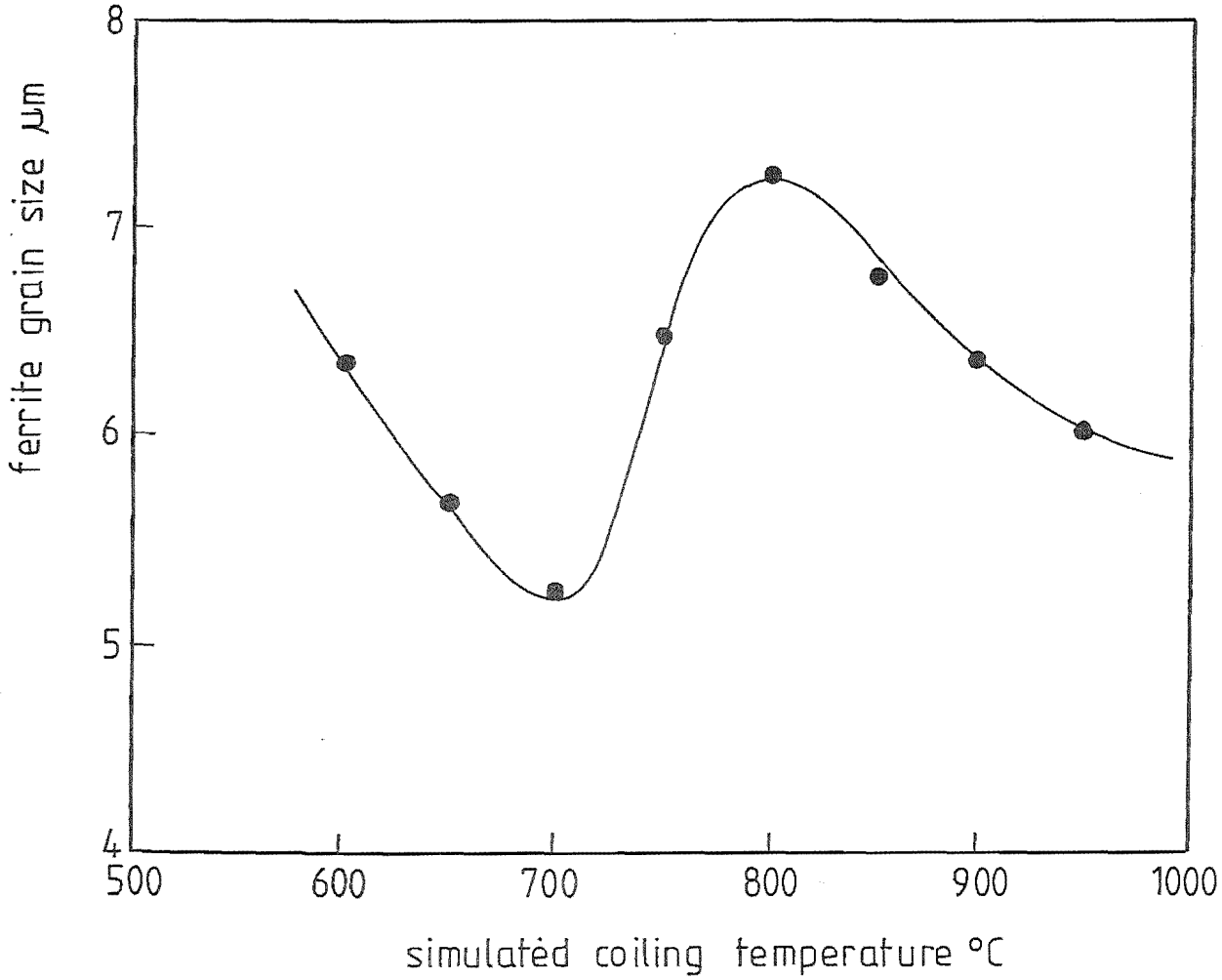

Figure 6.11: Changes in ferrite grain size with simulated coiling temperature (after normalizing at 900°C).

fraction of vanadium nitride is consequently almost constant and with consistent fine grain size and the lower yield stress is almost constant.

6.4.2 Effect of simulated coiling temperature on strain ageing

The variation in strain ageing index (ΔY) (see Figure 2.10) with simulated coiling temperature, is shown in Figure 6.12, for samples in the simulated hot rolled condition and after normalizing these samples. The minimum strain ageing index was recorded at a simulated coiling temperature of 700°C, where peak vanadium nitride precipitation was observed, with the strain ageing index increasing above and below this temperature. The peak ΔY value was recorded at 800°C, which corresponds to the condition of minimum vanadium nitride precipitation (see Figures 6.9 and 6.12). It is clear from the changes in vanadium nitride precipitation and strain ageing index (ΔY) that at all simulated coiling temperatures strain ageing was strongly controlled by vanadium nitride precipitation reducing the active nitrogen content. The effect of active nitrogen (N_{total} - N_{VN}) content on strain ageing shown in Figure 6.13 is consistent in trend with published data[3,62,128]. However, the degree of strain ageing is much less than expected, especially in the range of 0.0060% to 0.015% active nitrogen.

Another feature shown in Figure 6.12 is the strain ageing observed in these samples after normalizing. In this instance the variation in strain ageing index (ΔY) with simulated coiling temperature is smaller than that in the simulated hot rolled samples. This results from the constant value of vanadium nitride precipitate (0.0158% nitrogen precipitated as vanadium nitride) for all simulated coiling temperature leaving a constant active nitrogen content of

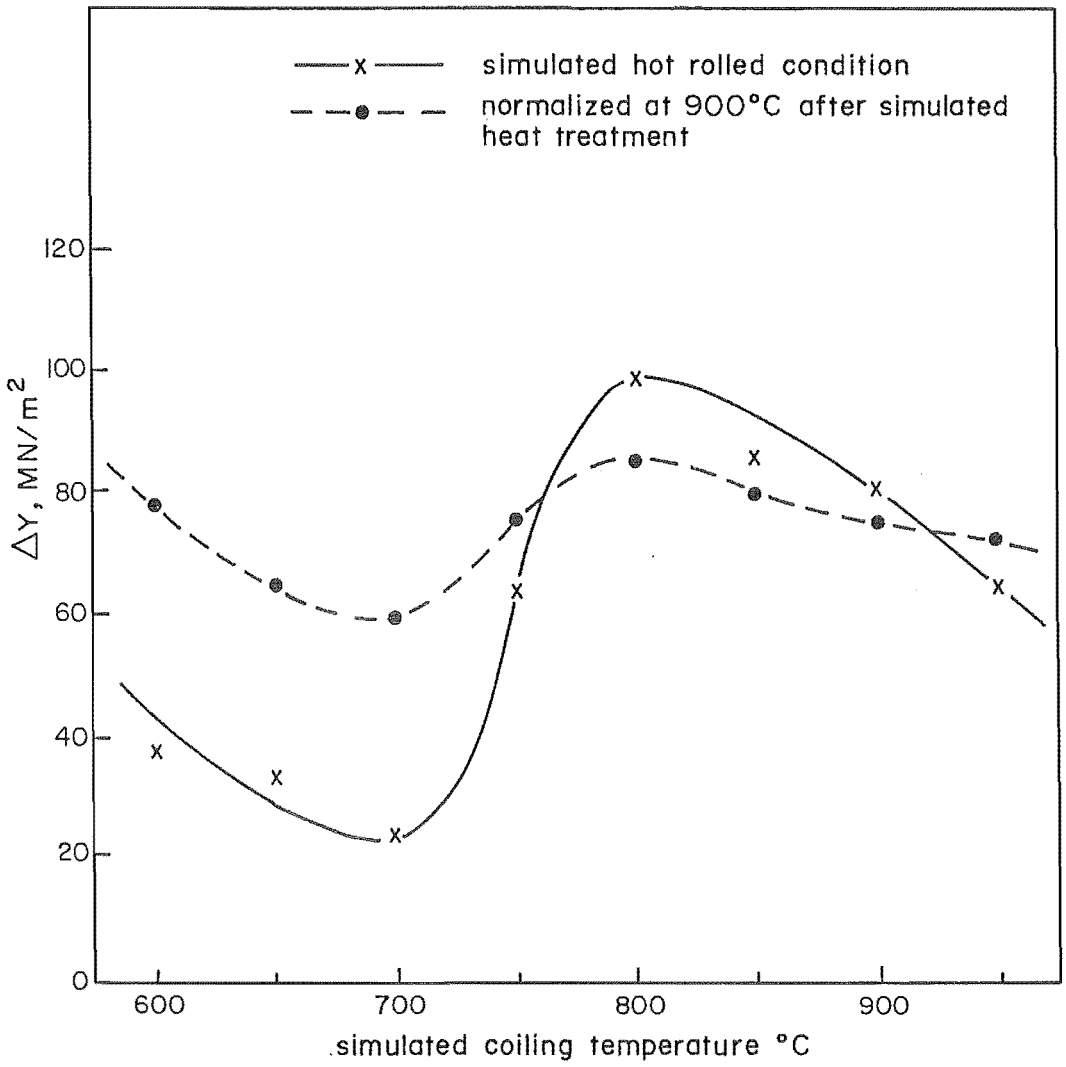

Figure 6.12: Variation in strain ageing index with simulated coiling temperature.

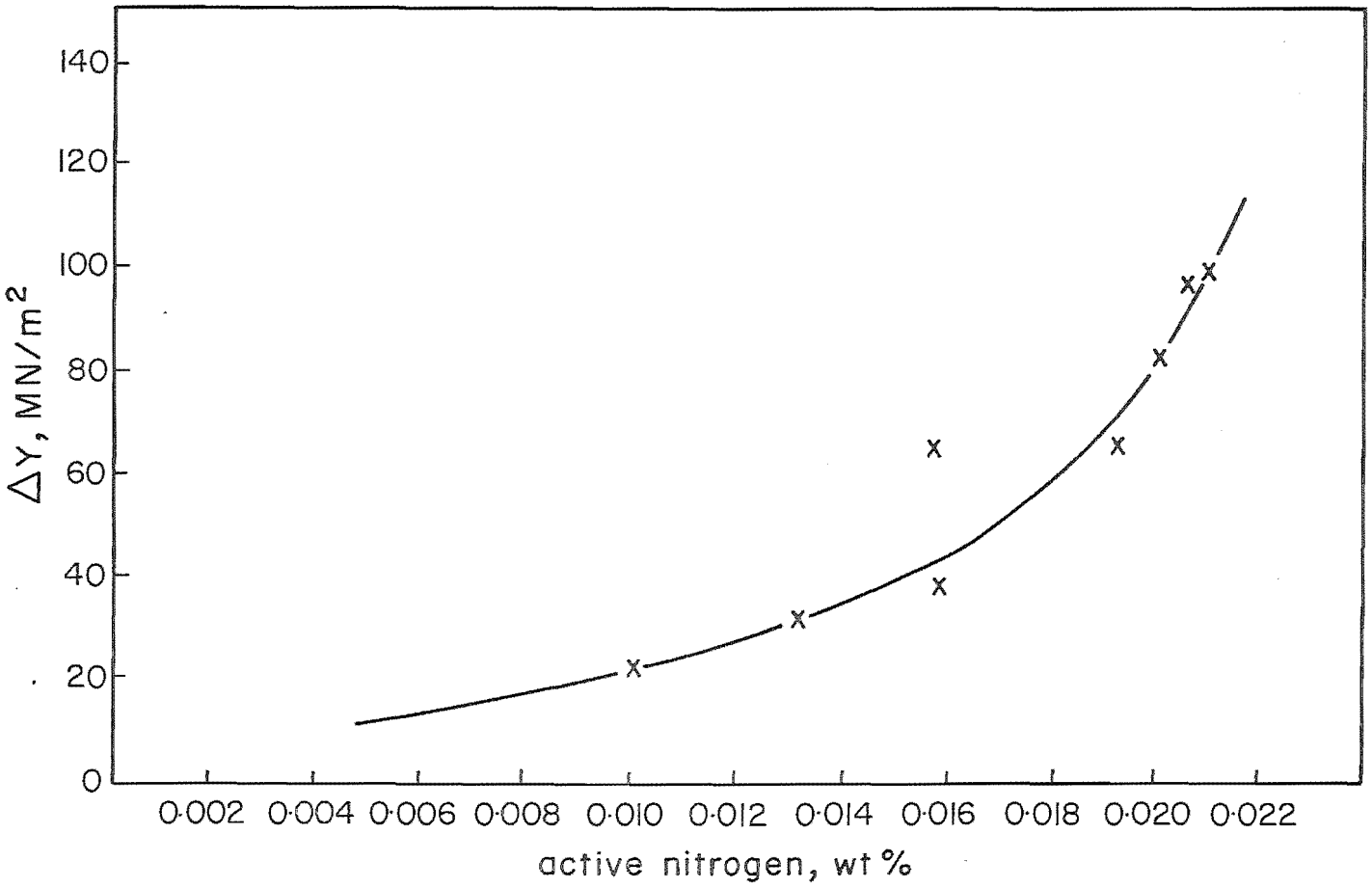

Figure 6.13: Effect of active nitrogen content on strain ageing.

0.0067%. The degree of strain ageing observed in normalized samples falls within the range normally expected for those active nitrogen levels [62], but the simulated hot rolled samples show a low degree of strain ageing, especially at simulated coiling temperatures of 600°C and 700°C. Although the simulated hot rolled samples have a higher active nitrogen content than normalized samples, the coarser ferrite grain size of these simulated hot rolled samples would reduce the degree of strain ageing observed[128].

6.4.3 Effect of simulated coiling temperature on impact-transition temperature

As can be seen in Table 6.2, the charpy 27 Joules impact-transition temperature increases with increasing coiling temperature for the simulated hot rolled samples. The impact-transition temperatures obtained are significantly higher than those normally found in HSLA steels. The coarse ferrite grain size observed in the simulated hot rolled samples will be responsible for this observation. On the other hand, low sub-ambient impact-transition temperatures were obtained for the normalized samples. The impact-transition temperature is strongly influenced by the ferrite grain size, and the much finer grain size of these normalized samples will have had a major influence on this result.

Cottrell [129] and Petch[13] have both proposed dislocation models of the transition temperature in single phase polycrystalline metals. From these models the following equation can be derived:

$$\varepsilon T_c = \sigma_o^* + c - \left[\frac{\beta G \gamma}{k_y} - k_y\right] d^{-\frac{1}{2}} \qquad \text{Eqn.6.1}$$

where T_c = impact-transition temperature

σ_o^* = temperature independent friction stress

ε and c = constants

β = constant representing state of stress

G = shear modulus

γ = surface energy

k_y = grain boundary strength coefficient

d = grain diameter

This equation shows that the impact-transition temperature decreases linearly with increasing $d^{-\frac{1}{2}}$, and increases linearly with increasing σ_o^* (assuming that both k_y and γ remain approximately constant). When the impact-transition temperatures determined by the charpy test were plotted against $d^{-\frac{1}{2}}$, as shown in Figure 6.14, a linear relationship was obtained. This graph of transition temperature against $d^{-\frac{1}{2}}$ gives a slope of $14.5°C/d^{-\frac{1}{2}}$, compared with $11.8°C/d^{-\frac{1}{2}}$ obtained in published data [55,86]. Since increases in σ_o^* would raise the transition temperature, the results obtained for the samples in the simulated hot rolled condition would be higher than for normalized samples of equivalent grain size, i.e. the results obtained for normalized samples should lie on the dotted line shown in Figure 6.14. The increased transition temperature of the simulated hot rolled samples above that predicted for normalized samples is consequently a result of an increase in σ_o^*.

Unfortunately there are too few sets of data available for a more detailed examination of this relationship.

6.5 SUMMARY

Change in lower yield strength, impact-transition temperature and strain age propensity of HSLA steels microalloyed with vanadium

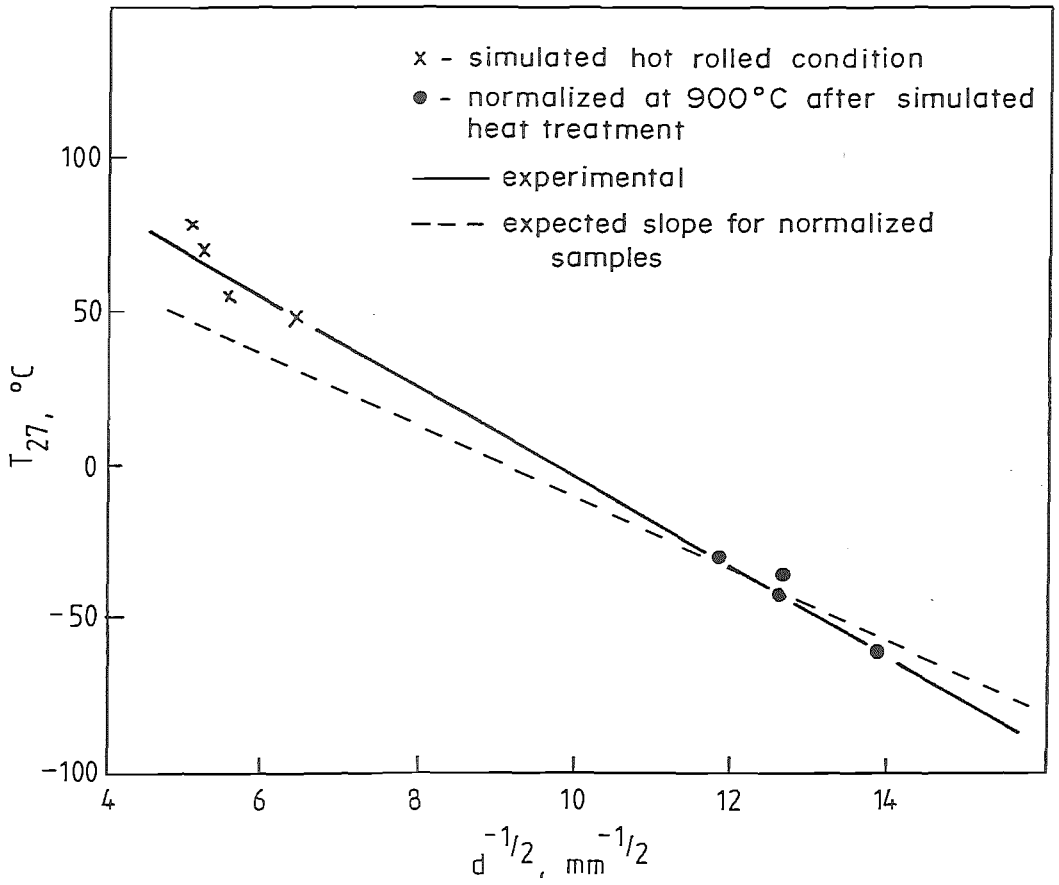

Figure 6.14: Effect of grain size on the impact-transition temperature.

have been determined after a simulated hot rolling thermal cycle. A second test series was conducted on samples normalized after the simulated thermal cycle.

Peak precipitation of vanadium nitride has been shown to occur at a simulated coiling temperature of 700°C for the V-Mn-N steel examined. Minimum ferrite grain size for the simulated rolling thermal cycle, and for samples subsequently normalized, suggest that vanadium nitride formed at the highest ferrite phase temperatures dominates ferrite grain size.

The lower yield strength and impact transition temperature have been shown to be dependent on grain size and the volume fraction of vanadium nitride precipitated during the simulated hot rolling thermal cycle.

The strain ageing index has been shown to be strongly controlled by the action of vanadium nitride precipitation on the active nitrogen content. It was found that the strain ageing was stronger in normalized samples than in simulated hot rolled samples. It is suggested that the finer ferrite grain size of the normalized samples is responsible for the observed difference.

The impact-transition temperature has been shown to be influenced by grain size and volume fraction of vanadium nitride precipitate. The vanadium nitride precipitate increases the transition temperature by increasing the σ_o^* value while finer grain size decreases the transition temperature. These observations are in good agreement with predictions made by equation 6.1.

CHAPTER 7

PARTITIONING OF NITROGEN IN DUAL PHASE STEELS

7.1 INTRODUCTION

While the principles of conventional HSLA steels are well understood, the development of ancillary properties, such as formability in the case of strip products, has become an important objective. The development of strength properties in isolation is of little value if the strip cannot be formed into an appropriate component. Formability is a generalized term relating to a number of properties which may have different metallurgical based principles. For example, bendability is a property involving resistance to fracture during bending and is controlled by the volume fraction and orientation of second phase particles, such as sulphides, in the metal. By comparison stretching is controlled by plastic instability, and depends on factors controlling the work-hardening characteristics and strain rate sensitivity. Deep-drawing characteristics depend on a selective through thickness which is controlled largely by crystallographic texture. In many practical applications, complex components may require combinations of these formability properties. Pressings can make demands on all these properties, depending on die design, blank-holding pressures, and other such factors.

Major drawbacks in the cold forming of HSLA steels are considered to be springback and poor formability. In the automobile industry the majority of components utilizing HSLA steels are formed by pressing, and their high strengths, specifically the yield strength, requires that the energy input for the forming operation is

extremely high. This results in high die wear, as well as causing the region of plastic deformation to be extremely localized. Local plastic deformation increases the production of Lüder bands, and thus increases cosmetic finish problems associated with these Lüder bands. To overcome these problems, dual phase steels were developed which combined the conflicting requirements of high strength and improved formability. In the automobile industry dual phase steels have attracted great interest because they offer an attractive combination of strength and ductility. These properties make dual phase steels interesting to apply where increased strength is required to save weight and where, at the same time, a good formability is required. Accordingly, a large potential use for HSLA steels is in automobiles where efforts to reduce fuel consumption require materials having such properties as these dual phase steels exhibit.

The significant properties of dual phase steels are summarized in Figure 7.1[131] and comprise:

(i) a combination of high tensile strength (UTS) and good ductility (total elongation at fracture),

(ii) the absence of a discontinuous yield point, with a smooth transition from elastic to plastic deformation at a relatively low off-set yield stress, and,

(iii) a high strain hardening rate over the initial three to five percent plastic strain.

The above characteristics ensure good formability, minimum springback after press-forming, and high strength in the formed component.

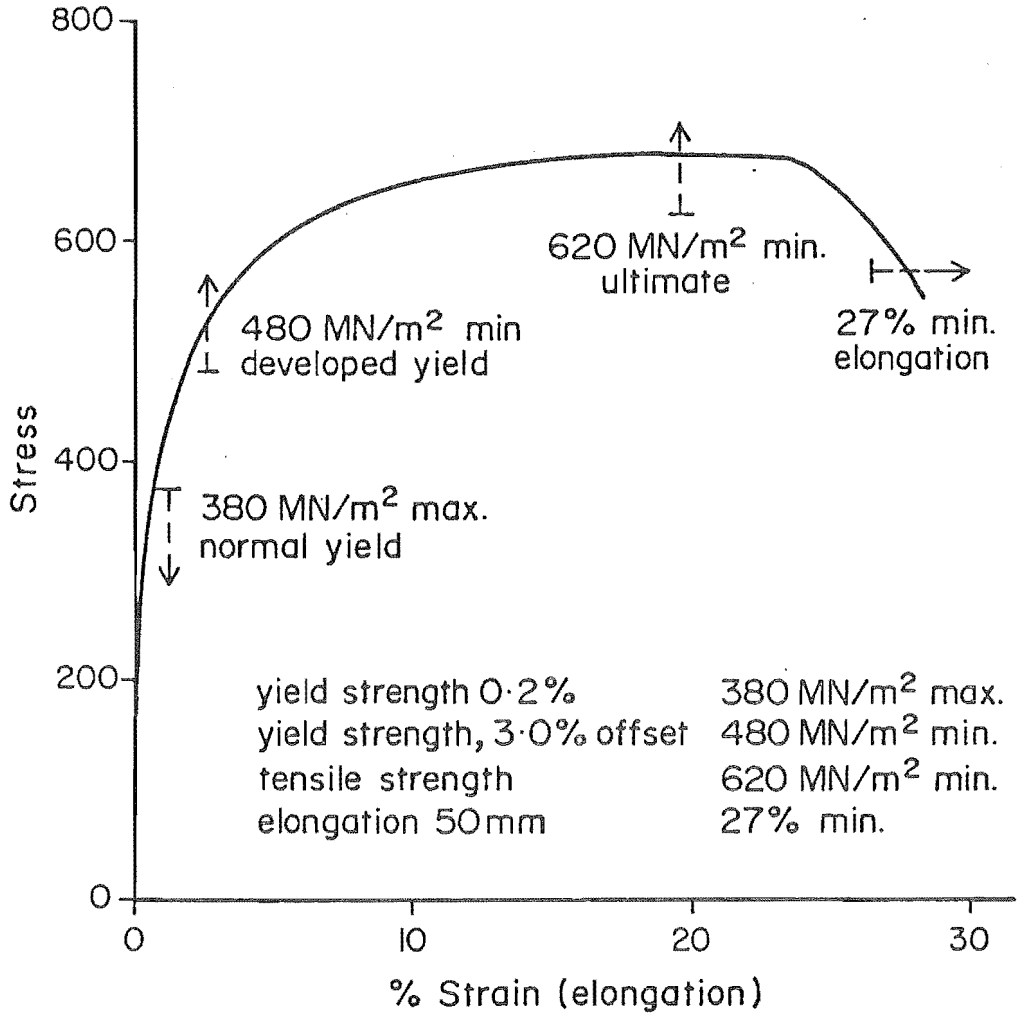

Figure 7.1: Target mechanical properties of dual phase steels for hot rolled thickness greater than 1.8 mm.

The yielding characteristics described in (ii) and (iii) above are attributed to the volume change on transformation of the second phase in the microstructure. This must be of sufficient magnitude to ensure the formation of a high residual stress and a high "active" dislocation density in the surrounding ferrite. It is therefore necessary that this transformation occurs at a low enough temperature to prevent auto-annealing or strain-ageing. The formation of martensite in the ferrite matrix usually fulfils these requirements and the resultant nonhomogeneous distribution of residual stress and mobile dislocation density in the ferrite ensures the absence of the discontinuous yield point and a high strain hardening rate over the initial three to five percent plastic strain.

The combination of high tensile strength (UTS) and good ductility, can therefore be considered the main characteristic of dual phase steels, and is mainly dependent on the microstructural variables:

(i) the volume fraction of second phase,

(ii) strength and ductility of the matrix ferrite phase, and,

(iii) strength and ductility of the secondary martensitic phase.

Other factors, such as grain size, are considered to have only a minor influence on tensile strength and ductility[131].

Although the dual phase microstructure (ferrite plus martensite) is readily obtained when quenching the steel from austenite plus

ferrite temperature range, low alloy steels are generally required in commercial practice to ensure sufficient hardenability for the austenite to transform into martensite. In order to accomplish the austenite to martensite transformation during cooling, an alloy content greater than some critical value is required, where the critical value depends on the cooling rate. The faster the cooling rate, the less alloy content is required. During intercritical annealing carbon atoms migrate from ferrite to austenite, resulting in the enrichment of carbon in austenite and accordingly stabilization of austenite. This, in turn, lowers the Ms temperature, permitting further diffusion of carbon from ferrite to austenite. To make full use of the scavenging effect of the austenite and to eliminate dissolved carbon in ferrite, a slower cooling rate is desirable[132]. As a matter of fact, slower cooling is possible only when the steel has a high alloy content.

A suitable alloying element to be added to a dual phase steel must have the following features;

(i) it should cause minimum solid solution hardening of ferrite phase,

(ii) it should retard the formation of ferrite, pearlite and bainite, thus assisting austenite to martensite transformation, and

(iii) it should be an austenite stabilizing element, which partitions between austenite and ferrite, resulting in a decrease of the alloy content in ferrite (i.e. minimum effect of solid solution hardening of ferrite).

The alloys generally used to give the required hardenability also suppress natural ageing either by interaction of the alloys with nitrogen or by precipitation of stable nitrides at higher temperatures (using additives of V, Ti, Aℓ, Nb, etc). As mentioned in previous Chapters 5 and 6, the nitride precipitates form in the ferrite matrix produce precipitation hardening, which reduces the ductility of dual phase steel. On the other hand nitrogen increases the hardenability of the austenite phase formed at intercritical annealing temperature by a partitioning effect of nitrogen.

The partitioning of interstitial nitrogen in low-alloy dual phase steel between co-existing ferrite and austenite is a diffusion controlled process, hence its kinetics will depend on the relevant diffusion coefficients. The partitioning of nitrogen in dual phase low-alloy steels is quite fast because of its high diffusivity in ferrite[133]. However, there is evidence to show that manganese retards the diffusion rate of nitrogen[134] and hence reduces the partitioning of nitrogen into austenite. Therefore the concentration of manganese in the ferrite phase must be reduced to increase the partitioning of nitrogen into austenite. Since manganese is an austenite stabilizing element, the manganese concentration in ferrite can be reduced by partitioning of manganese into austenite. The partitioning of substitutionally dissolved elements (e.g. Mn) in dual phase low-alloy steels is usually negligible in any practical heat treatment process, despite the existing thermodynamic driving force[133]. This is because of the low diffusivities of substitutional elements, compared with that of the interstitially dissolved elements. Therefore a systematic study was made on the partitioning

of manganese during an intercritical annealing process, and its effect on the partitioning of interstitial nitrogen between co-existing austenite and ferrite phases examined. This chapter reports the results of the study.

7.2 EXPERIMENTAL STEELS

There were 12 experimental steels used in this investigation. Of these 12 steels, 4 (DP1, DP5, DP6 and DP7) were specifically made for this investigation and the remainder were selected from steels used in the previous investigation. The 4 DP steels were produced by the air induction melting of 15 kg laboratory heats. The high nitrogen content was obtained by adding pre-determined amounts of nitrided scrap and nitrovan. These molten steels were cast at a temperature approximately 1600°C into 100 x 100 mm ingots. These ingots were then forged down into 40 x 40 mm billets. These billets were then hot rolled to 5 mm in several passes, and after air cooling to room temperature, were cold rolled to 1.5 mm thickness strip.

7.3 CHEMICAL ANALYSIS

The chemical composition of the steels was obtained spectrographically from the spectrometer in the Department of Mechanical Engineering, University of Canterbury. This analysis is given in Table 7.1.

The nitrogen content of the steels and the nitrogen combined as stable nitrides were determined by the chemical analysis method previously used[94]. The resultant nitrogen contents are given in Table 7.2. Details of this chemical analysis method are given in Appendix A.

Table 7.1: Composition of experimental steels.

CAST	C	Mn	Si	S	P	Ni	Cr	Mo	Cu	Sn	V	Al	N
DP1	0.11	2.67	0.02	0.012	0.012	0.03	0.02	-	0.01	-	0.01	0.003	0.0163
DP5	0.17	1.77	0.02	0.019	0.02	0.19	0.60	0.006	0.07	0.005	0.06	0.003	0.0292
DP6	0.13	1.52	0.02	0.019	0.019	0.14	0.40	0.005	0.11	0.007	0.06	0.002	0.0255
DP7	0.14	1.88	0.02	0.02	0.02	0.02	0.06	0.006	0.007	0.10	0.06	0.002	0.0224
A1	0.10	1.42	0.18	0.014	0.013	0.03	0.02	0.001	0.01	-	0.002	-	0.0065
A5	0.09	1.38	0.15	0.012	0.012	0.03	0.02	-	0.01	-	0.072	-	0.0067
D1	0.14	1.57	0.19	0.012	0.02	0.04	0.05	0.005	0.01	0.002	0.07	0.007	0.0370
D4	0.15	1.33	0.17	0.011	0.02	0.04	0.05	0.004	0.01	0.001	0.15	0.005	0.0393
N	0.14	0.63	0.001	0.01	0.003	0.01	0.01	-	0.01	0.001	-	-	0.0142
A	0.06	0.33	0.003	0.01	0.006	0.01	0.02	-	-	0.001	-	0.039	0.0042
O-Y	0.09	0.21	0.06	0.03	0.03	0.03	0.10	0.01	0.13	0.017	0.002	0.016	0.0141
S.T	0.14	1.48	0.25	0.01	0.02	0.14	0.14	0.03	0.25	0.02	0.004	0.035	0.0095

Table 7.2: Nitrogen determination of the experimental steels (intercritically annealed condition).

Cast	N_{sol} wt%	N_{insol} wt%	N_{total} wt%	$N_{A\ell N}$ wt%	N_{active} wt%
DP1	0.0143	0.0020	0.0163	0.0008	0.0135
DP5	0.0133	0.0159	0.0292	0.0008	0.0125
DP6	0.0095	0.0160	0.0255	0.0008	0.0087
DP7	0.0075	0.0149	0.0224	0.0008	0.0067
A1	0.0061	0.0004	0.0065	-	0.0061
A5	0.0003	0.0064	0.0067	-	0.0003
D1	0.0189	0.0181	0.0370	0.0018	0.0171
D4	0.0045	0.0348	0.0393	0.0010	0.0035
N	0.0137	0.0005	0.0142	-	0.0137
A	0.0037	0.0005	0.0042	0.0035	0.0002
O-Y	0.0121	0.0020	0.0141	0.0010	0.0111
S-T	0.0090	0.0005	0.0095	0.0046	0.0044

7.4 HEAT TREATMENT

Specimens of 10 x 10 mm size, cut from the cold rolled strip were used in this study of manganese partitioning in dual phase steels. These steel samples were held at appropriate intercritical annealing temperatures (see Table 7.3) for different time intervals (½ hr, 1 hr, 2 hrs, 4 hrs, 8 hrs, 16 hrs, 50 hrs and 100 hrs) in an argon atmosphere before quenching into water. Since the partitioning of substitutionally dissolved elements (manganese) in dual phase steels is very slow in any practical heat treatment process, samples were kept at intercritical annealing temperatures for longer than commercially practical periods to get a considerable degree of Mn partitioning.

Tensile specimens of 40 mm parallel length and 12.5 mm wide (see Figure 7.2) were machined prior to heat treatment from all of the above experimental steels. These tensile specimens were intercritically annealed in an argon atmosphere and were held at temperature for 30 minutes, 1 hr, 2 hrs and 4 hrs to provide some assessment of partitioning of nitrogen and the effect of manganese content on nitrogen partitioning during the intercritical annealing. All the specimens were then quenched in water from the heat treatment temperature.

7.5 METALLOGRAPHY

Scanning electron microscopy was carried out on the intercritically annealed specimens after polishing and etching in 2% nital.

Table 7.3: Intercritical annealing temperatures.

Cast	Intercritical Annealing Temperatures, °C
DP1	690
DP5	715
DP6	715
DP7	700
A1	720
A5	720
D1	715
D4	720
N	735
A	735
O-Y	735
S-T	720

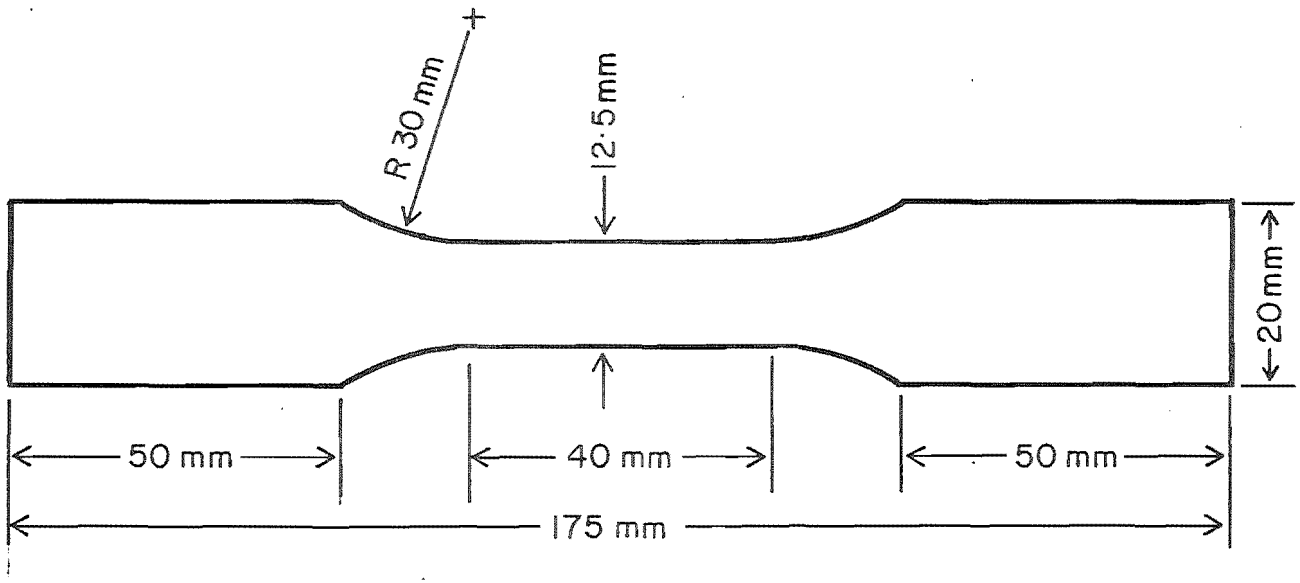

Figure 7.2: Details of the strip tensile specimen.

Partitioning of manganese and chromium was determined by using energy dispersive micro analysis. In order to get a good result about 10 analyses were done on each sample. The amount of manganese and chromium partitioned into austenite and ferrite was determined by a Link 290 energy dispersive X-ray analyser attached to JEOL JSM 35 scanning electron microscope.

The volume fraction of martensite was determined by using an image analyser.

7.6 TENSILE TESTING

The tensile testing was carried out on a 250 kN Instron universal testing machine using the following specified conditions at ambient temperature;

Cross-head speed	= 0.2 mm/min, giving an approximate strain rate of 1×10^{-4}/sec.
Maximum load range	= 20 kN.
Extensiometer sensitivity	= 5, 1% strain on 25 mm gauge length gives 26.25 mm on graph.

The 25 mm gauge length Instron strain gauge extensiometer was fixed to the specimen gauge length to provide recorded load-extension curves. Tensile specimens were pre-strained to 3%, unloaded and subsequently aged at 60°C for 88 hours (equivalent to ageing at ambient temperature 15°C for one year) before finally testing to fracture. The resultant tensile properties obtained from the recorded load-extension curves are summarized in Table 7.4.

Table 7.4: Tensile test results.

Cast	Tensile stress, MPa				ΔY , MPa				
	30 min. at temp., W.Q	1 hr at temp., W.Q	2 hrs at temp., W.Q	4 hrs at temp., W.Q	30 min. at temp., W.Q	1 hr at temp., W.Q	2 hrs at temp., W.Q	4 hrs at temp., W.Q	4 hrs at temp., F.C
DP1	676	723	750	820	46	33	18	0	72
DP5	496	575	590	619	53	31	9	0	65
DP6	469	500	532	537	45	21	7	0	50
DP7	527	630	663	682	30	34	20	0	37
A1	486	520	576	613	22	20	7	0	31
A5	490	508	534	591	10	7	7	0	7
D1	503	522	581	612	65	38	14	0	108
D4	517	536	579	652	14	16	7	0	17
N	482	498	520	534	7	0	0	0	78
A	453	487	514	520	0	0	0	0	7
O-Y	462	482	487	485	0	0	0	0	52
S-T	487	518	572	640	36	20	10	0	22

7.7 DISCUSSION OF RESULTS

7.7.1 Intercritically Annealed Structures

The microstructures of specimens intercritically annealed and quenched in water are shown in Figures 7.3(a) to 7.3(h). The structures of these specimens consists basically of ferrite with a martensite (plus retained austenite) second phase. A fine distribution of carbide particles was observed in samples annealed for short periods. The volume fraction of small carbide particles gradually decreased with increasing annealing time.

The important features of the formation of austenite that can be observed from Figures 7.3(a) to 7.3(h) are as follows;

(i) Austenite is nucleated during heating at Fe_3C particles situated in the ferrite grain boundaries and nucleation appears to continue throughout the isothermal holding period, i.e. some austenite grains nucleate after short holding periods whereas other austenite grains nucleate after relatively long holding times.

(ii) The austenite grains grow both into the ferrite matrix and along the ferrite grain boundaries. The distance that the austenite grains grow into the ferrite is much smaller than the growth along the grain boundaries. This difference in austenite grain dimension is presumably caused by the difference in diffusion coefficients perpendicular to and parallel to the ferrite grain boundaries.

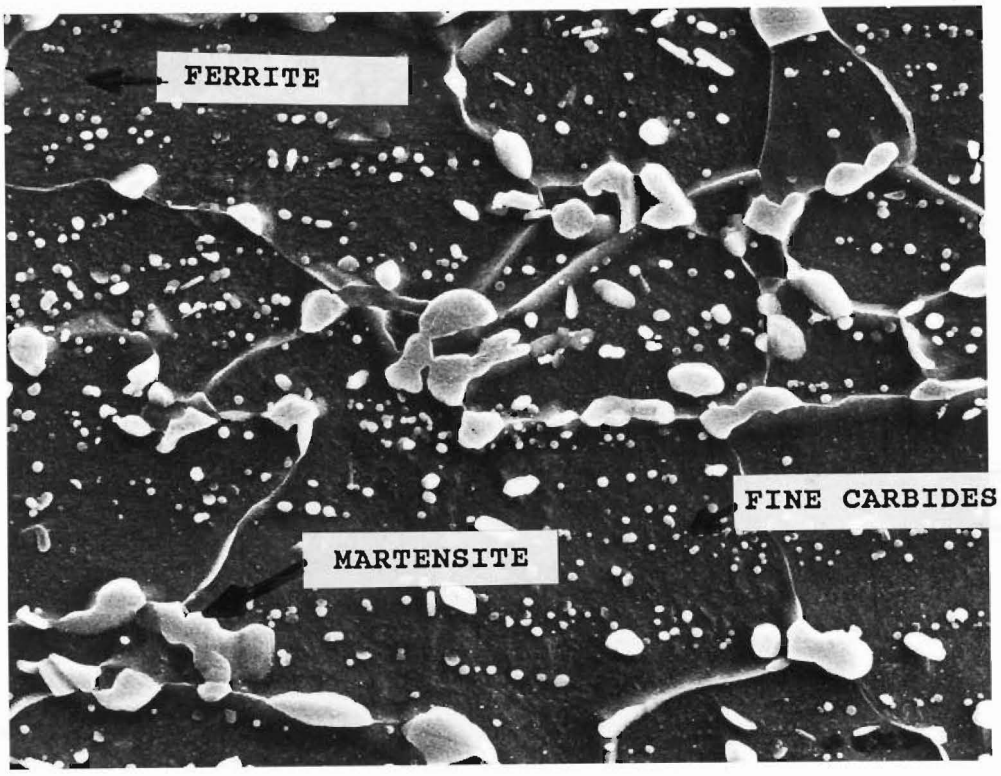

Figure 7.3(a): Scanning electron micrograph of steel DP7, after intercritically annealed at 700°C for ½ hr and water quenched.

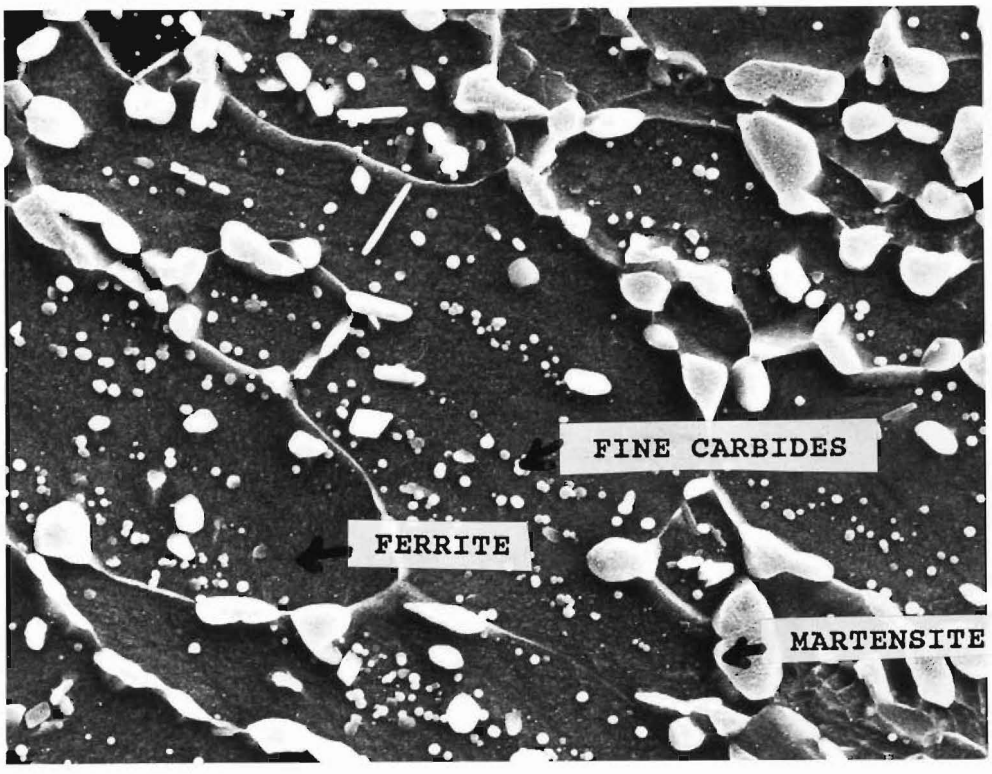

Figure 7.3(b): Scanning electron micrograph of steel DP7, after intercritically annealed at 700°C for 1 hr and water quenched. (X3000)

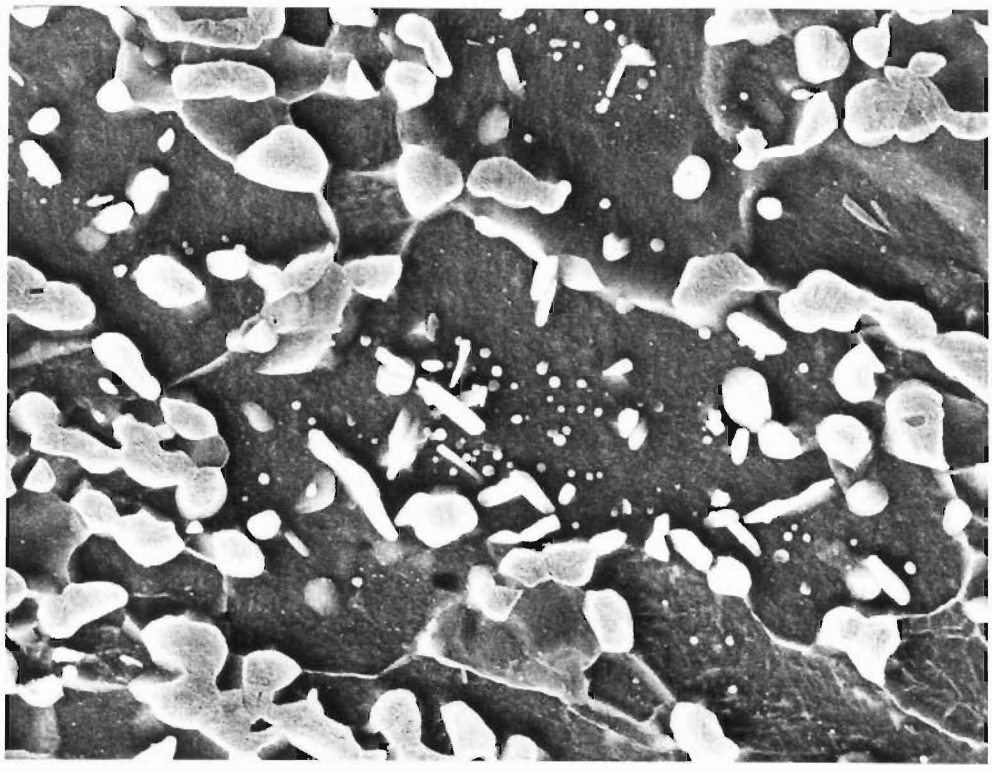

Figure 7.3(c): Scanning electron micrograph of steel DP7, after intercritically annealed at 700°C for 2 hrs and water quenched.

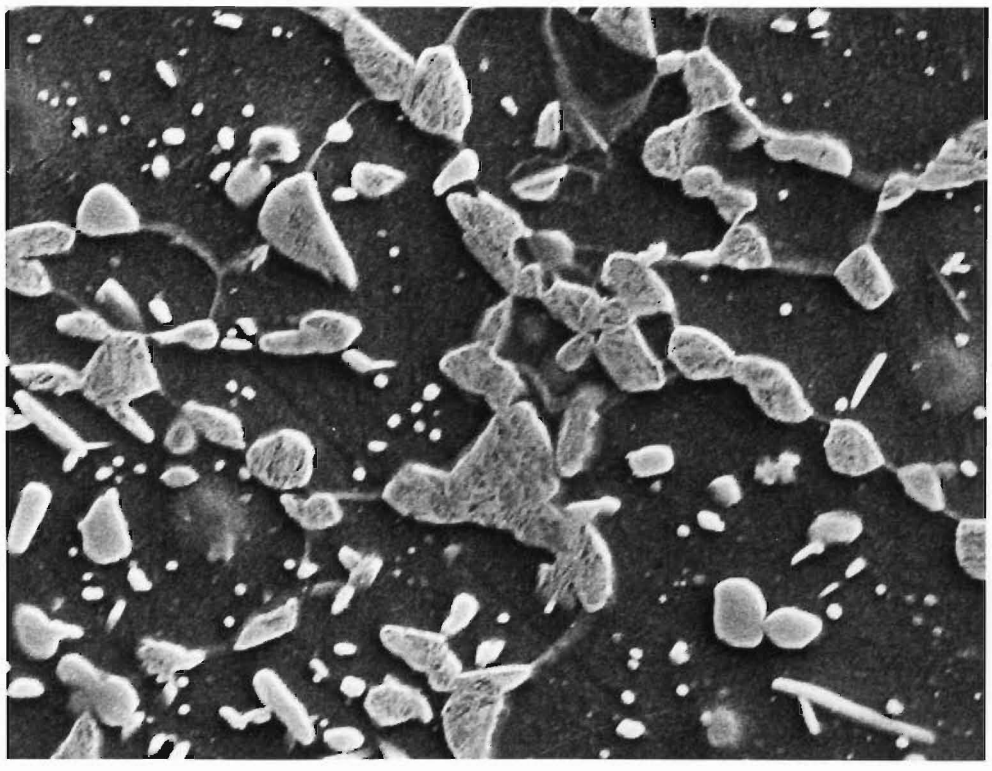

Figure 7.3(d): Scanning electron micrograph of steel DP7, after intercritically annealed at 700°C for 4 hrs and water quenched. (X3000).

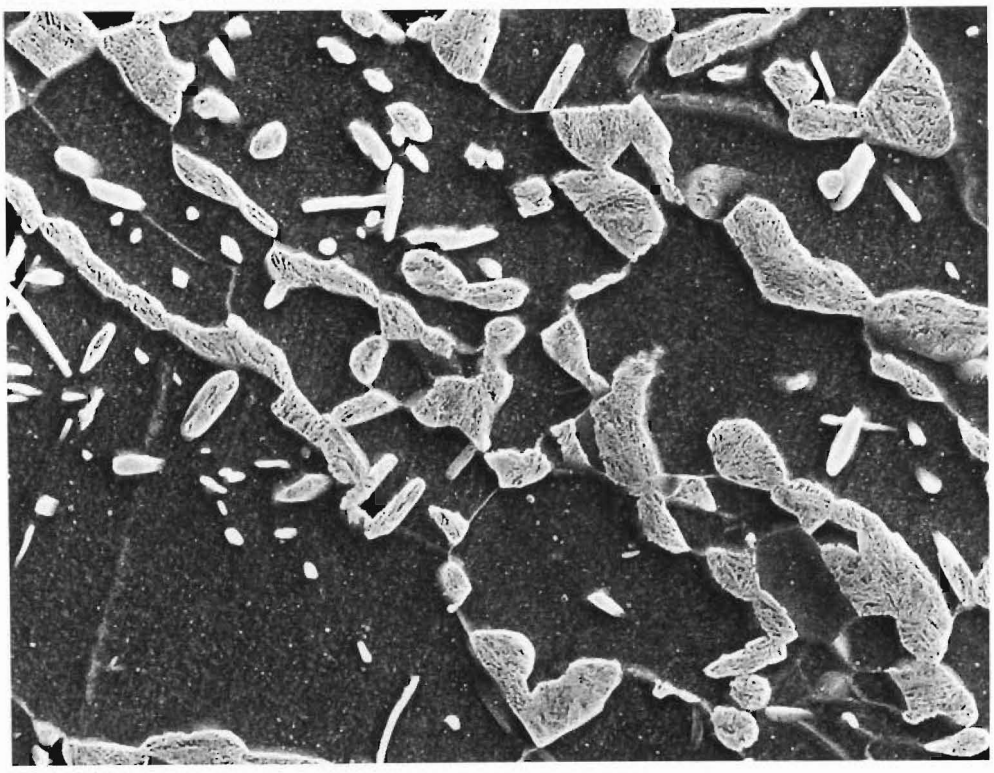

Figure 7.3(e): Scanning electron micrograph of steel DP7, after intercritically annealed at 700°C for 8 hrs and water quenched.

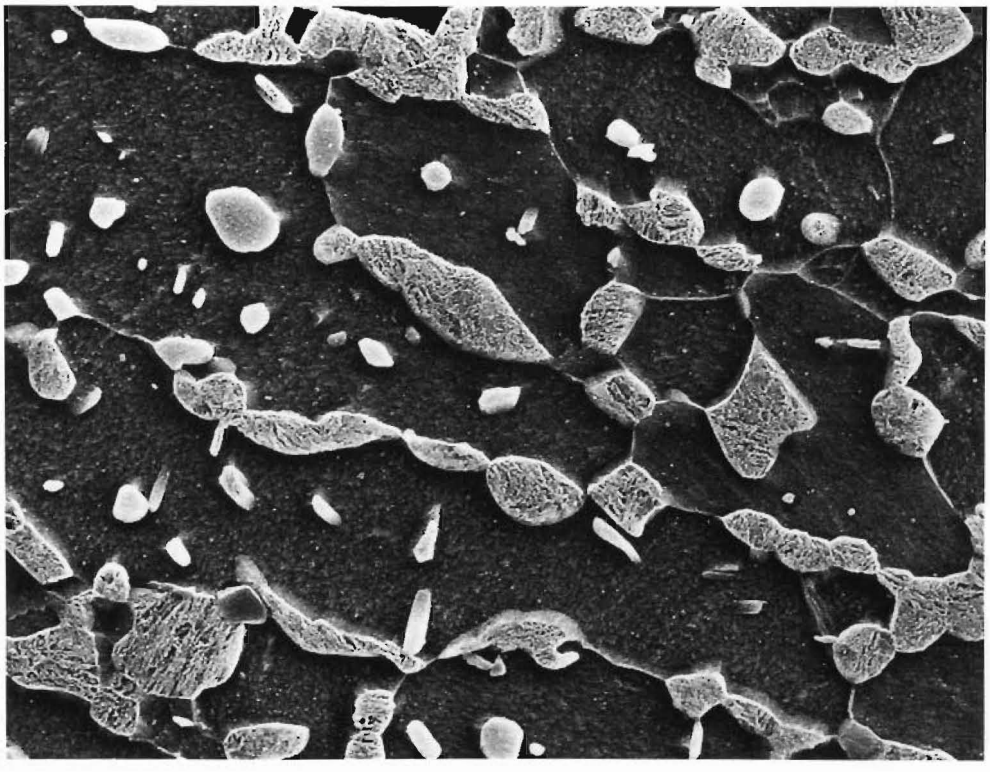

Figure 7.3(f): Scanning electron micrograph of steel DP7, after intercritically annealed at 700°C for 16 hrs and water quenched. (X3000)

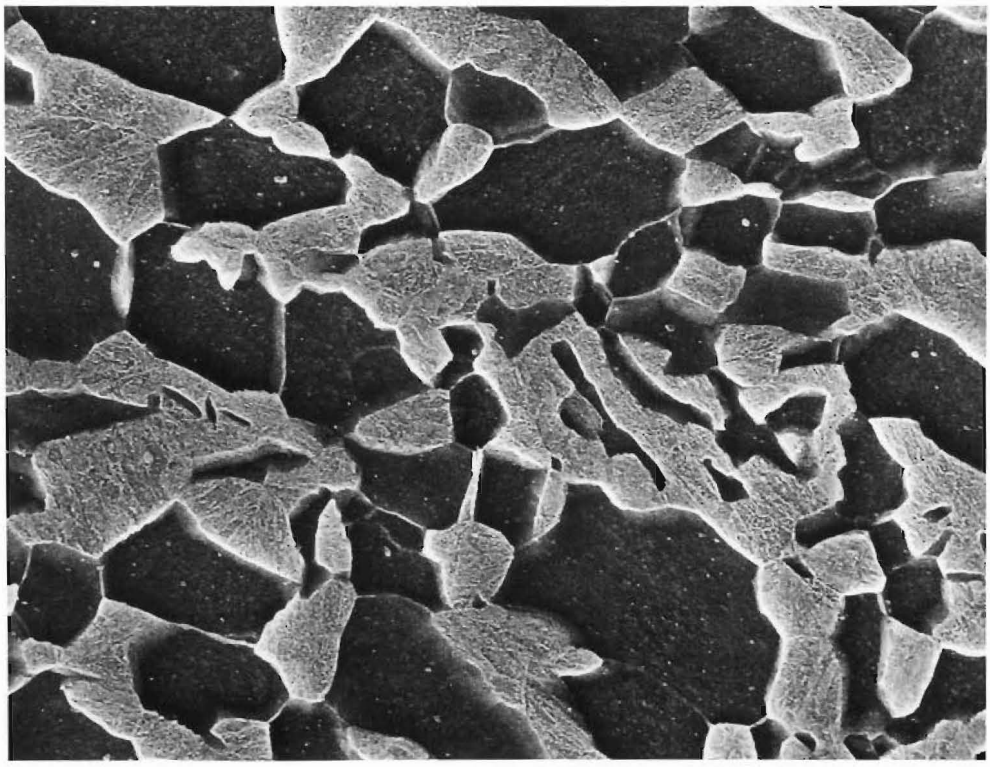

Figure 7.3(g): Scanning electron micrograph of steel DP7 after intercritically annealed at 700°C for 50 hrs and water quenched.

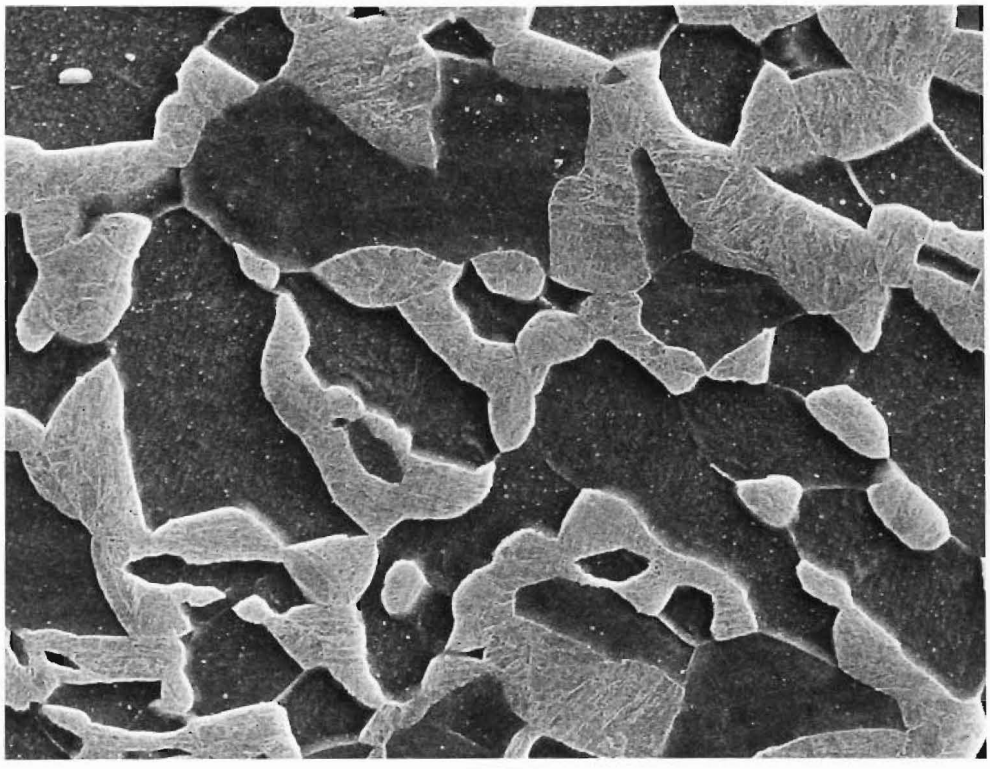

Figure 7.3(h): Scanning electron micrograph of steel DP7 after intercritically annealed at 700°C for 100 hrs and water quenched. (X3000)

7.7.2 Quantitative Metallography

As previously mentioned the volume fraction of 'second phase' was determined by an image analyser. When determining the volume fraction of second phase, it was assumed that particles of size less than 29.5 nm (100 pixels in frame grabber) were carbides and any particles larger than this were assumed the second phase (martensite). The distribution of all small particles of size less than 44.3 nm (150 pixels in frame grabber) in each sample is given in Appendix E..

Figure 7.4 illustrates the effect of intercritical annealing time on the volume fraction of small carbides. This shows that the volume fraction of carbide particles decreases with increasing intercritical annealing time and results from austenite phase growth. The austenite appeared to form and grow preferentially at Fe_3C particles located on ferrite grain boundaries and this has been observed in several earlier studies performed under approximately similar experimental conditions[135,136]. These carbide particles dissolve in the ferrite matrix during this isothermal treatment and the carbon from these particles then diffuses to the growing austenite phase located at the ferrite boundaries.

Another important feature that can be observed from the Figure 7.4 is the difference in volume fraction of carbide between steels DP5 and DP7. Although the samples from steel DP5 were intercritically annealed at slightly higher temperature (715°C) than that for steel DP7 (700°C), the volume fraction of carbide particles was found to be higher in samples from DP5. The significant chromium content of steel DP5 is the likely reason for this increased volume fraction of fine carbide particles, since chromium forms fine and more stable Cr_7C_3 and

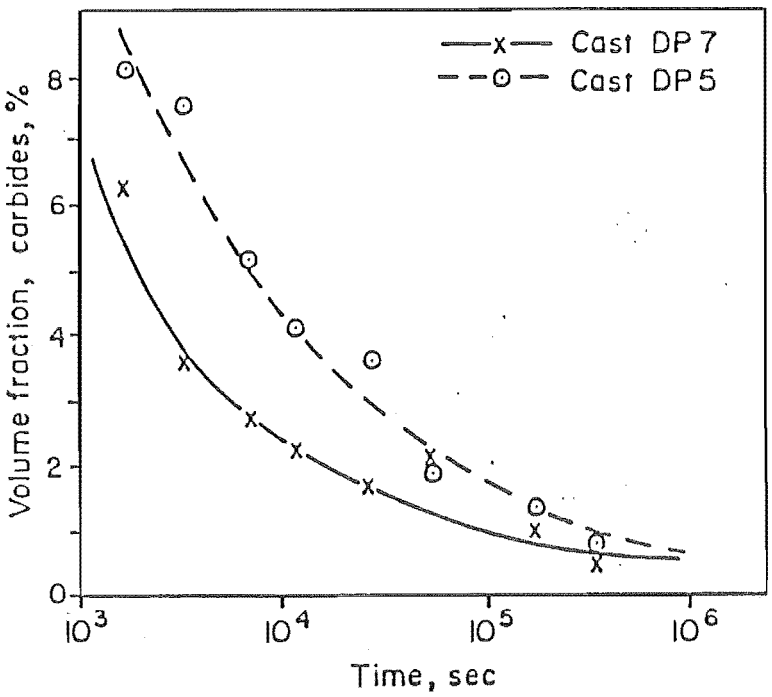

Figure 7.4: Effect of annealing time on volume fraction small carbides in the high and low Cr steels.

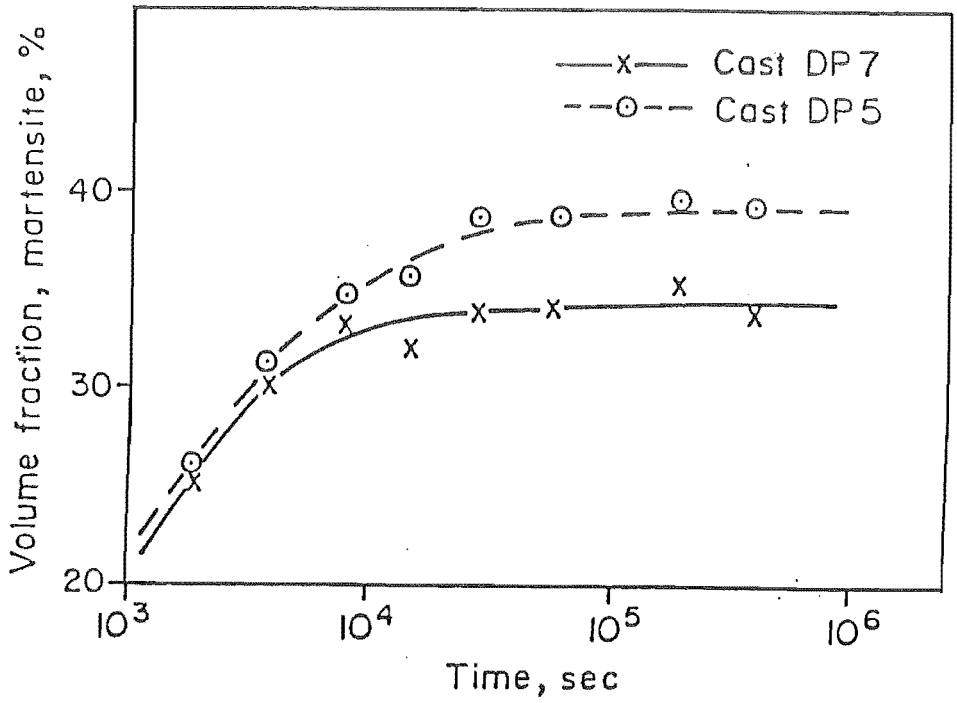

Figure 7.5: Effect of time at intercritical annealing temperature on volume fraction of martensite.

$Cr_{23}C_6$ carbides in the ferrite matrix. The Fe_3C, Cr_7C_3 and $Cr_{23}C_6$ all have physically the same appearance in SEM micrographs, and when measuring the volume fraction of carbides these chromium carbides Cr_7C_3 and $Cr_{23}C_6$ will have been included in the measurements. Similar results were observed by Nolfi[137] and Wever[138], both of whom found that the dissolution of Fe_3C during the formation of austenite was slowed by chromium additions.

The isothermal reaction curves for the formation of austenite at 700°C for steel DP7, and at 715°C for steel DP5 are shown in Figure 7.5. The volume fraction of martensite (austenite) increases up to a holding time of 8 hours, after which it remained constant. Another important feature appearing in Figure 7.5 is the time required for the complete formation of austenite. It can be seen that a longer time is required for the formation of maximum austenite in steel DP5. The slower dissolution of carbides in the high chromium steel DP5 would account for the slower formation of austenite in this steel.

It can also be seen in Figure 7.5 that the maximum amount of second phase in steel DP5 was greater than for steel DP7. The higher carbon content of steel DP5 (0.17%), compared with 0.14% carbon in steel DP7, causes this difference in second phase volume fraction.

The variation in hardness with martensite content of the dual phase steels is shown in Figure 7.6. It can be seen that the hardness is linearly dependent upon the volume fraction of martensite. It appears that the existence of fine carbide particles in samples, held at intercritical annealing temperature for short periods, have no

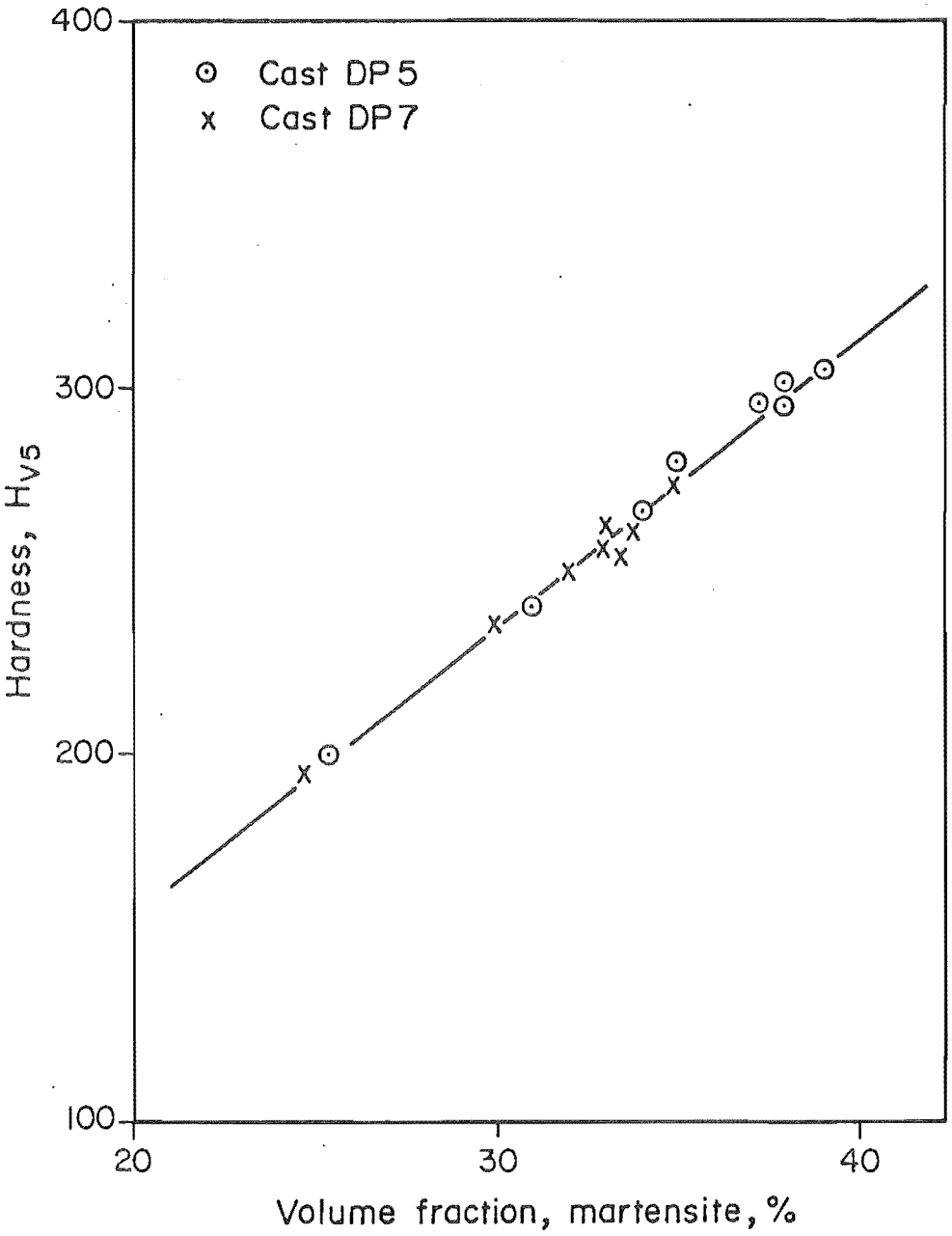

Figure 7.6: Variation of hardness of the dual phase steels with volume fraction of martensite.

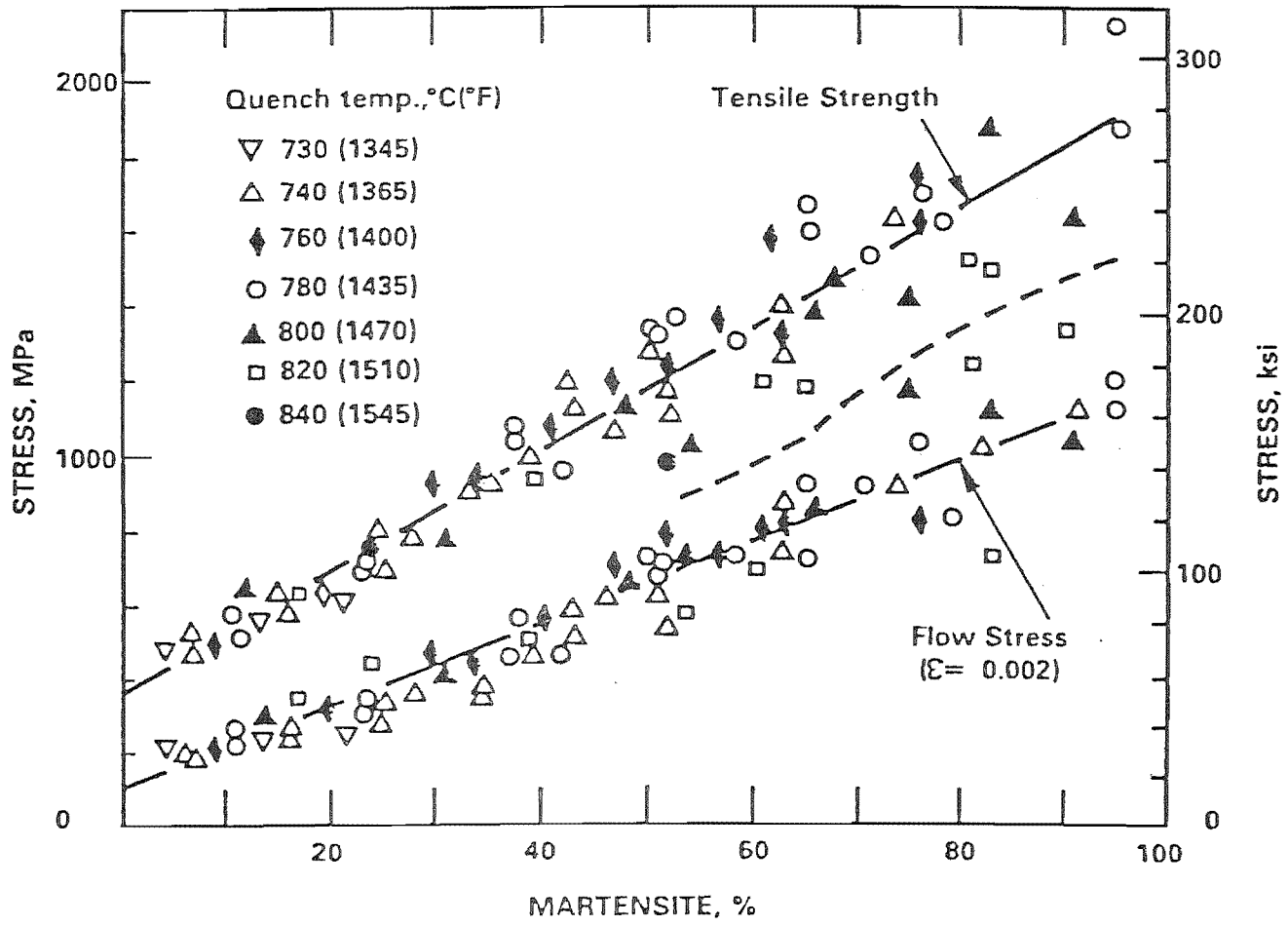

Figure 7.7: The 0.2% flow stress and tensile strength as a function of percent martensite for a series of Fe-Mn-C alloys. (Ref.139.)

effect on the linear variation of hardness. A similar linear variation was obtained for tensile strength and flow stress for a Fe-Mn-C dual phase steel[139], shown in Figure 7.7.

7.7.3 Partitioning of Manganese and Nitrogen During Intercritical Annealing of Dual Phase Steels

7.7.3.1 Manganese Partitioning

As it has been mentioned earlier in this chapter, the partitioning of manganese between co-existing ferrite and austenite phases was investigated by energy dispersive microanalysis. The manganese concentration in the martensite (austenite) grains and the ferrite matrix, determined by this analysis, is shown in Figures 7.8(a),(b), (c) and (d) for steels DP1, DP5, DP6 and DP7 respectively.

The degree of manganese partitioned into austenite can be seen to increase with intercritical annealing time and eventually reaches a maximum equilibrium value. Further increases in annealing time do not show any significant changes in the maximum equilibrium amount in all four steels. (See Figure 7.9.) It is also clear from Figure 7.9 that maximum equilibrium amount of manganese partitioned into austenite increases with increasing manganese content of steel. It has been reported[133] that this maximum equilibrium value primarily depends on the annealing temperature, but also some dependence on the parent structure.

Another interesting feature to be seen in Figures 7.8(a) to (d) is the variation in manganese concentration in the martensite (austenite) for each analysed sample. The curves representing the partitioned manganese in austenite were drawn through the mean values determined from 10 to 12 experimental results. This variation of

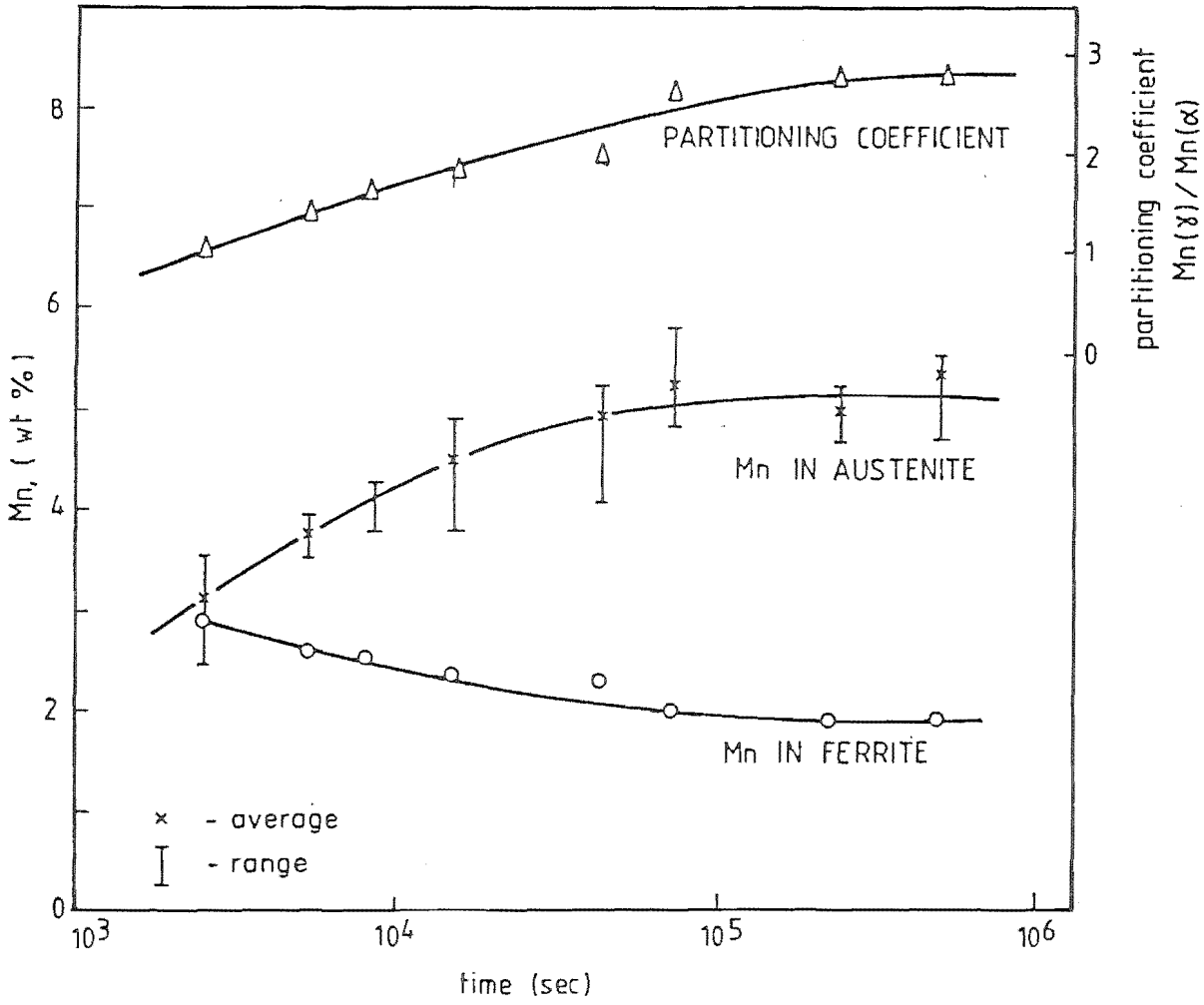

DP1

0·11% C
2·67%Mn
0·02%Si
0·06%Cr
0·01%V
0·0163%N

Heat treatment
690°C, WQ

Figure 7.8(a): Changes in Mn partitioning with time in steel DP1.

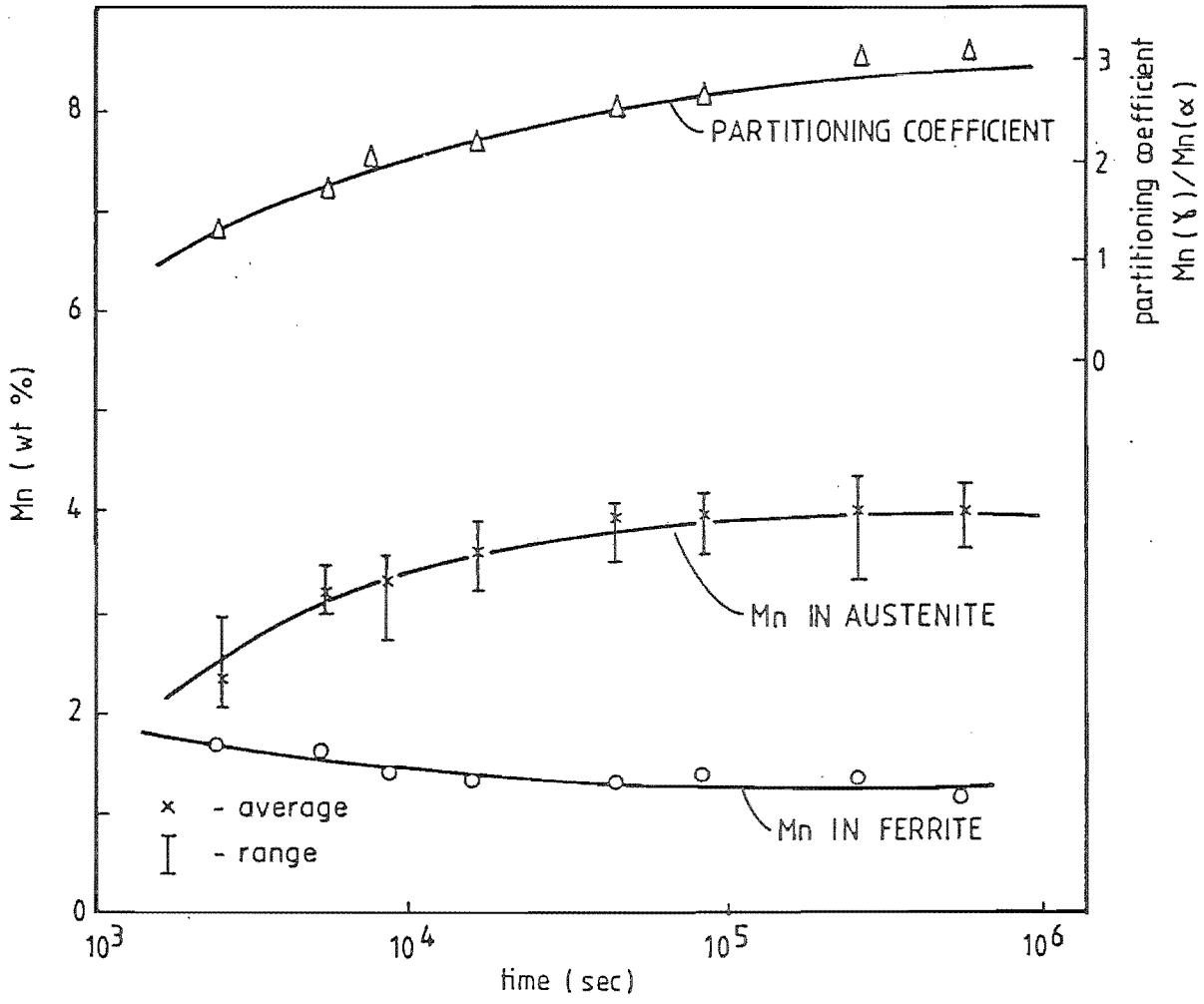

DP5

0·17%C
1·75%Mn
0·02%Si
0·60%Cr
0·06%V
0·0292%N

HEAT TREATMENT
715°C, WQ

Figure 7.8(b): Changes in Mn partitioning with time in steel DP5.

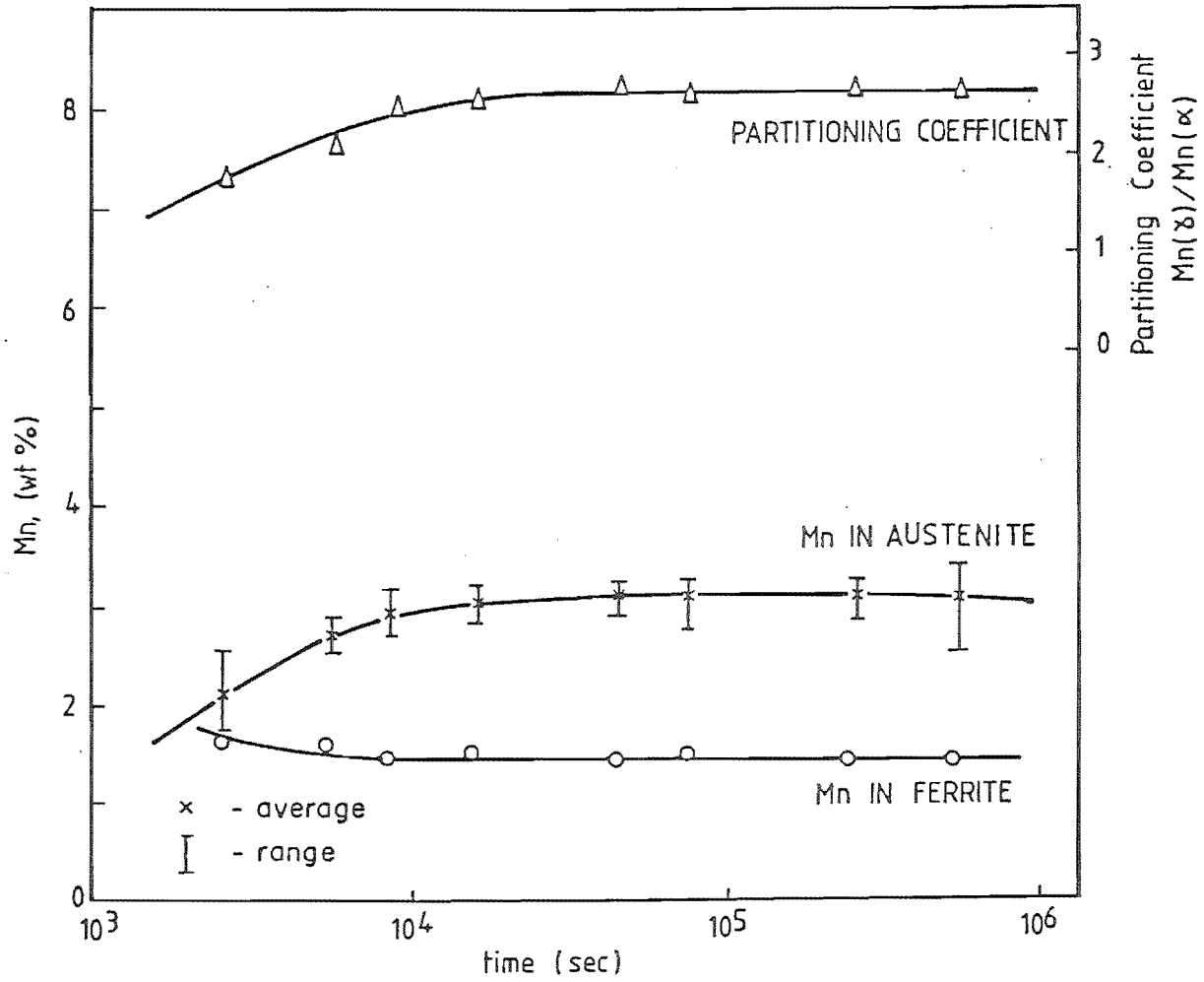

DP6

0·13% C
1·52% Mn
0·02% Si
0·40% Cr
0·06% V
0 0255%N

HEAT TREATMENT
715°C, WQ

Figure 7.8(c): Changes in Mn partitioning with time in steel DP6.

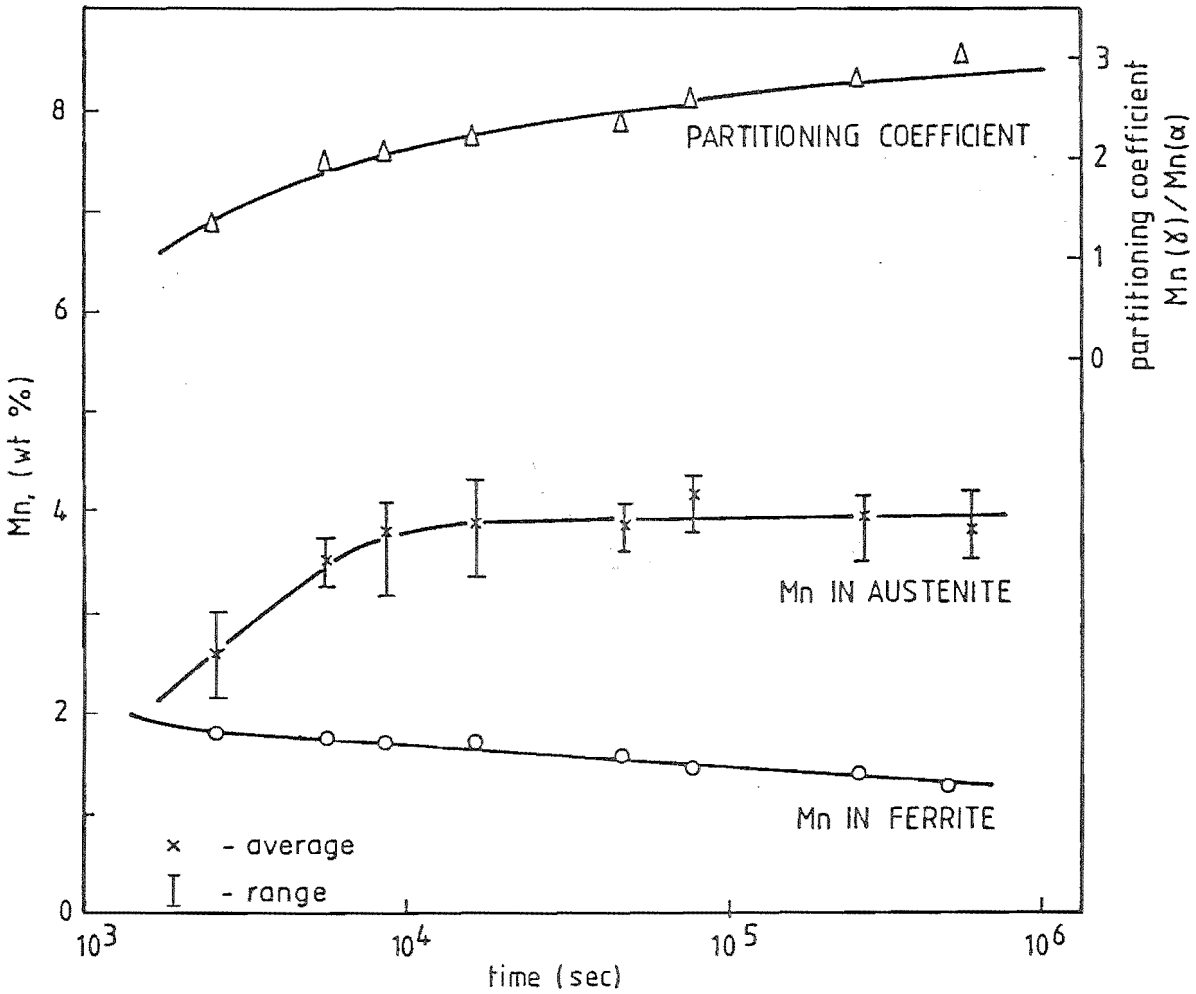

DP 7

0·14%C
1·88%Mn
0·02% Si
0·06% Cr
0·06% V
0·0224% N

Heat treatment
700°C, WQ

Figure 7.8(d): Changes in Mn partitioning with time in steel DP7.

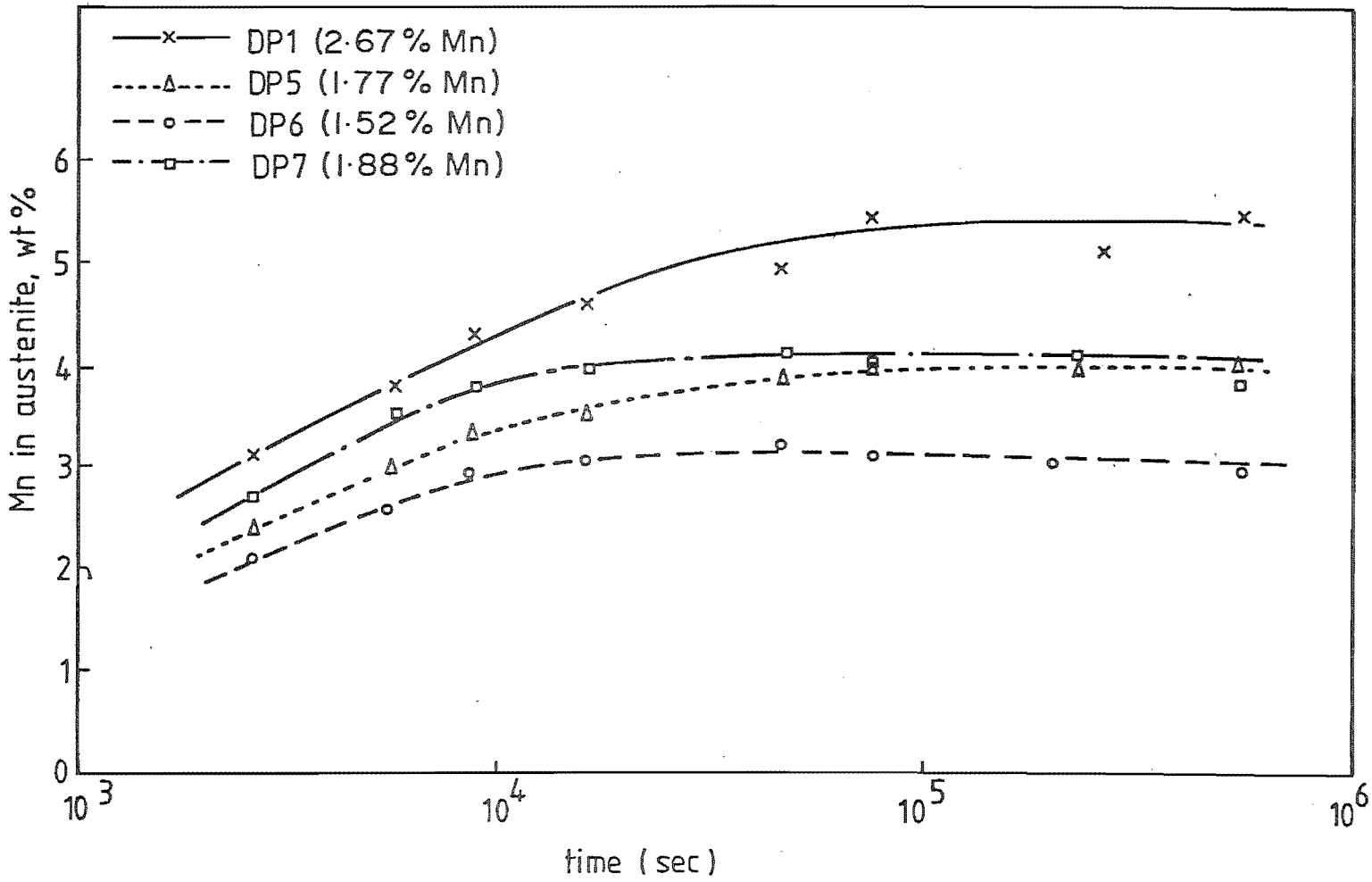

Figure 7.9: The variation in Mn content in austenite with time at intercritical annealing temperature.

manganese content in martensite (austenite) could be due to;

(i) Manganese concentration gradients within the martensite (austenite) grains. In the present work manganese content in martensite (austenite) was measured at arbitrarily selected points in martensite (austenite) grains. However, the distribution of manganese within martensite grain was investigated by Pussegoda et al[140] and this data is reproduced in Figure 7.10. These results suggest that it takes about 30 hours to eliminate manganese concentration gradients within austenite grains at 695°C. This may be the reason for the smaller variation observed in those samples heat treated for 50 and 100 hours ($\sim 10^5$ seconds), and shown in Figures 7.8(a) to (d).

(ii) Micro probe analysis gives results from a pear shaped volume below the surface and approximately 1 μm in diameter. Consequently some dilution in actual manganese content may be recorded when the analysed area penetrates into sub-surface ferrite. This results in a lower manganese concentration in martensite (austenite). Therefore, the higher values obtained in the energy dispersive microanalysis may give the correct amount of manganese partitioned into austenite.

The amount of manganese in ferrite, which was also determined by the energy dispersive microanalysis, is shown in Figures 7.8(a) to (d). The manganese content in the ferrite matrix initially decreases with increasing intercritical annealing time and reached a minimum equilibrium value after 10^5 seconds at all annealing temperatures.

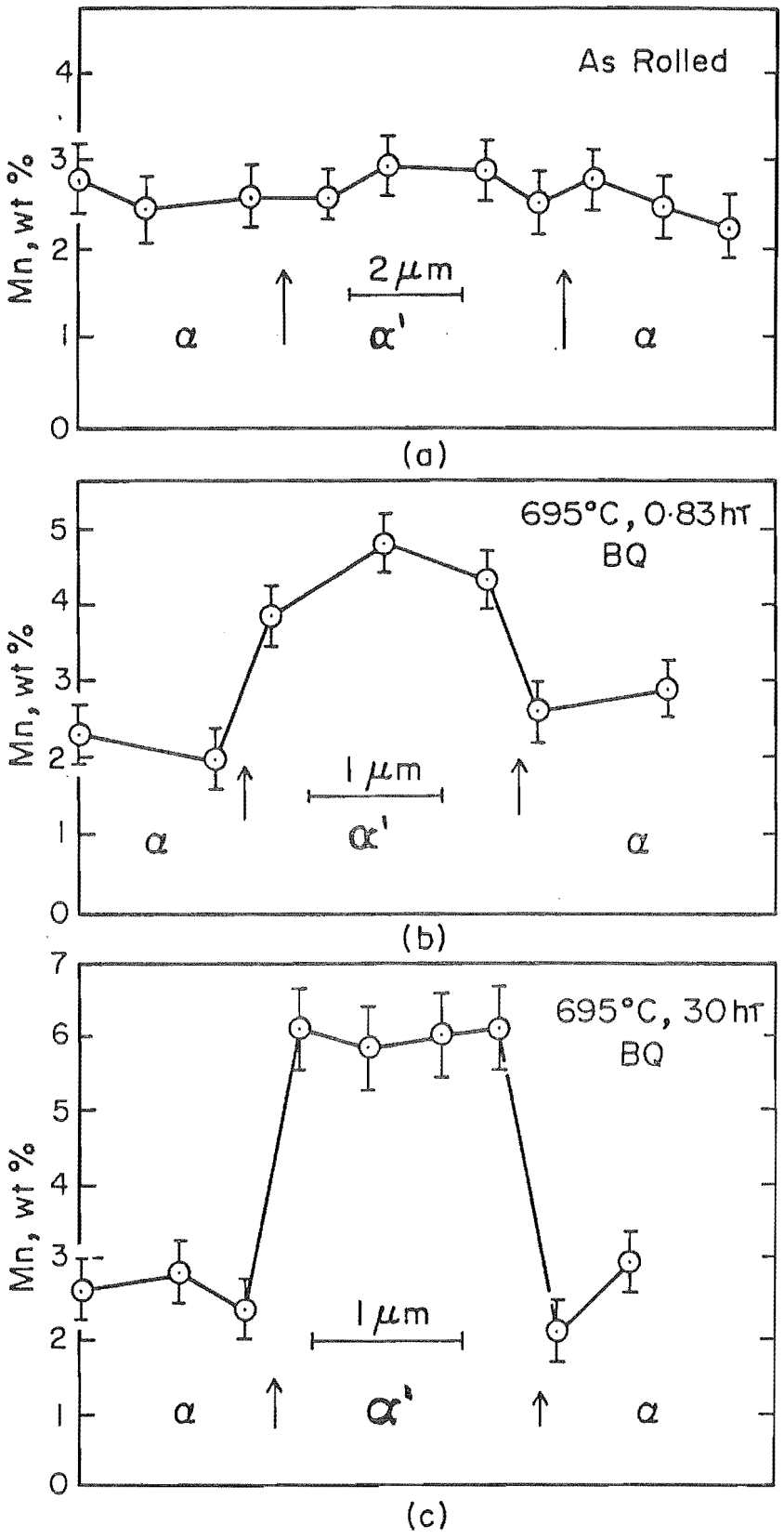

Figure 7.10: Mn distribution in ferrite and martensite: (a) as-rolled (before heat treatment), and after 695°C intercritical anneal for (b) 0.83 hr and (c) 30 hr followed by brine quenching. Positions of the α/α' boundaries are indicated. (Ref.140.)

Unlike the manganese content in martensite (austenite), very little variation in manganese concentration in the ferrite matrix was observed in any of the samples. This could be due to;

(i) The higher diffusion rate of manganese in ferrite than in austenite, (for example, the diffusivity of manganese in ferrite at 740°C is 1.2×10^{-16} m^2/s[141] while that in austenite at the same temperature is 6.8×10^{-19} m^2/s[142], i.e. smaller by a factor of over 175).

(ii) The volume analysed. Since the volume fraction of ferrite is greater than martensite and the ferrite grains are coarser than the martensite (austenite) grains, the analysed volume would more likely be free from martensite sub-surfaces, and the microprobe analysis give less variation of manganese content in ferrite than in martensite (austenite).

The partitioning coefficient, also shown in Figures 7.8(a) to (d), is defined as the ratio of average manganese content of the martensite (austenite) grains to manganese content in the adjacent ferrite matrix. The partitioning coefficient again increases with increasing intercritical annealing time to reach a maximum equilibrium value after 10^5 seconds.

Andrews[152] calculated the equilibrium partitioning coefficient using the following equation:

$$\frac{C^{\gamma}_{Mn}}{C^{\alpha}_{Mn}} = \exp\left(-\frac{\Delta H}{RT}\right) \qquad \text{Eqn.7.1}$$

in which C^{γ}_{Mn} and C^{α}_{Mn} are the concentration of manganese in austenite and ferrite, respectively, and ΔH is the difference between the heat of solution of manganese in ferrite and that of manganese in austenite. According to equation 7.1, the equilibrium partitioning coefficient should be approximately 3 at 840°C and increases with decreasing temperature to about 3.5 close to 700°C.

These values show reasonable agreement with experimental values from the present investigation, see Figures 7.8(a) to (d), Hillert[144], however, replaced the temperature independent ΔH values by a temperature dependent parameter based on the standard free energies of solution, and this refinement leads to a down-scaling of Andrew's partitioning coefficients and results in good agreement between the experimentally determined values of the present investigation, (see Table 7.5).

Figure 7.11 shows the effect of partitioned manganese content in martensite on the tensile strength of the experimental dual phase steels. The increase in tensile strength with manganese content in dual phase steels DP1, DP5, DP6 and DP7 is not unexpected. Manganese increases the strength of martensite phase by solid solution hardening, and thus increases tensile strength of dual phase steels of equal volume fraction of martensite.

7.7.3.2 Nitrogen Partitioning

A quantitative determination of nitrogen partitioning in the co-existing ferrite and austenite phases was attempted using the Jeol wave length dispersive X-ray analyser attached to JSM 35 scanning

Table 7.5: Comparison of experimental equilibrium partitioning coefficient values with calculated values.

Temperature °C	Equilibrium partitioning coefficient		
	Calculated by		Experimental Value From Fig.7.8(a) to (d)
	Andrew, (Ref.143)	Hillert, (Ref.144)	
690	3.51	3.02	2.85
700	3.50	3.00	2.85
715	3.43	2.92	2.80

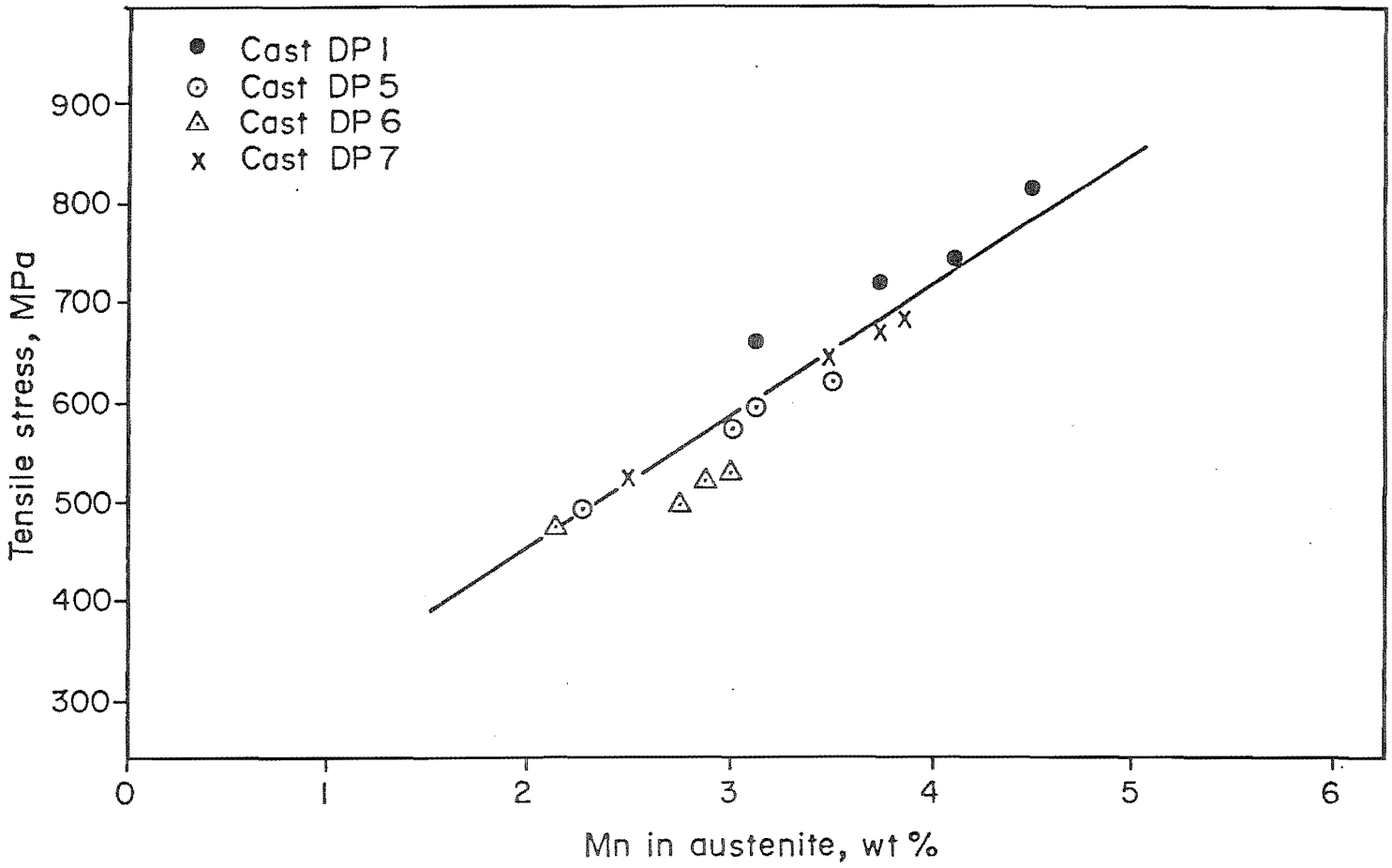

Figure 7.11: Change in tensile stress with Mn concentration in austenite.

electron microscope. However, this wave length X-ray analyser was unable to detect any significant differences in nitrogen content between the ferrite and austenite phases. It was consequently necessary to determine the partitioning of nitrogen by an indirect method.

Nitrogen is known to be solely responsible for strain ageing at ageing temperatures below approximately 150°C in hot rolled and/or annealed ferritic steels. It has been shown that the degree of strain ageing, as measured by changes in lower yield stress (ΔY), increases with active nitrogen content[62].

Nitrogen should diffuse into the austenite phase during the intercritical annealing process because of its higher solubility in austenite than that in ferrite. When quenching, the austenite transforms to martensite and since this transformation is "diffusionless", there will be no opportunity for nitrogen to migrate back to the ferrite phase. Consequently nitrogen atoms which have diffused into the austenite phase during intercritical annealing will be trapped in the martensite phase, leaving only that nitrogen retained in the ferrite phase available to cause strain ageing.

During strain ageing, the newly formed dislocations in the ferrite phase resulting from plastic straining are pinned in position by the segregation of the nitrogen atoms to these dislocation sites. Diffusion of the nitrogen atoms from the martensite phase into ferrite phase during ageing can probably be prevented by ageing at low temperatures (<60°C). The increase in lower yield stress (ΔY) due to the nitrogen pinning is therefore related to the active nitrogen

content in ferrite, with ΔY increasing with increasing active nitrogen content.

In order to determine ΔY, interrupted tensile tests were carried out on intercritically annealed tensile specimens (see section 7.6). During this test specimens were pre-strained by 3%, unloaded and subsequently aged at 60°C for an equivalent of one year at ambient temperature (determined by Hundy's equation[147]) before final tensile testing to fracture.

These results are summarized in Table 7.6, and the decrease in ΔY with increasing intercritical annealing time shows that nitrogen partitioning into the austenite occurs during the intercritical annealing treatment. For example, steel O-Y which contains about 0.01% active nitrogen, did not show any strain ageing, indicating that all the nitrogen is partitioned into the austenite phase even after short intercritical annealing times.

Figure 7.12 shows the effect of manganese content and intercritical annealing time on the partitioning of nitrogen in the experimental dual phase steels. These results suggest that manganese retards the partitioning of nitrogen, but does not suppress it. In high manganese steels (D1, DP5 and DP6), ΔY decreases with increasing intercritical annealing time and reaches zero in 4 hours (1.5×10^4 secs) at an intercritical annealing temperature of 715°C. This shows that in these high manganese steels (1.5 - 1.7% Mn) diffusion of all the active nitrogen into austenite phase takes about 4 hours. But in low manganese steels, e.g. experimental steel O-Y with 0.21% Mn, but with a similar active nitrogen content, all the active nitrogen diffused

Table 7.6: Variation of change in lower yield stress due to strain ageing (ΔY) with intercritical annealing time.

Cast	C wt%	Mn wt%	N_{active} wt%	ΔY , MPa				
				30 min. at temp., W.Q	1 hr at temp., W.Q	2 hrs at temp., W.Q	4 hrs at temp., W.Q	4 hrs at temp., F.C
DP1	0.11	2.67	0.0135	46	33	18	0	72
DP5	0.17	1.77	0.0125	53	31	9	0	65
DP6	0.13	1.52	0.0087	45	21	7	0	50
DP7	0.14	1.88	0.0067	30	34	20	0	37
A1	0.10	1.42	0.0061	22	20	7	0	31
A5	0.09	1.38	0.0003	10	7	7	0	7
D1	0.14	1.57	0.0171	65	38	14	0	108
D4	0.15	1.33	0.0035	14	16	7	0	17
N	0.14	0.63	0.0137	7	0	0	0	78
A	0.06	0.33	0.0002	0	0	0	0	7
O-Y	0.09	0.21	0.0111	0	0	0	0	52
S-T	0.14	1.48	0.0044	36	20	10	0	22

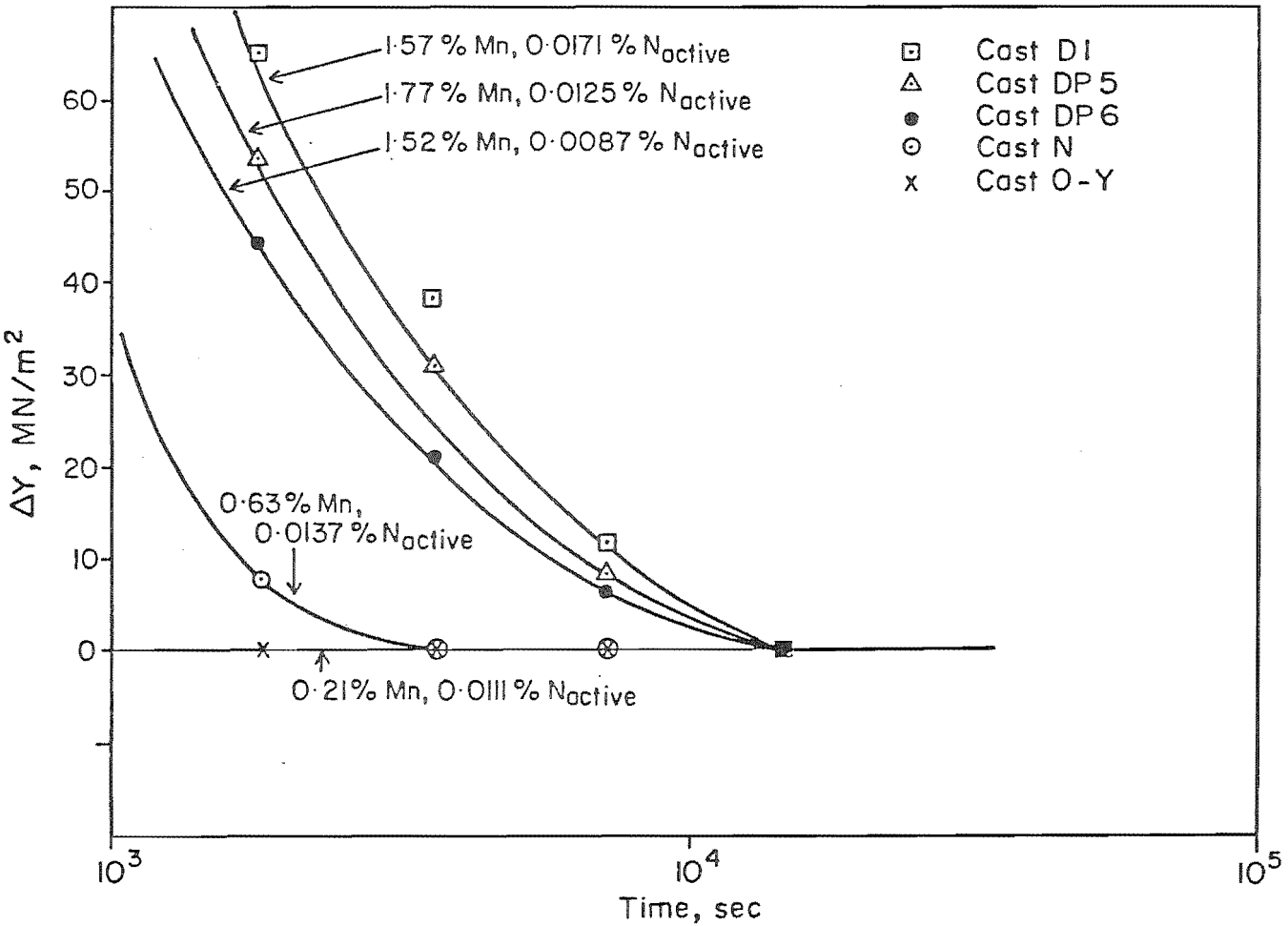

Figure 7.12: Partitioning of nitrogen in dual phase steel.

into austenite within less than 30 minutes ($1.8x10^3$ secs) at an intercritical annealing temperature of 735°C. Manganese is believed to form atom pairs within the iron lattice, and providing low energy sites for nitrogen atoms[32]. These sites would then be occupied in preference to the normal Fe-Fe interstitial sites, thus manganese reduces the diffusion rate of nitrogen in ferrite. This would account for the longer periods required at intercritical annealing temperatures for diffusion of all the active nitrogen into austenite of high manganese steels.

Figure 7.13 compares the partitioning of nitrogen and manganese in two of the experimental steels. It appears from this figure that the time taken for the diffusion of all the active nitrogen into austenite is similar to the time taken for manganese to reach its maximum equilibrium concentration in austenite. This suggests also that nitrogen atoms occupy the Mn-Mn interstitial sites and diffuse with manganese, which always takes place at a slower rate because of its lower diffusivity.

Figure 7.14 shows the variation of strain ageing parameter (ΔY) with active nitrogen content in water quenched and furnace cooled specimens from intercritical annealing temperature. The increase in ΔY with active nitrogen content obtained for furnace cooled specimens is not unexpected, but the corresponding water quenched specimens do not show strain ageing. Hence it would seem that all the active nitrogen has partitioned into austenite during intercritical annealing and no active nitrogen is left in the ferrite phase to show strain ageing.

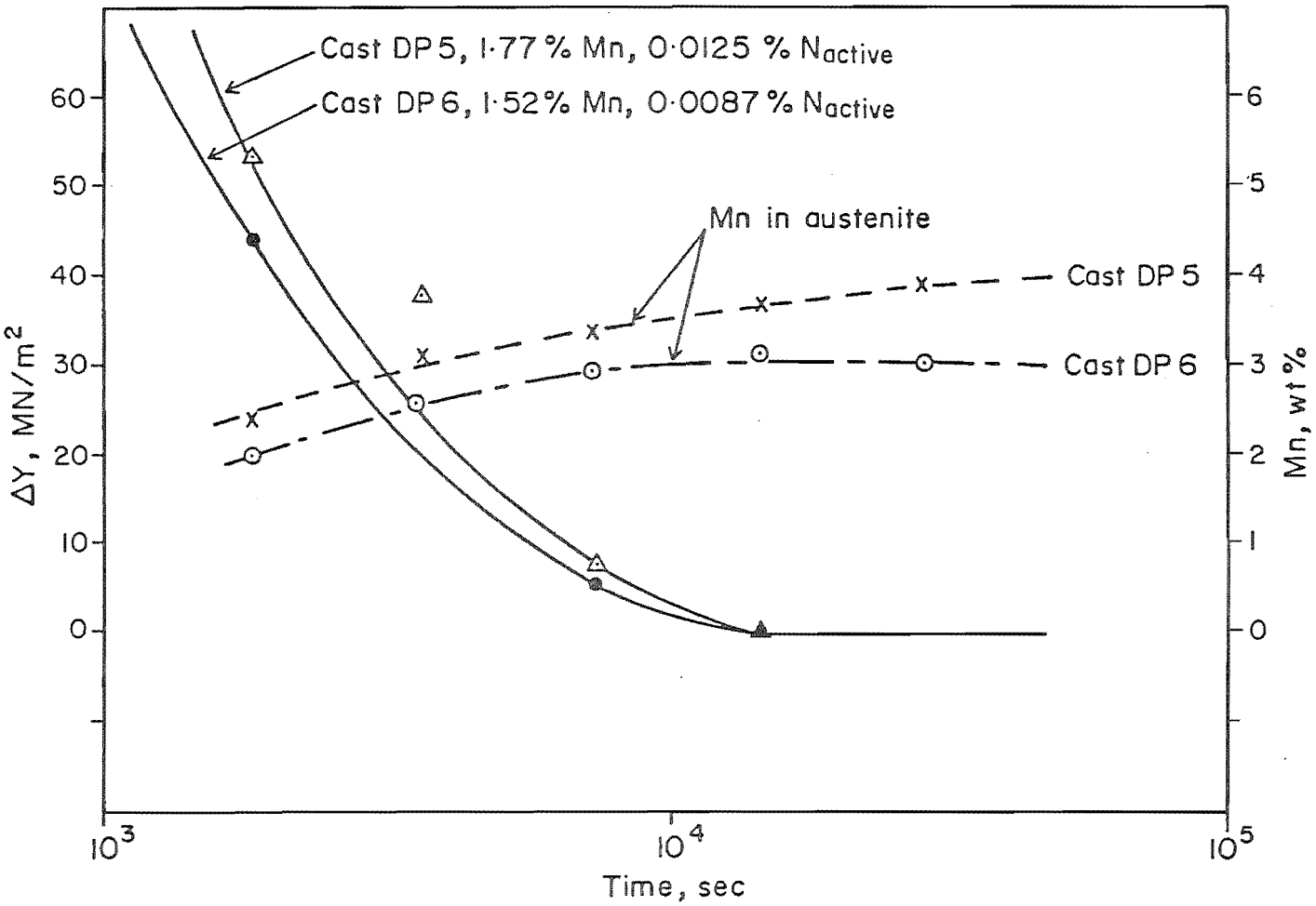

Figure 7.13: Effect of manganese on nitrogen partitioning.

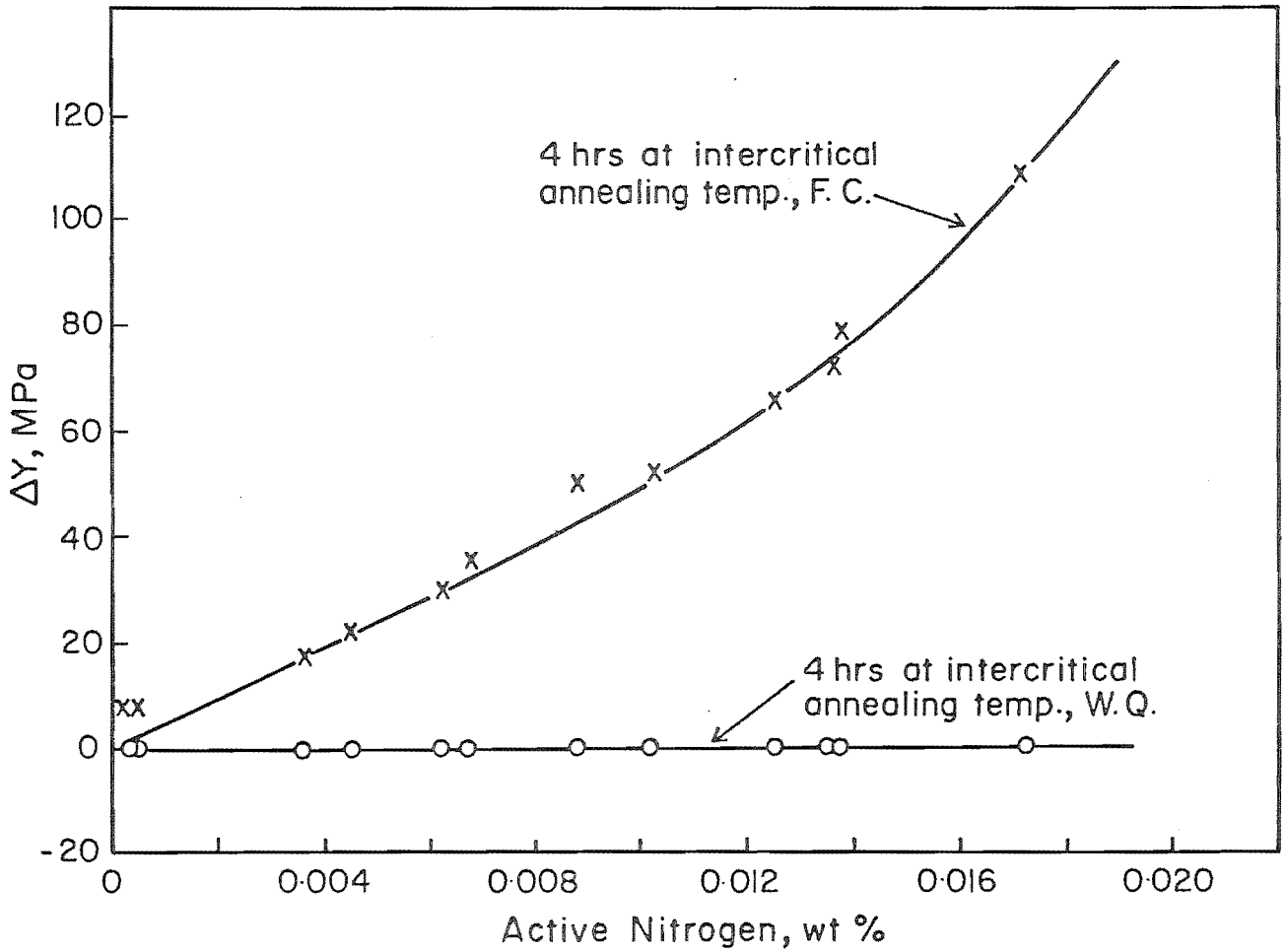

Figure 7.14: Effect of active nitrogen content on strain ageing in water quenched and furnace cooled specimens.

7.7.4. Chromium Partitioning

For the ideal dual phase steel combination of ductile ferrite with 10 to 20 percent high strength martensite, alloy additions are required which will have minimum effect on ferrite strength and ductility, but give good stability and hardenability of the austenite phase. Published data [145,146] suggest that chromium additions will least affect the ductility of the ferrite matrix while maintaining good hardenability for martensite phase formation, (see Figures 7.15 and 7.16). But chromium is a ferrite stabilizing element, and therefore it would be expected that chromium partitioning into ferrite during intercritical annealing would occur and reducing the ductility of the ferrite matrix.

As it has been mentioned earlier in this chapter, the partitioning of chromium between co-existing ferrite and austenite phases was also investigated by energy dispersive microanalysis. The chromium content in the martensite (austenite) grains and the ferrite matrix determined by this analysis is shown in Figure 7.17 for steel DP5.

The experimental results show that the partitioning of chromium during intercritical annealing is insignificant. This result is desirable for optimum dual phase properties. Chromium partitioning may occur with higher chromium contents, but the longer resolution time required to dissolve chromium rich carbides during the intercritical annealing would also present a problem.

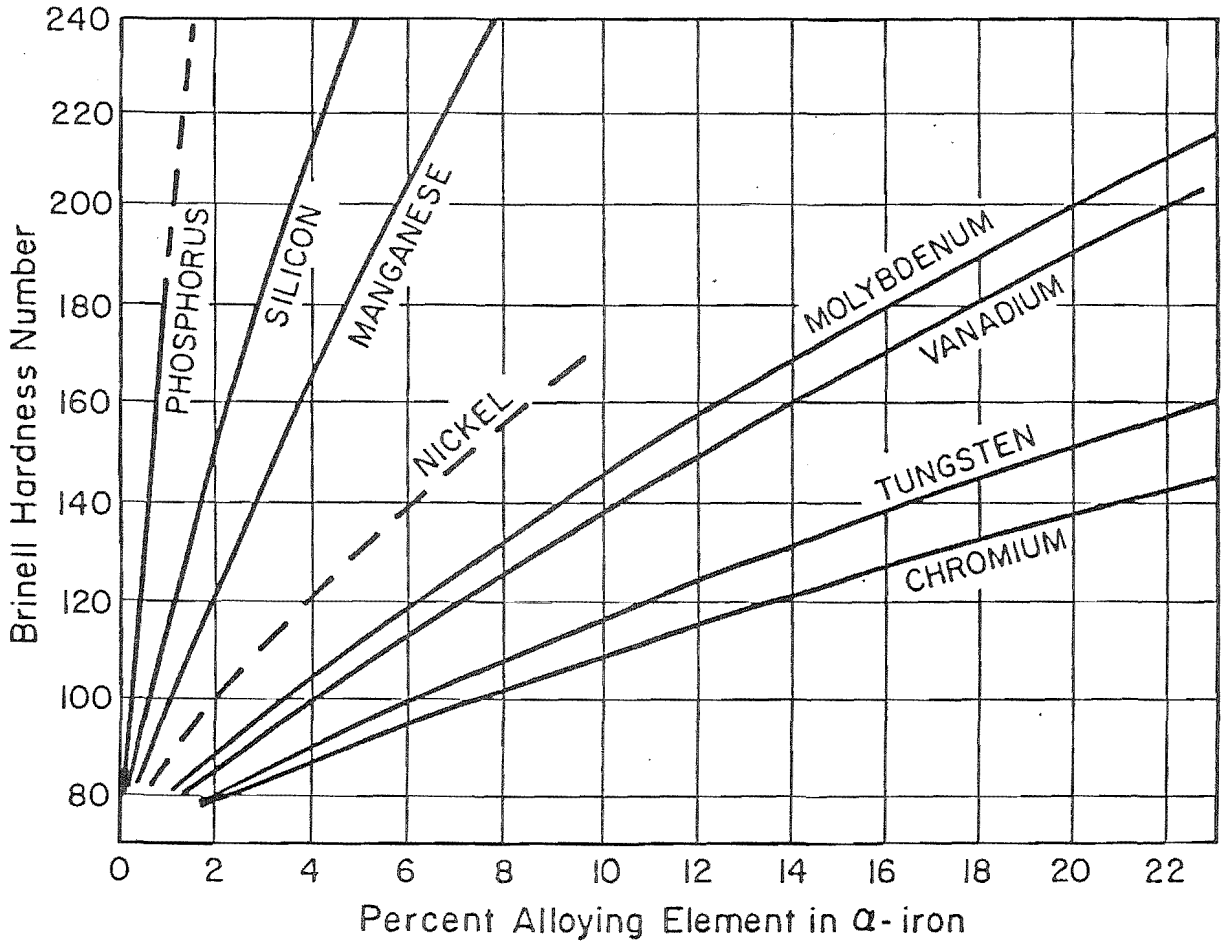

Figure 7.15: Hardness of alloy ferrites. (Ref. 146.)

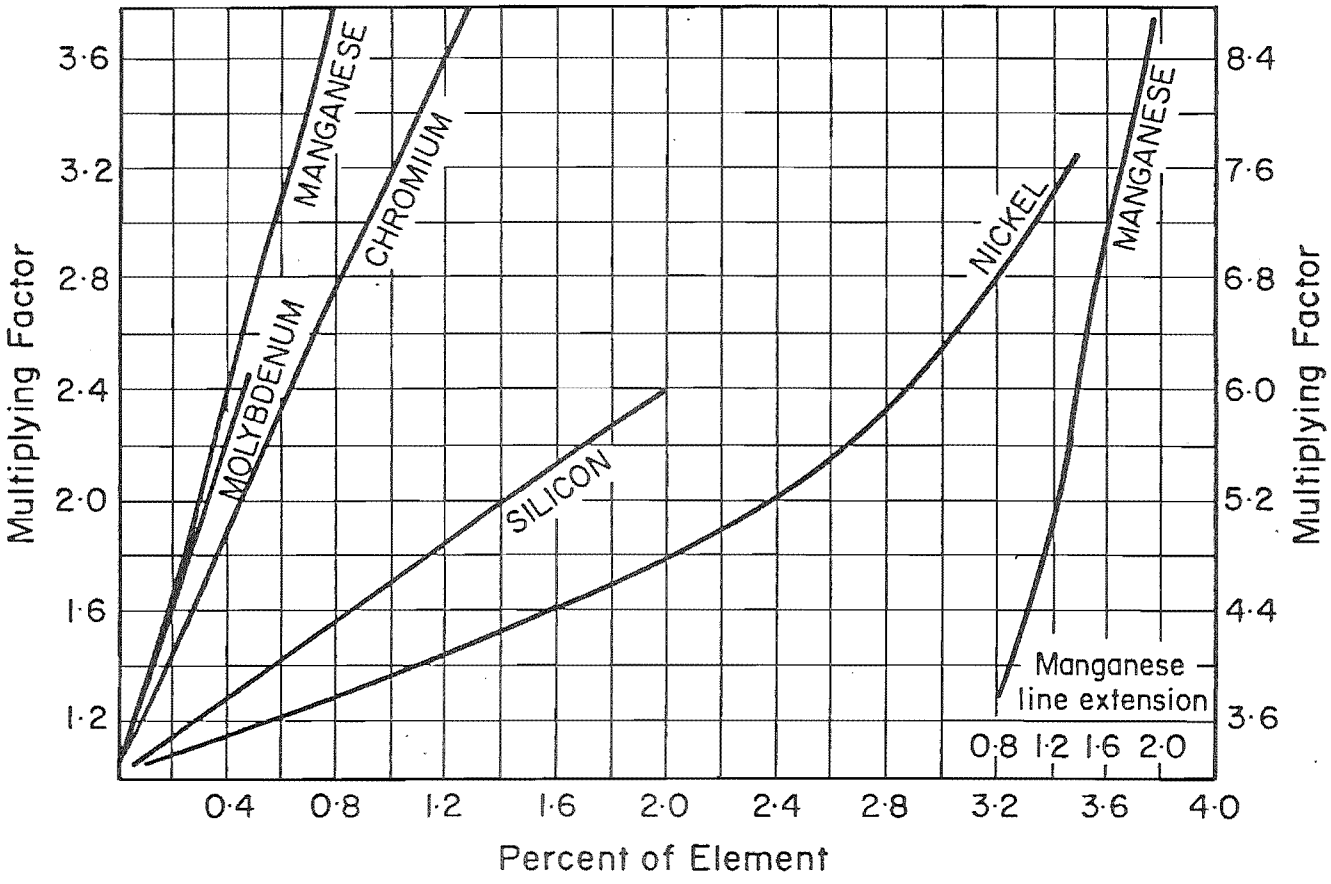

Figure 7.16: Hardenability factors for alloy steels.(Ref.146.)

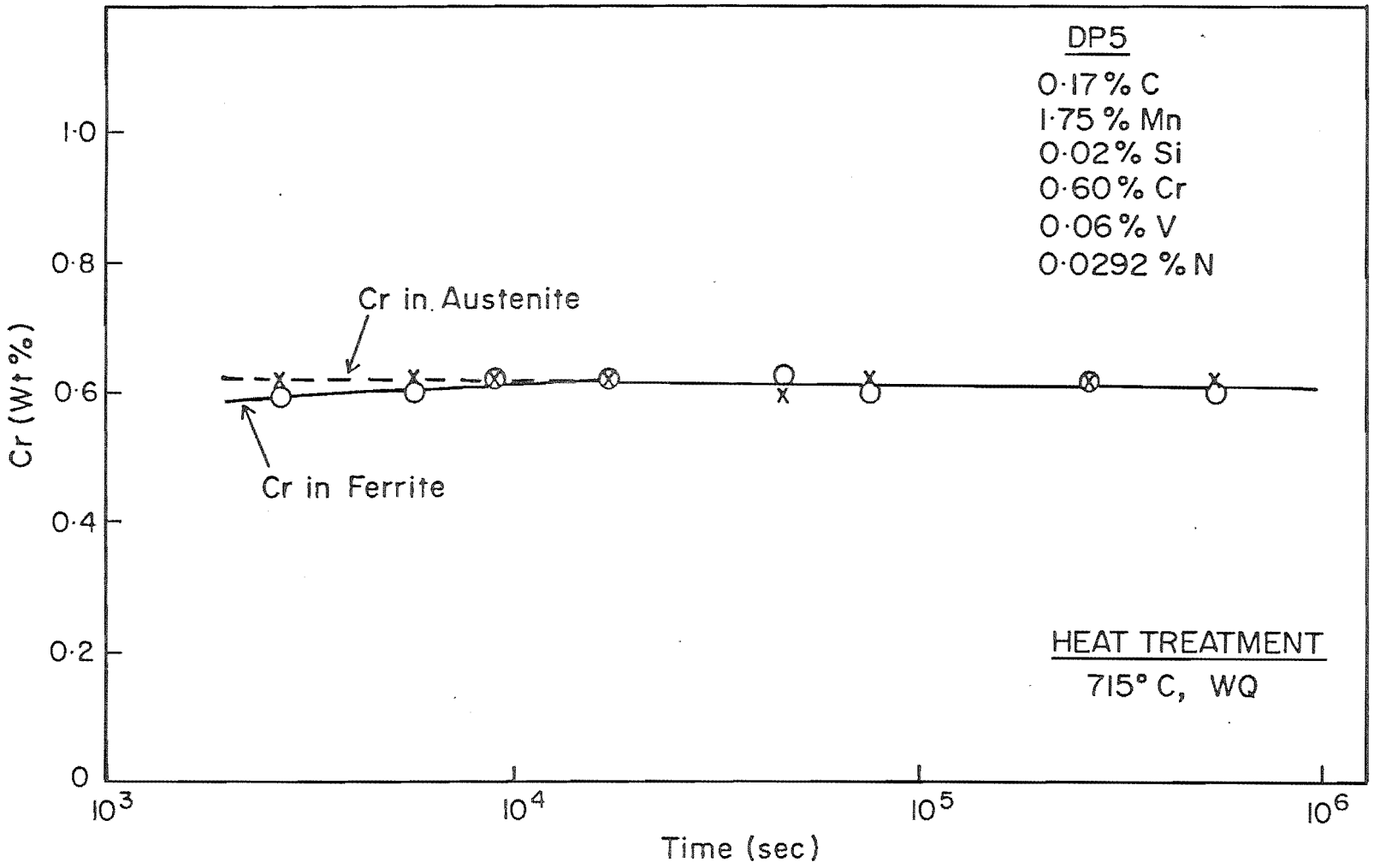

Figure 7.17: Effect of intercritical annealing time on Cr partitioning.

7.7.5 Effect of Manganese Partitioning on the Formation of Martensite During Slow Cooling

The development of a dual phase structure in steel requires that the steel be cooled relatively rapidly (e.g. as in continuous annealing) from the intercritical annealing temperature. Because of limited continuous annealing facilities in the domestic steel industry, there is interest in using other existing process facilities, such as batch annealing, to produce dual phase steels. Thus the purpose of the present investigation was to further explore earlier observations that high manganese steels can develop a dual phase microstructure during the slow cooling rates (e.g. 30°C/hr) that are associated with the batch annealing process at New Zealand Steel.

It has been observed in the present investigation that manganese partitions into austenite during intercritical annealing and takes about 10^5 second (~ 28 hours) to achieve maximum equilibrium concentration. It is intended that this manganese enriched austenite transforms to martensite on cooling.

Batch annealing at New Zealand Steel is carried out in three natural gas fired radiant tube furnaces in a reducing atmosphere of hydrogen and nitrogen. The method is known as the Uni-Flow Annealing System (U.A.S.) since the coils of strip are loaded in the furnace, proceed through, and are then discharged from the opposite end, travelling through the furnace in one direction. The coils are loaded with the coil bore vertical onto a coil transfer tray and charged to the heating chamber. The trays carry a maximum weight of 180 tonnes (9 coils of 20 tonnes each). Heating continues until the required

coil temperature is reached after which a soaking period of 4 hours is allowed to ensure uniform temperature throughout the coils. The coils are then transferred to the cooling chamber where cooling is carried out, still in a protective atmosphere, by air being blown through heat exchangers which cool the chamber atmosphere. The total annealing time for a tray of 9 coils is about 40 hours made up of a heating cycle including charging, purging and soaking of 17.5 hours and a cooling cycle, including purging and discharging, of 22 hours.

Samples from steels DP1, DP5, DP6 an DP7 were intercritically annealed at appropriate temperatures for two different periods, ½ hr and 4 hrs, and cooled at a rate of

(a) 15°C/hr;

(b) 30°C/hr, (cooling rate of coils in the batch annealing process at New Zealand Steel)

from the intercritical annealing temperature. Observed microstructures of the intercritically annealed samples are given in Table 7.7.

(a) Cooling Rate 15°C/hr

High temperature transformation product was found in all four steel samples intercritically annealed for both ½ hr and 4 hrs.

(b) Cooling Rate, 30°C/hr

Dual phase microstructures (ferrite plus martensite) were observed in all four steel samples intercritically annealed for 4 hrs, but high temperature transformation product was found in those samples annealed for only ½ hr, (see Figures 7.18(a) and (b)).

Table 7.7: Observed microstructures in intercritically annealed samples.

Cast	Intercritical annealing temp.°C	Microstructure			
		Cooling rate 15°C/hr		Cooling rate 30°C/hr	
		½ hr at temp.	4 hrs at temp.	½ hr at temp.	4 hrs at temp.
DP1	690	H.T.T.P.	H.T.T.P.	H.T.T.P.	D.P.
DP5	715	H.T.T.P.	H.T.T.P.	H.T.T.P.	D.P.
DP6	715	H.T.T.P.	H.T.T.P.	H.T.T.P.	D.P.
DP7	700	H.T.T.P.	H.T.T.P.	H.T.T.P.	D.P.

H.T.T.P. - High temperature transformation product.

D.P. - Dual phase (ferrite plus martensite)

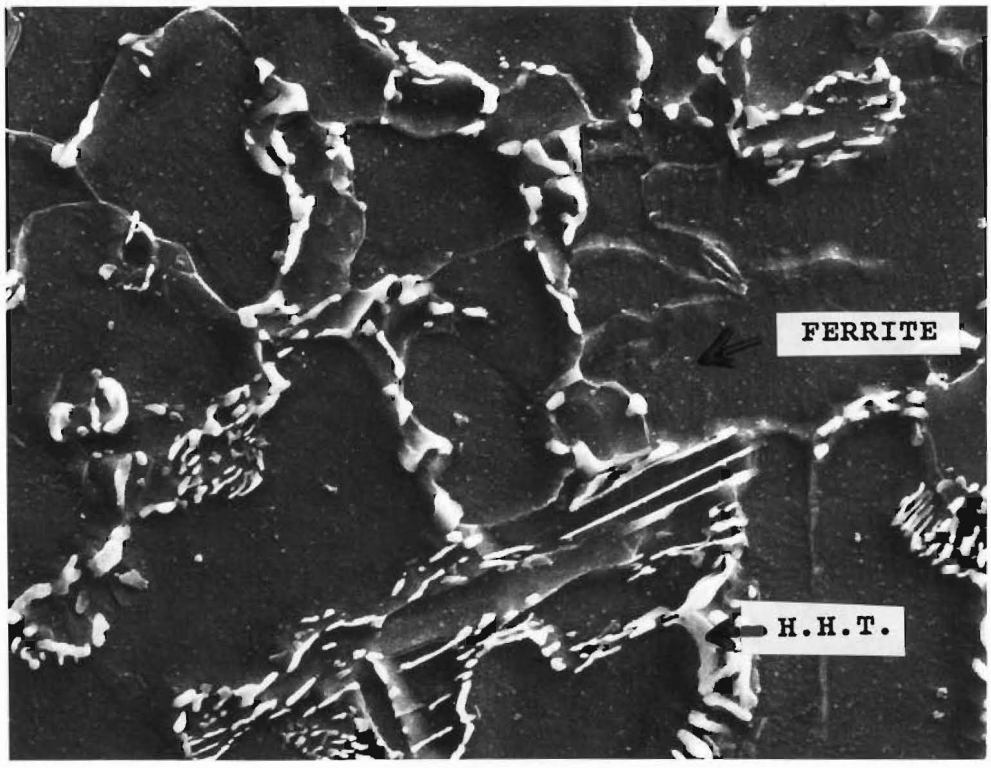

Figure 7.18(a): Scanning electron micrograph of steel DP5, intercritically annealed at 715°C for ½ hr, and cooled at 30°C/hr.

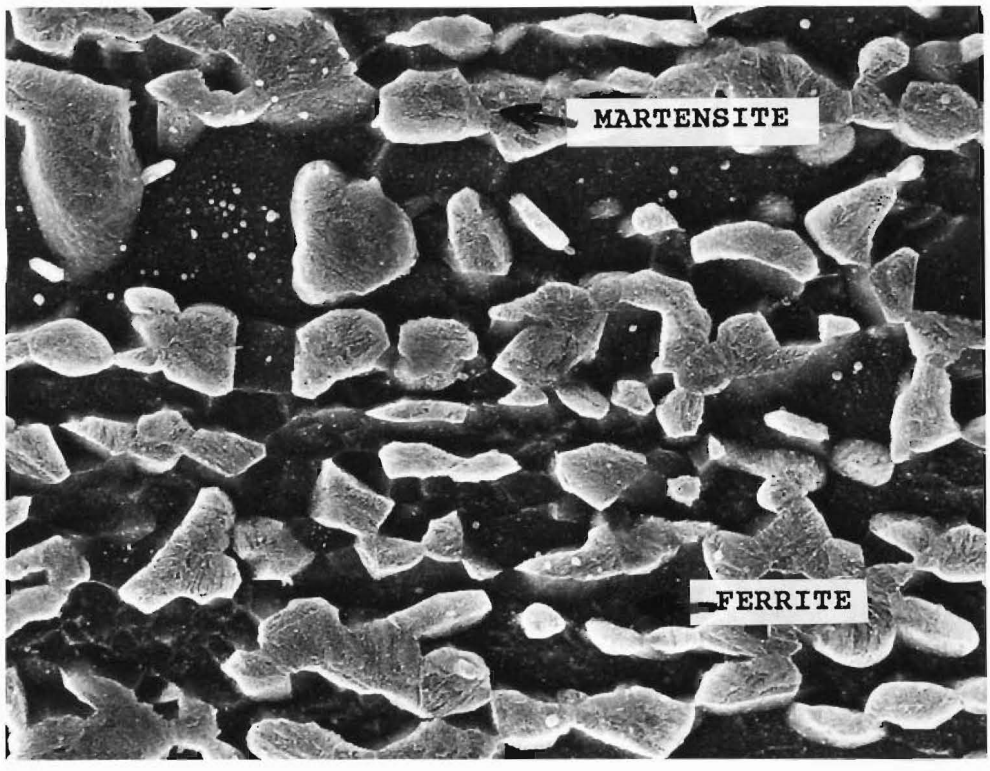

Figure 7.18(b): Scanning electron micrograph of steel DP5, intercritically annealed at 715°C for 4 hrs, and cooled at 30°C/hr.

A critical cooling rate is required for the formation of the dual phase microstructure. Tanaka et al[132] studied the effectiveness of manganese in raising the intercritical hardenability of austenite and derived the following empirical relation:

$$\text{Log CR}(^{\circ}\text{C/sec}) = -1.73\ Mn_{eq} + 3.95 \qquad \text{Eqn.7.2}$$

where CR is the critical cooling rate required for the transformation of austenite into martensite when cooled from intercritical temperature range, and Mn_{eq} is the manganese equivalent, given by:

$$Mn_{eq} = Mn + 1.3\ Cr + 2.67\ Mo \qquad \text{Eqn.7.3}$$

where the element symbols stand for their respective weight percentage.

It can be seen from equations 7.2 and 7.3 that the logarithm of the critical cooling rate decreases in a linear manner with increasing manganese content. Calculated critical cooling rates for all four experimental steels, using equations 7.2 and 7.3, are tabulated in Table 7.8. The amount of manganese partitioned into austenite is lower in samples annealed for ½ hr than in samples annealed for 4 hrs. Therefore the required critical cooling rate, for the formation of dual phase microstructures, is higher for those samples annealed for ½ hr and significantly greater than the cooling rate (30°C/hr) employed, (see Table 7.8). However full agreement between the achieved microstructures, Table 7.7, and the calculated critical cooling rate, Table 7.8 is not always obtained.

Table 7.8: Effect of Mn & Cr contents on critical cooling rate.

Cast	Intercritical annealing temp.	Mn content in austenite, wt%		Cr content in austenite, wt%		Calculated critical cooling rate from Eqn.7.2, °C/hr	
		½ hr at temp.	4 hrs at temp.	½ hr at temp.	4 hrs at temp.	½ hr at temp.	4 hrs at temp.
DP1	690	3.1	4.5	0.06	0.06	102	0.4
DP5	715	2.3	3.6	0.6	0.6	150	0.9
DP6	715	2.1	3.0	0.4	0.4	941	26
DP7	700	2.6	3.8	0.06	0.06	747	6

7.8 SUMMARY

The partitioning of nitrogen has been investigated in high (1.5 - 1.8%) and low (0.2%) manganese dual phase steels. It has been demonstrated that significant partitioning of nitrogen and manganese occurs between austenite and ferrite phases during intercritical annealing. It has also been shown that about 1.5% manganese retards the partitioning rate of nitrogen by retarding the long range diffusion of nitrogen.

A mechanism by which manganese can exert such a profound effect on the partitioning of nitrogen between austenite and ferrite phases has been suggested. i.e. that the formation of manganese atom pairs provides low energy sites for nitrogen atoms and these sites are then occupied in preference to the normal interstitial sites. This effectively pins the nitrogen atoms and restricts their long range diffusion.

It has also been demonstrated that dual phase microstructures can be produced by slow cooling from intercritical annealing temperatures. The manganese enriched austenite formed during intercritical annealing and resulting from manganese partitioning, will transform into martensite during cooling at 30°C/hr.

CHAPTER 8

CONCLUSIONS

This thesis has embraced the study of nitrogen in high strength, low alloy and dual phase steels. Sources and control of nitrogen in various steelmaking processes have been discussed. The effect of 'active' nitrogen and nitrogen combined as stable nitrides on steel properties has also been discussed.

A detailed investigation of the variation in nitrogen level during steel production at New Zealand Steel has been carried out with samples taken from iron leaving the melter, after the vanadium recovery unit (VRU), from steel samples after the oxygen blow in the (KOBM) converter, after a homogenizing purge at the ladle treatment station (LTS) and from the mould stream at the continuous casting machine (CCM). Multiple linear regression analysis has been used to establish a quantitative relationship between the nitrogen content and process variables.

It was found that hot metal from the melters had an average nitrogen content of 0.0027% and a further increase in nitrogen content was observed at VRU. However, there was a drop in nitrogen content after oxygen blowing in the KOBM. It is suggested that nitrogen in solution in the liquid steel is absorbed into gas bubbles passing through the steel bath giving a flushing action, consequently carbon monoxide bubbles formed during oxygen lancing will effectively reduce the nitrogen content. There was a significant increase in nitrogen content between the KOBM samples and LTS samples, and a further

increase in nitrogen content was observed in the CCM samples. These increases at the LTS and CCM seem to result from the absorption of nitrogen during tapping, transferring the ladle to the LTS and teeming at the CCM where there is little protection of the molten stream from the atmosphere and consequential nitrogen absorption.

The production of steels with a low nitrogen content needs the control of a great number of parameters during successive steps of liquid steel refining. At the converter stage (KOBM), special care must be taken with the amount of nitrogen introduced from feed materials (hot metal, scrap, oxygen etc.). A good combination of blowing condition and an avoidance of reblows are required to obtain low nitrogen levels before tapping. During the remaining process steps (ladle treatment, continuous casting), the main goal is to restrict nitrogen pick-up from the atmosphere. Efficient protection of the molten steel from the atmosphere at ladle treatment station and continuous casting machine represents the most important action for control of nitrogen level.

The effect of nitrogen on the properties of steel can be either beneficial or detrimental, depending on the steel composition, processing treatment, and the use of the product. During thermo-mechanical processing of microalloyed steels, micro alloying elements such as vanadium, aluminium, titanium etc. combine with nitrogen to form stable nitride precipitates. These nitride precipitates play a major role in controlling the mechanical properties of microalloyed steels. The investigation reported here had as its objective the simulation of a hot rolling mill thermal cycle typical for the production of high strength, low alloy steels. The effect of this

thermal cycle on precipitation, grain size and mechanical properties was studied using vanadium as the microalloy addition.

The solubility of vanadium nitride in high strength, low alloy steels was determined for the temperature range 900°C to 1250°C. Since there were no other strong nitride formers present in the experimental steels, the 'acid-soluble' component was assumed to represent the nitrogen combined as vanadium nitride. From these individual results, the solubility product (K_s) relationship with temperature for vanadium nitride in austenite was determined using linear regression analysis, and gave the following result:-

$$\text{Log}_{10}\ K_s = -\frac{7754}{T} + 3.02 \qquad \text{Eqn.4.19}$$

The solution temperature of vanadium of vanadium nitride in each experimental steel was found from the above equilibrium relationship.

The analysis N_{insol} content of simulated hot rolled samples suggests that the precipitation of vanadium nitride is most rapid in the ferrite phase, and is diffusion controlled. Peak precipitation consequently occurs at a simulated coiling temperature of 700°C in the HSLA steels examined and there was no evidence to show that the undissolved vanadium nitride present at the reheat furnace temperature acted as nuclei for precipitation at lower temperatures.

The ferrite grain size of samples subjected to the simulated thermal cycle for all 'coiling' temperatures is significantly coarser than that normally expected in HSLA steels, however there was no

mechanical deformation subsequent to reheating and the initial austenite grain size would consequently be coarser than normal.

When samples are normalized from 900°C after the simulated thermal cycle, the ferrite grain size is considerably reduced and lies within the range normally expected for high strength, low alloy steels. Analysis for N_{insol} on the normalized samples gave a consistent result for all simulated coiling temperatures. This shows that the precipitation of vanadium nitride is rapid on reheating to normalizing temperature. Minimum ferrite grain size for the simulated rolling thermal cycle, and for samples subsequently normalized, suggest that vanadium nitride formed in the ferrite phase dominates grain size effects.

Changes in lower yield strength, charpy transition temperature and strain age propensity of high strength, low alloy steels micro-alloyed with vanadium, have also been determined after the simulated hot rolling thermal cycle. A second test series was also conducted on samples normalized after the above simulated thermal cycle.

Although the ferrite grain size is significantly coarser than that normally expected in high strength, low alloy steels, the yield strength values fall within the normally expected range for these steels. This suggests then that the yield strength is strongly dependent on the volume fraction and size of the vanadium nitride precipitate. The resistance provided by this precipitate to free dislocation motion increases the friction stress and consequently increases the yield strength. There is also some variation in yield

strength resulting from grain size effects, however these are of second order in magnitude after precipitation strengthening.

The strain ageing index has been shown to be strongly influenced by the 'active' nitrogen content which in turn is controlled by the amount of vanadium nitride precipitated. The degree of strain ageing observed in simulated hot rolled samples is much less than expected, especially in the range of 0.0060% to 0.015% active nitrogen, but the degree of strain ageing in the normalized samples falls within the range normally expected for those active nitrogen levels. Although the simulated hot rolled samples have a higher active nitrogen content than normalized samples, the coarser ferrite grain size of these simulated hot rolled samples reduces the degree of strain ageing observed.

The effect of vanadium nitride precipitate during the simulated hot rolling thermal cycle on the impact-transition temperature has also been investigated. The impact-transition temperature has been shown to be influenced by both grain size and volume fraction of vanadium nitride precipitated. The vanadium nitride precipitate increases the transition temperature by increasing the σ_o^* value whilst finer grain size decreases the transition temperature.

Nitrogen also has influence on the microstructure and properties of the dual phase steels examined. Nitrogen increases the hardenability of the austenite phase formed at intercritical annealing temperature. It has been shown that nitrogen partitioning occurs during the intercritical annealing heat treatment, and that manganese retards nitrogen partitioning.

Manganese partitioning in dual phase steels has been investigated and it was found that the degree of manganese partitioned into austenite increases with annealing time and eventually reaches a maximum equilibrium value. The maximum equilibrium value has been shown to be primarily dependent on the intercritical annealing temperature and manganese content of steel.

The partitioning of nitrogen has been investigated in high (1.5% - 1.8%) and low (0.2%) manganese dual phase steels. It has been shown that significant partitioning of nitrogen occurs between austenite and ferrite phases during intercritical annealing. Experimental results shows that in the high manganese steels, partition of all the active nitrogen into the austenite phase takes about 4 hours at an intercritical annealing temperature of 720°C, but in steels of low manganese content with a similar active nitrogen content, all the active nitrogen partitioned into austenite in less than 30 minutes at an intercritical annealing temperature of 725°C. Manganese is believed to form atom pairs within the iron lattice, these couples providing low energy sites for nitrogen atoms. These sites would then be occupied in preference to the normal Fe-Fe interstitial sites, and thus manganese reduces the diffusion rate of nitrogen in ferrite. This would account for the longer periods required at intercritical annealing temperatures for partition of all the active nitrogen into austenite of high manganese steels.

It has also been demonstrated that dual phase microstructures can be produced by slow cooling from intercritical annealing temperatures. The critical cooling rate required for the austenite to martensite transformation is decreased with increasing manganese

content in the austenite phase. Therefore the critical cooling rate is dependent on the degree of manganese partitioning. It has been shown that manganese enriched austenite formed during intercritical annealing of high manganese (1.5%) steels transforms into martensite during cooling at 30°C/hour.

From this study it is possible to draw a clear conclusion, namely that nitrogen is and must always be considered an essential alloying element. In large measure its benefits lie in its interaction with the other alloying elements invariably present in the steels, and it is by understanding such interactions that the effects of nitrogen can be optimised and its sometimes less beneficial effects obviated.

By judicial use of nitrogen, and by capitalising on its undoubted beneficial effects, considerable improvements can be obtained in terms of steel properties, and by the use of what is probably the least expensive of alloying elements.

REFERENCES

(1) ERASMUS, L.A. Journ.Iron & Steel Inst., v202, January, 1964: pp.32-41.

(2) MORRISON, W.B. Ironmaking and Steelmaking, v16, February, 1989: pp.123-28.

(3) ERASMUS, L.A. and PUSSEGODA, L.N. Metallurgical Trans., v11A, February, 1980: pp.231-37.

(4) IRVINE, K.J. et al, Journ.Iron & Steel Inst., v205, February, 1967: pp.161-82.

(5) GLADMAN, T. and PICKERING, F.B. Journ.Iron & Steel Inst., v203, December, 1965: pp.1212-217.

(6) ERASMUS, L.A. and PUSSEGODA, L.N. New Zealand Engineering, v32, August, 1977: pp.178-83.

(7) BUTLER, J.F. and BUCHER, J.H. "Dual-Phase and cold pressing vanadium steels in the automobile industry". Seminar Proceedings, Vanadium International Technical Committee, London, October, 1978: pp.3-12.

(8) ERASMUS, L.A. Proceedings of Australasian Conference on "Materials for Industrial Development". Institute of Metals and Materials Australasia, Christchurch, New Zealand, August, 1987: pp.357-64.

(9) IRVINE, K.J. "Strong Tough Structural Steels". The Iron and Steel Institute publication no104, 1967: p.1.

(10) MAY, M.J. "Strong Tough Structural Steels". The Iron and Steel Institute publication no104, 1967: p.11.

(11) BARR, W. "The Fracture of Metals". Institution of Metallurgists, 1950: p.117.

(12) BARR, W. and HONEYMAN, A.J.K. Journ.Iron & Steel Inst., v157, October, 1947: pp.239-42.

(13) PETCH, N.J. Journ.Iron & Steel Inst., v174, May, 1953: pp.25-28.

(14) HALL, E.O. Proceedings Physics Society, Series B, v64, 1951: p.747.

(15) PICKERING, F.B. and GLADMAN, T. The Iron and Steel Institute's Special Report no81, 1963: p.10.

(16) WIESTER, H.J. and ULMER, H. Stahl und Eisen, v79, 1959: p.1120.

(17) MORRISON, W.B. and WOODHEAD, J.H. Journ.Iron & Steel Inst., v201, January, 1963: pp.43-47.

(18) LESLIE, W.C. "The Relationship Between Structure and Mechanical Properties of Metals". NPL Conference, Proceedings, Her Majesty's Stationery Office, 1963: p.334.

(19) KORCHYNSKY, M. and STUART, H. "Low-Alloy High Strength Steels". London-Scandinavian Conference, Nuremberg, 1970: p.17.

(20) MIHELICH, J.L. et al. Journ.Iron & Steel Inst., v209, June, 1971: pp.469-75.

(21) PHILLIPS, R. and CHAPMAN, J.A. Journ.Iron & Steel Inst., v204, June, 1966: pp.615-27.

(22) DUCKWORTH, W.E. et al. Journ.Iron & Steel Inst., v203, November, 1965: pp.1108-136.

(23) GROZIER, J.D. Microalloying '75. Conference Proceedings, Washington, D.C., U.S.A., October, 1975: pp.241-50.

(24) PLATTS, G.K. et al. The Metallurgist and Materials Technologist, v16, September, 1984.

(25) PICKERING, F.B. Microalloying '75. Conference Proceedings, Washington D.C. U.S.A. October, 1975, pp.9-31.

(26) GLADMAN, T. Metals Technology, v10, July, 1983: pp.274-81.

(27) TITHER, G. et al. Proceedings of 20th Mechanical Working Conference, AIME, Chicago, 1980: p.72.

(28) DAVIES, R.G. Journal of Metallurgy, v31, November, 1979: pp.17-22.

(29) COLDREN, A.P. and TITHER, G. Journal of Metallurgy, v30, April, 1978: pp.6-12.

(30) LANZILLOTTO, C.A.N. and PICKERING, F.B., Metal Science, v16, August, 1982: pp.371-82.

(31) BALLIGER, J.K. and GLADMAN, T. Metal Science, v15, March, 1981: pp.95-108.

(32) GLADMAN, T. and PICKERING, F.B. Journ.Iron & Steel Inst., v203, December, 1965: pp.1212-217.

(33) WARD, R.G. "An Introduction to the Physical Chemistry of Iron and Steel Making". Edward Arnold (Publishers) Ltd., London, 1962: p.179.

(34) PEHILKE, R.D. and ELLIOTT, J.F. Trans. of the Metallurgical Society of A.I.M.E., v218, December, 1960: pp.1088-101.

(35) CHIPMAN, J. and ELLIOTT, J.F. "Electric Furnace Steel Making, Theory and Fundamentals". John Wiley & Sons Inc., London, 1963: p.75.

(36) DARKEN, L.S. and GUNY, R.W. "Physical Chemistry of Metals". McGraw-Hill, London, 1953: p.394.

(37) WALKER, R.D. and MARITER, Z. Journ.Iron & Steel Inst., v210, August, 1972: pp.629-30.

(38) CHENG, T.W. and LOH, H.S. Project Report no23/75, Dept. Mechanical Engineering, University of Canterbury, Christchurch, New Zealand, 1975.

(39) OSBORNE, A.H. American Inst.Mining & Metallurgical Engineering. Open Hearth Proc. v36, 1953: p.67.

(40) BROWER, T.E. et al. Trans. A.I.M.E. v188, 1950: pp.851-60.

(41) MOORE, C. and MARSHALL, R.I. "Modern Steel Making Methods". The Institution of Metallurgists, U.K., 1981: pp.27-46.

(42) MARIQUE, C. et al. Ironmaking and Steelmaking, v15, January, 1988: pp.38-42.

(43) MOERKERKE, J. et al. "Factors Influencing The Nitrogen Level of Steels Produced in a Mixed Blowing Converter". Internal Report, SIDMAR, March, 1986: p.32.

(44) COESSENS, C. et al. Iron and Steelmaker, v14, July, 1987: pp.34-43.

(45) MARIQUE, C. and NILLES, P. Iron and Steelmaker, v11, August, 1984: pp.19-27.

(46) PLAMERS, A. and DEFAYS, J. in meeting on "Secondary Metallurgy in Oxygen Steelshops", Dusseldorf, September, 1986: Verein Deutscher Eisenhuttenleute, p.28.

(47) PETCH, N.J. Journ.Iron & Steel Inst., v174, May, 1953: pp.25-28.

(48) PICKERING, F.B. and GLADMAN, T. "Metallurgical Developments in Carbon Steels", Iron & Steel Inst. Special Report 81, London, 1963: pp.10-20.

(49) MINTZ, B. Metals Technology, v11, July, 1984: pp.265-72.

(50) BIRKBECK, G. Journ.Iron & Steel Inst., v206, September, 1968: pp.909-10.

(51) PETCH, N.J. Phil.Mag., v3, 1958: p.1089.

(52) CODD, I. and PETCH, N.J. Phil.Mag. v5, 1960: p.30.

(53) MINTZ, B. Journ.Iron & Steel Inst., v211, June, 1973: pp.433-39.

(54) MINTZ, B. Metals Technology, v1, May, 1974, pp. 226-32.

(55) ERASMUS, L.A. Aust.Inst.Metals, 27th Conference Proceedings, Christchurch, New Zealand, May, 1974: pp. 143-50.

(56) FAHY, F.W. et al. "Engineering Metallurgy", University of Canterbury, 2nd Edition, 1982.

(57) COTTRELL, A.H. and BILBY, B.A. Proc.Phy.Soc., vA62, 1949: p.49.

(58) HALL, E.O. "Yield Point Phenomena in Metals and Alloys", MacMillan, London, 1970: p.67.

(59) LI, J.C.M. Trans.AIME, v227, February, 1963: pp.239-47.

(60) HAHN, G.T. Acta.Metallurgica, v10, August, 1962: pp.727-38.

(61) BAIRD, J.D. Iron and Steel, v36, August, 1963: pp.186,326,368, 400,450.

(62) WILSON, D.V. and RUSSELL, B. Acta. Metallurgica, v8, June, 1960: pp.468-73.

(63) THOMAS, W.R. and LEAK, G.M. Proc.Phy.Soc., vB68, 1955: p.1001.

(64) LEAK, G.M. Iron and Steel Inst. Special Report no68. 1960: p.270.

(65) MORGAN, E.R. and SHYNE, J.C. Trans AIME, v209, 1957: p.65.

(66) KOSTER, W. et al. Archiv Eisenhuttenwesen, v25, 1954: p.567.

(67) KOSTER, W. and KAMPSCHUTTE, G. ibid v32, 1961: p.809.

(68) BUTLER, J.F. Trans Metallurgical Soc.AIME, v224, January 1962: p.89.

(69) LOW, J.R. and GENSAMER, M. Trans.AIME, v58, March 1944: p.207.

(70) STEPHENSON, E.T. and COHEN, M. Trans.ASM. v54. January, 1961: p.72.

(71) WILSON, D.V. Acta.Metallurgica, v5, June 1957: pp.293-302.

(72) PETCH, N.J. "Fracture", M.I.T. Wiley & Sons Inc., New York, 1959: p.20.

(73) ERASMUS, L.A. Journ.Aust.Inst.Metals, v19, June 1974: pp.116-27.

(74) GREENBERG, B. Metal Progress, v71, June 1957: p.78.

(75) BISRA Vacuum and Allied Techniques Working Group: "Vacuum Degassing of Steel", Special Report 92, Iron and Steel Inst., 1965: p.185.

(76) ENRICETTO, J.F. Journ.Iron & Steel Inst., v204, March, 1966: pp.252-58.

(77) MORGAN, E.R. and SHYNE, J.C. Trans.AIME, v209. January 1965: p.65.

(78) ERASMUS, L.A. Journ.Iron & Steel Inst., v202, February 1964: pp.128-34.

(79) ERASMUS, L.A. and RATNARAJ, R. Proceedings of International Conference on "Modernization of Steel Rolling", Beijing, China, April 1989: pp.505-12.

(80) ERASMUS, L.A. Iron and Steel, v39, October, 1966: pp.477-80.

(81) ERASMUS, L.A. and PUSSEGODA, L.N. Met.Trans.A, v11A, February, 1980: pp.231-37.

(82) KONIG, P. et al. Archiv Eisenhuttenwesen, v32, August, 1961: pp.541-56.

(83) PLATTS, G.K. et al. The Metallurgist and Materials Technologist, v16, September, 1984: pp.447-54.

(84) GLADMAN, T. and DULIEU, D. Met.Sci.Journ., v8, June, 1974: pp.167-76.

(85) GLADMAN, T. et al. Journ.Iron & Steel Inst., v208, February, 1970: pp.173-83.

(86) GLADMAN, T. et al. Microalloying '75. Conference Proceedings, Washington, D.C., U.S.A., October, 1975: pp.32-58.

(87) STEPHENSON, E.T. et al. Trans.ASM, v57, April, 1964: pp.208-19.

(88) IRVINE, K.J. et al. Journ.Iron & Steel Inst., v199, October, 1961: pp.153-75.

(89) NORSTROM, L.A., Met.Sci.Journ., v11, June, 1977: pp.208-12.

(90) HOPKIN, L.M.T. Journ.Iron & Steel Inst., v203, June 1965: pp.583-89.

(91) BAIRD, J.D. and JAMIESON, A. Journ.Iron & Steel Inst., v204, August, 1966: pp.793-803.

(92) HOLBOROW, K.A. "Engineering Technology, Past and Present", Proceedings of Annual IPENZ Conference, v2, May, 1987: pp.35-43.

(93) CHIN, N.E. Project Report no31/88, Dept. of Mechanical Engineering, University of Canterbury, Christchurch, New Zealand, 1988.

(94) "Standard Methods of Analysis". The United Steel Companies Limited, Sheffield, England, 1961: pp.85-92.

(95) ERASMUS, L.A. Proceedings of the New Zealand Metals and Materials Symposium, Lower Hutt, New Zealand, August, 1983: pp.7-12.

(96) DARKEN, L.S. Proc. Elec. Furnace Steel, A.M.I.E., v6, 1948: pp.55-59.

(97) VOLK, W. "Applied Statistics for Engineers", McGraw-Hill, London, 1958.

(98) WILLIAMS, E.J. "Regression Analysis", John Wiley and Sons Inc. New York, 1959.

(99) FISHER, R.A. and YATES. "Statistical Tables". 6th Edition, Oliver & Boyd Ltd., London, 1963.

(100) KOOTZ, T. Archiv. Eisenhuttenwesen, v.15, 1941: p.77.

(101) MARIQUE, C. and NILLES, P. Iron & Steelmaker, v11, August, 1984: pp.19-27.

(102) PLAMERS, A. and DEFAYS, J. Meeting on "Secondary Metallurgy in Oxygen Steelshops". Dusseldorf, Verein Deutscher, Eisenhuttenleute, September, 1986: p.28.

(103) PEHLKE, R.D. and ELLIOT, J.F. Trans. of the Metallurgical Society of AIME. v218, December, 1960.

(104) MACKOWIAK, J. "Physical Chemistry for Metallurgists". Allen & Unwin, London, 1965.

(105) DARKEN, L.S. et al. Trans AMIEE, v191, 1951: p.1174.

(106) FOUNTAIN, R.W. and CHIPMAN, J. Trans. sof the Metallurgical Society of AIME, v212, December, 1958: pp.737-48.

(107) FRAHBERG, M.G. and GRAF, H. Stahl.Eisen.,v80, 1960:pp.539-45.

(108) ERASMUS, L.A. Journ.Iron & Steel Inst. v202, February, 1964: pp.128-34.

(109) NARTIA, K. and KOYAMA, S. Tetsu-to-Hagane v52, 1966: pp.292-98.

(110) HARUE WADA. Trans.Iron & Steel Inst. Japan, v27, August, 1987: pp.649-57.

(111) KONIG, P. et al. Archiv Eisenhuttenwesen, v32, August, 1961: pp.541-56.

(112) PICKERING, F.B. "Physical Metallurgy and the Design of Steels". Applied Science Publishers Ltd., London, 1978: pp.60-87.

(113) BUNGANETT, K. et al. Archiv. Eisenhuttenwesen, v27, January, 1956: pp.61-69.

(114) SCKIME, INOVE and OGASWASA. Trans.Iron & Steel Inst. Japan. v8, February 1968: pp.101-109.

(115) GRAY, J.M. et al. Journ.Iron & Steel Inst., v203, August, 1965: pp.812-18.

(116) MORRISON, W.B. Journ.Iron & Steel Inst., v201, April, 1963: pp.317-25.

(117) McCANN, J. and RIDD, K.A. Journ.Iron & Steel Inst., v202, May, 1964: pp.441-47.

(118) DAVEPEAT, A.T. et al. Met.Sci.Journ., v2, January 1968: pp.104-10.

(119) GRAY, M. and YEO, R.B.G. Trans ASM, v61, March, 1968: pp.225-61.

(120) FAST, J.D. and VERRIJP, M.B. Journ.Iron & Steel Inst., v176, January, 1954: pp.24-27.

(121) BALLIGON, N. and HONEYCOMBE, R.W.K. Met.Trans.'A', v11A, March, 1980: pp.421-29.

(122) ERASMUS, L.A. Iron and Steel, v39, October, 1966: pp.477-80.

(123) CORDEA, J. and HOOK, R.E. Met.Trans,'A', v1A, January, 1970, pp.111-18.

(124) MINORU FUKUDA, et al. Microalloying '75, Conference Proceedings, Washington D.C., U.S.A., October, 1975: pp.136-52.

(125) Handbook of Hounsfield Tensometer Tensile Specimens, University of Canterbury, Christchurch, New Zealand, p.2.

(126) ROBERT R. PRESTON, Journ. of Metals, v29, January, 1977: pp.9-16.

(127) CHONG CHON JIN, Ph.D. Thesis, Dept.of Mech.Engineering, University of Canterbury, Christchurch, New Zealand, February, 1980: p.27.

(128) ERASMUS, L.A., Proceedings of Australasian Conference on "Materials for Industrial Development". Institute of Metals and Materials Australasia, Christchurch. New Zealand, August, 1987: pp.145-51.

(129) COTTRELL, A.H., "Fracture", Ed. AVERBACH.B.L. et al M.I.T., Wiley & Sons Inc., New York, 1959: p.20.

(130) WOODHEAD, J.H. and WEBSTER, D., Journ.Iron & Steel Inst., v209, January, 1969: pp.51-53.

(131) ERASMUS, L.A., Project Report 928-475, July, 1979: Stelco R & D, Canada, pp.1-28.

(132) TOMO TANAKA et al, "Structure and Properties of Dual Phase Steels", Conference Proceedings, The Metallurgical Society of AIME, February 19-21, 1979: pp.221-41.

(133) ERIK NAVARA, "High Strength Low Alloy Steels", Proceedings of an international conference sponsored by the Metallurgical Society of AIME and AIM, Wollongong, Australia, August 20-24, 1984: pp.302-7.

(134) GLADMAN, T. and PICKERING, F.B., Journ.Iron & Steel Inst., v203, December, 1965, pp.1212-17.

(135) JUDD, R.R. and PAXTON, H.W., Trans. of the Met.Soc.of AIME, v242, February, 1968: pp.206-15.

(136) SPEICH, G.R. and SZIRMAE, A., Trans. of the Met.Soc.of AIME, v243, May, 1969: pp.1063-74.

(137) NOLTI, F.V., Ph.D. Thesis, Carnegie Mellon University, Pittsburg, U.S.A., 1968.

(138) WEVER, H, and FLENDER, H., Arch.Eisenhuttenwes, v35, January, 1964: pp.65-73.

(139) DAVIES, R.G., Metallurgical Trans., v9A, January, 1978: pp.41-52.

(140) PUSSEGODA, L.N. et al, Metallurgical Trans., v15A, July, 1984: pp.1499-1502.

(141) FRIDBERG, J. et al, Jernkont, Ann. v153, 1969: p.263.

(142) SPEICH, G.R. et al, Metallurgical Trans., v12A, August, 1981: pp.1419-28.

(143) ANDREWS, K.W., Journ.Iron & Steel Inst., v184, December, 1956: pp.414-27.

(144) HILLERT, M., "Phase Transformations", papers presented at a seminar of the American Society for Metals, October 12 and 13, Metals Park, Ohio, 1970: pp.181-218.

(145) LACY, C.E. and GENSOMER, M. Trans. ASM, v32, 1944: p.88.

(146) United States Steel Corporation: The Making, Shaping and Treating of Steels, 9th Edition, 1971: pp.1132-37.

(147) HUNDY, B.B., Journ.Iron & Steel Inst., v178, September, 1954: pp.34-38.

(148) ROBERTS, W. and SANDBERG, A., "Institutet for Metalforskning", Swedish Institute for Metals Research, Report No.IM-1489, October, 1980: p.1.

(149) Properties and Selection of Metals, ASM Metals Handbook, v1, 8th Edition, 1972, p.50.

APPENDIX A

DETERMINATION OF NITROGEN IN STEEL

The total nitrogen content in steel is considered to be made up of two parts:

(i) Acid - insoluble nitrides, (N_{insol}), and

(ii) Acid - soluble nitrides, (N_{sol}), which consists mainly of iron nitride (Fe_4N, $Fe_{16}N_2$), aluminium nitride and interstitial nitrogen,

The total nitrogen content is given by:

$$N_{total} = N_{sol} + N_{insol} \qquad \text{Eqn.A.1}$$

The 'active' nitrogen content (representing nitrogen in solid solution and as iron nitride) is given by:-

$$N_{active} = N_{sol} - N_{A\ell N} \qquad \text{Eqn.A.2}$$

A.1 SUMMARY OF THE METHOD

A.1.1 Determination of Soluble and Insoluble Nitrogen Contents

Drillings from a sample are dissolved in dilute H_2SO_4 by heating in a steam bath. When the acid attack on the drillings is complete, the insoluble residue is separated by centrifuging. The clear solution contains all the 'acid-soluble' nitrogen as an ammonium salt. The insoluble residue is then decomposed by fuming with concentrated H_2SO_4 at its boiling point. This solution is then diluted and contains all the 'acid-insoluble' nitrogen as an ammonium

salt. The nitrogen in these two solutions is absorbed as ammonia into a boric acid solution by steam distillation with NaOH solution. The nitrogen contents are then determined from these ammonia solutions colorimetrically with Nessler's reagent. The procedure is summarised diagrammatically in Figure A.1.

A.1.2 Determination of Nitrogen Content as A&N

The sample is dissolved in methyl acetate-bromine solution. The insoluble residue from this solution is obtained by filtering through two layers of glass fibre filter paper. The bromine absorbed in the filter papers is washed off with methyl acetate. After drying this residue any aluminium nitride present in it is hydrolysed by digesting with NaOH in the steam distillation apparatus. The ammonia evolved is collected in a boric acid solution and the content of this solution is determined colorimetrically with Nessler's reagent.

A.2 PROCEDURE

A.2.1 Determination of N_{sol} and N_{insol}

3.5 grams of the sample was dissolved in a round bottomed flask by the addition of about 50 ml 20% V/V H_2SO_4 and warming over a steam bath. Once all reaction had ceased, the sample was cooled and transferred into a 50 ml centrifuge tube and centrifuged at 3000 r.p.m. for about 5 minutes. 2 ml of 2% W/V $BaCl_2$ was added to the solution and then centrifuged for a further 5 minutes. The clear solution was carefully poured into a 100 ml stopped bottle and kept for steam distillation.

The insoluble residue was transferred to the original flask washing it with ammonia-free distilled water. A splash head was

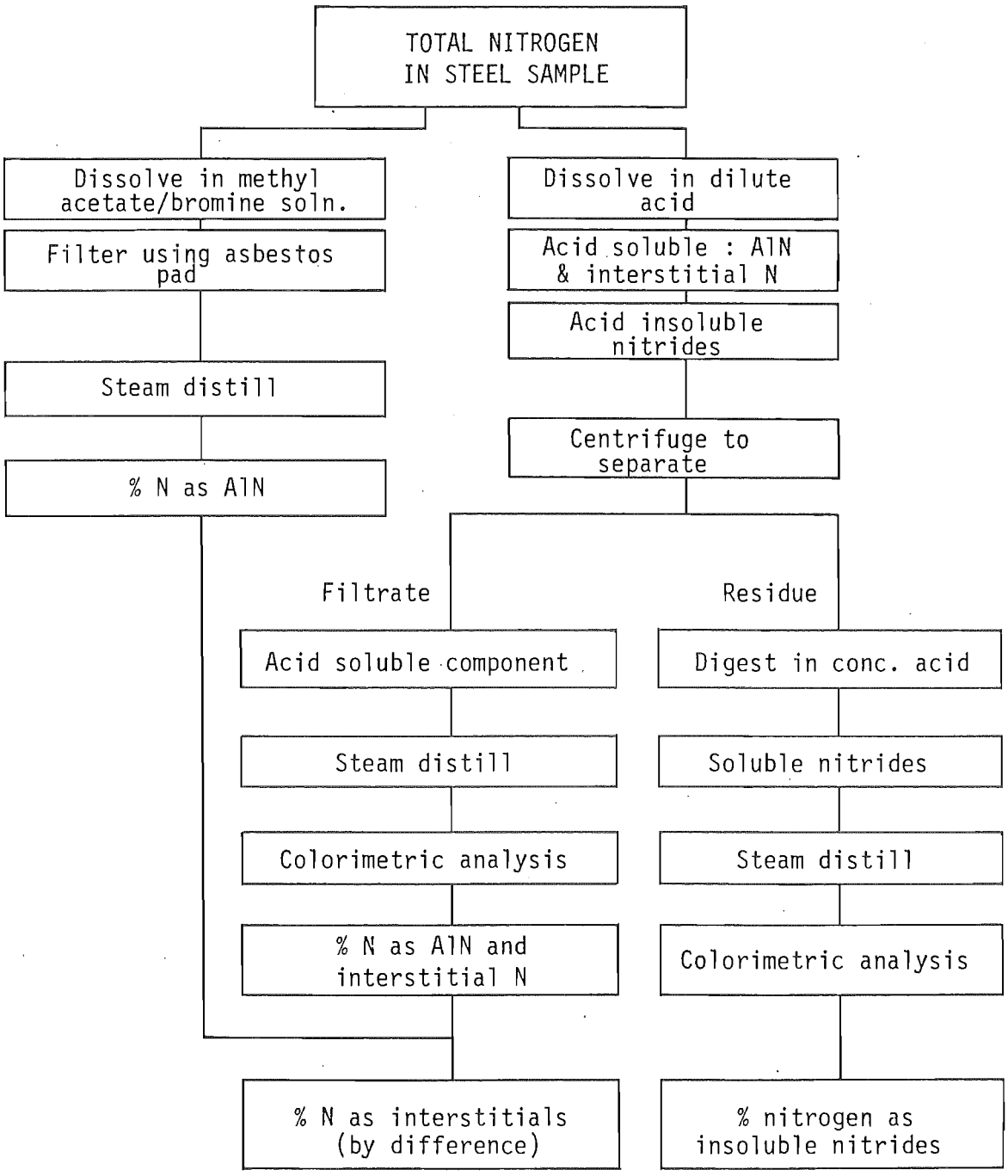

Figure A.1: Format for nitrogen analysis of steel

placed onto the flask and 8 - 9 ml of concentrated H_2SO_4 was added to the insoluble residue and evaporated to fumes using a bunsen flame. The fuming was continued at its boiling point until all the insoluble residue was decomposed. This solution was cooled to room temperature and then diluted by adding 40 ml of ammonia-free distilled water and kept for steam distillation.

The steam distillation was carried out on the apparatus shown in Figure A.2. Initially the apparatus was conditioned by adding about 40 ml of ammonia-free distilled water followed by 50 ml of 50% W/V NaOH solution (containing 0.1% W/V Devard's alloy) to the distillation flask E via funnel D and distilling for about 15 minutes by closing taps 1 and 2. The heat was turned off to the steam generator A and the contents in flask E were allowed to syphon into the evacuation flask C and then drained through tap 2. A sample kept of steam distillation was admitted to E followed by 100 ml of 50% W/V NaOH solution. The funnel D was then washed with a little ammonia-free distilled water. The distillation was carried out by closing taps 1 and 2 and the distillate collected at G in a 100 ml bottle containing 5 ml of 0.2% W/V boric acid. The bottle was kept with the outlet from the condenser F dipping into the boric acid before closing taps 1 and 2. The distillation was continued until about 80-90 grm of distillate collected. As earlier, the contents of E were drained through tap 2 by removing the heat source from the steam generator A. This process was repeated for other samples. A blank determination was carried out using 50 ml of 20% V/V H_2SO4 for each batch of tests.

The distillate solutions were brought up to a standard weight (90 grm of distillate in the bottle) by the addition of ammonia-free

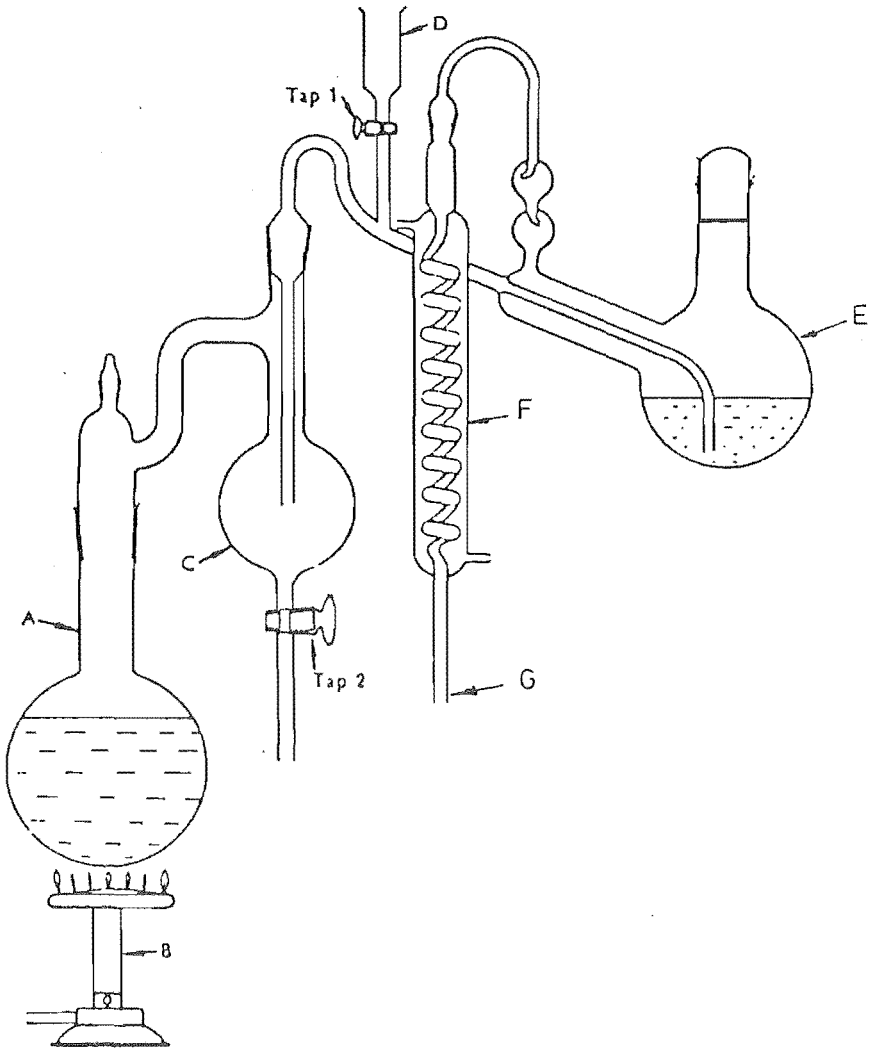

Figure A.2: Steam Distillation apparatus used for the determination of nitrogen in steel.

distilled water. A set of standard solutions was made from a standard ammonium chloride solution (strength, 1 ml contains 0.175×10^{-4} grm of nitrogen). The standard solutions were made by diluting different volumes of the standard ammonia solution by the addition of 5 ml of 0.2% W/V boric acid followed by ammonia-free distilled water until the standard weight (90 grm) was reached. 2 ml of Nessler's reagent was added to each of these solutions, mixed and allowed to stand for about 15 minutes. Readings were taken for each solution using a colorimeter. The nitrogen contents of the distillate solutions were determined using the colorimeter graph which was obtained from the standard solutions.

A.2.2 Determination of $N_{A\ell N}$

3.5 grm of sample was transferred to a clean, dry 100 ml round bottomed flask followed by 8-10 ml of bromine. A condenser was attached to the flask and about 40 ml of methyl acetate was added cautiously via the top of the condenser, a few ml at a time. The solution was boiled (at 60°C) gently with the solvent reflexing from the condenser. This process was continued until the sample was fully dissolved (checked using a small magnet). This solution was filtered through two layers of glass fibre filter paper in a dry funnel and filter disc, using suction. The flask was washed with methyl acetate to remove any adhering particles. The filter paper and residue were washed with methyl acetate until it was free from bromine and then transferred to a dry watch glass and dried in an air oven at about 100°C and finally cooled in a desiccator.

The dry filter paper containing the residue was transferred to the distillation flask E by opening it at the top, followed by 20 ml

of 50% W/V NaOH solution through funnel D. The funnel D was then washed with a little ammonia-free distilled water. The distillation of the sample was then carried out and the distillate was collected in a 100 ml bottle, as described earlier in A.2.1. The contents in E were sucked out from the top. The nitrogen content of the distillate was determined colorimetrically with Nessler's reagent.

When carrying out a new set of tests, the distillation apparatus was initially conditioned and a blank determination was made during the tests.

A.3 GENERAL PRECAUTIONS IN PROCEDURE

The tests were carried out in a chemical laboratory where every possible precaution was taken against contamination with ammonia. The reagents and glassware used were specially kept for the nitrogen determination. All reagents used were selected for very low ammonia content. For all dilution of reagents and washing glassware ammonia-free distilled water was used. The nitrogen content of the blanks ($< 0.0005\%$) confirmed that contamination with ammonia was below accepted levels.

APPENDIX B

Table B1. Nitrogen analysis results for the samples collected at New Zealand Steel.

Heat No.	Nitrogen as	Wt%, Nitrogen at				
		Melter	VRU	KOBM	LTS	CCM
304912	Sol	0.0010	0.0008	0.0015	0.0038	0.0061
	Insol	0.0026	0.0028	0.0007	0.0009	0.0005
	Total	0.0036	0.0036	0.0022	0.0047	0.0066
304909	Sol	0.0009		0.0020	0.0034	0.0046
	Insol	0.0013	-	0.0003	0.0007	0.0007
	Total	0.0022		0.0023	0.0041	0.0053
304688	Sol	0.0011		0.0016	0.0036	0.0051
	Insol	0.0022	-	0.0007	0.0010	0.0013
	Total	0.0033		0.0023	0.0046	0.0064
305186	Sol	0.0004	0.0008	0.0016	0.0039	0.0061
	Insol	0.0012	0.0011	0.0011	0.0015	0.0007
	Total	0.0016	0.0019	0.0027	0.0054	0.0068
305137	Sol	0.0007	0.0010	0.0023	0.0032	0.0048
	Insol	0.0023	0.0015	0.0005	0.0010	0.0004
	Total	0.0030	0.0025	0.0028	0.0042	0.0052
304766	Sol	0.0006		0.0015	0.0033	0.0032
	Insol	0.0019	-	0.0011	0.0008	0.0008
	Total	0.0026		0.0026	0.0041	0.0040
304949	Sol	0.0005		0.0017	0.0031	0.0046
	Insol	0.0020	-	0.0004	0.0009	0.0004
	Total	0.0025		0.0021	0.0040	0.0050
305135	Sol	0.0005	0.0007	0.0021	0.0031	0.0042
	Insol	0.0027	0.0032	0.0011	0.0010	0.0007
	Total	0.0032	0.0039	0.0032	0.0041	0.0049
305048	Sol	0.0004	0.0006	0.0019	0.0036	0.0048
	Insol	0.0020	0.0024	0.0008	0.0015	0.0007
	Total	0.0024	0.0030	0.0027	0.0051	0.0055

Table B1: (Continued)

Heat No.	Nitrogen as	Wt%, Nitrogen at				
		Melter	VRU	KOBM	LTS	CCM
305106	Sol	0.0008	0.0007	0.0020	0.0036	0.0051
	Insol	0.0015	0.0028	0.0020	0.0015	0.0008
	Total	0.0023	0.0035	0.0040	0.0051	0.0059
305088	Sol	0.0005	0.0007	0.0018	0.0024	0.0042
	Insol	0.0015	0.0023	0.0008	0.0011	0.0004
	Total	0.0020	0.0030	0.0026	0.0035	0.0046
305107	Sol	0.0005	0.0008	0.0019	0.0032	0.0041
	Insol	0.0016	0.0017	0.0007	0.0012	0.0005
	Total	0.0021	0.0025	0.0026	0.0044	0.0046
304385	Sol	0.0007		0.0019	0.0024	0.0051
	Insol	0.0027	-	0.0006	0.0012	0.0005
	Total	0.0034		0.0025	0.0036	0.0056
305073	Sol	0.0005	0.0005	0.0021	0.0047	0.0060
	Insol	0.0016	0.0023	0.0003	0.0012	0.0007
	Total	0.0021	0.0028	0.0024	0.0059	0.0067
305105	Sol	0.0011	0.0010	0.0010	0.0024	0.0062
	Insol	0.0018	0.0033	0.0009	0.0012	0.0003
	Total	0.0029	0.0043	0.0019	0.0036	0.0065
304950	Sol	0.0009		0.0017	0.0030	0.0036
	Insol	0.0020	-	0.0003	0.0008	0.0001
	Total	0.0029		0.0020	0.0038	0.0037
305109	Sol	0.0009	0.0005	0.0023	0.0032	0.0046
	Insol	0.0020	0.0038	0.0004	0.0012	0.0008
	Total	0.0029	0.0043	0.0027	0.0044	0.0054
304888	Sol	0.0004	0.0005	0.0023	0.0037	0.0050
	Insol	0.0028	0.0036	0.0007	0.0008	0.0008
	Total	0.0032	0.0041	0.0030	0.0045	0.0058

Table B2: Melter Data

Sample No.	% N_{tot}	% C	% Si	% S	% P	% Mn	% V	% Ti	% Al	Temp.(°C)
800244 C212Q	0.0036	2.953	0.234	0.031	0.090	0.369	0.463	0.150	0.002	1486
800243 C236Q	0.0022	3.088	0.193	0.048	0.071	0.306	0.467	0.139	0.006	1484
800051 C204Q	0.0033	3.423	0.249	0.040	0.104	0.362	0.474	0.250	0.007	1492
700103 C373Q	0.0016	3.223	0.353	0.042	0.088	0.341	0.469	0.219	0.005	1364
800420 C279Q	0.0030	2.796	0.208	0.050	0.088	0.285	0.451	0.132	0.007	1395
800125 C296Q	0.0026	3.114	0.186	0.036	0.100	0.330	0.452	0.170	0.007	1423
800277 C170Q	0.0025	3.146	0.258	0.038	0.065	0.365	0.466	0.271	0.008	1455
700081 C342Q	0.0032	2.719	0.193	0.058	0.096	0.253	0.469	0.065	0.009	1348
800358 C154Q	0.0024	2.749	0.260	0.032	0.090	0.349	0.428	0.181	0.008	1420
700082 C359Q	0.0023	2.786	0.197	0.056	0.097	0.257	0.480	0.067	0.001	1571
800378 C288Q	0.0020	2.878	0.436	0.026	0.111	0.481	0.461	0.436	0.002	1446
800403 C244Q	0.0021	3.283	0.272	0.042	0.093	0.327	0.512	0.265	0.005	1426
800374 C162Q	0.0021	2.717	0.361	0.027	0.089	0.379	0.403	0.259	0.008	1424
800224 C177Q	0.0032	2.862	0.119	0.049	0.081	0.238	0.462	0.080	0.007	1444
800400 C186Q	0.0029	3.327	0.243	0.046	0.092	0.309	0.520	0.252	0.007	1443
800278 C254Q	0.0029	3.044	0.298	0.037	0.080	0.437	0.463	0.296	0.001	1451
800336 C321Q	0.0029	3.078	0.212	0.035	0.094	0.338	0.459	0.206	0.008	1428
800676 C341Q	0.0034	3.143	0.230	0.039	0.112	0.348	0.450	0.183	0.009	1478

Table B3: VRU Data

Sample No.	N_{total}	% C	% Ti	% Si	% Mn	% P	% Al	% S	% V	Temp.°C	FeSi(kg)	$O_2(m^3)$
402120 C214Q	0.0036	2.866	0.029	0.280	0.204	0.089	0.001	0.030	0.317	1406	100	200
402369 C375Q	0.0019	3.145	0.071	0.219	0.211	0.092	0.005	0.041	0.329	1455	400	470
402323 C281Q	0.0025	2.662	0.045	0.318	0.185	0.089	0.007	0.050	0.354	1428	300	300
502321 C344Q	0.0039	2.626	0.016	0.286	0.119	0.098	0.009	0.055	0.311	1479	300	300
502322 C360Q	0.0035	2.701	0.023	0.406	0.171	0.097	0.001	0.053	0.355	1370	300	300
402274 C290Q	0.0030	2.850	0.109	0.373	0.278	0.114	0.001	0.025	0.335	1423	300	400
502293 C245Q	0.0025	3.202	0.112	0.624	0.232	0.094	0.006	0.041	0.390	1402	250	400
402254 C164Q	0.0028	2.588	0.052	0.277	0.189	0.100	0.009	0.034	0.317	1452	200	350
402102 C179Q	0.0041	2.745	0.033	0.255	0.170	0.082	0.008	0.047	0.356	1389	200	200
402288 C190Q	0.0043	3.052	0.009	0.074	0.042	0.095	0.010	0.047	0.133	1441	100	740
402206 C323Q	0.0043	2.930	0.034	0.033	0.142	0.098	0.007	0.035	0.324	1501	350	450
402228 C156Q	0.0030	2.606	0.031	0.362	0.176	0.088	0.007	0.032	0.310	1502	350	400

Table B4: KOBM Data

Sample No.	% N_{tot}	% C	% Si	% Mn	% P	% Al	% S	% V
304912 C215Q	0.0022	0.02	0	0.118	0.009	0.0020	0.017	0.005
304909 C238Q	0.0023	0.01	0	0.098	0.009	0.0015	0.018	0.005
304688 C206Q	0.0023	0.02	0.003	0.209	0.038	0.0024	0.014	0.016
305186 C377Q	0.0027	0.01	0	0.076	0.009	0.0019	0.016	0.003
305137 C282Q	0.0028	0.00	0	0.093	0.008	0.0025	0.016	0.003
304766 C298Q	0.0026	0.01	0	0.046	0.013	0.0032	0.018	0.003
304949 C172Q	0.0021	0.01	0	0.103	0.007	0.0016	0.017	0.003
305135 C345Q	0.0032	0.04	0.005	0.324	0.007	0.0870	0.019	0.005
305048 C157Q	0.0027	0.01	0	0.052	0.004	0.0027	0.013	0.002
305106 C361Q	0.0040	0.00	0	0.044	0.005	0.0020	0.016	0.002
305088 C291Q	0.0026	0.01	0	0.083	0.007	0.0021	0.009	0.003
305107 C246Q	0.0026	0.01	0	0.097	0.009	0.0023	0.012	0.004
304385 -	0.0025	0.01	0	0.086	0.007	0.0019	0.012	0.003
305073 C165Q	0.0024	0.00	0	0.095	0.009	0.0022	0.012	0.003
305105 C191Q	0.0019	0.00	0	0.034	0.011	0.0028	0.017	0.002
304950 C256Q	0.0020	0.03	0	0.101	0.002	0.0060	0.018	0.006
305019 C324Q	0.0027	0.01	0	0.109	0.013	0.0018	0.009	0.006

Table B4: KOBM Data (Continued)

SAMPLE NO.	LIME (kg)	DOLOMITE (kg)	LIMESTONE (kg)	ALUMINIUM BARS (kg) M.B.	R.B.	TOTAL	BELOW TIMES (Mins) M.B.	R.B.	TOTAL	SCRAP (kg)	RUN OUT TIME (Mins)	T.D. TEMP.
304912 C215Q	3958	696	1491	0	56	56	20.33	0.00	20.33	5	7.7	1692
304909 C238Q	4763	773	1015	0	0	0	19.33	0.00	19.33	0	4.32	1674
304688 C206Q	5468	249	0	17	0	17	21.07	0.00	21.07	5	4.95	1733
305186 C377Q	5872	609	0	272	0	272	18.55	1.80	20.35	6	5	1733
305137 C282Q	4919	512	0	96	20	112	16.53	1.30	17.83	6	7.7	1687
304766 C298Q	5482	999	0	231	36	267	18.47	1.10	19.57	5	3.78	1688
304949 C172Q	4958	885	2038	0	44	44	19.15	1.08	20.23	0	6.333	1649
305135 C345Q	5922	661	827	0	0	0	27.60	2.00	19.60	0	5.133	1705
305048 C157Q	5003	687	2930	0	85	85	22.56	1.82	24.38	0	4.083	1622
305106 C361Q	4279	447	0	5	0	5	18.23	3.80	22.03	0	3.883	1705
305088 C291Q	5158	763	3697	0	0	0	16.92	0.00	16.92	0	4.4	1706
305107 C246Q	5934	709	1363	0	84	84	20.15	1.78	21.93	6	3.55	1712
304385 -	5928	205	0	196	0	196	19.00	0.00	19.00	8	5.5	1676
305073 C165Q	4665	492	44	0	0	0	18.55	0.00	18.55	4	5.95	1711
305105 C191Q	4774	492	0	361	37	398	17.42	0.00	17.42	0	3.883	1705
304950 C256Q	4969	875	2054	0	0	0	19.53	0.00	19.53	0	6.417	1675
305019 C324Q	5680	0	579	0	0	0	14.05	1.08	15.13	0	3.833	1766

Table B4: KOBM Data (Continued)

SAMPLE NO.	TOP 02 (m^3)	BOTTOM 02 (m^3)			NITROGEN (m^3)			NATURAL GAS (m^3)		
		M.B.	R.B.	TOTAL	M.B.	R.B.	TOTAL	M.B.	R.B.	TOTAL
304912 C215Q	837	2059	0	2059	671	98	769	581	61	642
304909 C238Q	837	1964	0	1964	444	0	444	439	0	439
304688 C206Q	1136	2132	0	2132	191	419	610	478	597	1075
305186 C377Q	1319	1888	186	2074	264	0	264	464	0	464
305137 C282Q	1175	1682	129	1811	179	73	253	397	46	443
304766 C298Q	1094	1873	97	1970	160	69	229	335	31	366
304949 C172Q	1123	1939	113	2052	170	72	242	326	32	358
305135 C345Q	1081	1786	200	1986	203	0	203	427	0	427
305048 C157Q	0	2551	181	2732	553	93	646	671	63	734
305106 C361Q	1087	1348	400	1748	258	0	258	333	0	333
305088 C291Q	1401	1909	0	1909	354	0	354	484	0	484
305107 C246Q	1517	2050	200	2250	348	86	434	513	61	574
304385 -	782	2233	0	2233	165	0	165	283	0	283
305073 C165Q	810	1885	0	1885	283	0	283	444	0	444
305105 C191Q	1273	1751	0	1751	327	119	446	465	60	525
304950 C256Q	1129	1982	0	1982	259	0	259	335	0	335
305019 C324Q	1149	1432	90	1522	249	0	249	360	0	360

Table B5: LTS Data

Sample No.	% N_{tot}	% C	% Ti	% Si	% Mn	% P	% Al	% S	% V
304912 C218Q	0.0047	0.041	0.005	0.002	0.263	0.008	0.0522	0.015	0.006
304909 C240Q	0.0041	0.039	0.006	0.003	0.271	0.011	0.0559	0.018	0.009
305186 C380Q	0.0054	0.150	0.006	0.137	0.716	0.010	0.0466	0.017	0.013
305137 C285Q	0.0042	0.051	0.006	0.004	0.294	0.010	0.0473	0.017	0.010
304949 C174Q	0.0040	0.028	0.005	0.002	0.254	0.009	0.0541	0.015	0.007
305135 C348Q	0.0041	0.056	0.006	0.003	0.309	0.009	0.0597	0.019	0.007
305048 C159Q	0.0051	0.024	0.006	0.003	0.199	0.007	0.0395	0.013	0.005
305088 C293Q	0.0035	0.037	0.006	0.005	0.240	0.008	0.0547	0.009	0.007
305107 C251Q	0.0044	0.122	0.006	0.005	0.339	0.011	0.0553	0.013	0.010
305073 C167Q	0.0059	0.058	0.006	0.002	0.347	0.009	0.0525	0.013	0.006
304888 C183Q	0.0045	0.140	0.006	0.006	0.972	0.020	0.0490	0.018	0.018
305105 C193Q	0.0036	0.143	0.006	0.004	0.305	0.012	0.0799	0.015	0.005
304950 C258Q	0.0038	0.041	0.006	0.001	0.252	0.009	0.0584	0.015	0.007
305019 C326Q	0.0045	0.068	0.006	0.006	0.396	0.010	0.0658	0.011	0.010
304688 C209Q	0.0047	0.137	0.006	0.010	0.745	0.026	0.0482	0.014	0.019
304766 C301Q	0.0041	0.050	0.005	0.008	0.343	0.015	0.0652	0.018	0.006
304385	0.0036	0.036	0.006	0.008	0.259	0.012	0.0546	0.014	0.010

Table B5: LTS Data (Continued)

Sample No.	Rinse Time (Min.)	Temp. (°C)	ΔT (°C)	Carbon (kg)	Al wire (m)	LCFeMn (kg)	RHA (kg)	Ladie Additions (kg) C	FeMn	Al	Lime (kg)
304912 C218Q	12	1577	58	0	50	0	50	23	205	105	0
304909 C240Q	9	1579	48	0	0	0	0	20	164	96	60
305186 C380Q	10	1567	58	0	50	0	50	103	693	73	105
305137 C285Q	11	1580	44	14	59	0	60	41	243	106	80
304949 C174Q	10	1577	38	7	80	10	0	22	158	102	80
305135 C348Q	10	1579	55	14	0	0	60	34	246	100	0
305048 C159Q	9	1576	45	7	30	30	60	10	124	92	0
305088 C293Q	12	1577	46	14	210	35	50	10	156	99	60
305107 C251Q	21	1577	87	30	170	50	50	114	268	108	80
305073 C167Q	5	1576	54	0	0	0	0	30	262	100	90
304888 C183Q	9	1569	53	28	80	0	50	33	872	84	0
305105 C193Q	10	1570	60	7	0	30	60	95	283	99	60
304950 C258Q	8	1578	46	0	20	0	50	22	163	102	60
305019 C326Q	12	1585	43	11	10	0	50	34	260	85	0
304688 C209Q	15	1570	104	7	220	40	50	115	580	88	0
304766 C301Q	15	1582	63	18	25	6	50	35	233	96	45
304385 C303Q	8	1580	56	0	58	14	50	33	146	113	0

Table B6: CCM Data

HEAT NO.	N_{total}
304912	0.0066
304909	0.0053
304688	0.0064
305186	0.0068
305137	0.0052
304766	0.0040
304949	0.0050
305135	0.0049
305048	0.0055
305106	0.0059
305088	0.0046
305107	0.0046
304385	0.0056
305073	0.0067
305105	0.0065
304950	0.0037
305019	0.0054
304888	0.0058

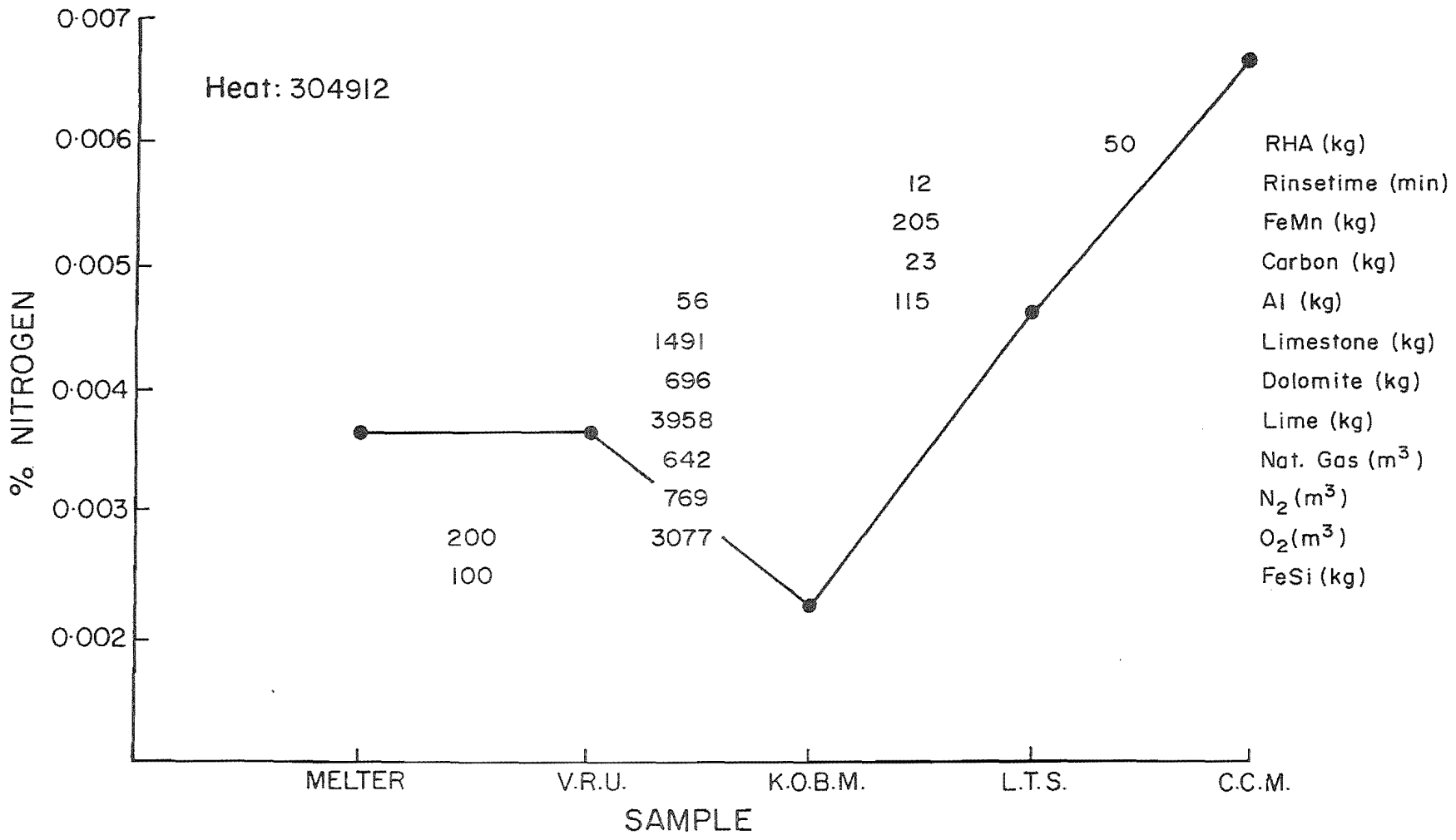

Figure B1: Variation in total nitrogen content

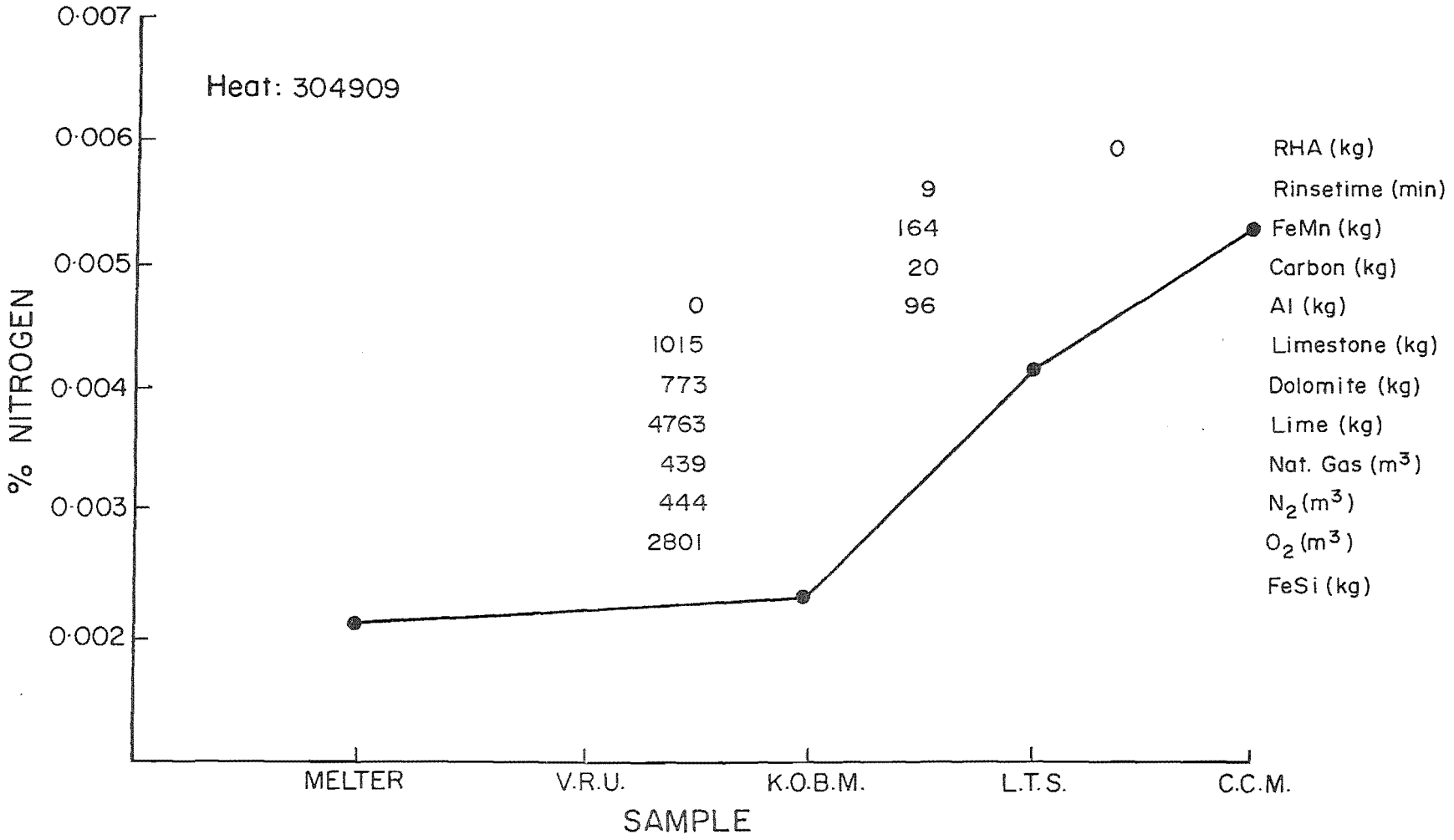

Figure B2 : Variation in total nitrogen content

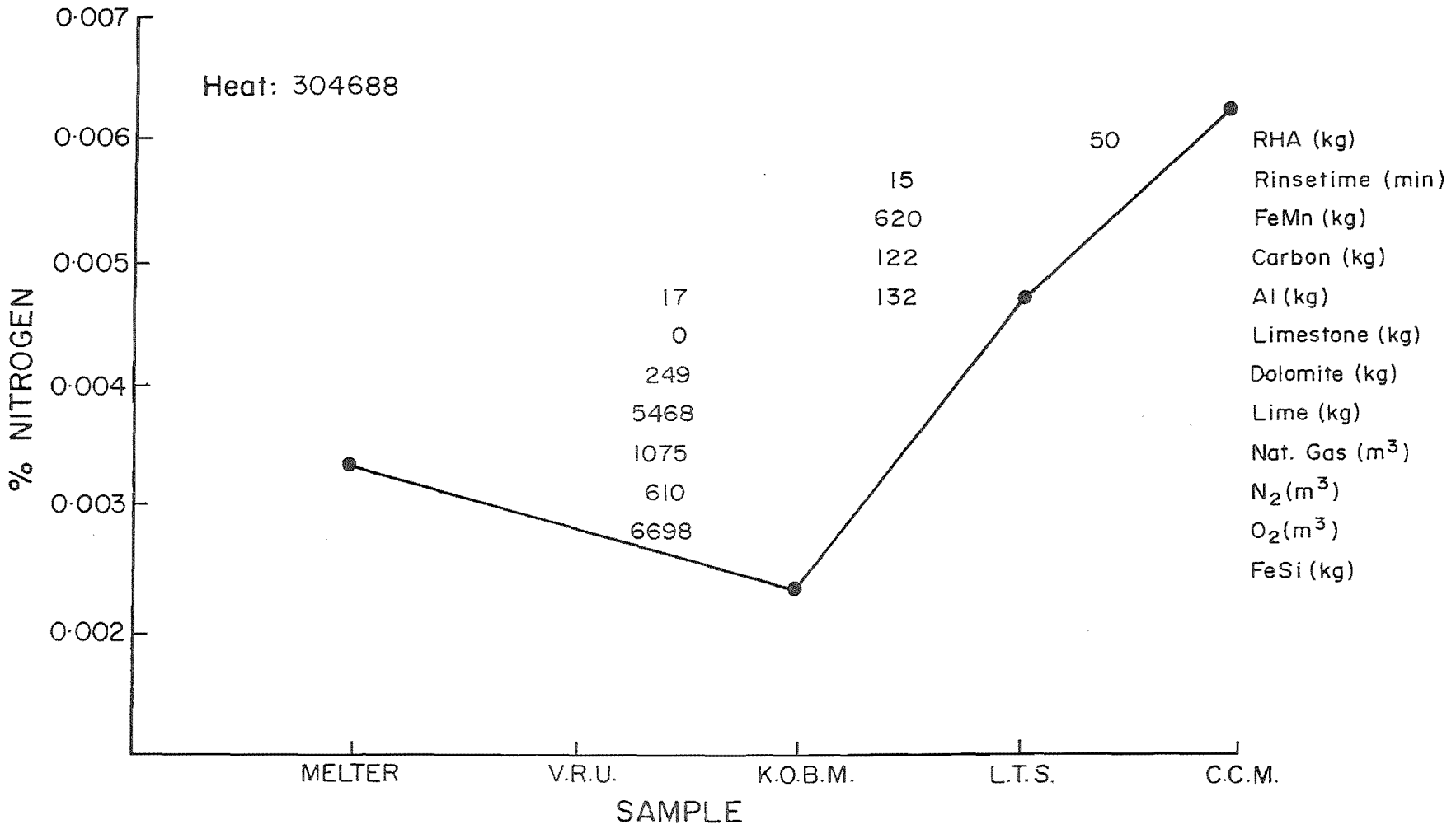

Figure B3 : Variation in total nitrogen content

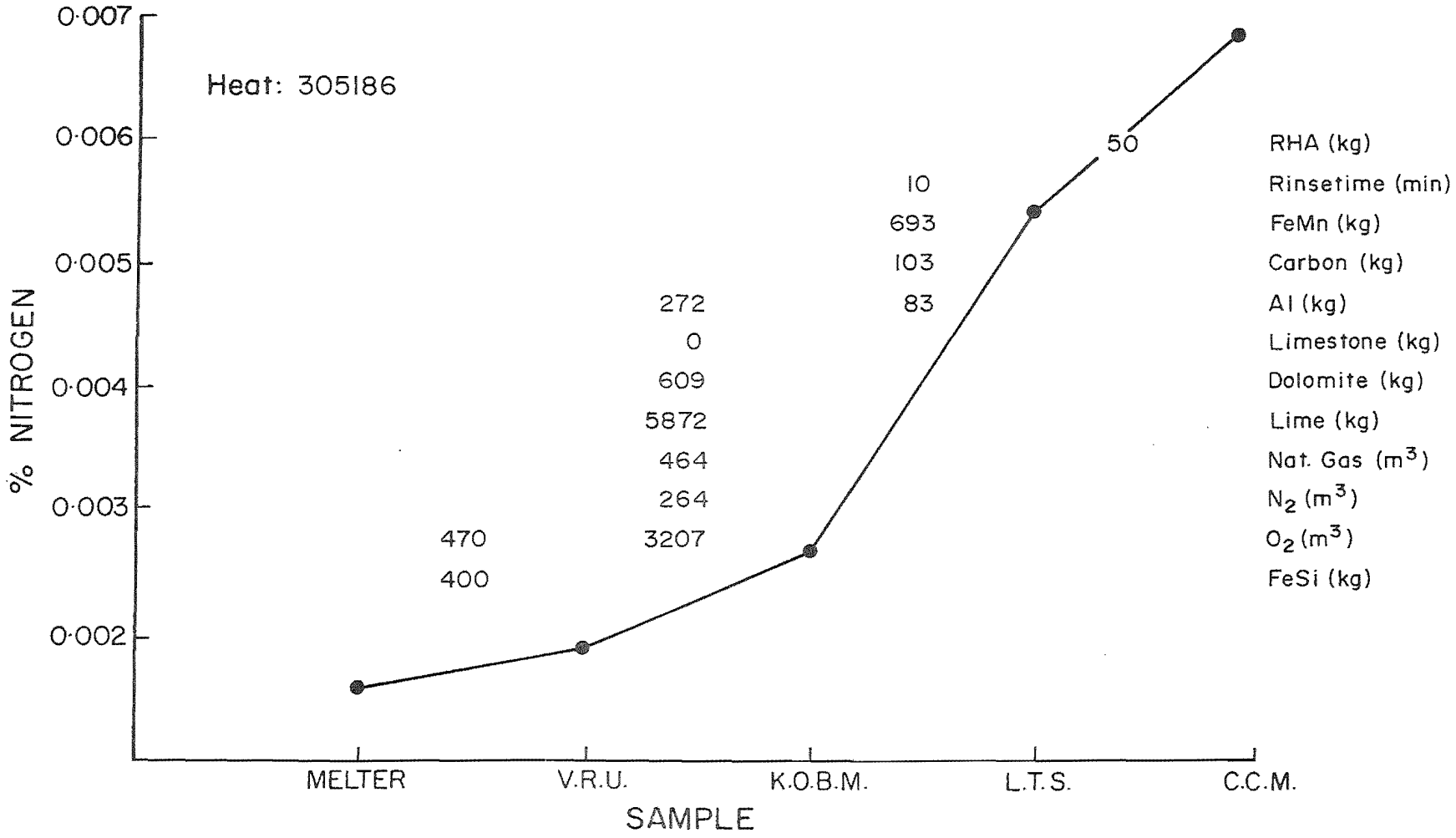

Figure B4 : Variation in total nitrogen content

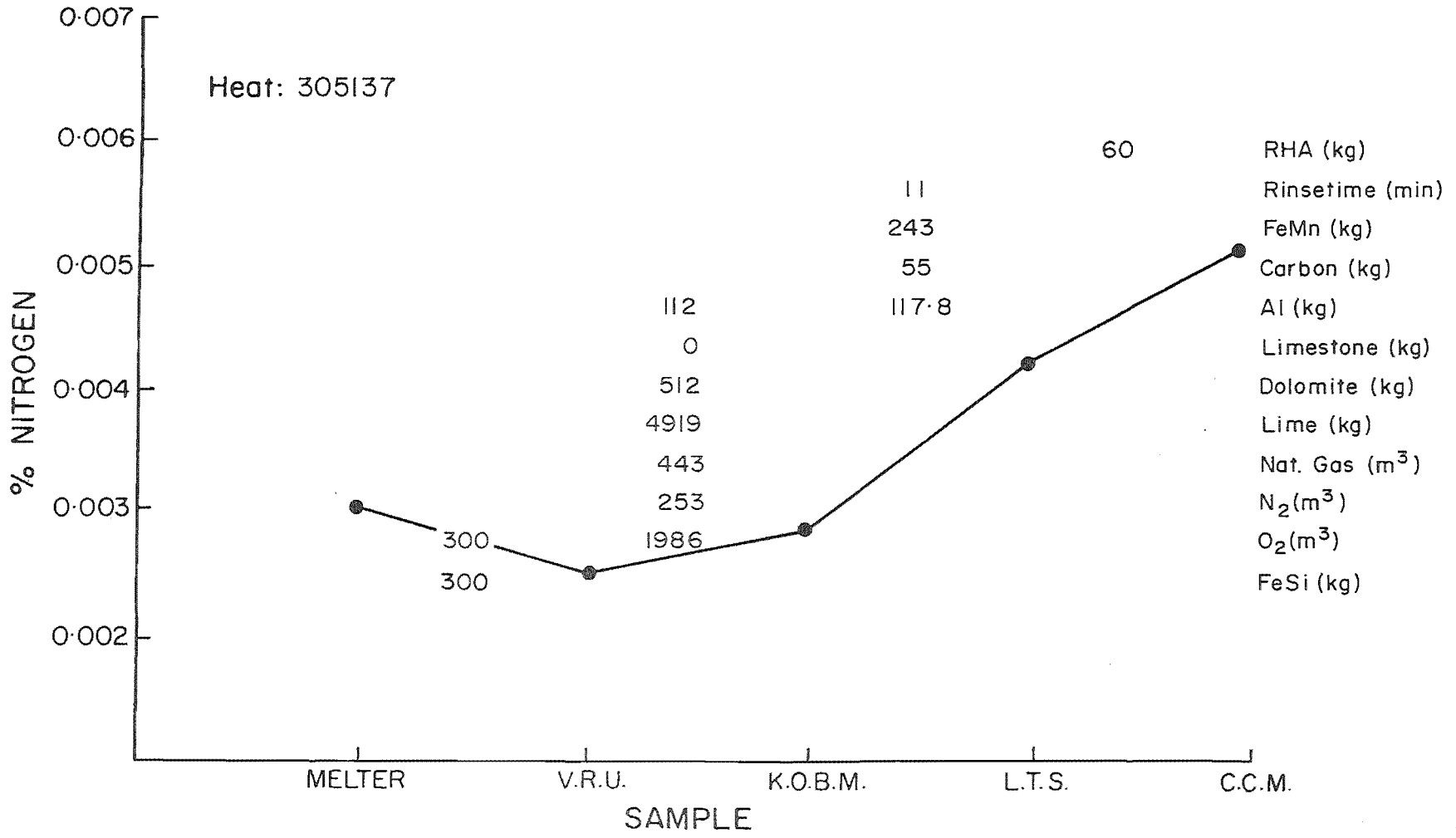

Figure B5 : Variation in total nitrogen content

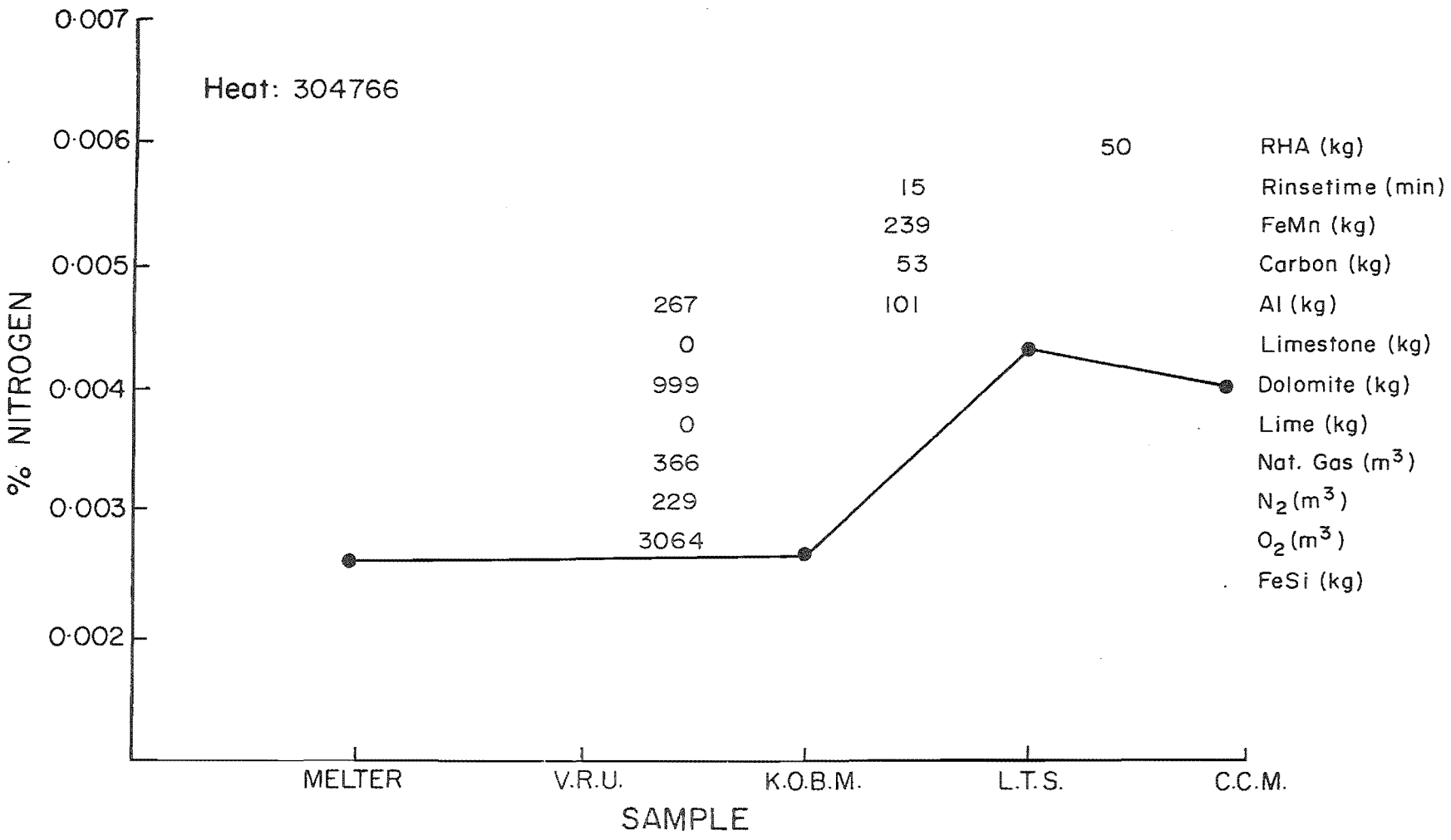

Figure B6 : Variation in total nitrogen content

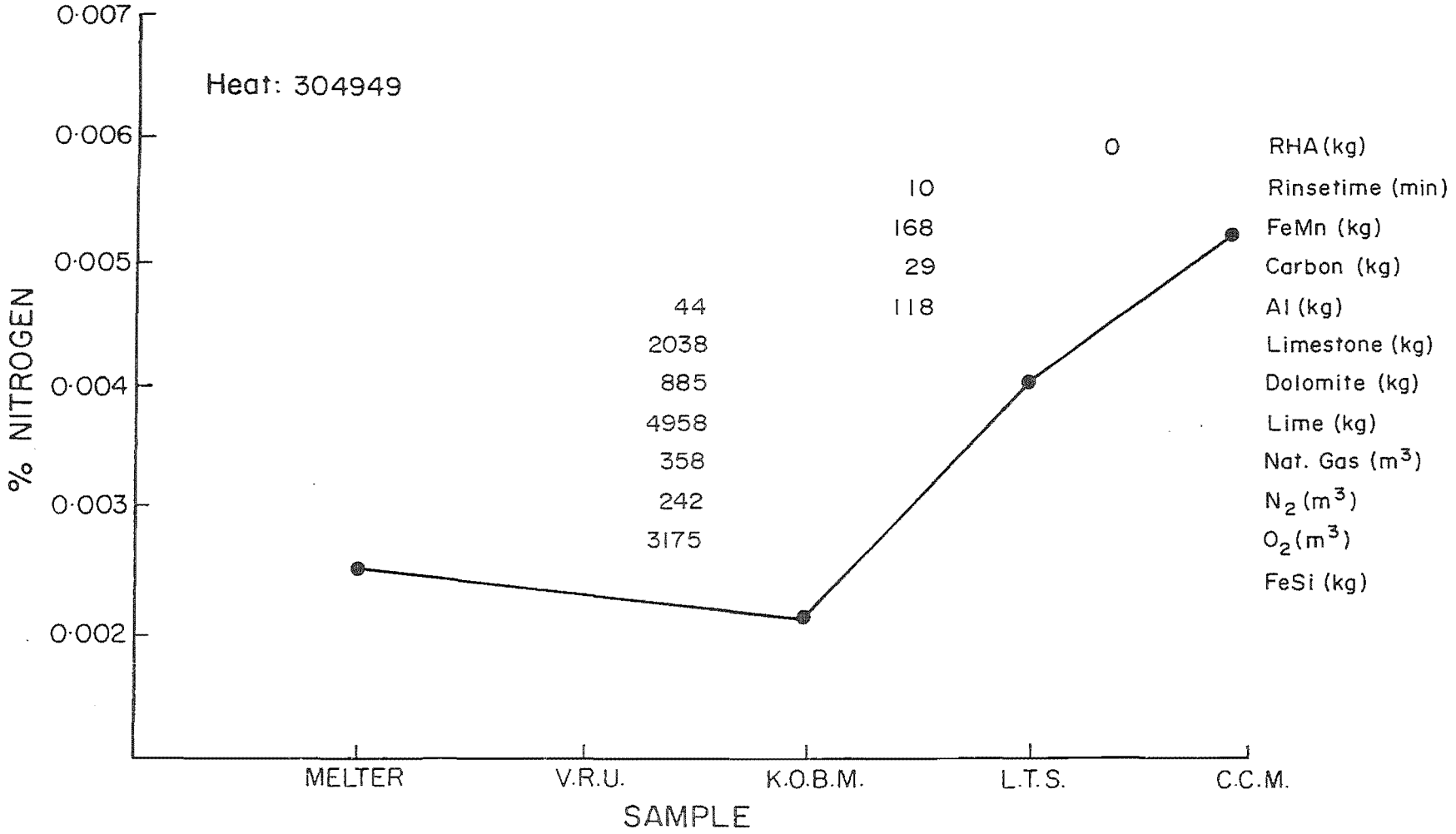

Figure B7 : Variation in total nitrogen content

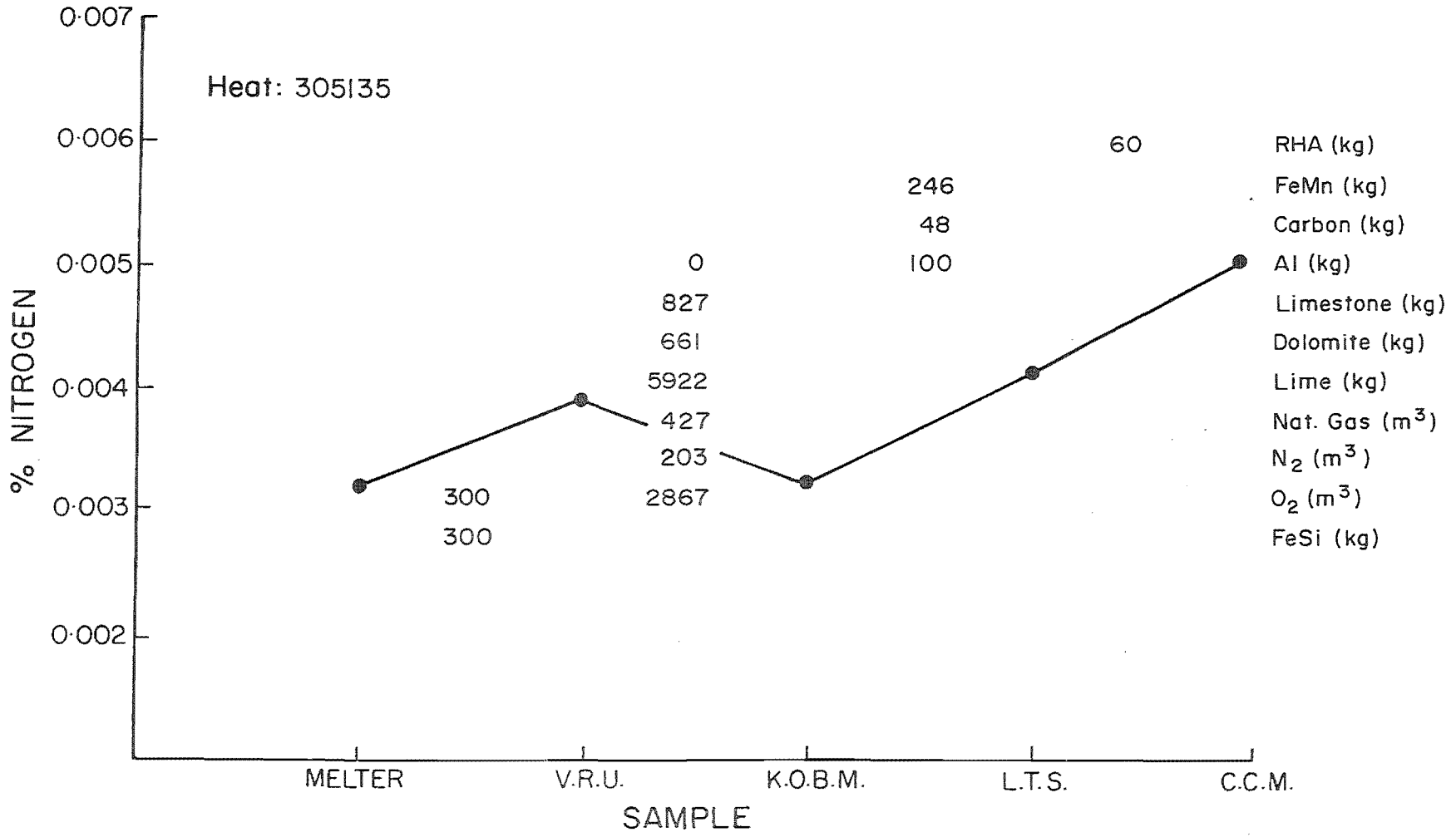

Figure B8 : Variation in total nitrogen content

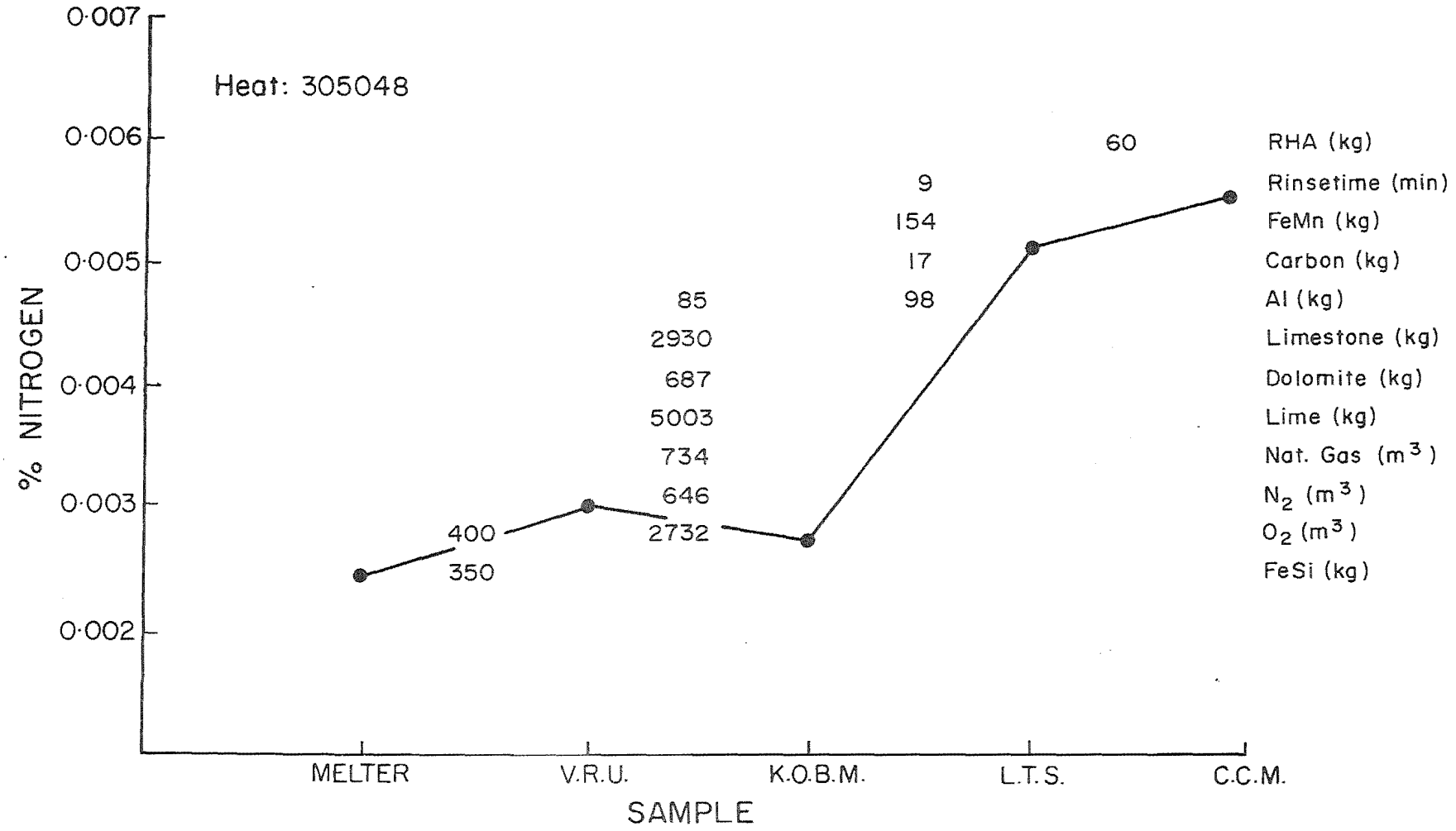

Figure B9 : Variation in total nitrogen content

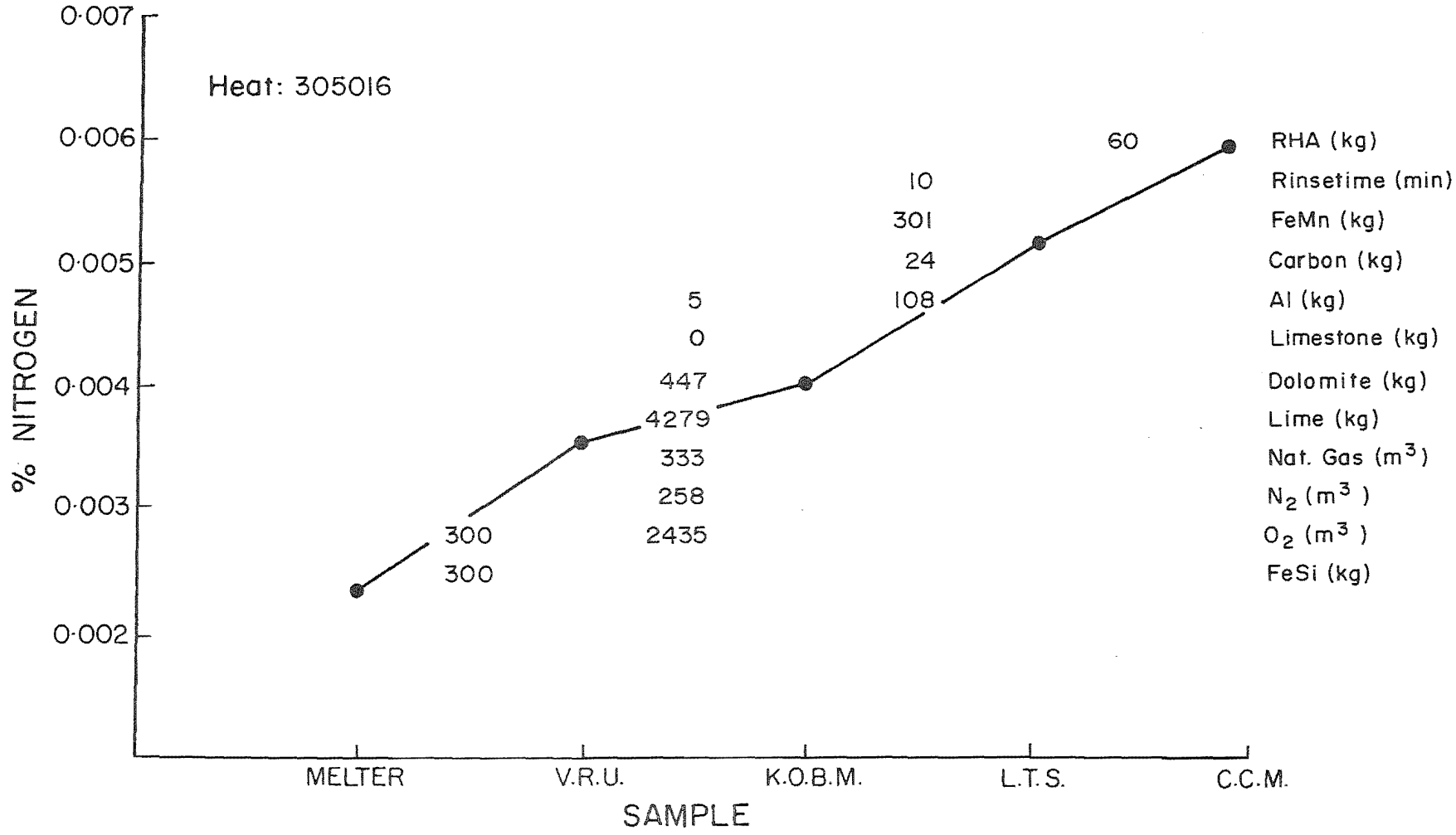

Figure B10 : Variation in total nitrogen content

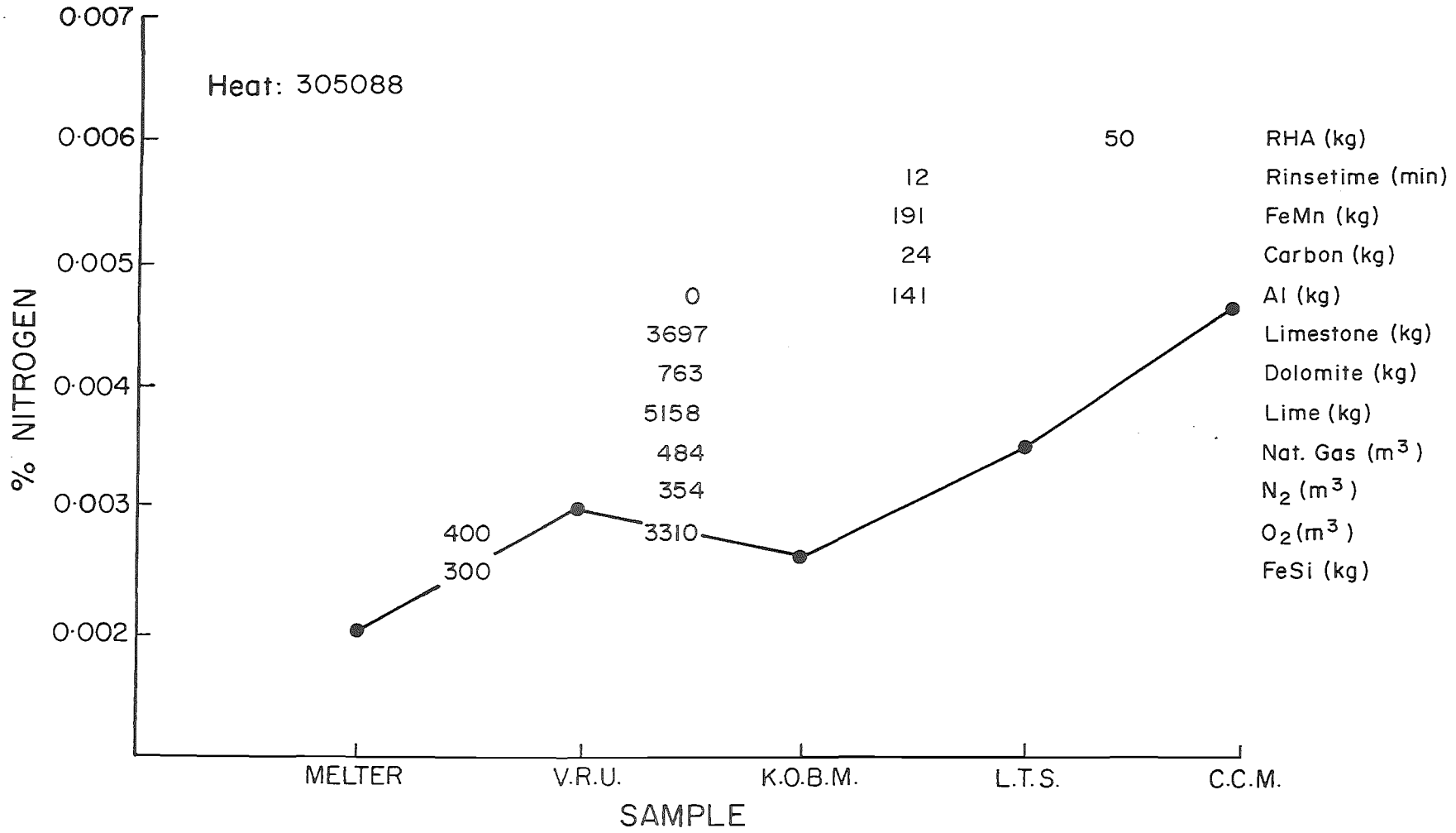

Figure B11 : Variation in total nitrogen content

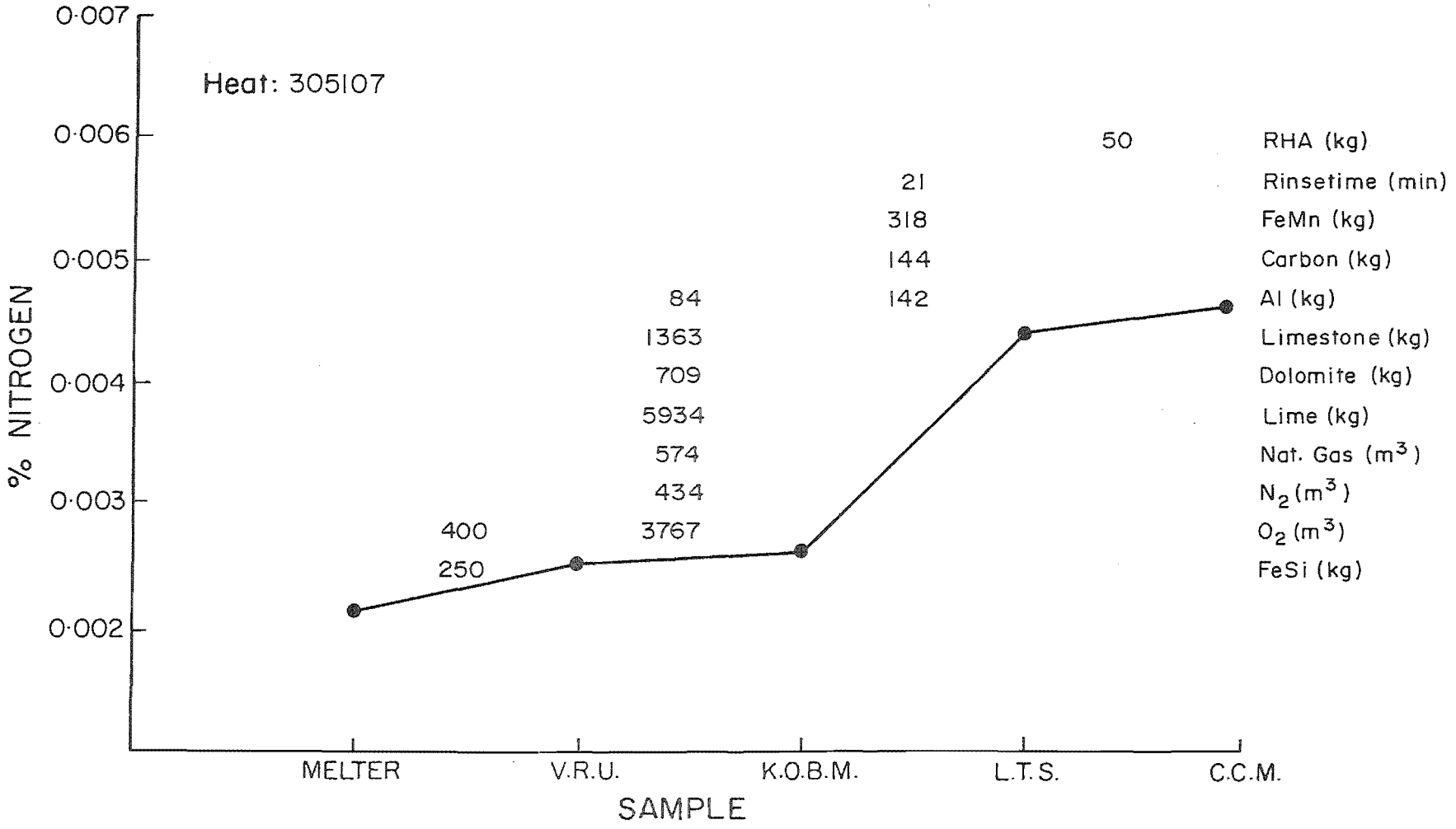

Figure B12 : Variation in total nitrogen content

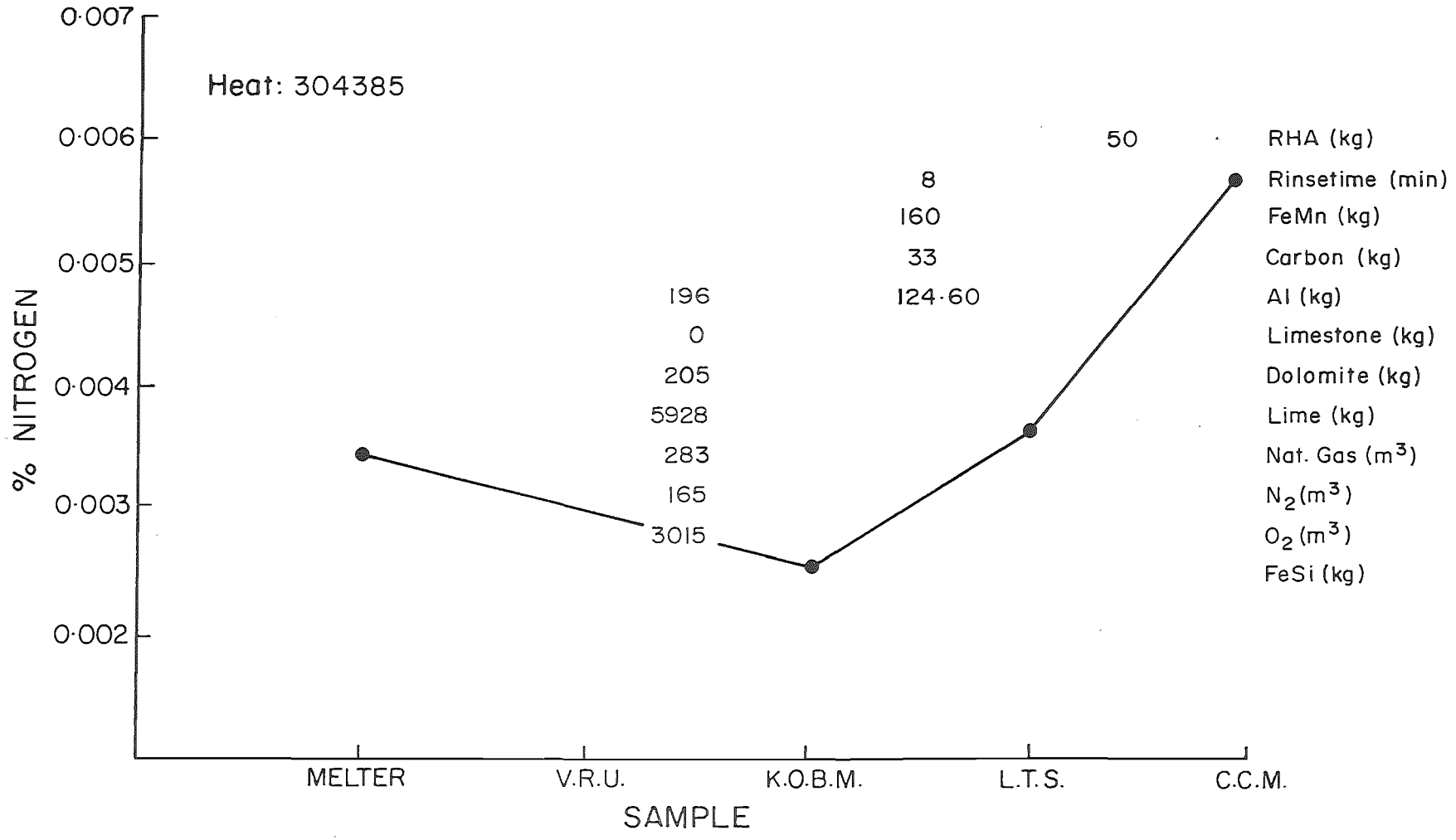

Figure B13 : Variation in total nitrogen content

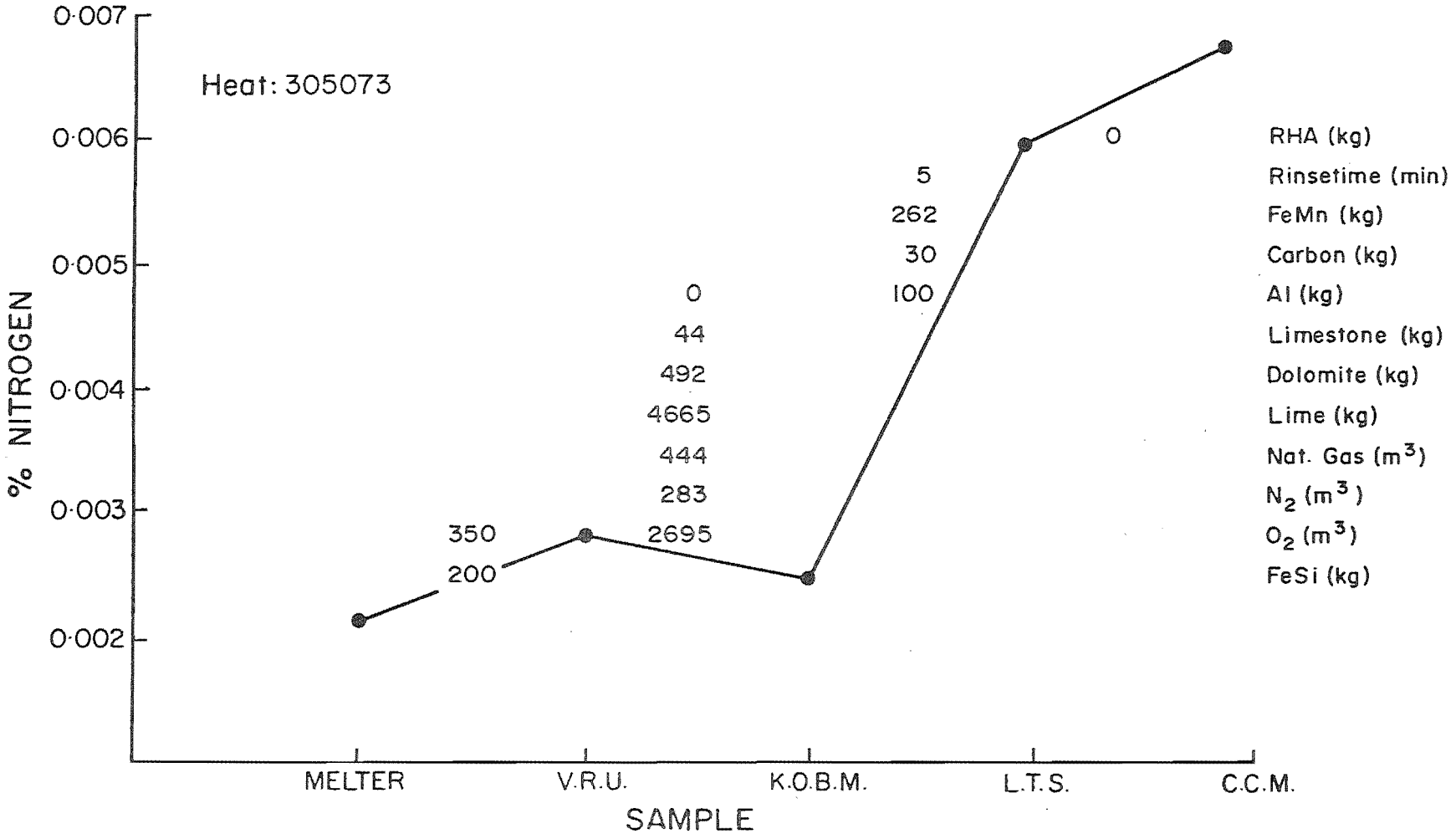

Figure B14 : Variation in total nitrogen content

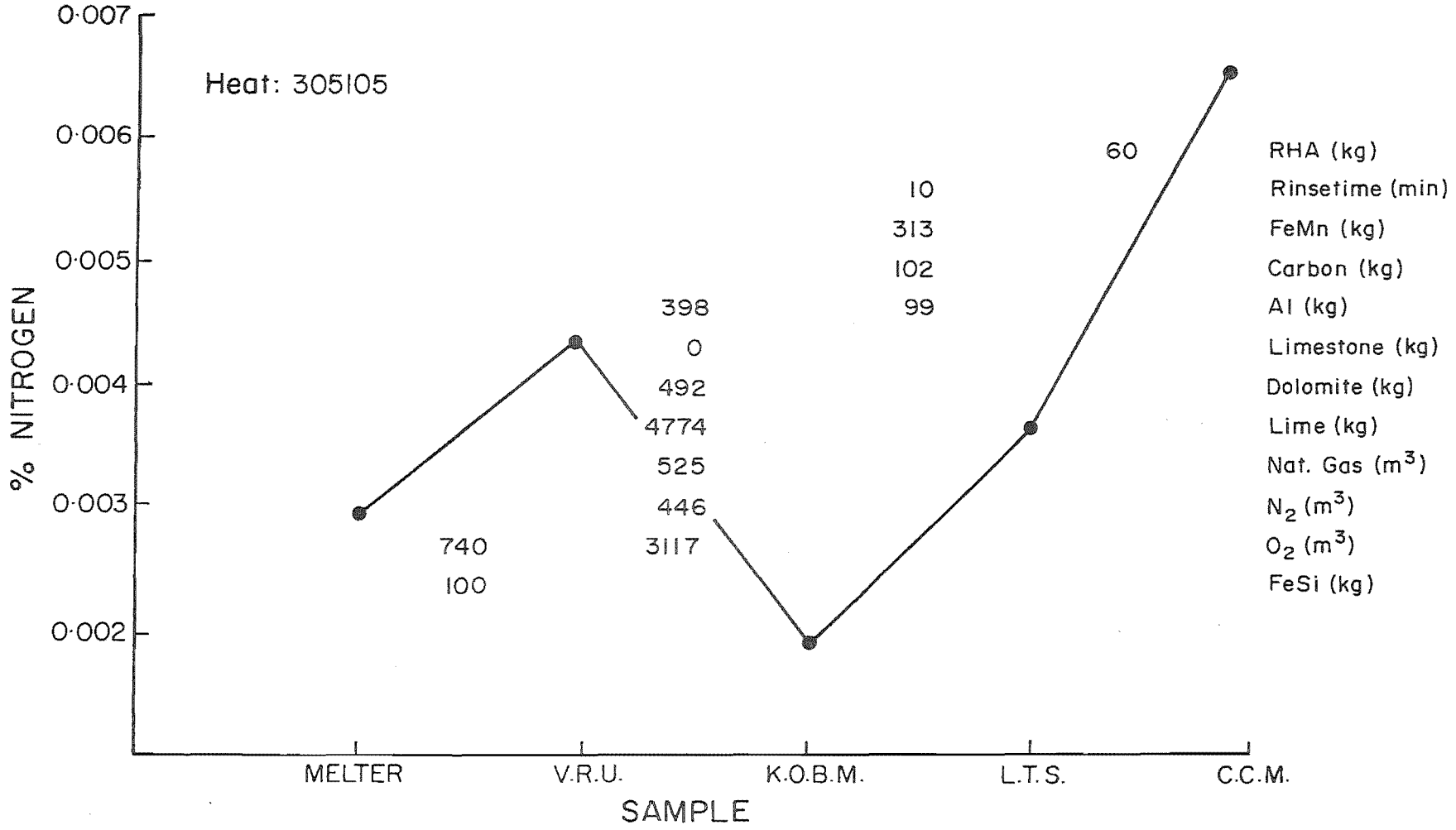

Figure B15 : Variation in total nitrogen content

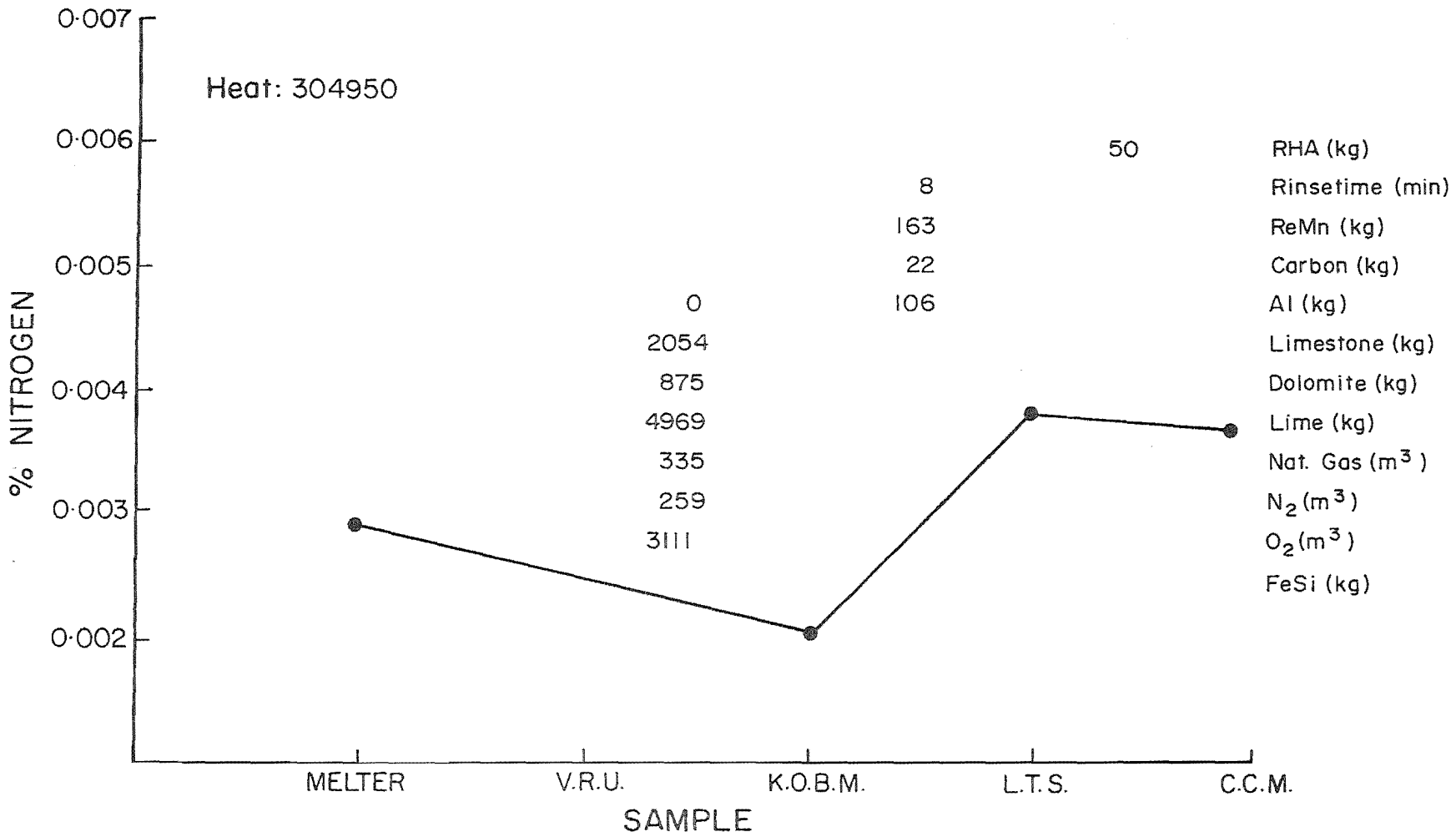

Figure B16 : Variation in total nitrogen content

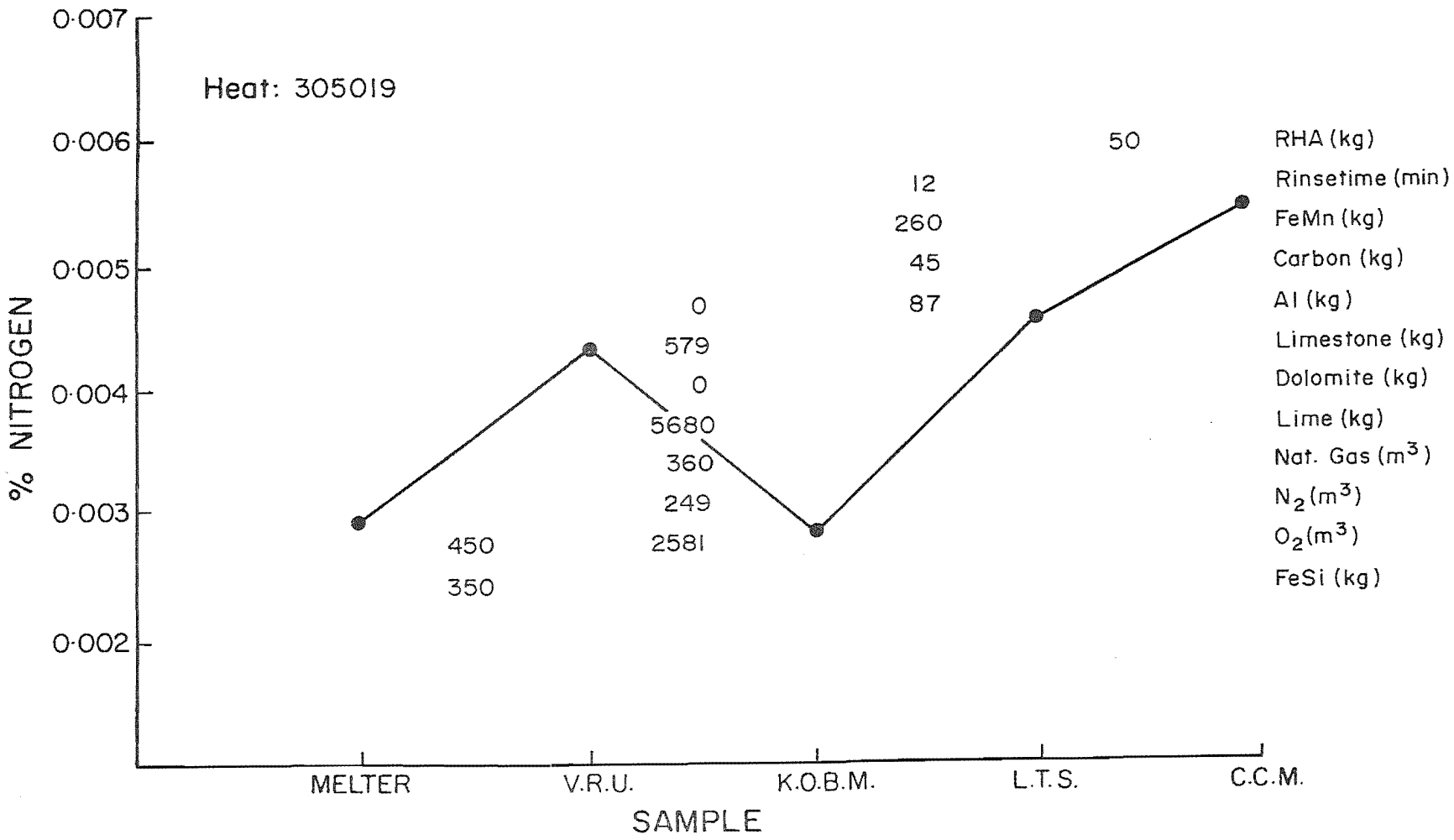

Figure B17 : Variation in total nitrogen content

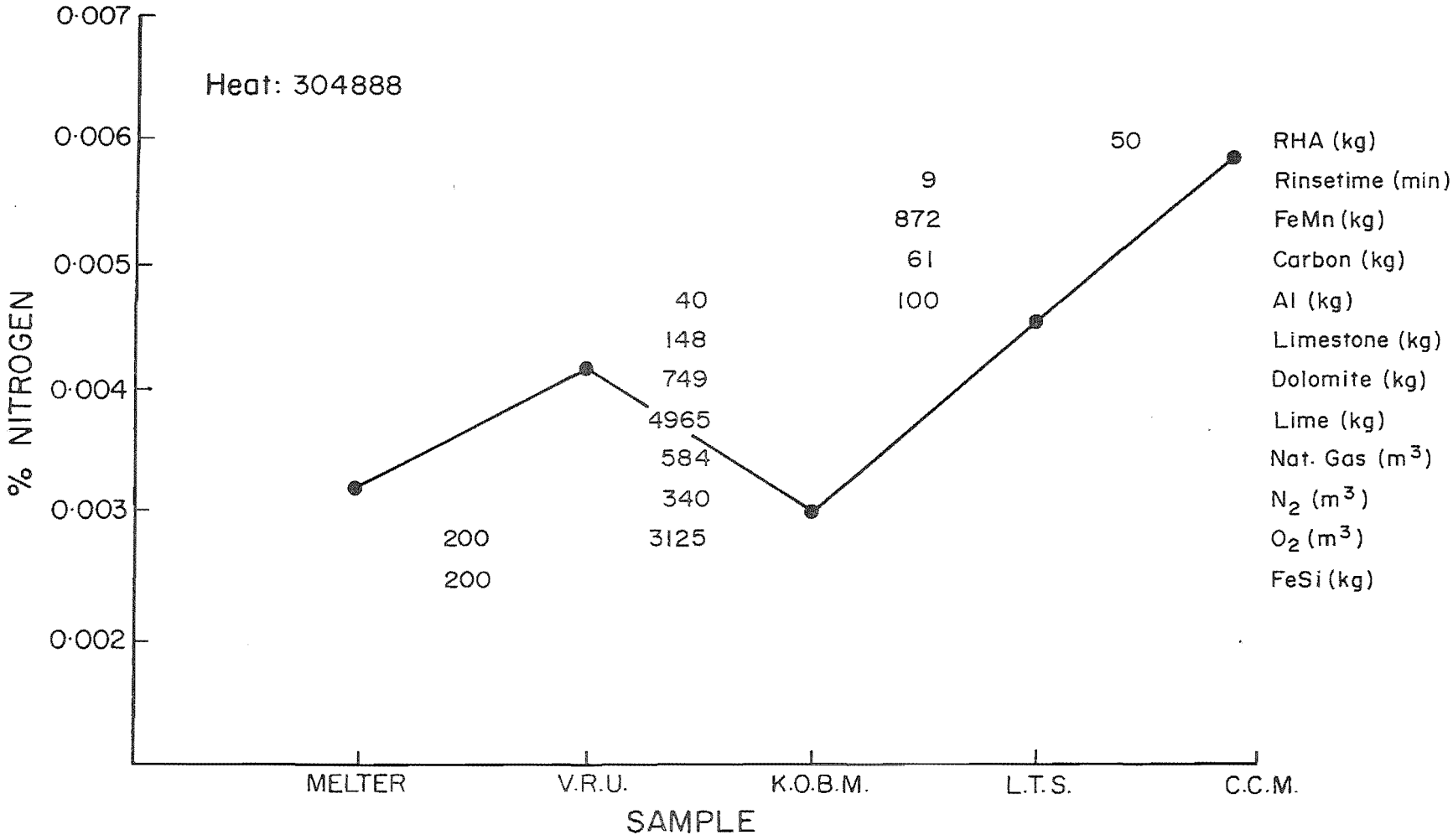

Figure B18 : Variation in total nitrogen content

APPENDIX C

Table C.1: Nitrogen determination of the heat treated HSLA steel Samples (for solubility product determination)

CAST	NITROGEN	TEMPERATURE °C													
		925	950	975	1000	1025	1050	1075	1100	1125	1150	1175	1200	1225	1250
B_2	SOL 1	0.0192	0.0192	0.0205											
	INSOL 1	0.0047	0.0034	0.0016											
	TOTAL:	0.0239	0.0226	0.0221											
	SOL 2	0.0144	0.0194	-											
	INSOL 2	0.0052	0.0032	-											
	TOTAL:	0.0196	0.0226	-											
C_2	SOL 1	0.0227	0.0245	0.0223	0.0223										
	INSOL 1	0.0074	0.0038	0.0044	0.0047										
	TOTAL:	0.0301	0.0283	0.0267	0.0270										
	SOL 2	-	-	0.0227	0.0221										
	INSOL 2	-	-	0.0043	0.0047										
	TOTAL:	-	-	0.0270	0.0268										
B_3	SOL 1	0.0149	0.0158	0.0189	0.0198										
	INSOL 1	0.0078	0.0074	0.0037	0.0023										
	TOTAL:	0.0227	0.0232	0.0226	0.0221										
	SOL 2	0.0150	0.0160	0.0196	0.0201										
	INSOL 2	0.0078	0.0075	0.0044	0.0024										
	TOTAL:	0.0228	0.0235	0.0240	0.0225										

Table C1: (Continued)

CAST	NITROGEN	TEMPERATURE °C													
		925	950	975	1000	1025	1050	1075	1100	1125	1150	1175	1200	1225	1250
C_3	SOL 1	0.0190	0.0201	0.0207	0.0224	0.0236	0.0259								
	INSOL 1	0.0114	0.0091	0.0088	0.0063	0.0025	0.0014								
	TOTAL:	0.0304	0.0292	0.0295	0.0287	0.0261	0.0273								
	SOL 2	0.0202	0.0211	0.0210	0.0231	0.0280	0.0269								
	INSOL 2	0.0116	0.0096	0.0093	0.0064	0.0026	0.0018								
	TOTAL:	0.0318	0.0307	0.0303	0.0295	0.0306	0.0287								
B_4	SOL 1	0.0122	0.0110	0.0150	0.0167	0.0181	0.0217								
	INSOL 1	0.0112	-	0.0085	0.0061	0.0056	0.0012								
	TOTAL:	0.0234	-	0.0235	0.0228	0.0237	0.0229								
	SOL 2	0.0120	0.0112	0.0151	0.0171	0.0183	0.0268								
	INSOL 2	0.0108	0.0119	0.0083	0.0064	0.0053	0.0016								
	TOTAL:	0.0228	0.0231	0.0234	0.0235	0.0236	0.0284								
C_4	SOL 1	0.0170	0.0153	0.0209	0.0200	0.0247	0.0264								
	INSOL 1	0.0152	0.0167	0.0111	0.0111	0.0078	0.0048								
	TOTAL:	0.0322	0.0320	0.0320	0.0311	0.0325	0.0312								
	SOL 2	0.0174	0.0143	0.0210	0.0216	0.0238	0.0261								
	INSOL 2	0.0156	0.0142	0.0110	0.0117	0.0078	0.0049								
	TOTAL:	0.0330	0.0285	0.0320	0.0333	0.0316	0.0310								

Table C1: (Continued)

CAST	NITROGEN	TEMPERATURE °C													
		925	950	975	1000	1025	1050	1075	1100	1125	1150	1175	1200	1225	1250
A_5	SOL 1	0.0051	0.0061												
	INSOL 1	0.0017	0.0006												
	TOTAL:	0.0068	0.0067												
	SOL 2	0.0051	0.0064												
	INSOL 2	0.0013	0.0006												
	TOTAL:	0.0064	0.0070												
B_5	SOL 1	0.0090	0.0110	0.0140	0.0140	0.0187	0.0223	0.0236							
	INSOL 1	0.0129	0.0113	0.0085	0.0078	0.0045	0.0018	0.0015							
	TOTAL:	0.0219	0.0223	0.0225	0.0218	0.0232	0.0241	0.0251							
	SOL 2	0.0091	0.0111	0.0141	0.0144	0.0180	0.0202	0.0210							
	INSOL 2	0.0130	0.0114	0.0084	0.0077	0.0037	0.0014	0.0012							
	TOTAL:	0.0221	0.0225	0.0225	0.0221	0.0217	0.0216	0.0222							
C_5	SOL 1	0.0144	0.0129	0.0171	0.0182	0.0287	0.0255	0.0279							
	INSOL 1	0.0180	0.0188	0.0146	0.0141	0.0085	0.0063	0.0029							
	TOTAL:	0.0324	0.0317	0.0317	0.0323	0.0372	0.0318	0.0308							
	SOL 2	0.0144	0.0137	0.0176	0.0183	0.0288	0.0234	0.0278							
	INSOL 2	0.0179	0.0191	0.0150	0.0142	0.0086	0.0062	0.0029							
	TOTAL:	0.0323	0.0328	0.0326	0.0325	0.0374	0.0296	0.0307							

Table C1: (Continued)

CAST	NITROGEN	TEMPERATURE °C												
		925	950	975	1000	1025	1050	1075	1100	1125	1150	1175	1200	1225	1250
D_1	SOL 1				0.0241	0.0288	0.0283	0.0314	0.0325	0.0348	0.0360	0.0362			
	INSOL 1				0.0135	0.0096	-	0.0035	0.0019	0.0013	0.0010	0.0008			
	TOTAL:				0.0376	0.0384	-	0.0349	0.0344	0.0361	0.0370	0.0370			
	SOL 2				0.0237	0.0285	0.0298	0.0340	0.0340	0.0344	0.0357	0.0363			
	INSOL 2				0.0136	0.0088	0.0057	0.0037	0.0019	0.0013	0.0011	0.0007			
	TOTAL:				0.0373	0.0373	0.0355	0.0377	0.0359	0.0357	0.0368	0.0370			
D_2	SOL 1				0.0194	0.0223	0.0244	0.0272	0.0298	0.0324	0.0857	0.0362			
	INSOL 1				0.0175	0.0143	0.0131	0.0095	0.0060	0.0030	0.0015	0.0008			
	TOTAL:				0.0369	0.0366	0.0375	0.0367	0.0358	0.0354	0.0372	0.0370			
	SOL 2				0.0202	0.0220	0.0250	0.0283	0.0300	0.0340	0.0360	0.0360			
	INSOL 2				0.0180	0.0152	0.0126	0.0094	0.0060	0.0031	0.0017	0.0008			
	TOTAL:				0.0382	0.0372	0.0376	0.0377	0.0360	0.0371	0.0377	0.0368			
D_3	SOL 1				0.0173	0.0189	0.0221	0.0299	0.0301	0.0305	0.0326	0.0369	0.0389		
	INSOL 1				0.0208	0.0213	0.0168	0.0120	0.0096	0.0090	0.0071	0.0026	0.0008		
	TOTAL:				0.0381	0.0402	0.0389	0.0419	0.0397	0.0395	0.0397	0.0395	0.0397		
	SOL 2				-	0.0174	0.0218	0.0267	0.0300	0.0301	0.0338	0.0371	0.0388		
	INSOL 2				-	0.0223	0.0170	0.0122	0.0096	0.0099	0.0057	0.0025	0.0007		
	TOTAL:				-	0.0397	0.0388	0.0389	0.0396	0.0400	0.0395	0.0396	0.0395		

Table C1: (Continued)

CAST	NITROGEN	TEMPERATURE °C												
		925	950	975	1000	1025	1050	1075	1100	1125	1150	1175	1200	1225	1250
D_4	SOL 1				0.0140	0.0155	0.0177	0.0280	0.0325	0.0316	0.0342	0.0372	0.0382		
	INSOL 1				0.0255	0.0227	0.0201	0.0120	0.0103	0.0082	0.0045	0.0017	0.0007		
	TOTAL:				0.0395	0.0382	0.0378	0.0400	0.0428	0.0398	0.0387	0.0389	0.0389		
	SOL 2				0.0141	0.0160	0.0169	0.0296	0.0324	0.0333	0.0344	0.0374	0.0381		
	INSOL 2				0.0256	0.0227	0.0200	0.0100	0.0091	0.0079	0.0051	0.0020	0.0009		
	TOTAL:				0.0397	0.0387	0.0369	0.0396	0.0415	0.0412	0.0395	0.0394	0.0390		
D_5	SOL 1				-	0.0099	0.0168	0.0219	0.0206	0.0265	0.0295	0.0364	0.0380	0.0389	
	INSOL 1				0.0292	0.0278	0.0251	0.0210	0.0199	0.0124	0.0103	0.0046	0.0020	0.0010	
	TOTAL:				-	0.0377	0.0419	0.0429	0.0405	0.0389	0.0398	0.0410	0.0400	0.0399	
	SOL 2				0.0114	0.0102	0.0162	0.0200	0.0196	0.0269	0.0298	0.0358	0.0378	0.0392	
	INSOL 2				0.0329	0.0293	0.0233	0.0226	0.0205	0.0120	0.0105	0.0054	0.0023	0.0008	
	TOTAL:				0.0443	0.0395	0.0395	0.0426	0.0401	0.0389	0.0403	0.0412	0.0401	0.0400	
D_6	SOL 1				0.0057	0.0107	0.0132	0.0178	0.0225	0.0243	0.0265	0.0288	0.0316	0.0357	0.0369
	INSOL 1				0.0310	0.0270	0.0238	0.0194	0.0171	0.0135	0.0109	0.0099	0.0062	0.0021	0.0009
	TOTAL:				0.0367	0.0377	0.0370	0.0372	0.0396	0.0378	0.0374	0.0387	0.0378	0.0378	0.0378
	SOL 2				0.0058	0.0112	0.0135	0.0182	0.0200	0.0233	0.0265	0.0283	0.0315	0.0355	0.0370
	INSOL 2				0.0309	0.0281	0.0235	0.0199	0.0171	0.0148	0.0118	0.0097	0.0065	0.0024	0.0009
	TOTAL:				0.0367	0.0393	0.0370	0.0381	0.0371	0.0381	0.0383	0.0380	0.0380	0.0379	0.0379

APPENDIX D

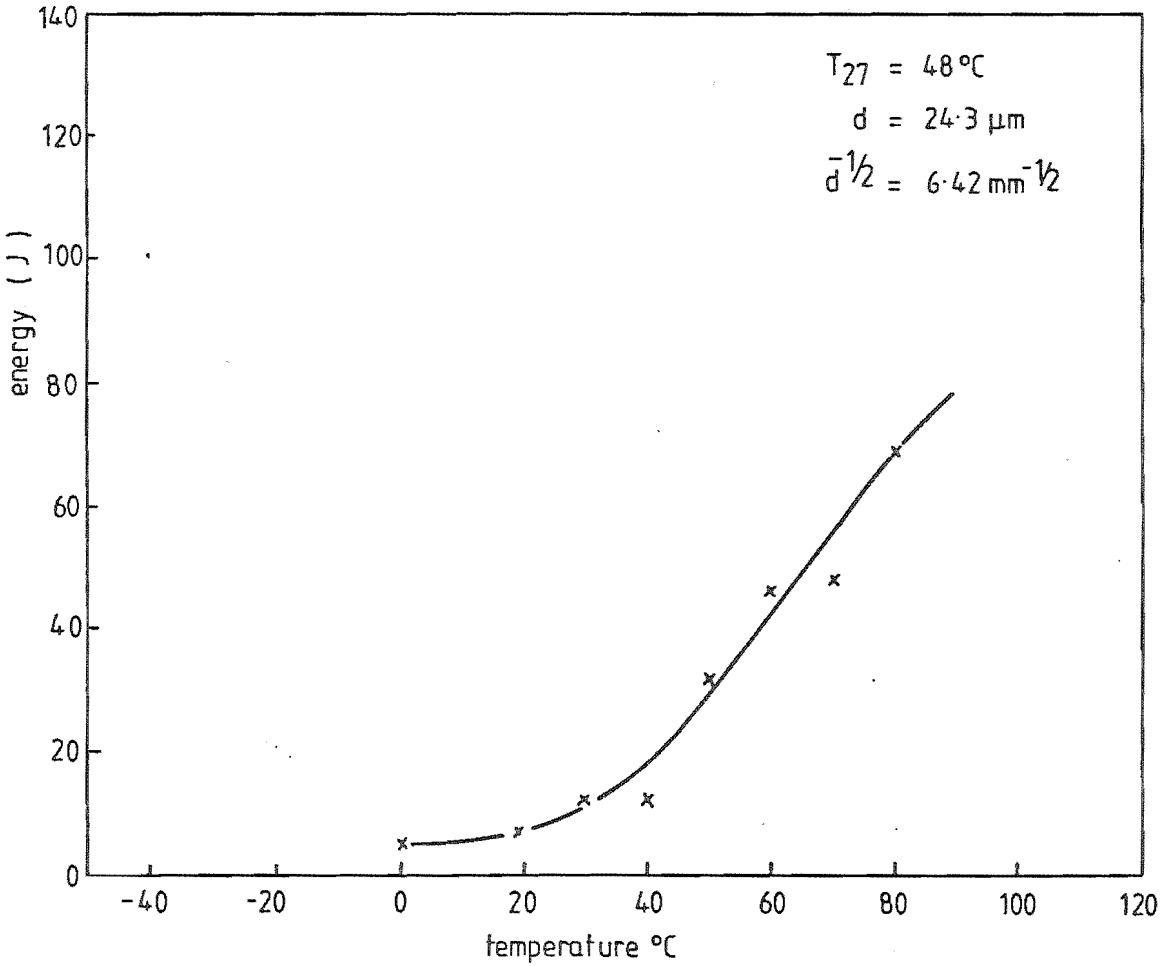

Figure D1: The V-notched charpy impact energy curve for steel B5; Simulated heat treated at 600°C

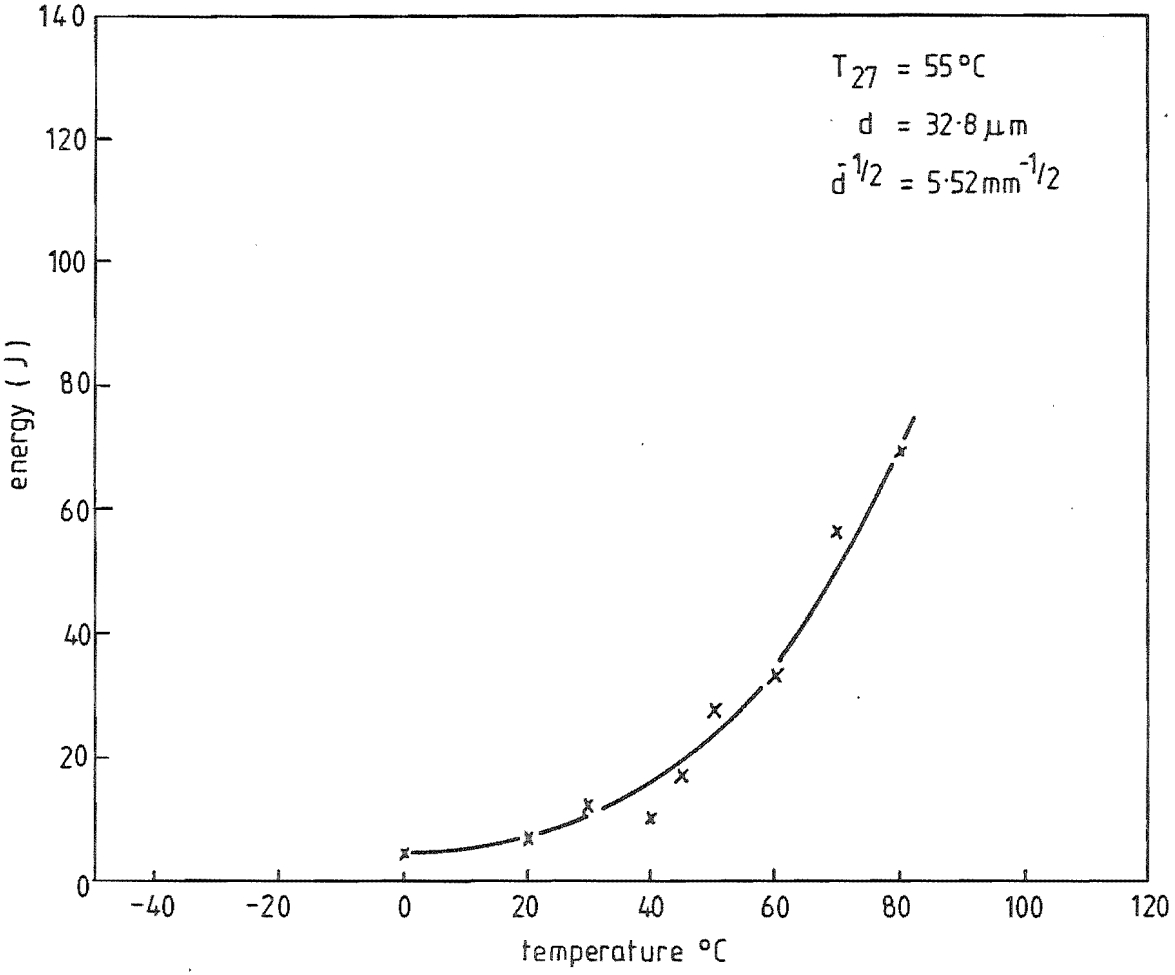

Figure D2: The V-notched charpy impact energy curve for steel B5; Simulated heat treated at 700°C

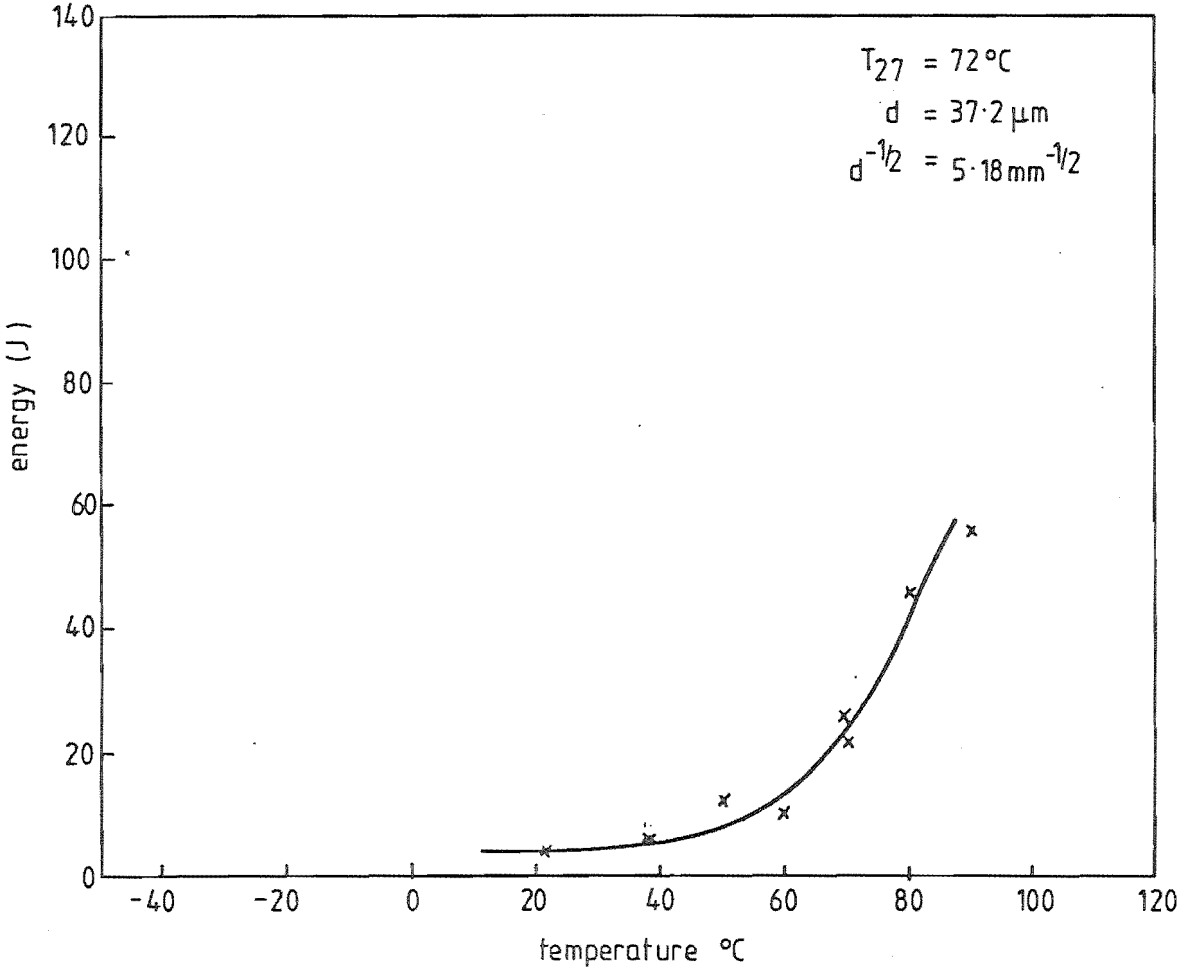

Figure D3: The V-notched charpy impact energy curve for steel B5; Simulated heat treated at 800°C

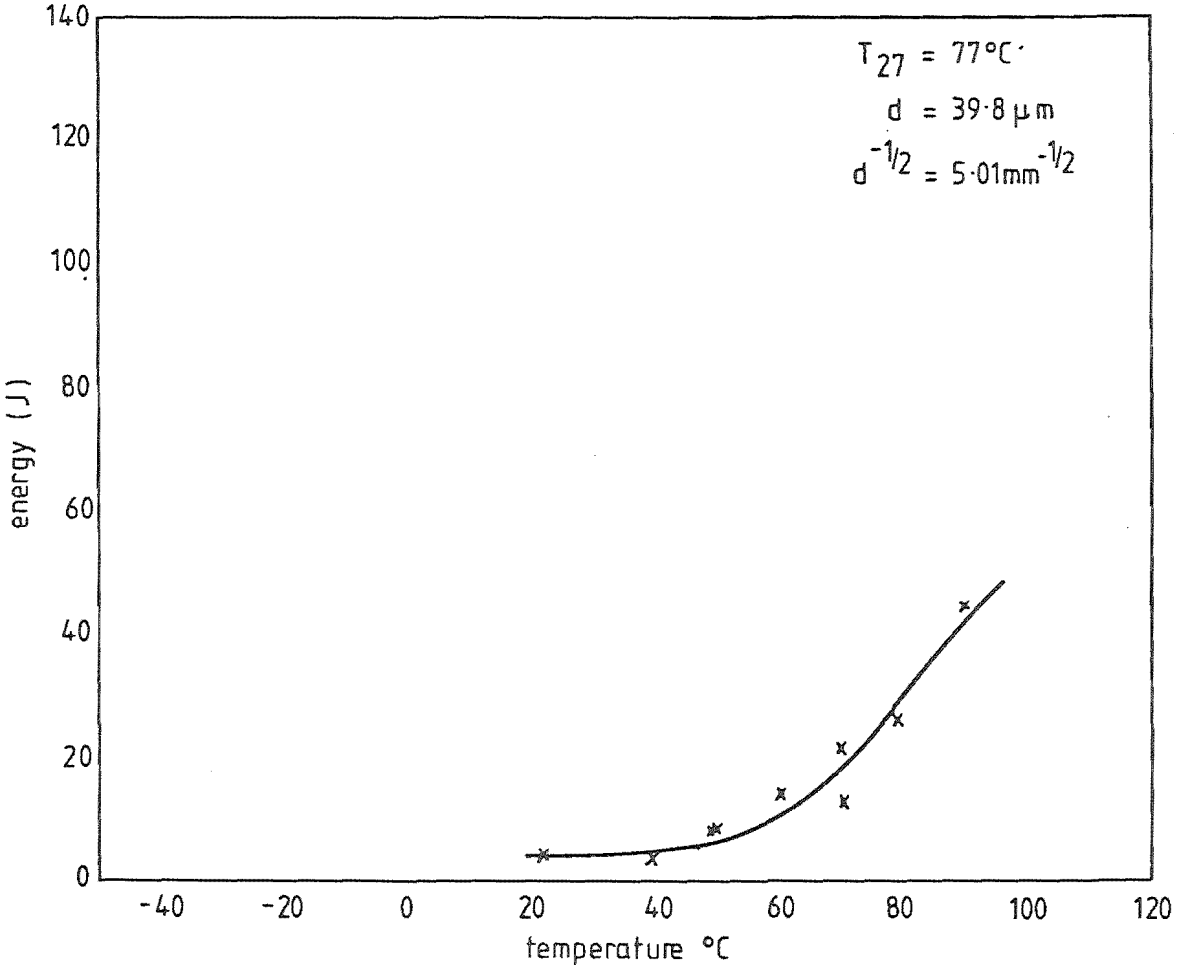

Figure D4: The V-notched charpy impact energy curve for steel B5; Simulated heat treated at 900°C

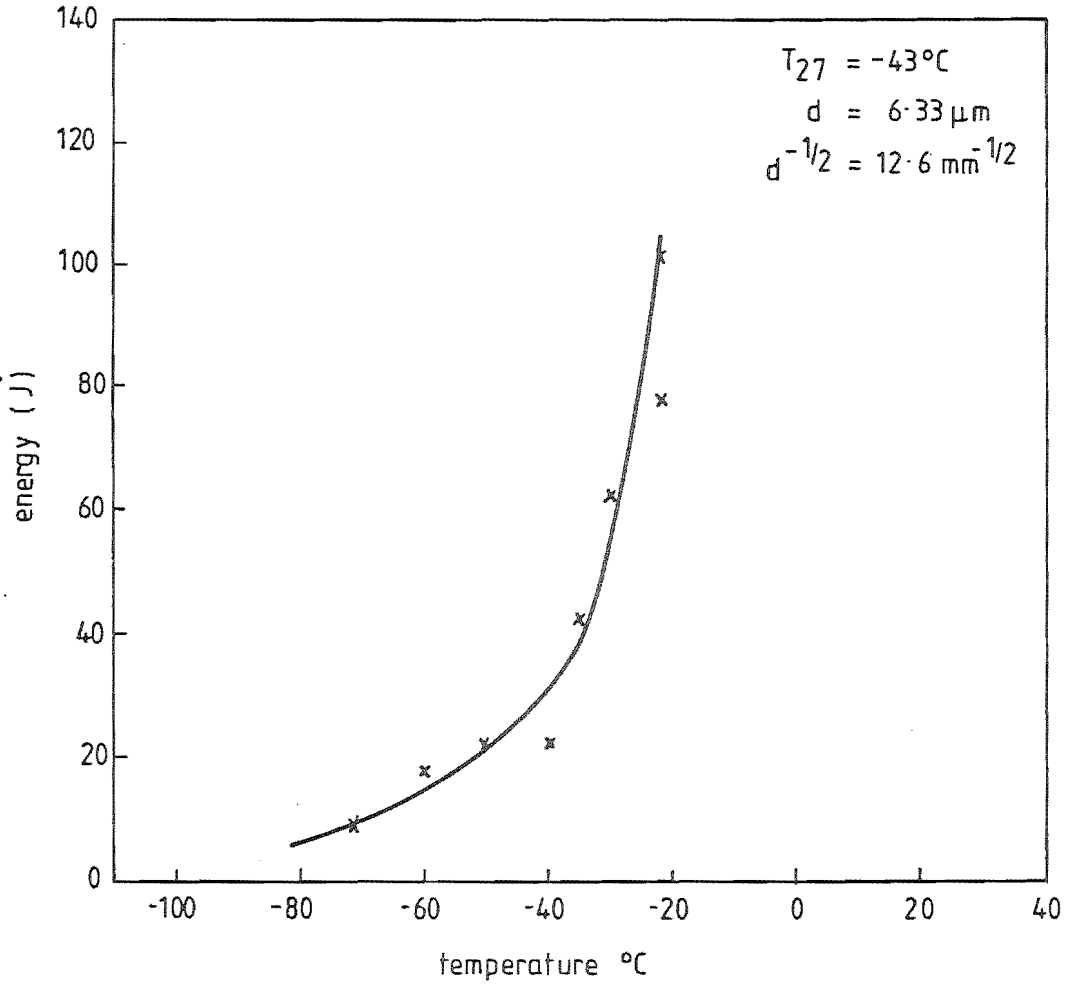

Figure D5: The V-notched charpy impact energy curve for steel B5; Normalized at 900°C after simulated heat treated at 600°C

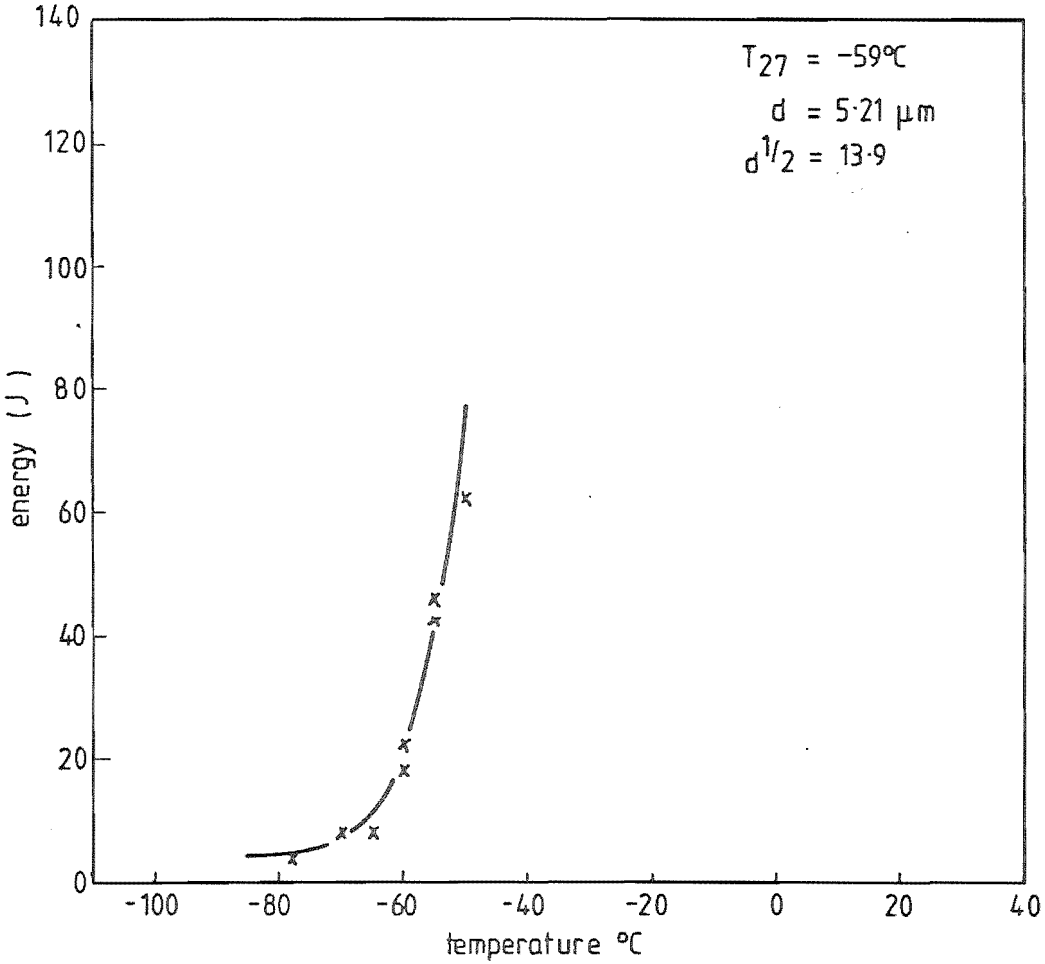

Figure D6: The V-notched charpy impact energy curve for steel B5; Normalised at 900°C after simulated heat treated at 700°C

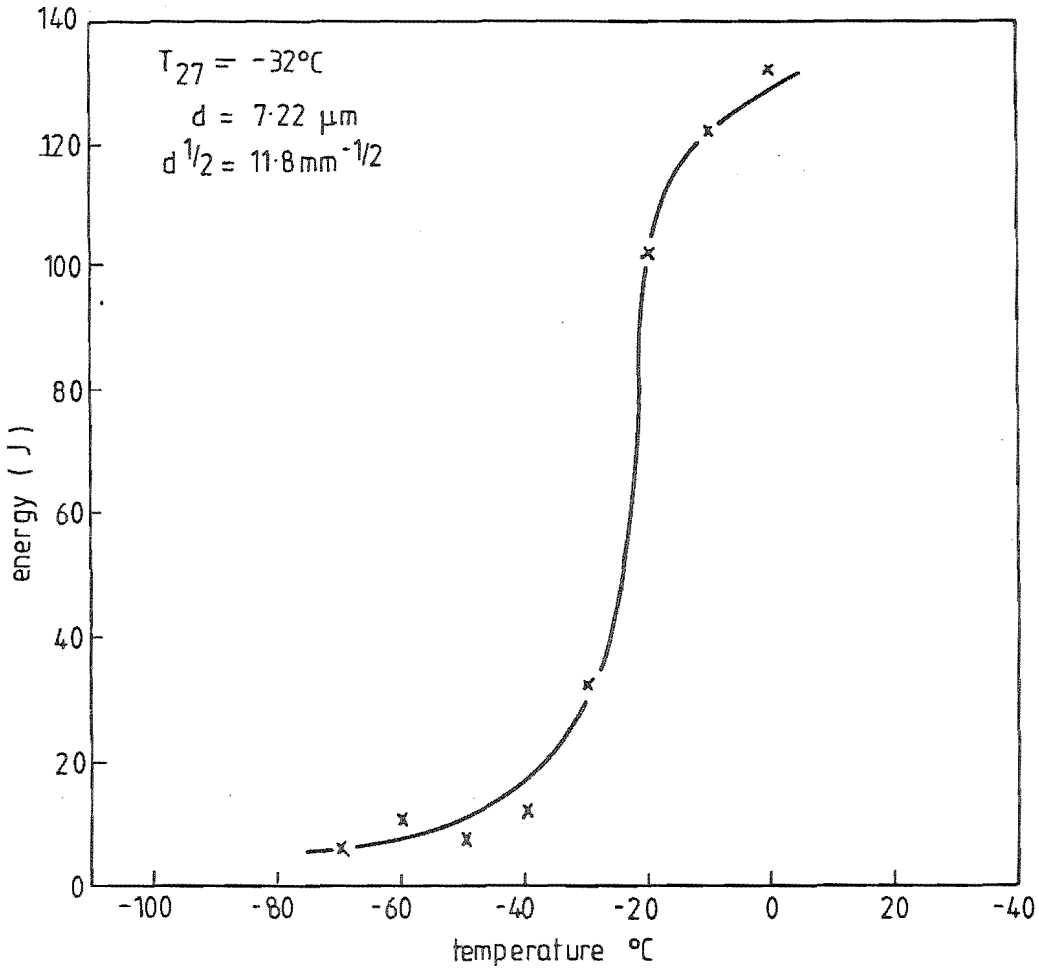

Figure D7: The V-notched charpy impact energy curve for steel B5; Normalized at 900°C after simulated heat treated at 800°C

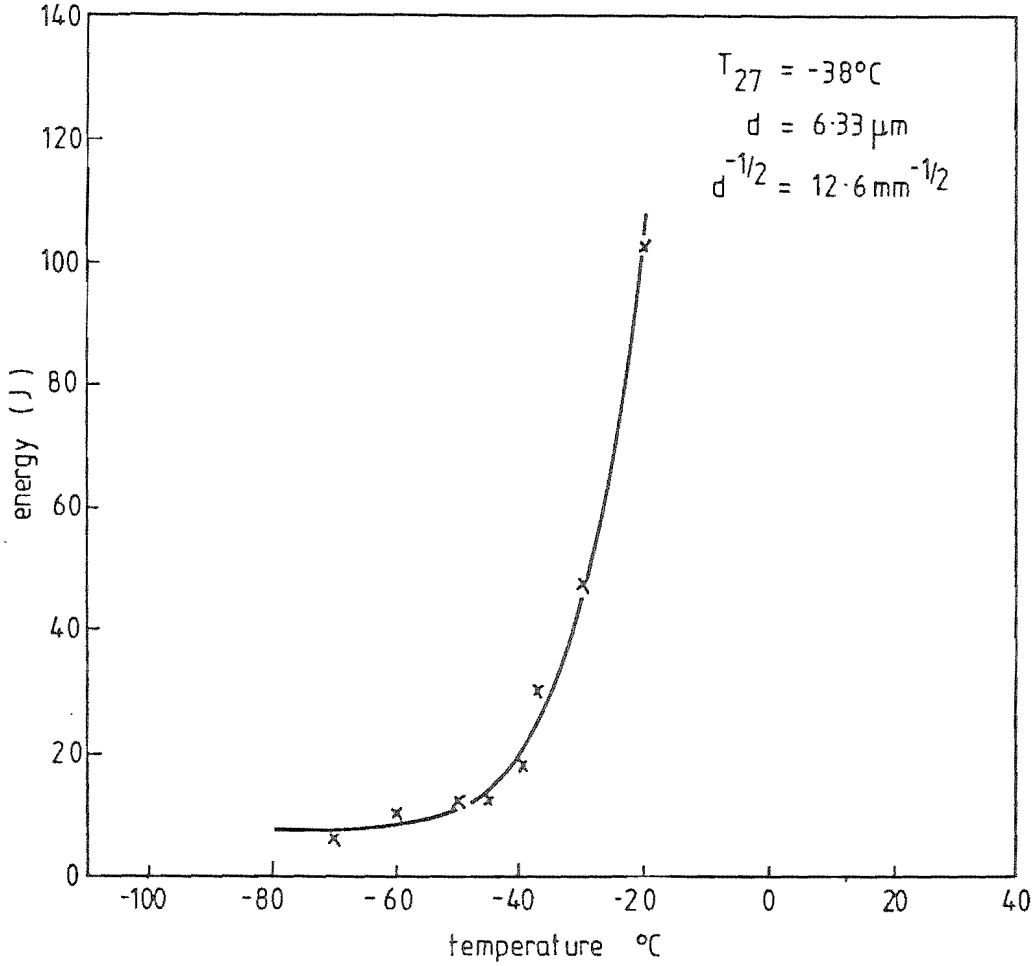

Figure D8: The V-notched charpy impact energy curve for steel B5; Normalized at 900°C after simulated heat treated at 900°C

APPENDIX E

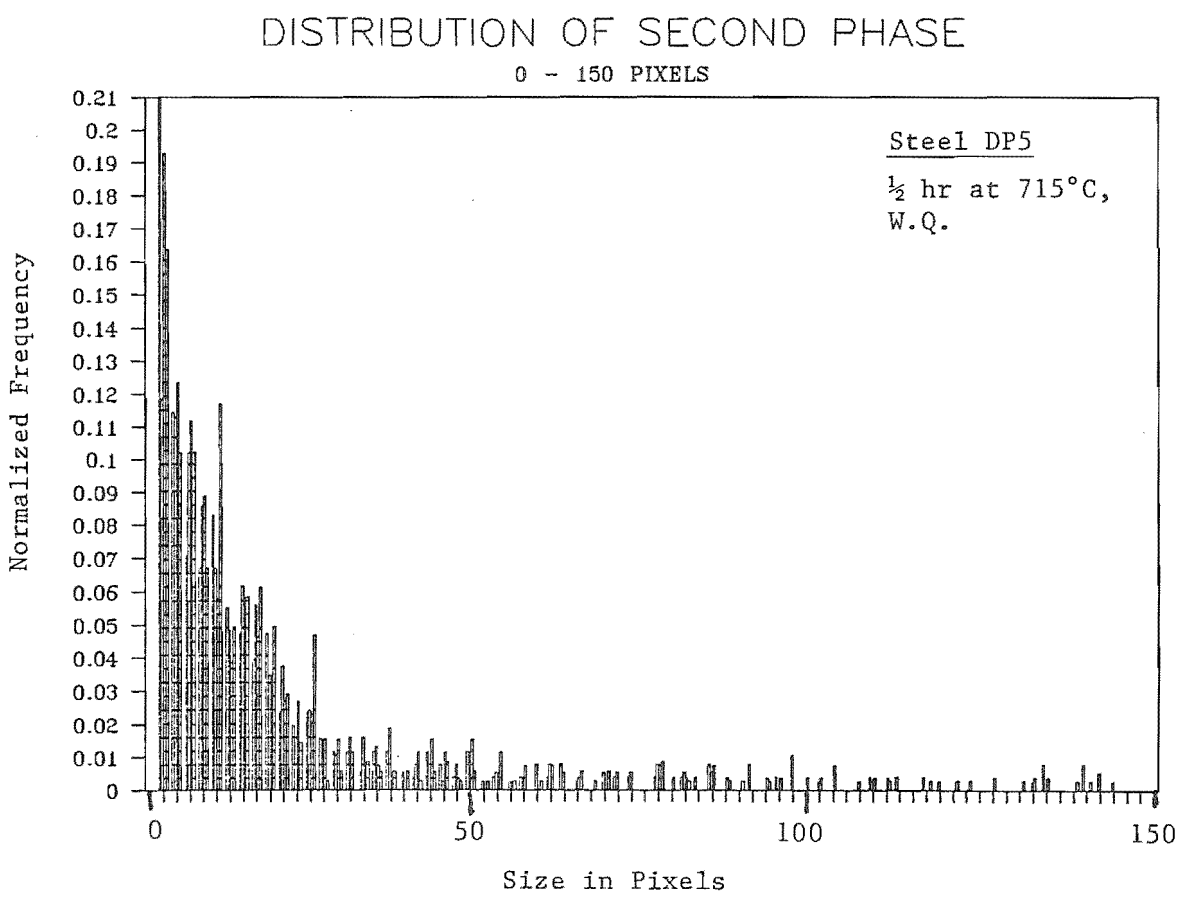

Figure E1: Distribution of Second Phase

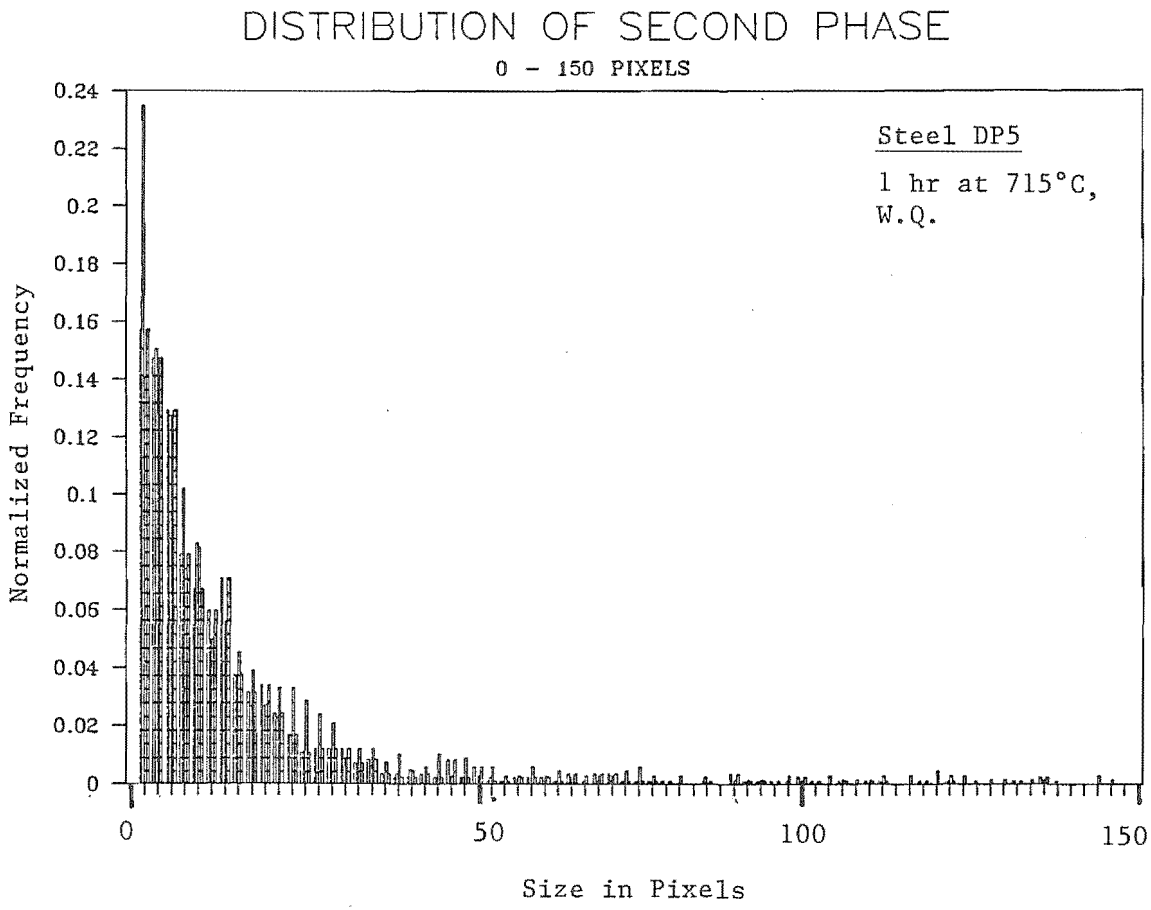

Figure E2: Distribution of Second Phase

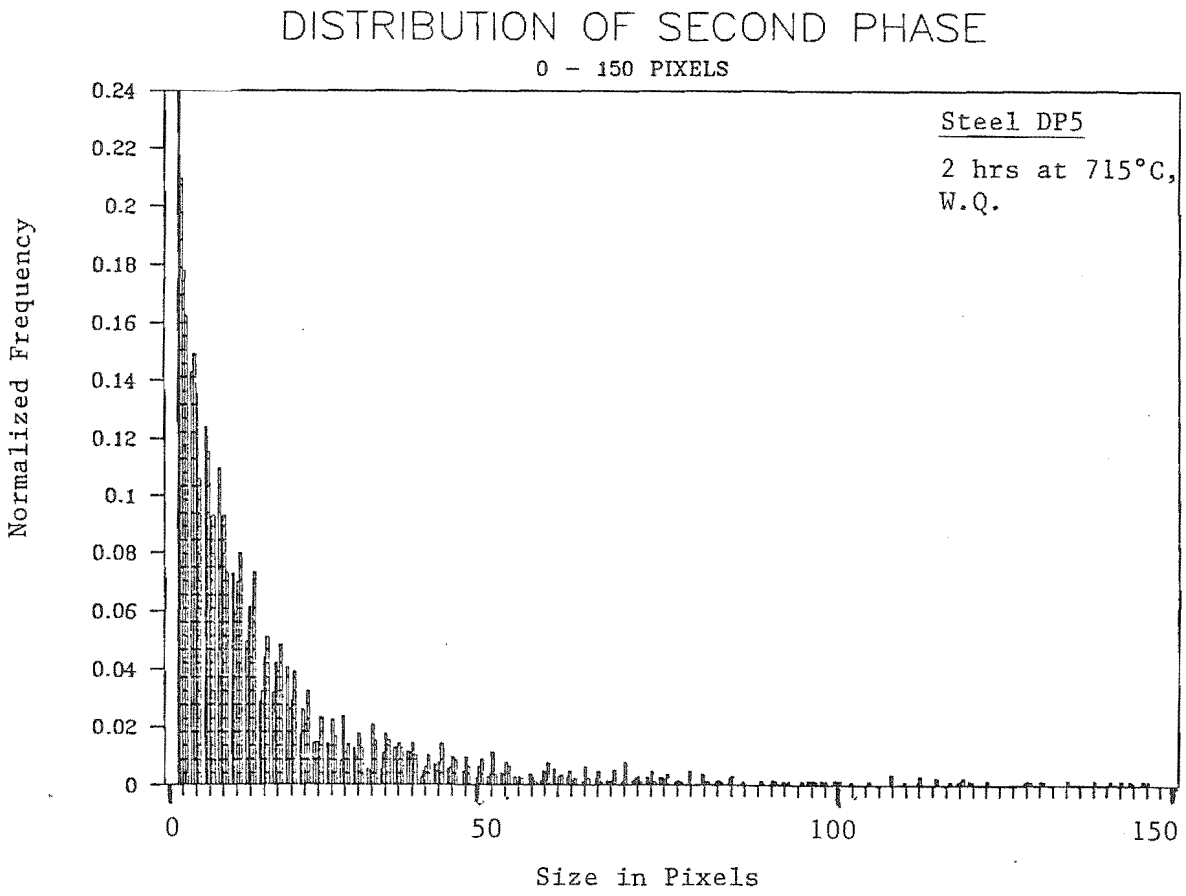

Figure E3: Distribution of Second Phase

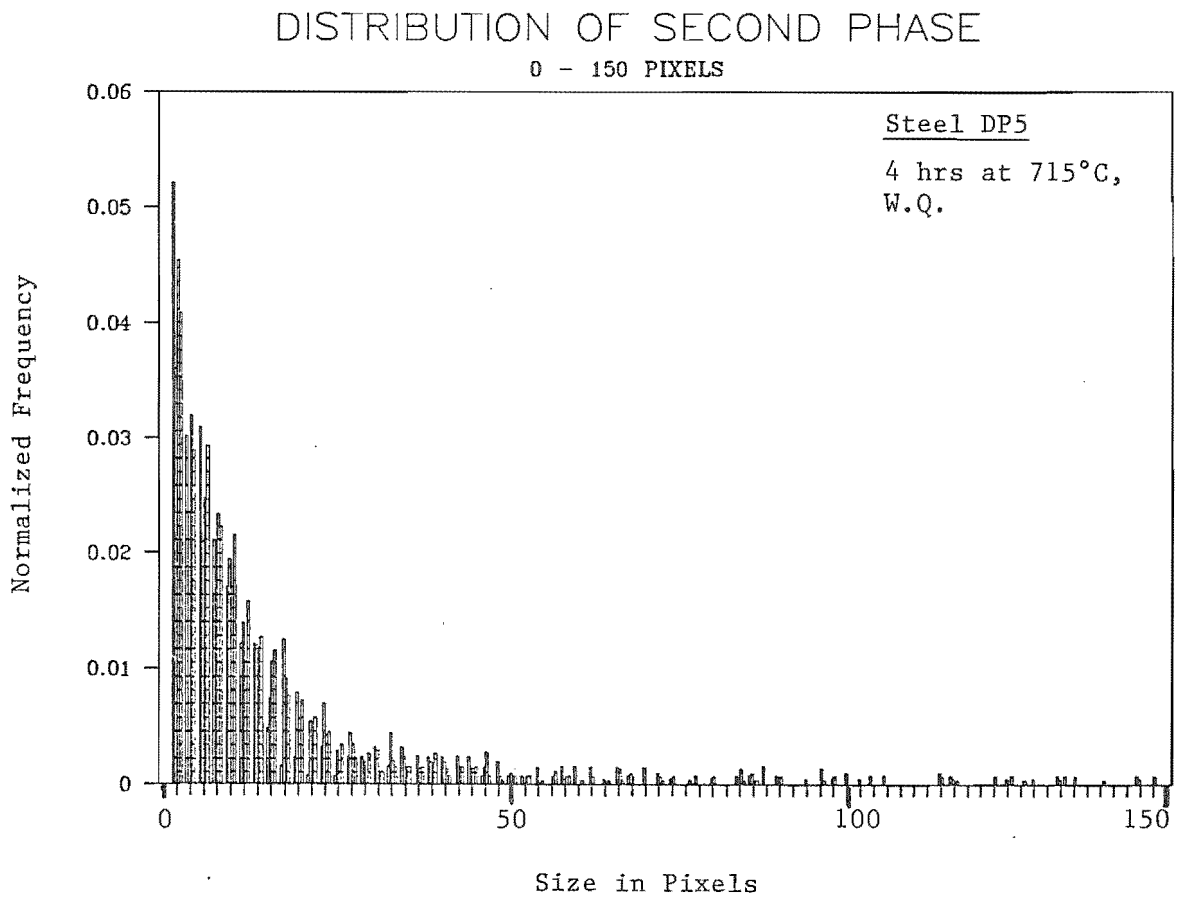

Figure E4: Distribution of Second Phase

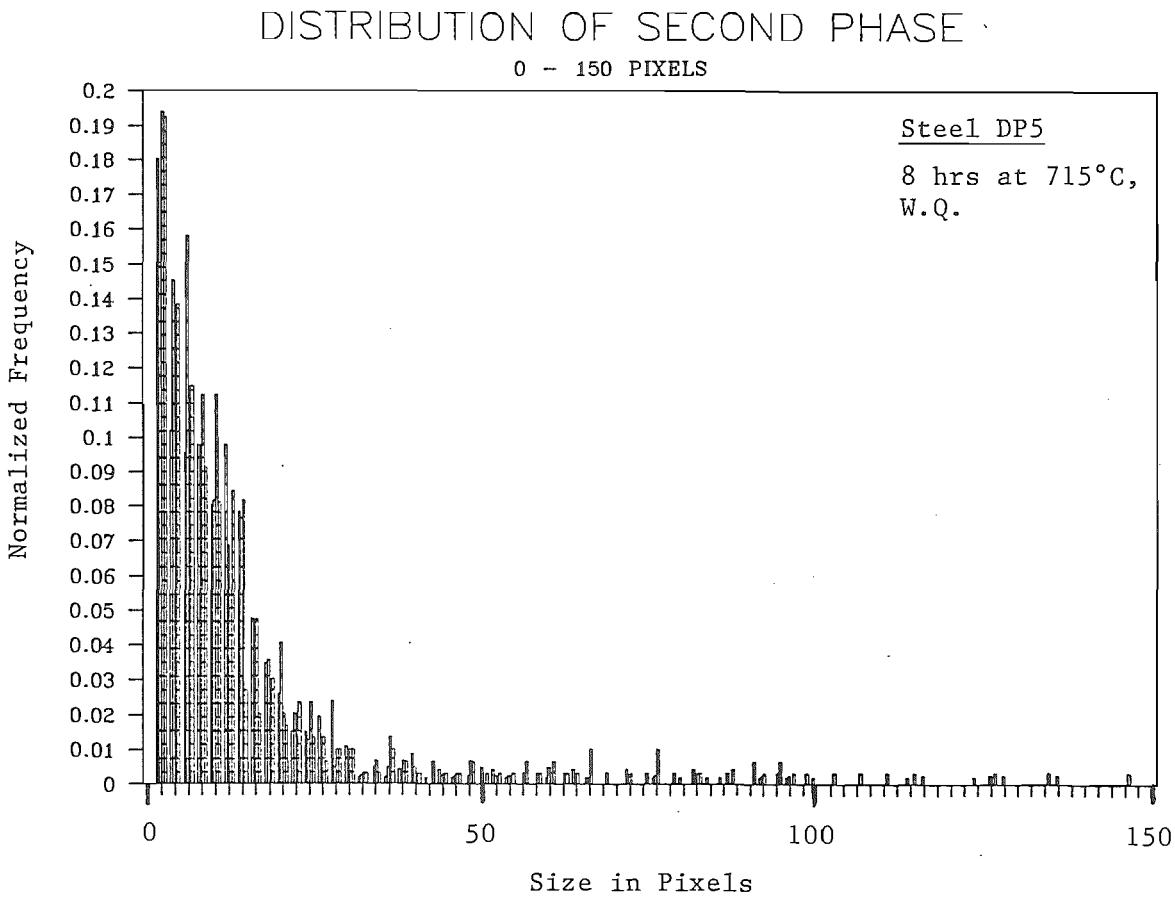

Figure E5: Distribution of Second Phase

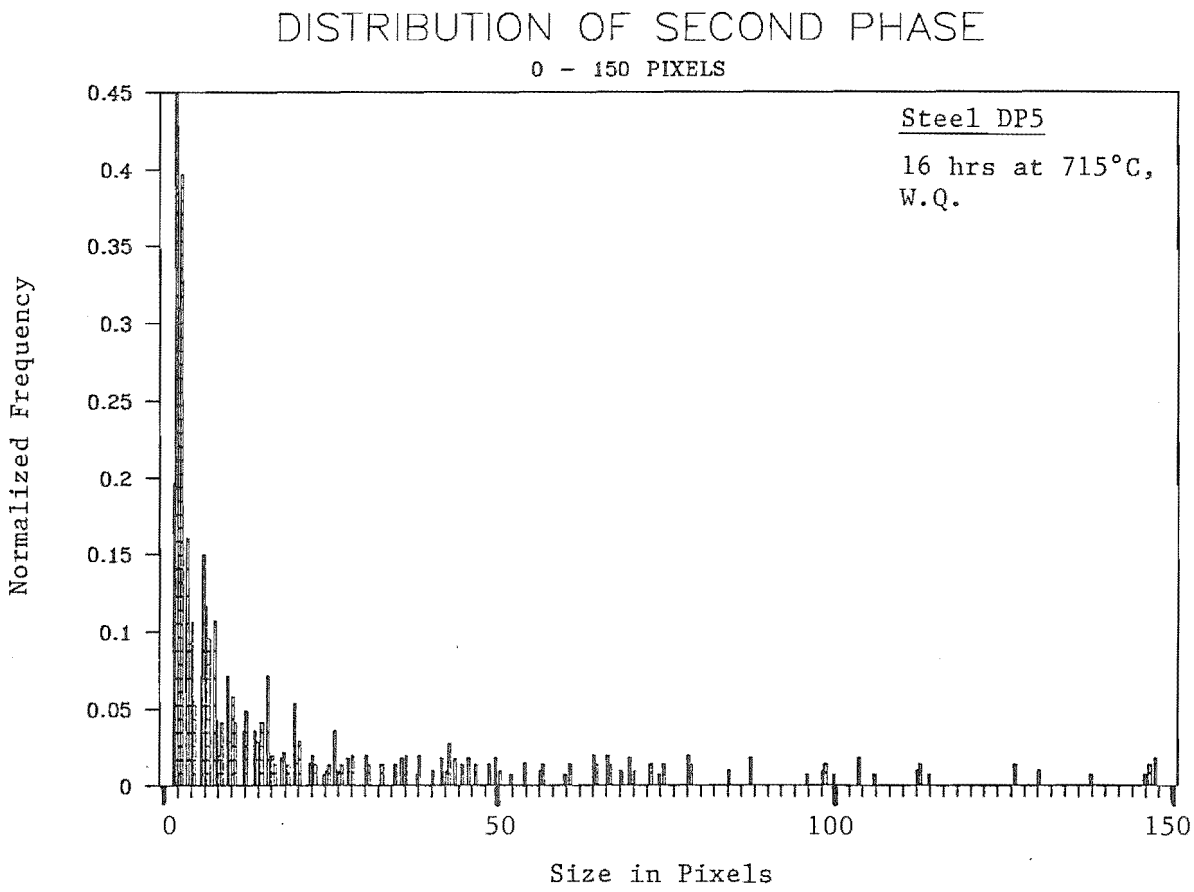

Figure E6: Distribution of Second Phase

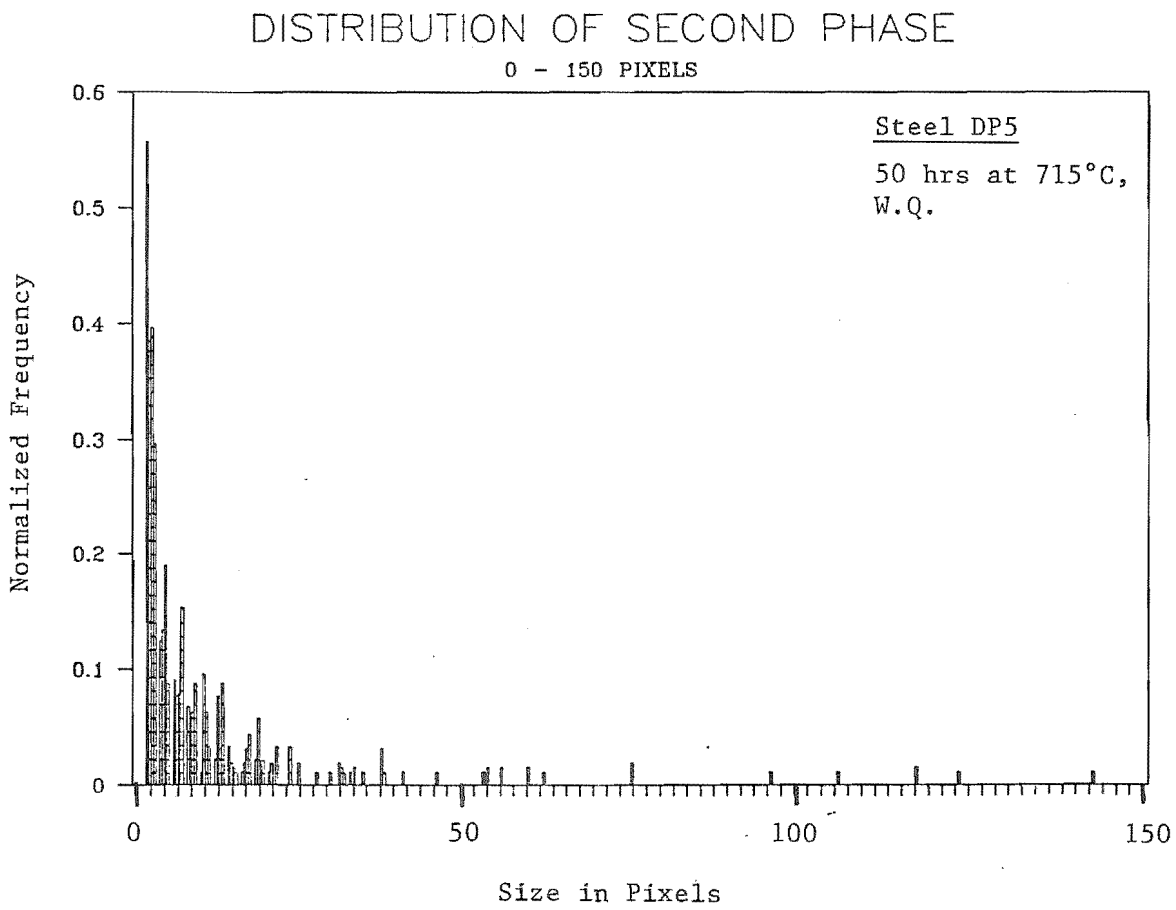

Figure E7: Distribution of Second Phase

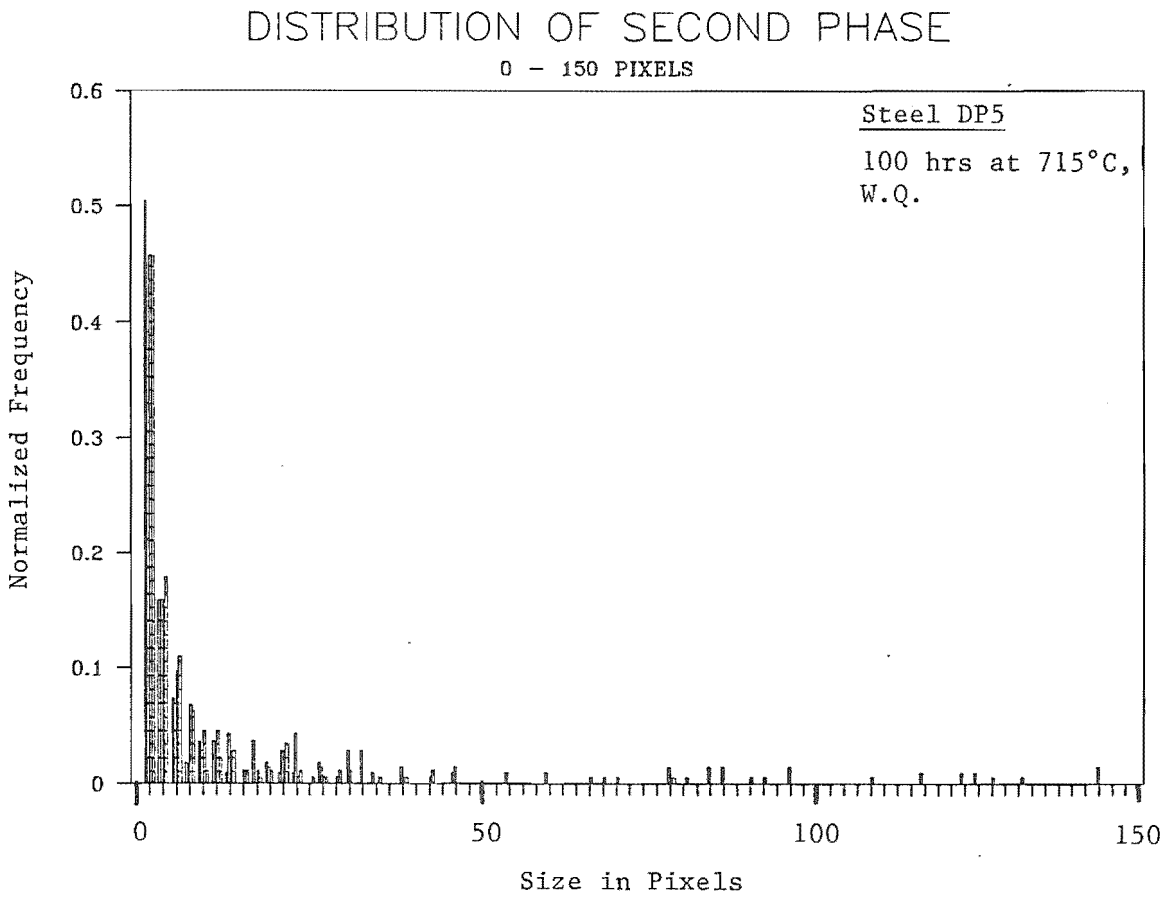

Figure E8: Distribution of Second Phase

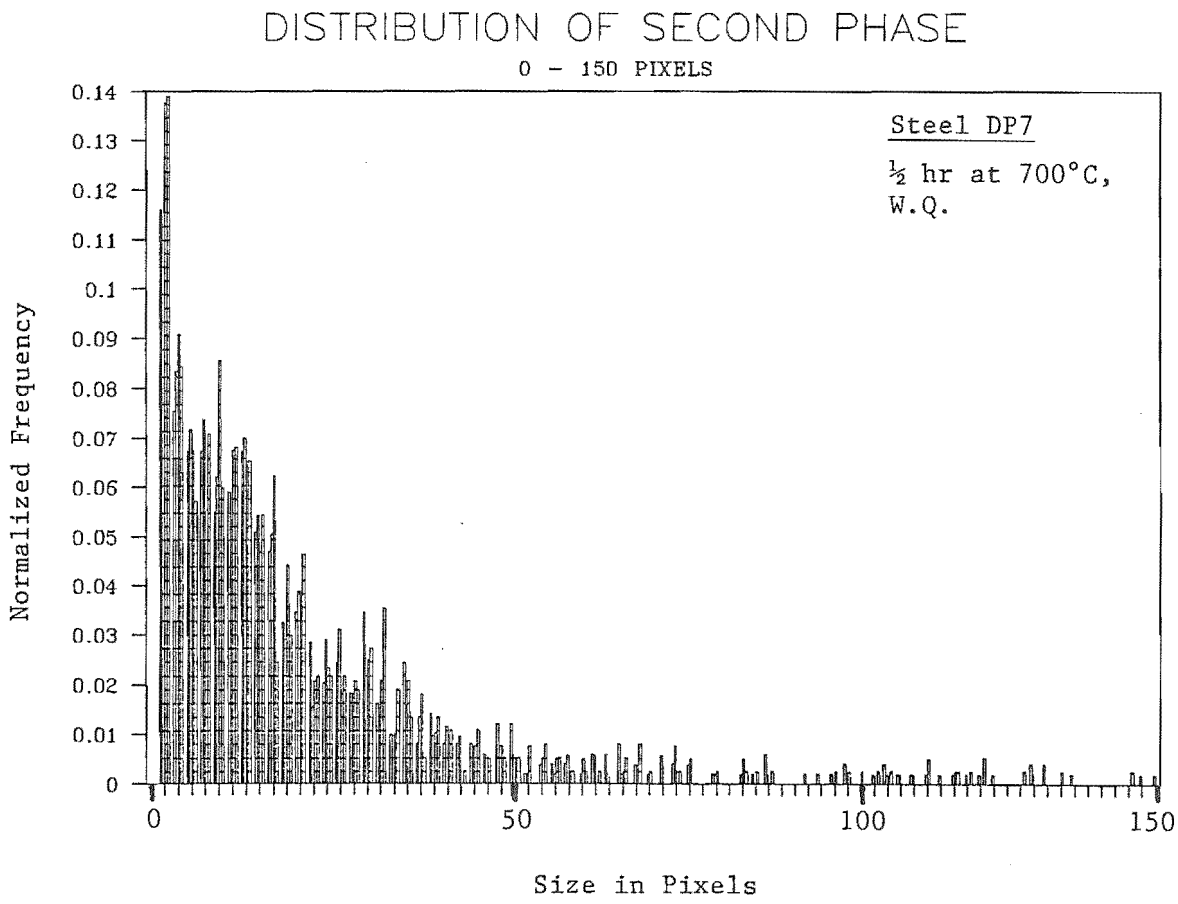

Figure E9: Distribution of Second Phase

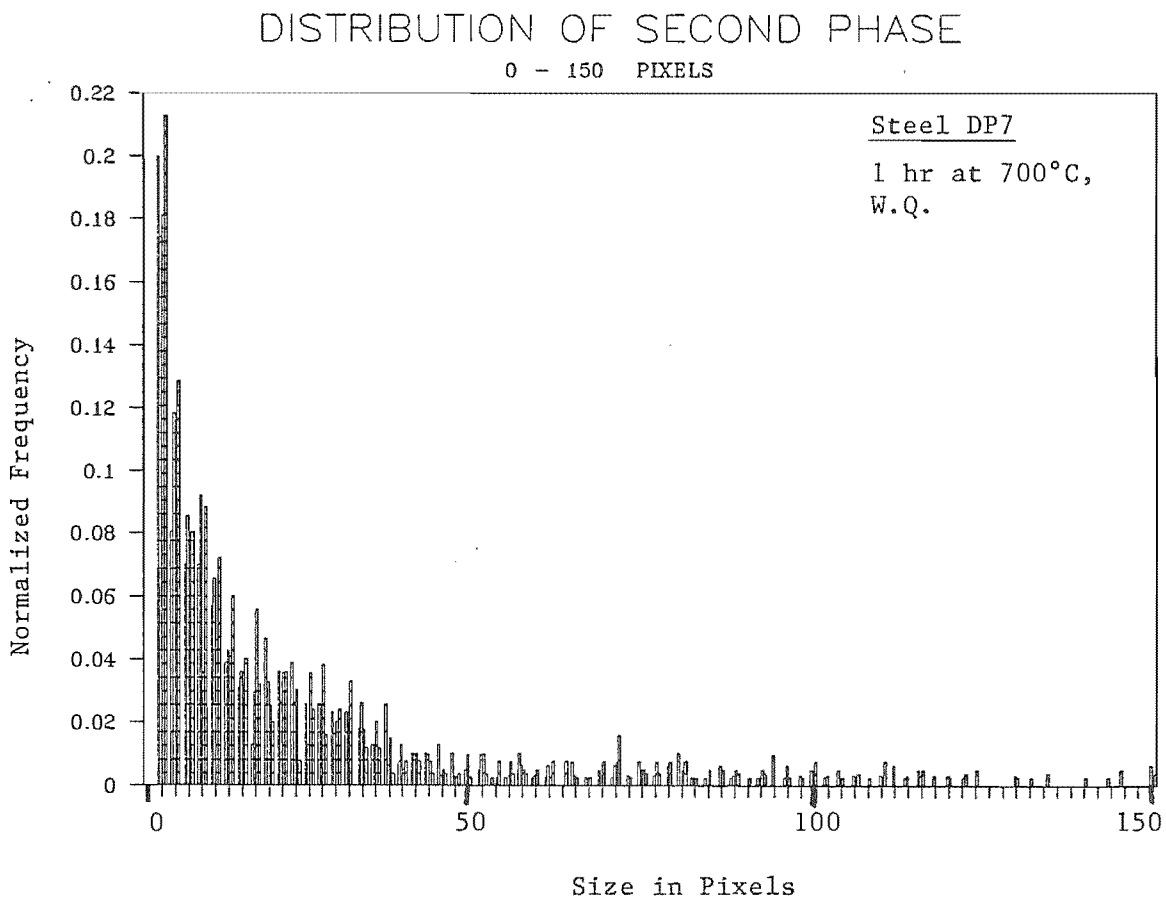

Figure E10: Distribution of Second Phase

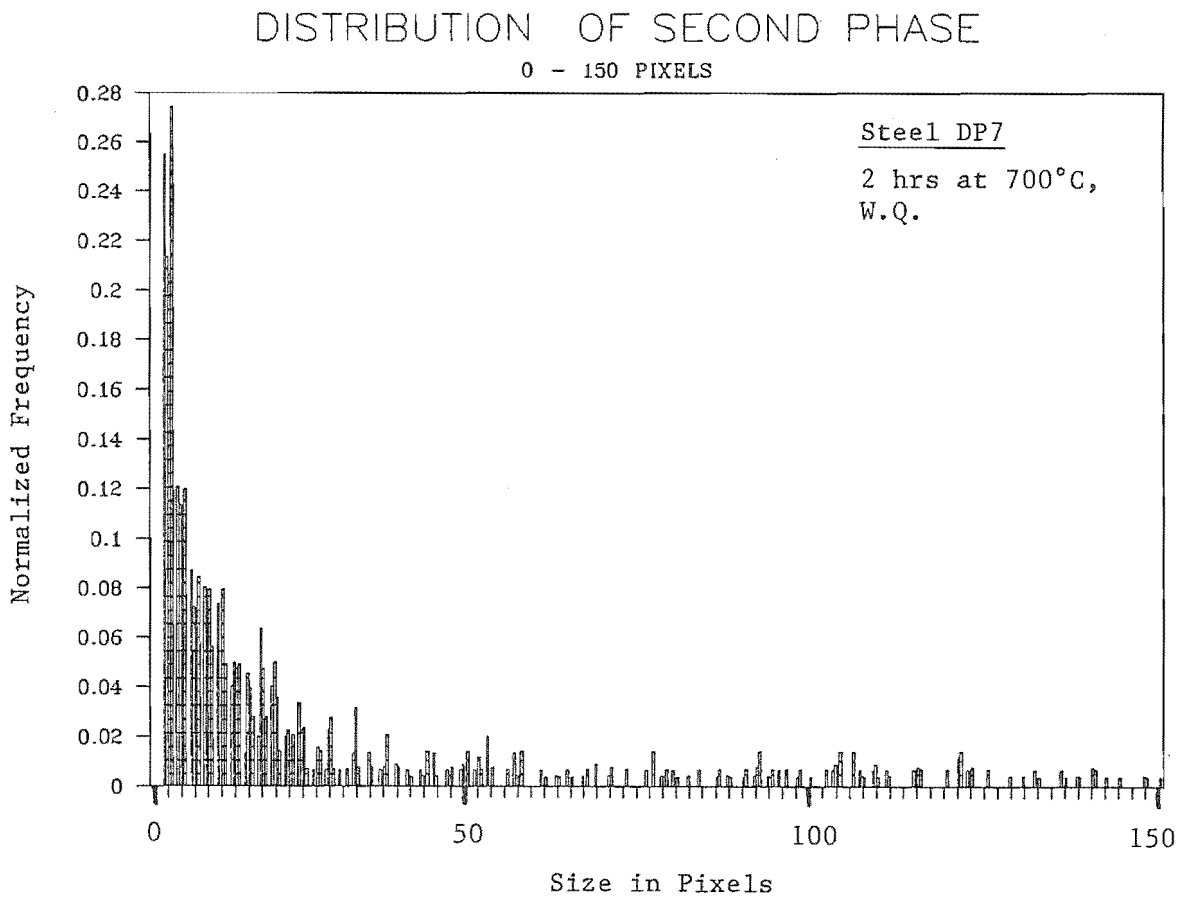

Figure E11: Distribution of Second Phase

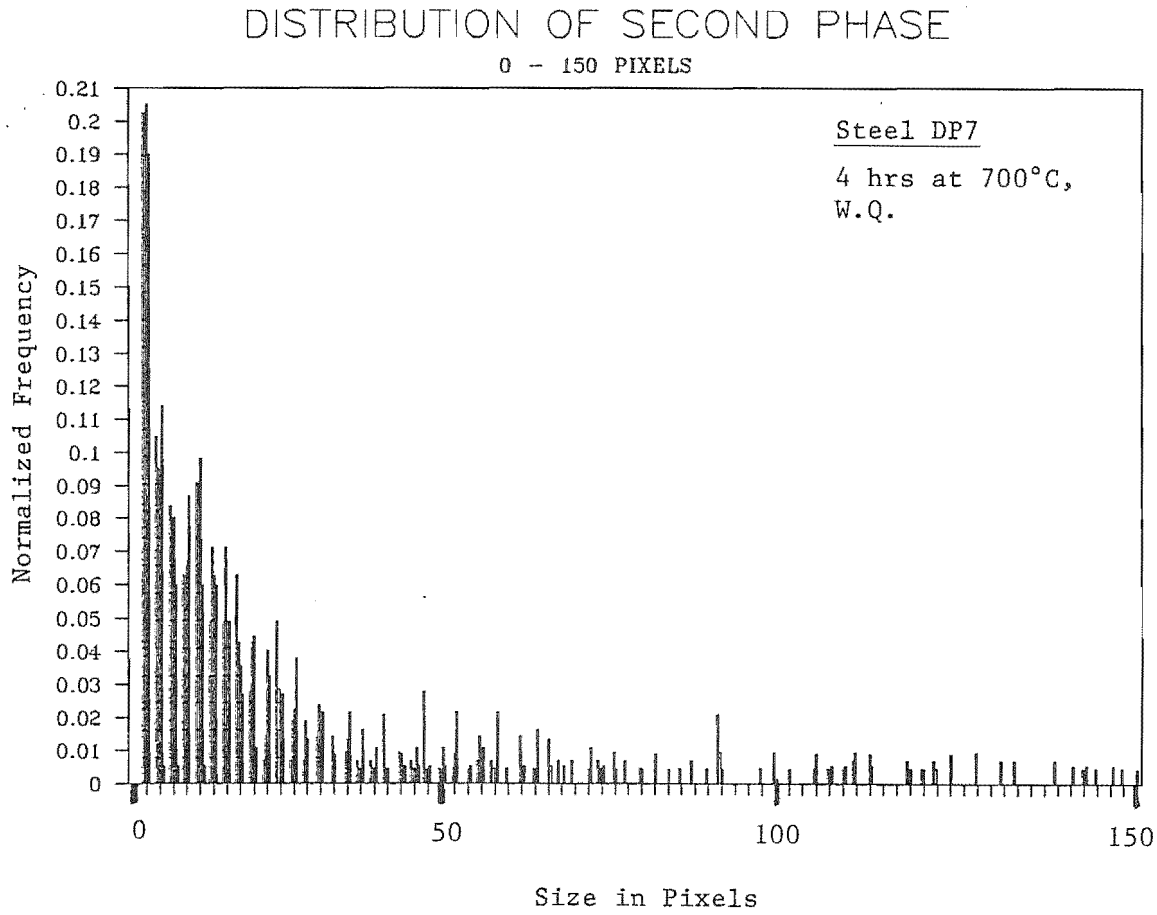

Figure E12: Distribution of Second Phase

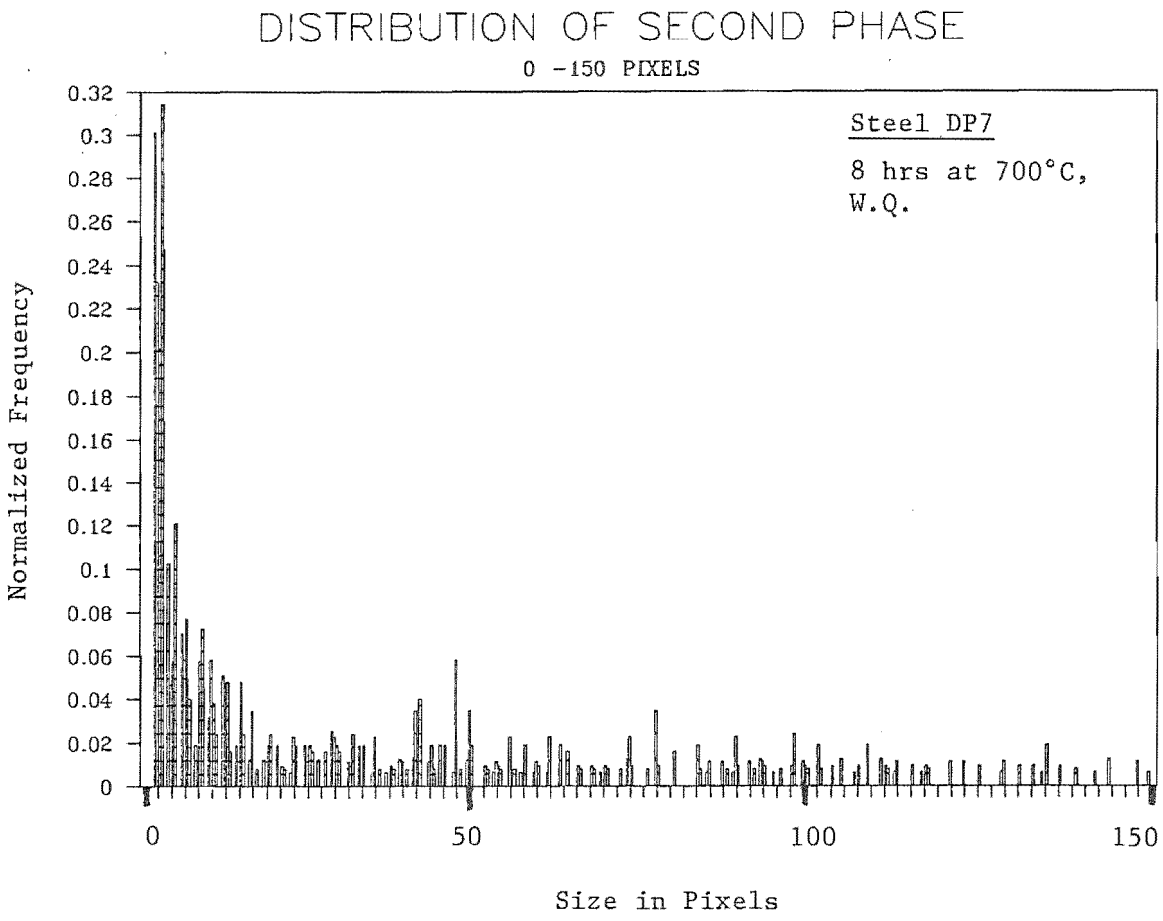

Figure E.13: Distribution of Second Phase

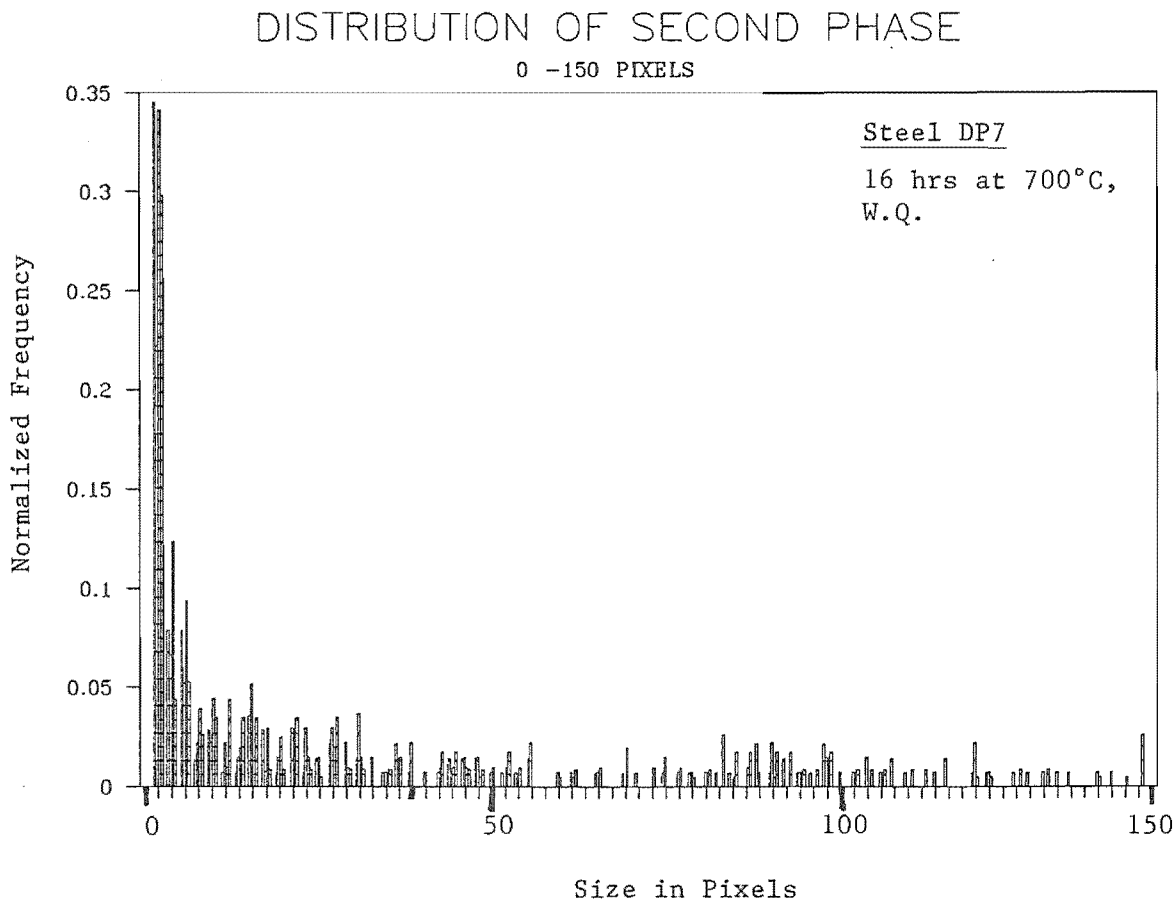

Figure E14: Distribution of Second Phase

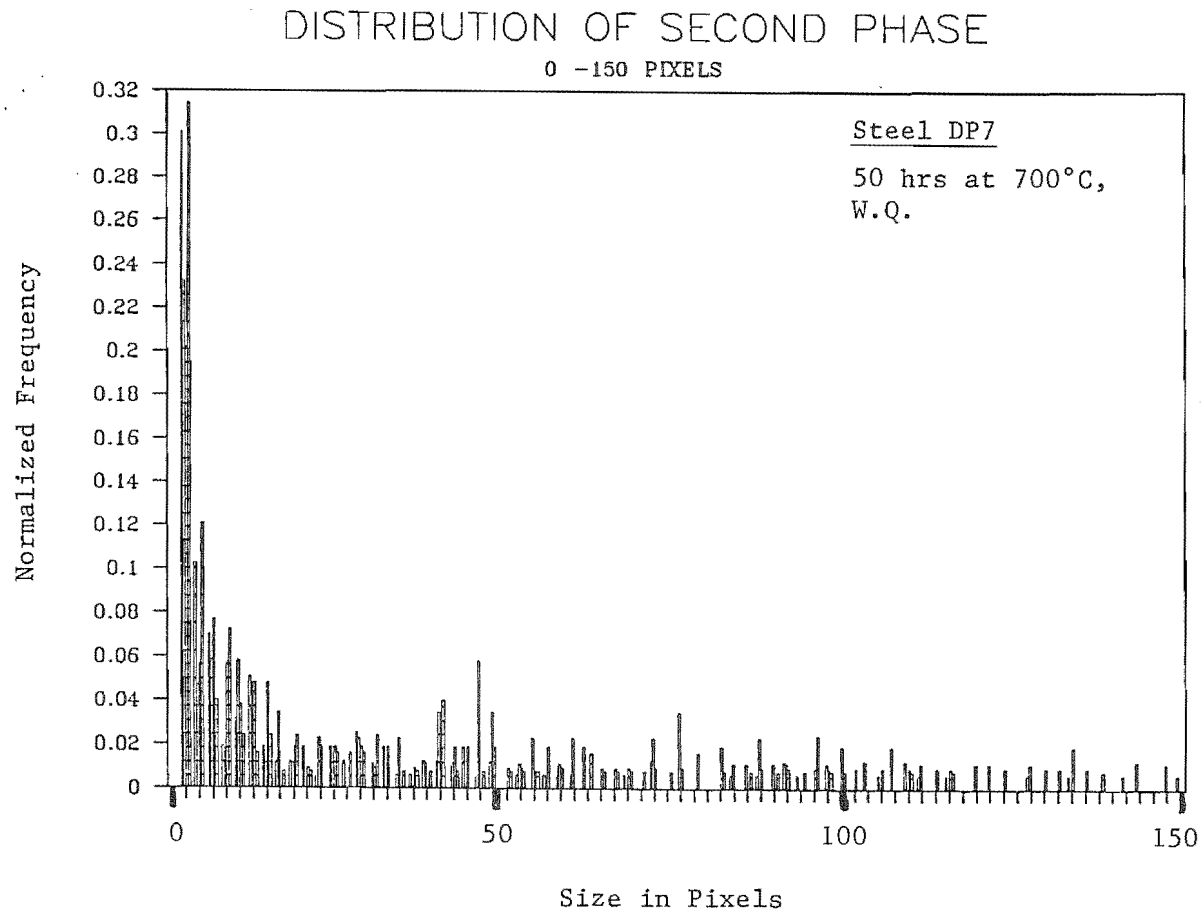

Figure E15: Distribution of Second Phase

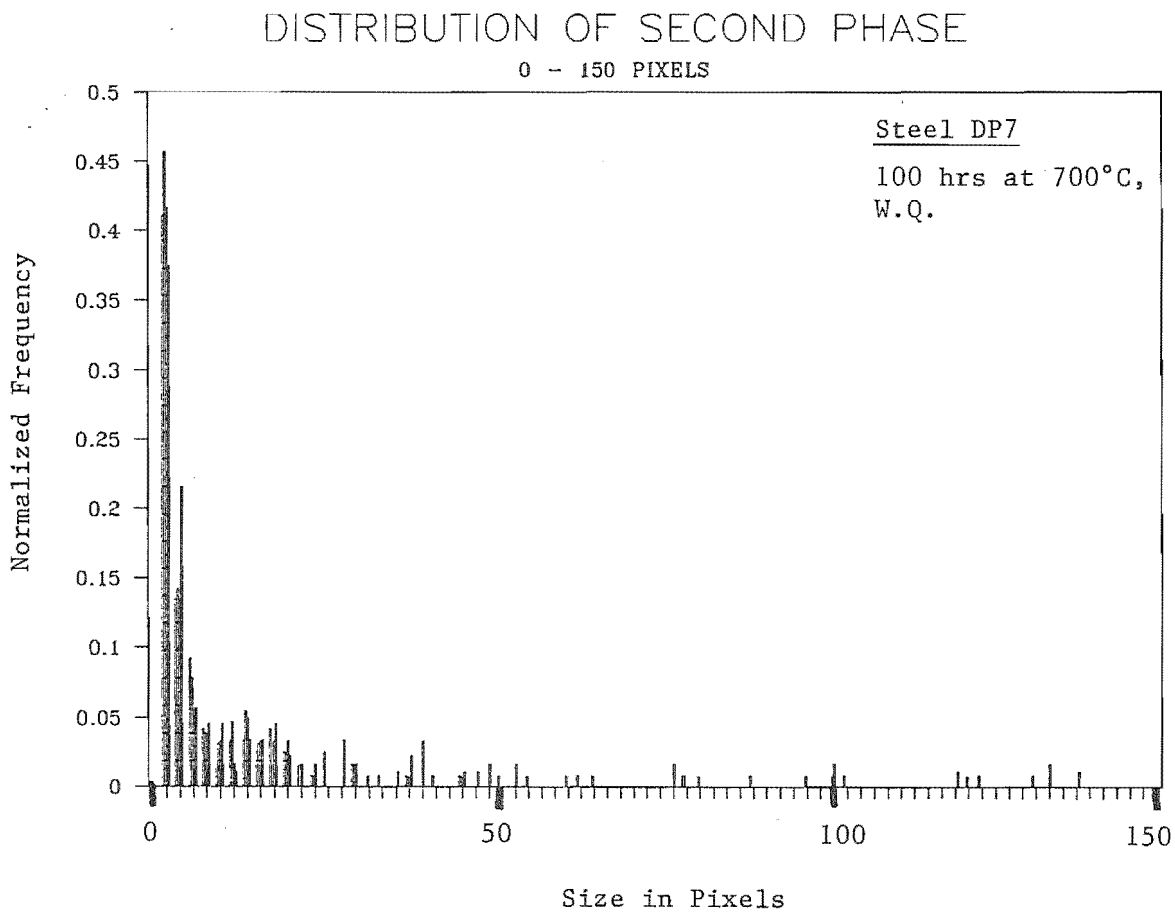

Figure E16: Distribution of Second Phase

APPENDIX F

THE PRECIPITATION OF VANADIUM NITRIDE DURING A SIMULATED HOT ROLLING THERMAL CYCLE FOR HSLA STEELS *

L.A. Erasmus, Professor of Mechanical Engineering
University of Canterbury
R. Ratnaraj, Postgraduate Student

ABSTRACT

The thermal cycle of a hot rolling strip mill has been simulated in the laboratory. In this simulation steel samples were held at 1125°C for four hours to represent slab time in the reheat furnace, after which samples were transferred to a second furnace set to represent strip coiling temperature. The temperature of this latter furnace was varied between 600°C - 950°C to simulate mill run-out table cooling, and held at these temperatures from 30 minutes to 2 hours to investigate precipitation of vanadium nitride during the slow cooling of coils.

In order to determine if prior precipitation at the reheat furnace temperature influenced precipitation of vanadium nitride at coiling temperature, two steels were used in the above investigation. In one, a small proportion of the vanadium and nitrogen was precipitated as vanadium nitride at the reheat furnace holding temperature (1125°C), and in the second all vanadium nitride precipitate was

---

* Presented in the International Conference on "Modernization of Steel Rolling", Beijing, China, May, 1989.

dissolved and the vanadium and nitrogen existed only in solid solution These tests showed that there was no significant acceleration of vanadium nitride precipitation resulting from the precipitate formed at the reheat furnace temperature.

The solubility of vanadium nitride in HSLA steels was determined for temperatures from 900°C to 1250°C, and the ferrite grain size after the simulated thermal cycle determined. The effect of a normalizing heat treatment subsequent to the simulated thermal cycle was also examined.

INTRODUCTION

High Strength Low Alloy (HSLA) steels have been produced and used in a wide range of industries for many years. These steels are generally of the low carbon, 1½% manganese type microalloyed with titanium, vanadium, niobium or aluminium, or a combination of these alloys, usually augmented by controlled temperature hot rolling schedules to give an optimum combination of high yield strength, low fracture mode transition temperature and good weldability. The high strength of these steels is attributed to fine ferrite grain size and precipitate dispersion hardening. The fine grain size in turn results from suppressed austenite grain growth during hot rolling caused by grain boundary pinning from any residual dispersion of precipitate, and from strain induced precipitation as the solubility of the precipitate phase falls with rolling temperature. It is generally agreed that precipitation hardening results principally from fine austenite-ferrite interphase precipitation and precipitation in the ferrite phase. The precipitate formed in the austenite temperature

range is considered too coarse to contribute substantially to dispersion hardening.

Many different controlled rolling processes have been and are used to produce HSLA steels In order to appropriate condition the austenite phase, heavy reductions late in the rolling process are employed. With heavy plate this is difficult to achieve and leads to large mill loads and other problems. As a result, controlled rolling is not considered economic nor technically feasible for plate above 20 mm thickness, or for thin plate where fabrication requires hot forming. It is also not feasible for shaped structural sections.

To by-pass the rather sophisticated controlled rolling technology required to ensure adequate control of finish rolling temperature, recent research has been aimed at alloy adjustments to the composition of HSLA steels which would give a fine recrystallized grain austenite without recourse to heavy low temperature deformations.

The investigation reported here had as its objective the simple simulation of a hot rolling mill thermal cycle without the thermo-mechanical treatment normally associated with HSLA steel production. The effect of this thermal cycle on precipitation and grain size was to be studied, initially using only vanadium as the microalloy addition. In the visualized hot rolling mill, slabs would be soaked at temperature in the reheat furnace for four hours. During subsequent rolling there would be only a small loss in temperature. The significant temperature drop would occur on completion of rolling, when the strip would be cooled rapidly by water sprays before coiling.

The temperature of the strip would become stabilized in the coil after which cooling would continue at a much reduced rate.

EXPERIMENTAL PROCEDURE

The simple simulation used for the above thermal cycle comprised the solution treatment of samples in an argon atmosphere at 1125°C for 4 hours, after which each sample was transferred immediately to a second furnace set at the coiling temperature. Samples were held at different coiling temperatures between 600°C and 950°C for 30 minutes, 1 and 2 hours to provide some assessment of precipitation and grain size changes which may occur after coiling, and then air cooled to ambient temperature.

Since the equilibrium solubility of vanadium carbide is much greater than the nitride in both austenite and ferrite[1], the progress of precipitation was measured by monitoring the acid insoluble nitrogen content. In this analysis technique the sample is divided into two fractions after dissolution in dilute sulphuric acid. Ammonia is separated from each fraction by steam distillation and the determination completed photometrically using Nessler's reagent. Previous experience with this method has shown the N_{insol} content to be vanadium nitride[2,3].

To provide data on the solubility of vanadium nitride in the reheat furnace, samples of HSLA type steels with a range of vanadium and nitrogen contents (see Appendix A) were held at temperatures from 900°C to 1250°C for 4 hours and then quenched. The vanadium nitride

content was again determined as N_{insol} using the technique outlined above.

Ferrite grain size was determined by the linear intercept method on samples subjected to the simulated rolling thermal cycle, and also on samples subsequently normalized from 900°C.

RESULTS AND DISCUSSION

The chemically determined N_{insol}(nitrogen as vanadium nitride) following the 4 hour heat treatments is shown in Figure 1 for the 15 steels of Appendix A. From these individual results the solubility product (K_s) relationship with temperature for vanadium nitride in austenite has been determined using linear regression analysis and is shown in Figure 2. The resultant calculated solubility curves for each of the individual steels has then been transferred back to Figure 1.

Figure 2 gives the solubility product for vanadium nitride in austenite as:-

$$\log K_s = - \frac{7754}{T} + 3.02 \qquad (1)$$

where K_s = [N][V] and T = absolute temperature.

A previously published[4] relationship for manganese steels, corrected to 1.3% manganese, gives

$$\log K_s = - \frac{8330}{T} + 3.56 \qquad (2)$$

Equations (1) and (2) give reasonable agreement when considering that a 4 hour heat treatment is probably too short to represent equilibrium conditions. Only steels B5 and D2 were used for the simulated hot rolling thermal cycle. Steel B5 has a vanadium content slightly in excess of stoichiometric for VN, and in steel D2 the vanadium content is less than stoichiometric (0.0095% excess nitrogen). When these steels are held at 1125°C for 4 hours to simulate slab reheating, all the vanadium nitride is dissolved in steel B5. However, approximately 0.003% nitrogen should still be combined as vanadium nitride in steel D2.

The N_{insol} (nitrogen as vanadium nitride) contents of the two steels after being subjected to the simulated hot rolling thermal cycle, is shown in Figure 3(a) for 'coil' furnace holding times of 30 minutes, 1 and 2 hours.

It can be seen from Figure 3(a) that vanadium nitride precipitation peaks at a 'coiling' temperature of about 700°C and decreases sharply above and below this temperature. Precipitation is a minimum at 800°C, and although the rate of precipitation increases again with higher simulated coiling temperatures, precipitation of vanadium nitride throughout the austenite temperature range is slow. For example, the precipitated vanadium nitride at a simulated coiling temperature of 900°C is less than 20% of solubility equilibrium predicted from Figure 2, even after holding at 'coiling' temperature for 2 hours. This indicates that the precipitation of vanadium nitride in the austenite temperature range is controlled almost entirely by diffusion and not by the decreased solubility of vanadium nitride, viz. diffusion rate decreases with decreasing temperature,

whereas decreasing solubility with decreasing temperature requires increased vanadium nitride precipitation.

The N_{insol} peak occurring at 700°C in Figure 3(a) appears also to be diffusion controlled, but in this instance by diffusion in ferrite. The diffusion coefficient for nitrogen in ferrite at 700°C is about 53 times that for nitrogen in austenite at the same temperature[5]. The total weight of vanadium nitride detected as N_{insol} will be the sum of precipitated vanadium nitride in both the ferrite and austenite phases. If appreciably more precipitate forms in the ferrite relative to austenite, the N_{insol} content will depend largely on the volume fraction ferrite phase. This will approach maximum at about 700°C, giving a corresponding maximum in N_{insol}, despite the higher diffusion rate of nitrogen in the ferrite formed at higher temperatures.

At simulated coiling temperatures below 700°, there would not be any significant change in the volume fraction ferrite phase. Since the N_{insol} content decreases rapidly at simulated coiling temperatures below 700°C, precipitation of vanadium nitride must again be controlled by diffusion as opposed to nitride solubility (which would predict increased precipitation). Diffusion control in the ferrite temperature range is also confirmed by increased vanadium nitride precipitated with 'coil' temperature holding time.

There is no evidence in Figure 3(a) to suggest that the undissolved vanadium nitride precipitate present at the reheat furnace temperature (1125°C) acted as centres for precipitation at lower temperatures, the difference between the N_{insol} contents of steels B5

and D2 being equal to or less than the initial 0.003% nitrogen as vanadium nitride for the full 'coiling' temperature range examined.

The ferrite grain size of samples subjected to the simulated thermal cycle is shown in Figure 3(b). The resultant ferrite grain size for all 'coiling' temperatures is significantly coarser than that normally expected in HSLA steels, however there was no mechanical deformation subsequent to reheating at 1125°C for 4 hours and the initial austenite grain size would be coarse for all simulated cooling cycles. The difference in grain size between steels B5 and D2 is consistent with impeded austenite grain coarsening from the 0.003% nitrogen as vanadium nitride in steel D2 at the reheat furnace temperature. This undissolved precipitate may exert a more important influence on grain size when combined with hot working.

There is some coarsening of grain size for all simulated coiling temperatures with increased holding time (slower coil cooling) indicating continued grain coarsening in both ferrite and austenite with time and despite the corresponding increase in nitride precipitation, see Figure 3(a). There is, however, a significant decrease in grain size at 'cooling' temperatures below 750°C. Since cooling through the austenite-ferrite transformation range would be more rapid in those samples held at 'coiling' temperatures in the austenite temperature range, this reduction in ferrite grain size must be precipitate related and dependent on the nitride precipitate formed in the ferrite phase.

When samples are normalised from 900°C after the simulated thermal cycle, Figure 3(c), the ferrite grain size is considerably

reduced and now lies within the range normally expected for HSLA steels. Again there is a consistent step in grain size at 750°C with minimum grain size corresponding to the peak in precipitated vanadium nitride and formed in the ferrite phase during the simulated rolling thermal cycle. Analysis for N_{insol} on the normalized samples gave a consistent result for all simulated coiling temperatures, e.g. 0.0155% in steel B5 (equalibrium prediction from Figure 2 gives 0.0145%). This shows that the precipitation of vanadium nitride is rapid on re-heating to normalizing temperature, but that the large volume fraction of precipitate in ferrite at the simulated coiling temperature of 700°C continues to influence the grain size after normalizing. Steel D2 has more nitrogen precipitated as vanadium nitride, and this too is reflected in the normalized grain size.

CONCLUSIONS

The analysed N_{insol} content suggests that the precipitation of vanadium nitride is most rapid in the ferrite phase, and is diffusion controlled. Peak precipitation consequently occurs at 700°C in the V-N-Mn steels examined. If any interphase nitride precipitate formed during the simulated rolling thermal cycle, its volume fraction was too small to be detected by chemical analysis. Minimum ferrite grain size for the simulated rolling thermal cycle, and for samples subsequently normalized, suggest that vanadium nitride formed in the ferrite phase dominates grain size effects.

REFERENCES

1. Woodhead, J.H., Proc.Conf. on Vanadium in High Strength Steel, Chicago, Nov.1979.

2. Konig, P. et al., Archiv Eisenhuttenwesen, vol.32, Aug. 1961, pp 541-556.

3. Erasmus, L.A. and Pussegoda, L.N., Met.Trans.A., vol.11A, Feb.1980, pp 231-237.

4. Irvine, K.J. et al., JISI, vol.205, Feb.1967, pp 161-182.

5. Fast, J.D. and Verrijp, M.B., JISI, vol.176, Jan.1954, pp 24-27.

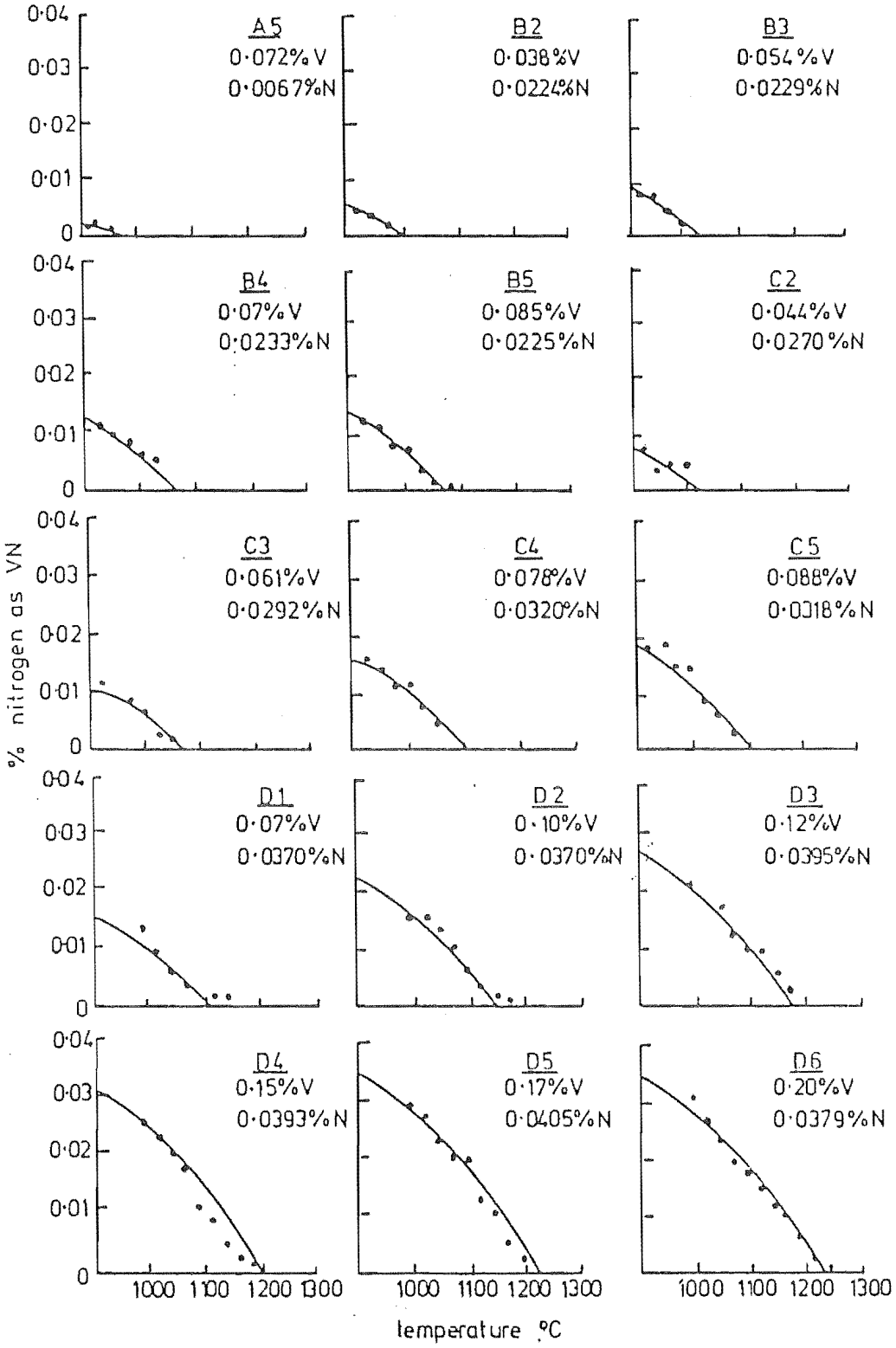

Fig 1 Solution of vanadium nitride in experimental HSLA steels after holding at temperatures for four hours

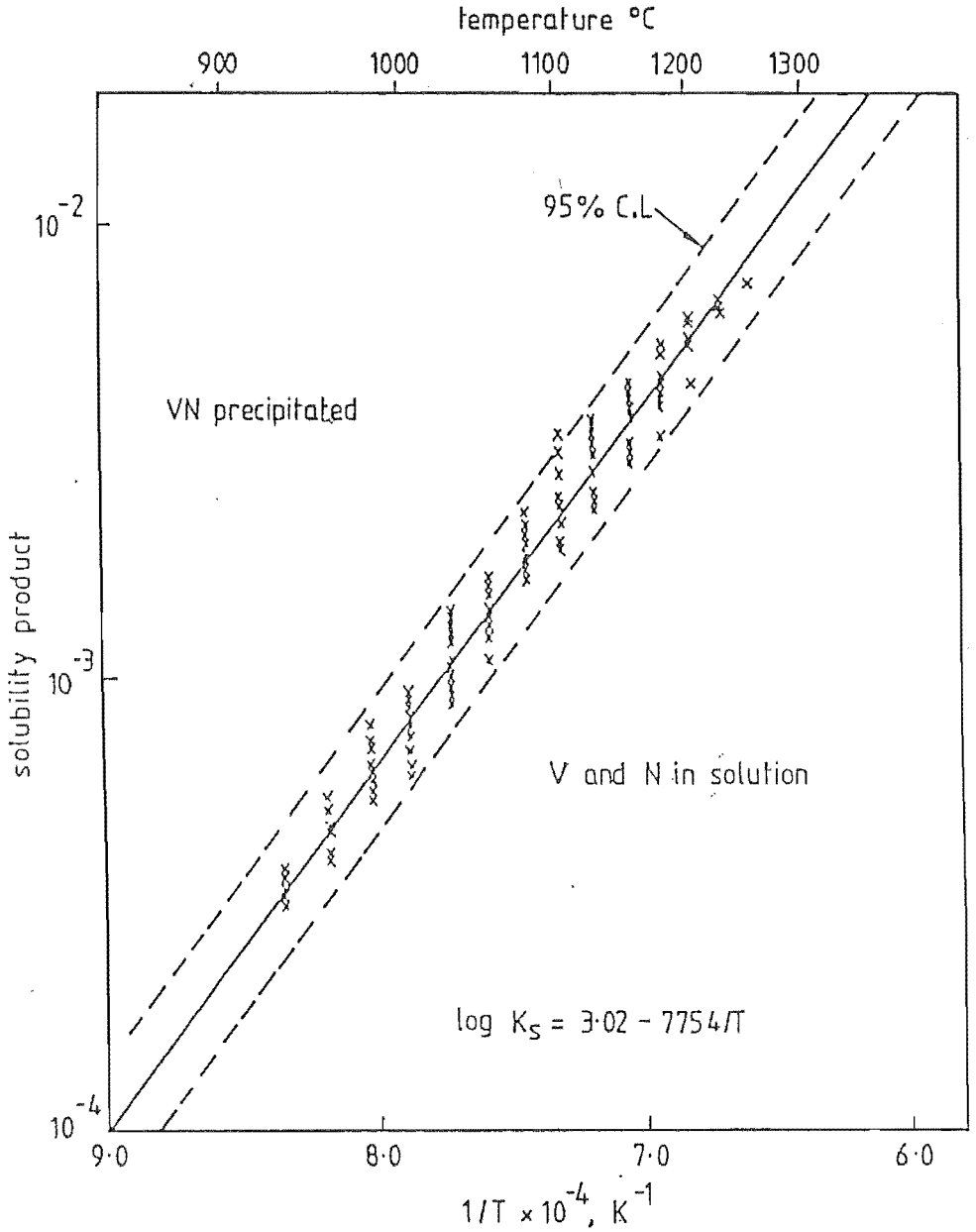

Fig 2 Solubility product of vanadium nitride in austenite as a function of temperature

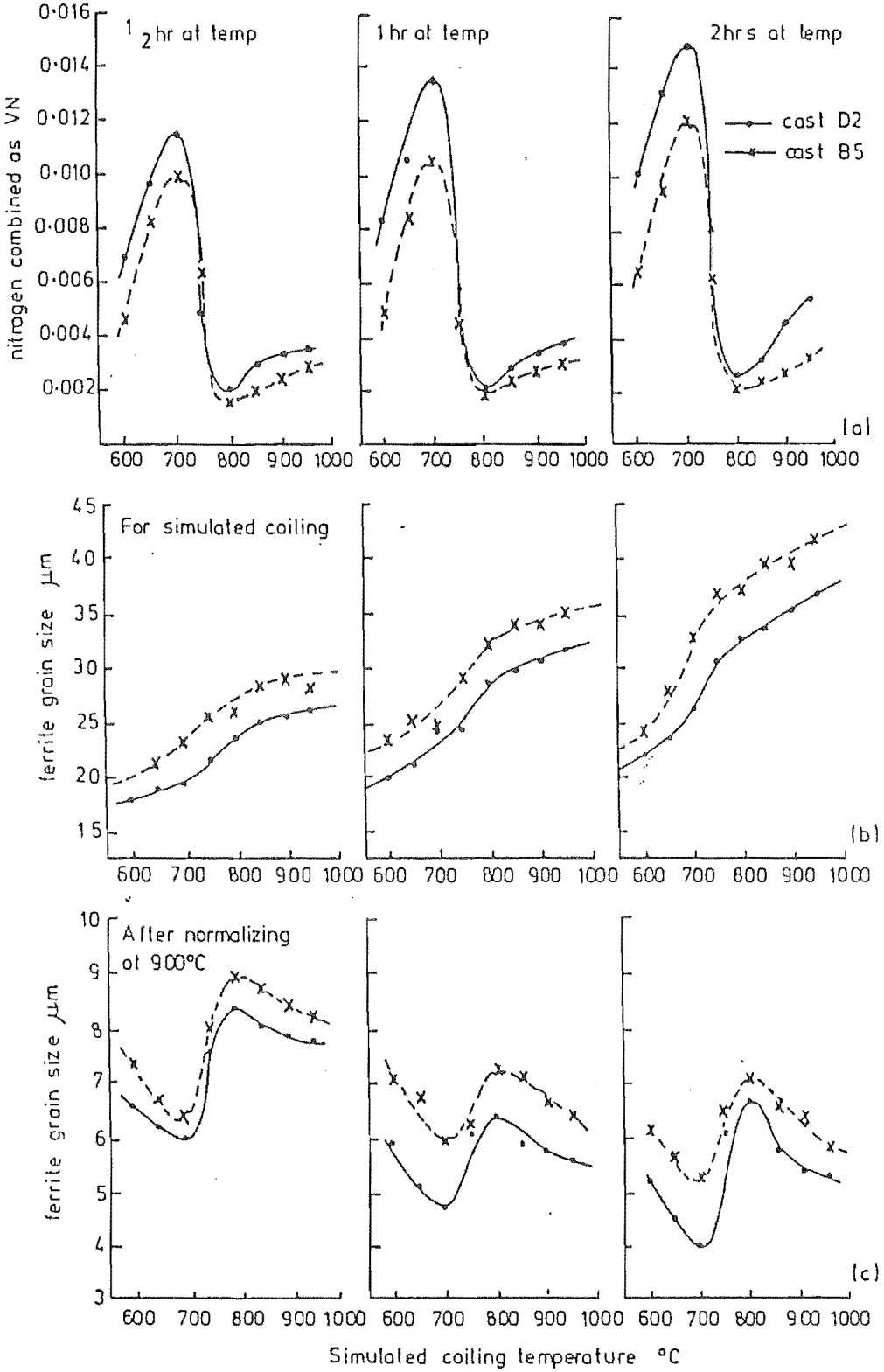

Fig 3 Changes in precipitated vanadium nitride ferrite grain size and ferrite grain size after normalizing for experimental steels D2 and B5

CAST	C	Mn	Si	S	P	Ni	Cr	Mo	Cu	Sn	V	Al	N
A5	0.09	1.38	0.15	0.012	0.012	0.03	0.02	-	0.01	-	0.072	-	0.0067
B2	0.11	1.35	0.31	0.016	0.014	0.03	0.01	-	0.01	-	0.038	-	0.0224
B3	0.09	1.30	0.30	0.012	0.011	0.03	0.01	-	0.01	-	0.054	-	0.0229
B4	0.10	1.29	0.30	0.012	0.011	0.03	0.01	0.004	0.01	0.004	0.070	0.001	0.0233
B5	0.12	1.33	0.30	0.015	0.013	0.03	0.01	0.002	0.01	0.001	0.085	-	0.0225
C2	0.11	1.28	0.20	0.011	0.011	0.03	-	-	0.01	-	0.044	-	0.0270
C3	0.12	1.29	0.20	0.014	0.012	0.03	-	-	0.01	-	0.061	0.004	0.0292
C4	0.12	1.27	0.19	0.014	0.012	0.03	-	0.001	0.01	-	0.078	-	0.0320
C5	0.11	1.25	0.18	0.013	0.011	0.03	-	-	0.01	-	0.088	-	0.0318
D1	0.14	1.57	0.19	0.012	0.020	0.04	0.05	0.005	0.01	0.002	0.07	0.007	0.0370
D2	0.14	1.35	0.18	0.011	0.019	0.04	0.05	0.004	0.01	0.001	0.10	0.007	0.0370
D3	0.14	1.34	0.18	0.011	0.019	0.04	0.05	0.005	0.01	0.002	0.12	0.006	0.0395
D4	0.15	1.33	0.17	0.011	0.019	0.04	0.05	0.004	0.01	0.001	0.15	0.005	0.0393
D5	0.15	1.27	0.15	0.011	0.019	0.04	0.05	0.004	0.01	0.001	0.17	0.005	0.0405
D6	0.16	1.24	0.13	0.012	0.020	0.04	0.05	0.003	0.01	-	0.20	0.005	0.0379

APPENDIX A: COMPOSITION OF EXPERIMENTAL STEELS

APPENDIX G

CALCULATION OF EQUIVALENT VOLUME FRACTION OF VANADIUM NITRIDE

The weight percentage of nitrogen in steel is given by:

$$\frac{\omega t\%\ N}{\omega t\%\ Fe} = \frac{(\text{Number of N atoms}) \times (\text{atomic } \omega t \text{ of N})}{(\text{Number of Fe atoms}) \times (\text{atomic } \omega t \text{ of Fe})} \qquad \text{Eqn.G.1}$$

For example, assume 0.01% nitrogen and 99.99% iron

$$\frac{\text{Number of N atoms}}{\text{Number of Fe atoms}} = \frac{0.01 \times 55.84}{99.99 \times 14} \qquad \text{Eqn.G.2}$$

Vanadium nitride possesses an f.c.c (NaCℓ type) crystal structure with ideal, stoichiometric composition VN, and has lattice parameter a_o of 4.137 $\mathring{A}$(148). This gives 4 nitrogen atoms per unit cell of 70.8 $\mathring{A}^3$

∴ We have a space equivalent of 17.70 $\mathring{A}^3$ per nitrogen atom.

For the b.c.c structure of iron the lattice parameter a_o is 2.86 $\mathring{A}$(149)

This gives 2 iron atoms per unit cell of 23.39 $\mathring{A}^3$. Therefore, we have a space equivalent of 11.70 $\mathring{A}^3$ per iron atom

$$\therefore \text{ Volume fraction of VN} = \frac{\text{Vol per N atom x Number of N atom}}{\text{Vol per Fe atom x Number of Fe atom}}$$

From equation G2, we have

$$\text{Volume fraction of VN} = \frac{17.70 \times 0.01 \times 55.84}{11.70 \times 99.99 \times 14}$$

$$= 6.03 \times 10^{-4}$$

∴ <u>Volume fraction VN = 0.06%.</u>